The Dissertation Committee for Rajeev Satish Prabhakar certifies that this is the approved version of the following dissertation:

Low Hydrocarbon Solubility Polymers: Plasticization-resistant Membranes for Carbon Dioxide Removal from Natural Gas

Committee:

Benny D. Freeman, Supervisor

Donald R. Paul

Isaac C. Sanchez

R. Bruce Eldridge

Gregory K. Fleming

Low Hydrocarbon Solubility Polymers: Plasticization-resistant Membranes for Carbon Dioxide Removal from Natural Gas

by

Rajeev Satish Prabhakar, B.Tech.(Hons), M.S.

Dissertation

Presented to the Faculty of the Graduate School of

The University of Texas at Austin

in Partial Fulfillment

of the Requirements

for the Degree of

Doctor of Philosophy

The University of Texas at Austin

December 2004

To my maternal grandmother, Rajkumari Sharma, and my paternal grandfather, Shyamsunder Prabhakar, for the strong positive influence they have had on my life

ACKNOWLEDGEMENTS

"It is not our abilities or gifts which define who we are, but the choices we make."

- Albus Dumbledore
in Harry Potter and the Sorcerer's Stone
by J. K. Rowling

I have several people to thank for helping me make the right choices in life. Several more have been there to help me in implementing these decisions, and I am indebted to them all. This dissertation would not have seen the light of day without the advice, help and support of the people below.

First and foremost, I would like to express my deepest gratitude to my advisor, Dr. Benny Freeman, for his encouragement and mentorship on various aspects of both research and life. I hope to continue having engaging discussions with him, which have benefited me immensely over the past few years. I am also thankful to my thesis committee members - Dr. Donald Paul, Dr. Isaac Sanchez, Dr. Bruce Eldridge and Dr. Greg Fleming - for their helpful discussions and guidance on this project. I am especially thankful to Dr. Greg Fleming for discussions during the initial stages of this project, which helped me define the focus of this research endeavor. A very special thanks also goes to my undergraduate senior thesis advisor, Dr. Sunando Dasgupta, for introducing me to the world of polymer membranes and the benefits this technology can bring to mankind.

Several people have contributed to this project in various ways. In particular, I am thankful to Dr. Mike Coughlin of DuPont-Dow Elastomers for providing the polymer, TFE/PMVE49, and Dr. Ingo Pinnau of Membrane Technology & Research, Inc. for providing composite poly(dimethylsiloxane) films. Dr. Timothy Merkel and Zhenjie He of Membrane Technology and Research, Inc. allowed me to use some of their unpublished data to make comparisons with my results, and for this I am grateful. Ian Roman of MEDAL L. P. is responsible for all the mixed-gas permeation data in this work, and I am indebted to him for providing me with results of these industrially-relevant tests. I also gratefully acknowledge the funding sources for this research. This research was partially supported by the United States Department of Energy under grant number DE-FGO2-99ER14991. This research was also partially supported with funding from the United States Department of Energy's National Energy Technology Laboratory under a subcontract from Research Triangle Institute through their Prime Contract No.: DE-AC26-99FT40675. The Chemical Sciences, Geosciences and Biosciences Division, Office of Basic Energy Sciences, Office of Science, U.S. Department of Energy (DE-FG03-02ER15362) also contributed funds to this research.

Past and present members of the Freeman Polymer Research Group are also thanked for their technical advice, support and encouragement. In particular, interactions with the following members have been helpful: Dr. Timothy Merkel, Dr. Sushil Dhoot, Dr. Kazukiyo Nagai, Dr. Hyuck J. Lee, Haiqing Lin, Dr. Nikunj Patel, Scott Matteucci, Scott Kelman and Roy Raharjo. A special thanks is in order for Scott Matteucci for making my dissertation writing phase cheerful with his constant attempts at humor. A very special thanks goes out to Dr. Michelle Arnold and Dr. Lora Toy for their friendship

– you made life in the lab fun with humorous stories, 'scientific' songs and discussions on all topics, and for this I am extremely grateful.

I owe a great deal to my dear friend, Urshit Parikh. He was there to keep me focused on the job at hand when other options seemed too tempting to stay committed to scientific research. Several other friends are thanked for being there during these graduate school years and providing good times and fond memories: Amit Khandelwal, Sandesh Joshi, Varsha Damle, Tushar Mahale, Srinivas Siripurapu, Swapnil Chhabra, Ketan Bhatt, Greg Clayson, Keith Shockley and Jason Kelly.

Finally, I thank my parents and sister for supporting my decisions and providing lots of love and encouragement, and my fiancée, Deepannita Ghosh, for her constant love, patience and companionship.

Low Hydrocarbon Solubility Polymers: Plasticization-resistant Membranes for Carbon Dioxide Removal from Natural Gas

Publication No._____

Rajeev Satish Prabhakar, Ph.D.

The University of Texas at Austin, 2004

Supervisor: Benny D. Freeman

Hydrocarbon polymers developed for CO_2 removal from natural gas often lose their superior separation ability at field conditions. This deterioration in performance is primarily a result of polymer plasticization by natural gas components like higher hydrocarbons, which have high solubilities in these polymers. Polymers that have low solubilities for higher hydrocarbons may be less susceptible to plasticization by these penetrants and therefore exhibit more stable separation properties in actual field conditions. This study was undertaken to investigate the above premise through identification of low-hydrocarbon-solubility polymers and performing a fundamental study to assess the potential of such materials to be stable membranes for CO_2 removal from natural gas.

Hydrocarbon and fluorocarbon gas solubility measurements in hydrocarbon polymers and fluoropolymers reveal that interactions between hydrocarbon and fluorocarbon species result in lower solubilities of hydrocarbons in fluorocarbon polymers, and *vice versa*, than expected on the basis of empirical correlations. The influence of these interactions on gas permeability is greater in lower free volume materials. Interestingly, hydrocarbon solubility in fluoropolymers increases much less with increasing penetrant condensability than in hydrocarbon polymers, implying that large hydrocarbon compounds will exhibit much lower solubility in fluoropolymers than in hydrocarbon polymers.

A commercial fluoropolymer, Hyflon AD 80, has much higher CO_2 permeability than typical hydrocarbon polymers, but its CO_2/CH_4 selectivity is lower than these polymers. However, Hyflon AD 80 exhibits more stable gas separation properties than typical hydrocarbon polymers in the presence of CO_2 and moderate amounts of large hydrocarbons.

Materials selection guidelines for using fluoropolymers as plasticization-resistant coatings on existing hydrocarbon membranes require the fluoropolymer to have a lower ratio of higher hydrocarbon to CO_2 (or CH_4) solubility than the hydrocarbon polymer. The guidelines also require the coating to have a similar, or greater, diffusivity selectivity (size-selectivity) for gases than that of the hydrocarbon polymer.

Permeability of highly condensable penetrants is often a function of their sorbed concentration in the polymer. A model is presented to rationally predict concentration and temperature dependent gas permeability in rubbery polymers, based on limited

experimental data. The model satisfactorily describes vapor permeation in a commercial membrane, poly(dimethyl siloxane), and in poly(ethylene).

Table of Contents

List of Tables

List of Figures

CHAPTER 1

Introduction

1.1 NATURAL GAS

Natural gas is a vital component of the world's energy supply. It is one of the cleanest and safest energy sources available today [1]. Until the past few decades, natural gas encountered while drilling for oil was often simply flared, because the infrastructure necessary to capture the gas and transport it to potential users was not available. Today, natural gas pipelines are in place to serve a large portion of the industrialized world. World natural gas consumption is now on par with coal use on a BTU basis, supplying 23% of the world's commercial energy needs [1,2]. Environmental concerns such as global warming have resulted in calls for increased use of natural gas because natural gas yields only one half as much carbon dioxide per unit of energy produced as coal and 25% less than oil [1]. According to the Energy Information Administration of the US Department of Energy, natural gas is expected to be the fastest growing source of energy in the coming decades (*cf.* Figure 1.1), nearly doubling in amount consumed during the period 2003-2025 [2].

Natural gas, as used by consumers, is quite different from the natural gas brought from underground up to a wellhead. Raw natural gas varies substantially in composition from source to source; a typical composition is shown in Table 1.1. As seen from the table, natural gas is composed primarily of methane but also includes light hydrocarbons such as ethane, propane and butanes [3] as well as higher hydrocarbons (C_{5+}). Non-hydrocarbon impurities such as carbon dioxide, hydrogen sulfide, water, nitrogen, helium and argon may also be present in natural gas.

1.2 NATURAL GAS PROCESSING

Although raw natural gas has a wide range of compositions, the composition of gas delivered to consumers is tightly controlled. U.S. pipeline specifications for natural gas are shown in Table 1.2. All natural gas requires some treatment to meet these specifications, and approximately 20% requires extensive treatment before it can be delivered to the pipeline [4]. Traditionally, removal of acid gas components and water has been achieved by absorption-type processes (*e.g.,* amine- and glycol-based systems) [4]. However, in recent years, membrane processes have been shown to be very effective for performing some of these separations [5-8], especially for treating small to moderate size gas streams [4].

Membranes have several advantages over the absorption-type processes for natural gas treatment [9]:

1. Membrane-based separations are less energy intensive than traditional processing methods.
2. Glassy, size-selective polymer membranes are more permeable to CO_2, H_2S and water vapor than to CH_4 and higher hydrocarbons. Thus, the desired methane product is obtained in the high-pressure retentate stream without significant loss in pressure, as desired for transport through pipelines.
3. Membrane units are modular and, hence, flexible with respect to the capacity they can handle. Additional membrane units can be easily added to handle higher capacities.
4. Membrane units are compact and, hence, they can be installed on offshore platforms. Thus, natural gas from the well can be processed on the platform

before being transported. This on-site processing capability eliminates the need to use expensive materials of construction for the pipelines to carry corrosive gases like CO_2 and H_2S. Also, smaller pipelines can be used because contaminants in the stream no longer have to be transported to on-shore processing plants for removal, thereby reducing material and pumping costs.

Due to these significant advantages, membranes have generated interest in the natural gas processing industry, especially for the removal of CO_2. Currently, more than 200 membrane plants have been installed to perform this separation [4].

1.3 POLYMER MEMBRANES FOR CO_2 REMOVAL FROM NATURAL GAS

Gas transport through a non-porous polymeric membrane is known to follow the solution-diffusion mechanism [10]. According to this three-step mechanism, the gas first sorbs into the membrane on the high-pressure side, then diffuses across the membrane under a partial pressure driving force and finally desorbs from the low pressure side of the membrane. Therefore, gas permeability in the membrane is dependent both on the solubility of the gas in the polymer as well as its diffusion coefficient in the polymer. Gas solubility in polymers typically increases with an increase in gas condensability, in the absence of specific interactions between the gas molecules and polymer chains [11]. Gas diffusion coefficients decrease with an increase in penetrant size [11]. Thus, differences in molecular size and/or gas condensability can result in different gas permeation rates through a polymer. Differential permeation rates result in an increase in the concentration of the faster permeating species on the downstream side of the membrane as compared to

its concentration in the feed stream, thus effecting a separation of the gases in the mixture. This phenomenon is the underlying principle of membrane-based gas separation.

CO_2 is smaller and more condensable than CH_4, so both diffusivity and solubility favor CO_2 transport over CH_4 in polymers. Materials science research in this area has mainly concentrated on increasing gas diffusion coefficients and diffusivity selectivity of the membrane (*i.e.*, the ability of the membrane to separate molecules based on size) to achieve higher CO_2 permeability and CO_2/CH_4 selectivity simultaneously. These efforts have produced high performance materials like aromatic polyimides which now compete with cellulose acetate, a polymer widely used in this application [4,9]. However, when exposed to natural gas in actual field conditions, many of these membranes exhibit only modest CO_2/CH_4 selectivities, underperforming significantly in comparison to their superior separation performance observed under laboratory conditions.

The deterioration in membrane separation performance under field conditions is primarily due to the action of CO_2 and higher hydrocarbon contaminants present in natural gas. Large hydrocarbons are highly condensable and have high solubilities in the hydrocarbon polymers currently used for this application. Upon sorbing into a polymer, these higher hydrocarbons can act as plasticizers, increasing polymer chain mobility and decreasing the size-sieving ability (or diffusivity selectivity) of the polymer. Plasticization theory attributes this effect of low molar mass compounds on polymer chain mobility and diffusivity selectivity to an increase in free volume of the polymer [12]. Just as an increase in the number of chain ends in a polymer increases its free volume due to greater mobility of these end groups, similarly, the low molar mass compounds impart greater free volume to the polymer due to their higher mobility. The

plasticizer molecules can also decrease inter-chain interactions by interposing between chains and providing a screening effect [12]. This increases the mobility of the polymer chains and hence decreases their size-sieving ability.

Figure 1.2 presents results from an experimental study of the effect of plasticization on diffusion coefficients in poly(vinyl chloride), which is a glassy, rigid, strongly size-sieving polymer [13,14]. From Figure 1.2, in the unplasticized polymer, diffusion coefficients decrease dramatically with increasing penetrant size. For example, as penetrant critical volume, V_c, increases from 57.4 cm^3/mol to 370 cm^3/mol (from helium to *n*-hexane), diffusivity decreases by about 10 orders of magnitude. However, in plasticized poly(vinyl chloride), diffusivity decreases by only two orders of magnitude over the same penetrant size range, thus showing that the polymer loses its size-sieving ability to a very large extent due to plasticization.

As mentioned above, polymer membranes can also be plasticized by CO_2. Due to CO_2-induced plasticization, the actual CO_2/CH_4 separation performance of polymer membranes cannot be predicted from pure gas measurements, which are often used to estimate permanent gas separation performance. Figure 1.3 shows the difference between the prediction of CO_2/CH_4 separation performance in cellulose acetate, a commercially used membrane material, based on pure gas measurements and the actual separation performance determined from mixture permeation experiments [15]. With increasing feed pressure, the pure gas measurements predict an increase in CO_2/CH_4 selectivity. This is because, at the higher pressures, CO_2 plasticizes the polymer, which increases its diffusivity and hence its permeability. Therefore, the ratio of CO_2 to CH_4 permeability, *i.e.*, pure gas CO_2/CH_4 selectivity, increases with increasing pressure. However, in the

mixture experiments, due to CO_2-induced plasticization, the diffusion coefficient of CH_4 increases to a greater extent than that of CO_2, and this causes a decrease in the overall selectivity. Higher hydrocarbon-induced plasticization can further decrease the selectivity.

Figure 1.4 shows an example of the negative effect of higher hydrocarbon induced plasticization on CO_2/CH_4 separation [16]. In the presence of toluene or hexane, the polyimide membrane exhibits a significant reduction in CO_2/CH_4 mixed-gas selectivity from that determined in the absence of these compounds. A decrease in CO_2/CH_4 selectivity results in more of the desired methane product appearing in the low pressure permeate stream from the membrane unit, which either forces the use of a second membrane stage to recover the permeated methane and repressurize it to pipeline conditions or results in larger losses of methane from the separation system. Both of these options increase the cost of purifying the gas. To promote the use of polymer membranes for natural gas processing, it is imperative to develop membranes that will maintain their superior separation properties in actual field conditions.

1.4 GOALS AND ORGANIZATION OF THIS RESEARCH

Efforts have been made to suppress plasticization of hydrocarbon polymers in natural gas environments. Strategies such as using polymer blends [17,18], thermal treatment of polymer membranes [19] and crosslinking of polymers [20-22] has resulted in some success in delaying the onset of plasticization to higher partial pressures of the plasticizing components. However, these approaches attempt to treat the symptom rather

than the underlying fundamental cause of the plasticization phenomenon, *i.e.*, the high solubility of large hydrocarbon compounds in currently-used polymer membranes. An alternate materials design strategy is to identify polymers with inherently low solubility for large hydrocarbon compounds. Such polymers might be more resistant to plasticization and, therefore, maintain their separation capabilities under field conditions for extended periods of time. This research project was undertaken with the aim of identifying such polymers and performing a fundamental study to assess the potential of this materials design strategy for obtaining plasticization-resistant membranes for CO_2 removal from natural gas. Such membranes may also find application in other separations involving hydrocarbon compounds.

This dissertation is comprised of nine chapters, including this introductory chapter which provides background information and motivation for pursuing the goal of developing plasticization-resistant polymer membranes for CO_2 removal from natural gas. Chapter 2 outlines the theory of membrane-based gas separation and describes the experimental techniques utilized in this study. It also provides an overview of the literature that formed the basis for this research.

Chapter 3 presents the results of an experimental investigation of the energetics of hydrocarbon and fluorocarbon sorption and permeation in two hydrocarbon-based polymers, rubbery poly(dimethylsiloxane) (PDMS) and high-free-volume, glassy, poly(1-trimethylsilyl-1-propyne) (PTMSP). This study provides quantitative evidence of less favorable interactions between hydrocarbons and fluorocarbons than between hydrocarbons themselves. The study shows that fluorocarbon-hydrocarbon interactions

have a greater effect on transport properties in the rubbery polymer (PDMS) than in the high-free-volume, glassy polymer (PTMSP).

The above study led to an investigation of the effect of hydrocarbon-fluorocarbon interactions on the sorption and permeation of hydrocarbons in a rubbery fluoropolymer, and the results are presented in Chapter 4. The study reveals much lower hydrocarbon sorption in the rubbery fluoropolymer than expected on the basis of empirical correlations. The study also shows that hydrocarbon-fluorocarbon interactions play a major role in determining hydrocarbon transport properties in this fluoropolymer.

Since most polymers derive their CO_2/CH_4 selectivity in large part from their strong size-sieving abilities, a detailed study of gas sorption, pure gas permeation and mixed-gas permeation of permanent gases and hydrocarbon penetrants was undertaken in a commercial, low free volume, glassy fluoropolymer, called Hyflon AD 80. In Chapter 5, the CO_2/CH_4 separation performance of this polymer is compared with currently-used membrane polymers both under pure and mixed gas conditions. Hyflon AD 80 shows excellent stability in separation performance in the presence of plasticizing penetrants.

Chapter 6 presents a theoretical analysis of the strategy of using fluoropolymers as coatings on existing hydrocarbon membranes to minimize plasticization of the underlying hydrocarbon membranes. Materials selection guidelines are developed to aid in selection of the appropriate coating. The benefits and limitations of this strategy are illustrated by using model cases.

Transport of condensable penetrants such as large hydrocarbons through polymers often depends on gas concentration in the polymer, and hence on the operating conditions (*i.e.*, temperature, feed pressure, permeate pressure, *etc.*) of the membrane separation

process. Often, permeability data are not available over the complete range of conditions of interest in considering design alternatives. Therefore, it becomes necessary to estimate permeation properties based on extrapolation from known experimental data. Chapter 7 presents results of an effort to develop a rational framework to guide the estimation of permeability at conditions away from those where experimental data are available, when permeability is dependent on the operating conditions.

Chapter 8 presents an overview of the investigations reported in literature to understand the interactions between hydrocarbon and fluorocarbon species. Chapter 9 presents the conclusions of this research project and outlines possibilities for future work in this area.

A list of critical volumes and critical temperatures of the penetrants mentioned in this dissertation is provided in the Appendix at the end of this dissertation.

Table 1.1 Composition of non-associated natural gas found in Lacq, France [3].

Component	***Composition (% v/v)***
Methane	69.1
Ethane	2.8
Propane	0.8
Butanes	1.5
C_{5+}	0.6
Hydrogen sulfide	15.4
Carbon dioxide	9.7
Nitrogen	-
Helium	-
Argon	-

Table 1.2 Composition of natural gas required for delivery to the U.S. national pipeline grid [4].

Component	***Specification***
CO_2	< 2%
H_2O	< 120 ppm
H_2S	< 4 ppm
C_{3+} content	950-1050 BTU/scf Dew point: -20 ^oC
Total inert gases	< 4%

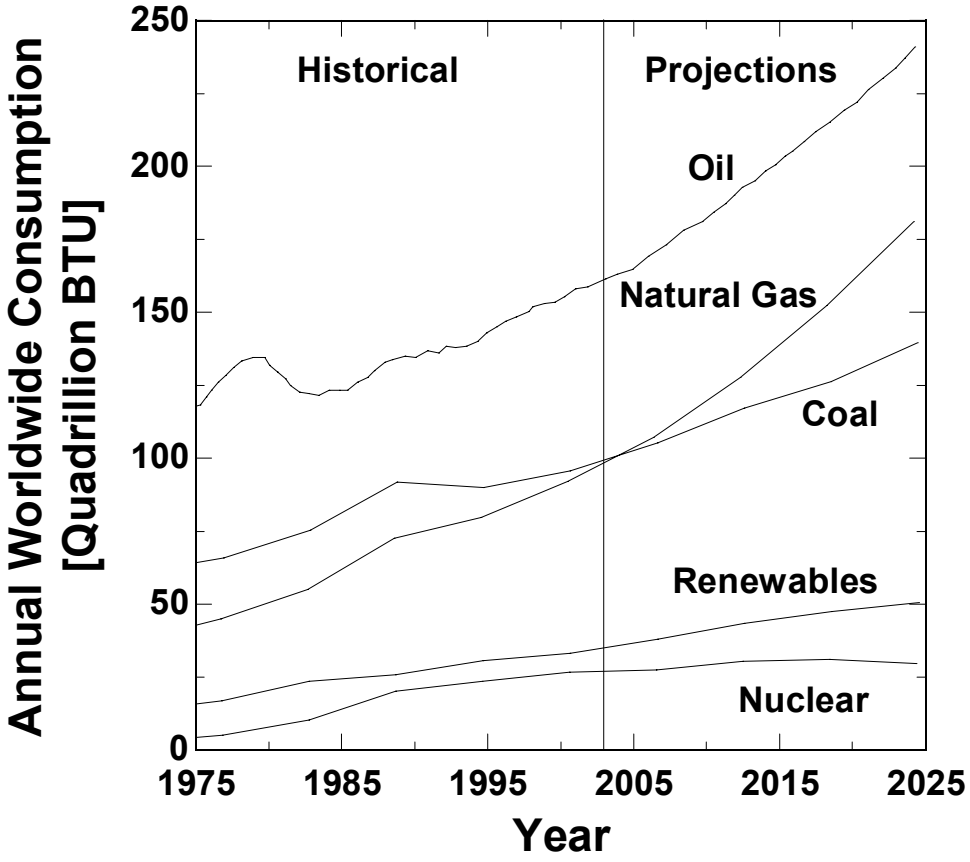

Figure 1.1: Historical and projected world energy consumption by fuel type [2].

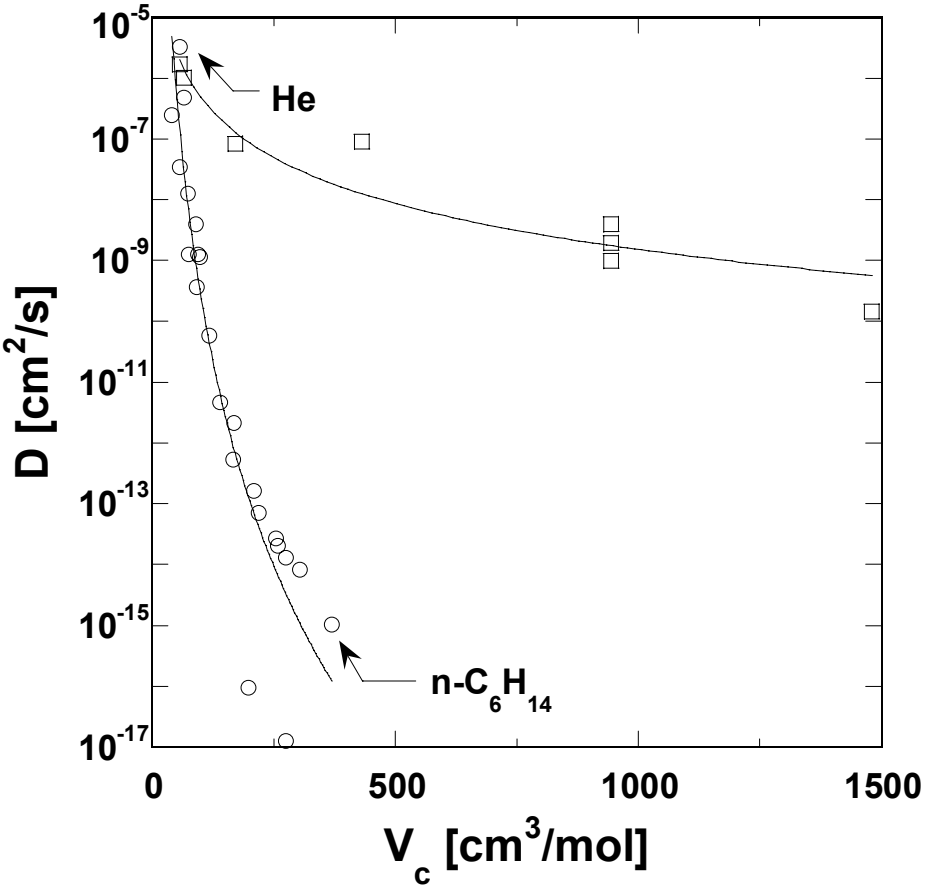

Figure 1.2: Diffusion coefficients in poly(vinyl chloride) in the unplasticized (○) and plasticized (□) state [13,14].

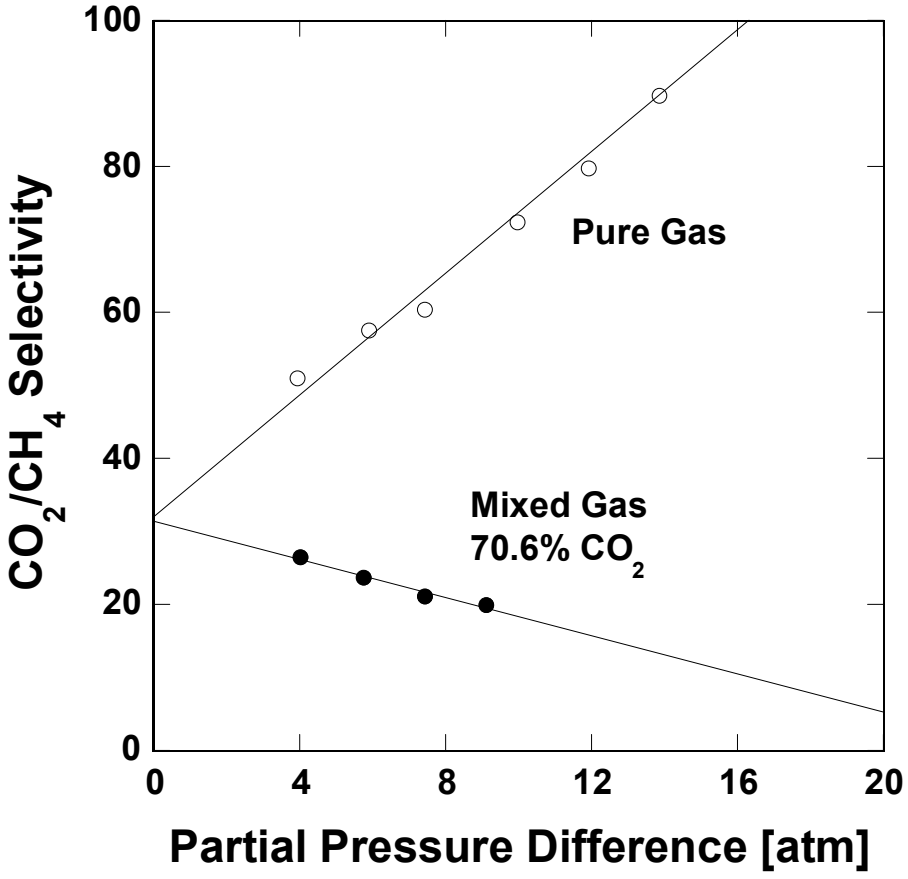

Figure 1.3: Pure and mixed-gas CO_2/CH_4 selectivity in cellulose acetate [15].

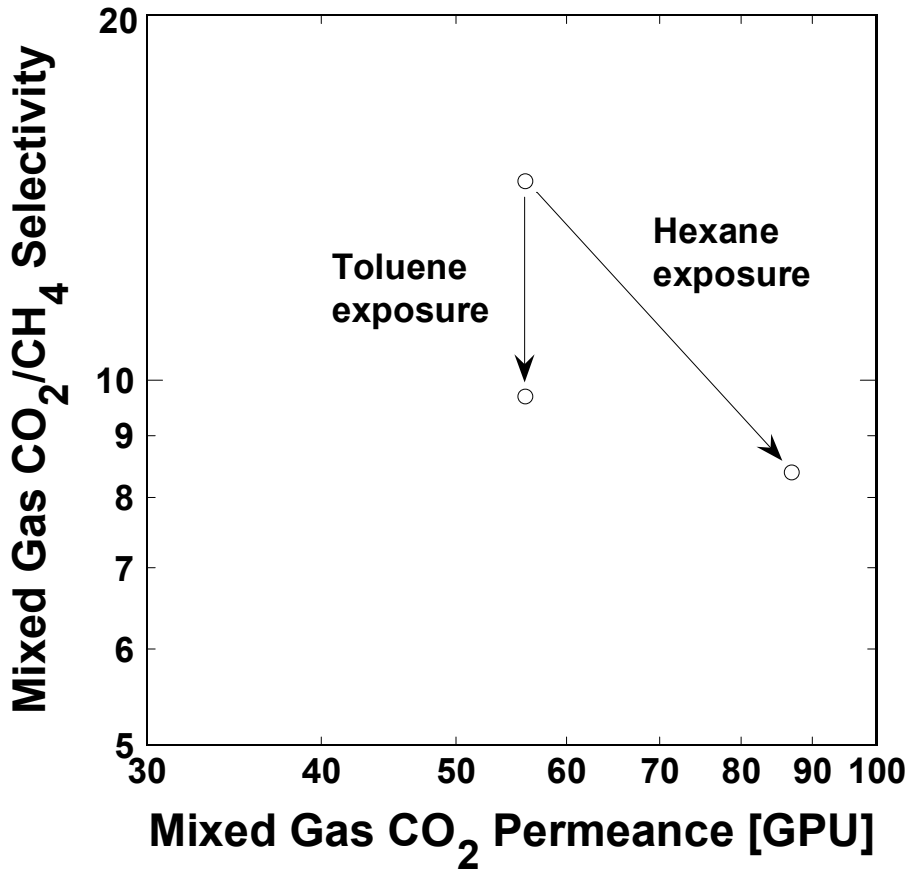

Figure 1.4: Mixed gas CO_2 permeance (permeability per unit membrane thickness) and CO_2/CH_4 selectivity of a polyimide membrane (6FDA-DMB) [16]. The feed gas was 10 mol % CO_2 and 90 mol % CH_4, and the experiments were performed at 48 ^oC using a feed pressure of 1000 psi. To obtain the results for membranes exposed to hydrocarbons, the CO_2/CH_4 feed stream was saturated with 0.055 vol. % toluene or 0.23 vol. % *n*-hexane [16]. 1 GPU = 1×10^{-6} $cm^3(STP)/(cm^2 \cdot s \cdot cmHg)$.

CHAPTER 2

Background and Approach

2.1 THEORY

2.1.1 Gas Permeability

Small molecule transport in polymer membranes is widely modeled using the solution-diffusion mechanism and is expressed by a permeability coefficient, P, defined as follows:

$$P = \frac{N\,l}{p_2 - p_1} \tag{2.1}$$

where N is the steady-state gas flux through a polymer membrane of thickness l due to a partial pressure difference (p_2-p_1) across the film, p_2 is the feed (upstream) pressure and p_1 is the permeate (downstream) pressure. In the simplest case, penetrant diffusion is modeled using Fick's law of diffusion [23]:

$$N = -\frac{D_{loc}}{(1-\omega)}\left(\frac{dC}{dx}\right) \tag{2.2}$$

where D_{loc} is the local diffusion coefficient, C is penetrant concentration and ω is penetrant mass fraction in the polymer. Combining eqs 2.1 and 2.2 and integrating across the film thickness yields:

$$P = \frac{1}{p_2 - p_1} \int_{C_1}^{C_2} D\, dC \tag{2.3}$$

where C_2 and C_1 are penetrant concentrations at the upstream and downstream faces of the polymer membrane, respectively, at a given temperature and D is the local, effective diffusion coefficient in the polymer, defined for convenience as follows:

$$D \equiv \frac{D_{loc}}{1 - \omega} \tag{2.4}$$

If the diffusion coefficient is not a function of concentration,

$$P = \frac{C_2 - C_1}{p_2 - p_1} D \tag{2.5}$$

In the limit of negligible permeate pressure, this equation gives the result,

$$P = S \times D \tag{2.6}$$

where, the solubility coefficients, S, is defined as follows:

$$S = \frac{C}{p} \tag{2.7}$$

In eq 2.6, S should be evaluated at the upstream conditions. Eq 2.6 is also obtained from eq 2.5 if penetrant sorption obeys Henry's law (see eq 2.10 in section 2.1.3) [11]. Eq 2.6 is widely used to rationalize gas transport properties in polymer membranes.

2.1.2 Selectivity

The ideal selectivity, $\alpha_{A/B}$, of component A over B is a measure of the potential separation ability of the membrane material. The ideal selectivity can be written as the ratio of the pure gas permeabilities [11]:

$$\alpha_{A/B} \equiv \frac{P_A}{P_B} \tag{2.8}$$

From eqs 2.6 and 2.8,

$$\alpha_{A/B} = \left(\frac{S_A}{S_B}\right) \times \left(\frac{D_A}{D_B}\right) \tag{2.9}$$

where the first term on the right hand side of eq 2.9 is the solubility selectivity and the second is the diffusivity selectivity. In addition to operating conditions (*i.e.*, temperature, pressure and gas composition), penetrant solubility depends on condensability and polymer-penetrant interactions [11]. In the absence of specific interactions (*e.g.*, hydrogen bonding), the first effect is dominant, and solubility increases as penetrant condensability, characterized by critical temperature, normal boiling point or Lennard-

Jones force constant, increases [11]. Thus, solubility selectivity increases as the difference in condensability between two penetrants in a mixture increases. Often, larger penetrants are more condensable and, therefore, more soluble than smaller penetrants. The diffusion coefficient decreases as penetrant size increases and, therefore, diffusivity selectivity increases as the relative size difference between two penetrants increases, with the smaller penetrant having higher diffusivity [11]. Thus, a tradeoff often exists between solubility selectivity and diffusivity selectivity, with the overall selectivity depending on the relative magnitudes of these two terms.

2.1.3 Solubility

The sorption of sparingly soluble gases in rubbery polymers is qualitatively similar to the sorption of gases in low molecular weight liquids, and gas concentration in the polymer, C, often obeys Henry's law [11]:

$$C = k_D p \tag{2.10}$$

where k_D is the Henry's law constant and p is the gas pressure in contact with the polymer. The uptake of more soluble vapors in uncrosslinked rubbery polymers is frequently described using the Flory-Huggins expression [24]:

$$\ln a = \ln \phi_2 + (1-\phi_2) + \chi(1-\phi_2)^2 \tag{2.11}$$

where a is penetrant activity in the vapor phase, ϕ_2 is the volume fraction of sorbed penetrant and χ is the Flory-Huggins interaction parameter. For crosslinked rubbery polymers, a modified form of the above equation, called the Flory-Rehner expression is often used [24]:

$$\ln a = \ln \phi_2 + (1-\phi_2) + \chi(1-\phi_2)^2 + V_2\left(\frac{\upsilon_e}{V_o}\right)\times\left[(1-\phi_2)^{1/3} - \left(\frac{1-\phi_2}{2}\right)\right] \qquad (2.12)$$

where V_2 is the penetrant molar volume and ν_e/V_o is the effective number of crosslinks per unit volume of penetrant-free polymer (expressed in moles of crosslinks per unit volume of penetrant-free polymer). Throughout this study, penetrant activity in the above two equations is set equal to the relative pressure, p/p_{sat}, where p_{sat} is the saturation vapor pressure of the penetrant. The volume fraction of sorbed penetrant, ϕ_2, is calculated from the equilibrium penetrant concentration in the polymer, C, as follows:

$$\phi_2 = \left[1 + \frac{22,414}{C\bar{V}_2}\right]^{-1} \qquad (2.13)$$

where $\bar{V}_2$ is the penetrant partial molar volume and is estimated as described by Merkel *et al.* [25]. In this equation, C and $\bar{V}_2$ have units of cm^3(STP)/cm^3polymer and cm^3/mol, respectively. 22,414 is a conversion factor (cm^3(STP)/mol).

Sorption isotherms for gases in glassy polymers are usually concave to the pressure axis at low pressures and linear at higher pressures [11]. Such isotherms are often described using the dual mode sorption model [26]. In this model, penetrant molecules are viewed as being partitioned into two populations which are in dynamic equilibrium with each other: (i) penetrant molecules sorbed by a dissolution mechanism in the dense polymer matrix (Henry's law population), and (ii) penetrant molecules filling unrelaxed, molecular-scale gaps (microvoids) frozen into the glassy state (Langmuir population) [26]. The dual mode model is expressed analytically as a sum of these two contributions to penetrant sorption:

$$C = k_D p + \frac{C_H' b p}{1 + b p} \tag{2.14}$$

where C is the total concentration of penetrant in the polymer, C_H' is the hole saturation constant or Langmuir sorption capacity parameter, and b is the Langmuir affinity parameter.

2.1.4 Diffusivity

The local effective diffusion coefficient, D, defined in eq 2.4, can be estimated from the slope of the sorption isotherm and the pressure dependence of permeability as follows [27]:

$$D(C_2) = \left[P + \Delta p \frac{dP}{d\Delta p} \right]_{p_2} \left(\frac{dp}{dC} \right)_{p_2} \tag{2.15}$$

2.1.5 Temperature Dependence of Transport Coefficients

The temperature dependence of permeability, diffusivity and solubility at temperatures far removed from polymer thermal transitions are described as follows [11]:

$$P = P_o \exp\left(-\frac{E_P}{RT} \right) \tag{2.16}$$

$$D = D_o \exp\left(-\frac{E_D}{RT} \right) \tag{2.17}$$

$$S = S_o \exp\left(-\frac{\Delta H_S}{RT} \right) \tag{2.18}$$

where P_o, D_o and S_o are pre-exponential constants, E_P is the activation energy of permeation, E_D is the activation energy of diffusion, and ΔH_S is the enthalpy of sorption. Because permeability is the product of solubility and diffusivity (eq 2.6), the activation energies of permeation and diffusion and the enthalpy of sorption are related:

$$E_P = E_D + \Delta H_S \tag{2.19}$$

The above equation is a consequence of eqs 2.6 and 2.16-2.18, and is, therefore, subject to the assumptions inherent in these equations. For example, eq 2.19 does not hold if the downstream pressure cannot be neglected in comparison to the upstream pressure (or if Henry's law is not applicable) due to the assumptions underlying eq 2.6. Also, if penetrant transport properties (*i.e.*, P, D and S) are functions of concentration, eq 2.19 is expected to be a simplified form of a more general model which is presented in Chapter 7. Nevertheless, eqs 2.16-2.19 are the standard model for describing the temperature dependence of gas solubility, diffusivity, and permeability in polymers.

2.2 EXPERIMENTAL TECHNIQUES

The following experimental techniques were employed in this study to determine the transport coefficients of gases and vapors in polymer membranes.

2.2.1 Sorption Measurements

Penetrant sorption in polymers was determined using a high-pressure barometric apparatus [28]. This apparatus consists of two stainless steel chambers of known volume, called the 'charge cell' and the 'sample cell'. The chambers are connected to each other by a stainless steel valve. The gas pressure in each chamber is monitored using sensitive pressure transducers and recorded automatically by a data acquisition system employing LabTech software. A water bath is used to maintain the apparatus at a constant temperature (within ± 0.1 °C). A vacuum pump is connected to this apparatus to degas the chambers, whenever required. The experimental procedure is outlined below.

Initially, a polymer film is placed in the sample cell and exposed to vacuum to remove sorbed gases from the polymer. Gas is introduced into the charge cell until a fixed target pressure is reached. The number of moles of the gas in the charge cell can be calculated from the chamber pressure, water bath temperature and known chamber volume. The valve connecting the two chambers is then opened briefly to allow gas to flow into the sample cell. After closing the valve, the system is allowed to return to equilibrium. Once the pressures in both chambers are constant, the moles of gas in the gas phase in both chambers can be calculated based on known chamber volumes, known polymer volume, water bath temperature and gas pressures in the two chambers. The difference between initial and final moles of gas in the charge cell is the moles of gas introduced into the sample cell. The difference between this amount of gas and the final moles of gas in the gas phase of the sample cell is the amount of gas sorbed into the polymer at the pressure in the sample cell. Additional penetrant is then introduced into the sample cell and the procedure is repeated. In this incremental manner, penetrant uptake is determined as a function of pressure.

2.2.2 Pure-gas Permeability Measurements

The experimental technique employed to measure pure gas permeability coefficients in polymers was selected based on the flowrate of gas through the polymer membrane at the operating conditions of interest.

When the flowrate of the gas permeating the polymer was greater than about 1 cm^3/min, the permeability coefficient was determined using a constant

pressure/variable volume apparatus [29]. The apparatus consists of a Millipore filter holder (called a permeation cell, henceforth) with a membrane area of 13.8 cm^2. Gas is fed to the upstream side of the cell at fixed pressure. The downstream pressure is atmospheric. The system temperature is controlled to ± 0.5 °C using a DYNA-SENSE temperature control system. Prior to each experiment, the upstream and downstream sides of the permeation cell are purged with penetrant gas. During the experiment, the gas is fed to the upstream side with the vent line closed, thus forcing the gas to permeate through the polymer. The flowrate of the gas permeating through the polymer is measured by a bubble flowmeter. When pseudo-steady-state conditions are attained, the following expression is used to evaluate permeability, P (cm^3(STP)·cm/(cm^2·s·cm Hg)):

$$P = \frac{22414}{A} \frac{l}{p_2 - p_1} \frac{p_1}{RT} \frac{dV}{dt} \tag{2.20}$$

where A is the membrane area (cm^2), l is the membrane thickness (cm), p_2 is the upstream pressure (atm), p_1 is the downstream pressure (atmospheric pressure in this case), R is the universal gas constant (6236.56 cm^3·cm Hg/(mol·K)), T is the absolute temperature (K) and dV/dt is the volumetric displacement rate of the soap film in the bubble flowmeter (cm^3/s).

For conditions of low flowrates of permeating gases, pure gas permeability coefficients were measured in a constant volume/variable pressure apparatus [30]. This apparatus differs from the constant pressure/variable volume system described above only in the measurement of the amount of gas permeating the membrane. In this

apparatus, the gas permeating the membrane is collected in a chamber of known volume, maintained at a constant temperature (± 0.5 °C) using an Omega CN76000 temperature controller. The increase in pressure in the downstream chamber is measured by a sensitive pressure transducer and recorded using a data acquisition system employing LabTech software, as a function of experimental time. The pressure is allowed to increase only up to a maximum of 10 mm Hg to maintain the condition of negligible downstream pressure as compared to the upstream pressure. Prior to each experiment, the upstream and downstream sides of the permeation cell are evacuated to below 0.5 mm Hg. During the experiment, when the rate of pressure increase in the downstream volume, *dp/dt* (cm Hg/s), attains its pseudo-steady-state value, the following expression is used to calculate the permeability, *P* (cm^3(STP)·cm/(cm^2·s·cm Hg)):

$$P = \frac{22414}{A}\frac{l}{p_{abs}}\frac{V}{RT}\frac{dp}{dt} \tag{2.21}$$

where p_{abs} is the upstream pressure (cm Hg), and *V* is the downstream volume (cm^3).

2.2.3 Mixed-gas Permeability Measurements

Mixed-gas permeabilities were measured at MEDAL L. P., using a constant volume/variable pressure permeation apparatus similar to the one described by O'Brien *et al.* [31]. The apparatus consists of a permeation cell, similar to the one used for pure-gas permeation, with ports for a feed stream and a retentate stream on the upstream side of

the sample film and for a permeate stream on the downstream side of the film. Feed gas is made to flow across the upstream side of the membrane at a rate that is high enough to maintain the maximum stage cut (ratio of permeate to feed flowrate) below 1%. The permeate gas is collected in a chamber of known volume. The increase in pressure on the downstream side of the film is recorded using a data acquisition system employing Labview software. When the rate of pressure increase on the downstream side attains its pseudo-steady-state value, the permeability of each gas is calculated using the expression:

$$P_A = \frac{22414}{A} \frac{l}{x_A p_{abs}} \frac{V}{RT} y_A \frac{dp}{dt} \tag{2.22}$$

where P_A is the permeability of gas A (cm^3(STP)·cm/(cm^2·s·cm Hg)), x_A and y_A are the mole fractions of A in the feed and permeate streams, respectively, p_{abs} is the total upstream pressure (cm Hg) and dp/dt is the steady rate of total pressure increase with time in the downstream volume (cm Hg/s). The compositions of the feed and permeate streams are measured by a HP 5890 Gas Chromatograph with a thermal conductivity detector and high-purity He as carrier gas. The mixed-gas selectivity is the ratio of the two gas permeabilities calculated using eq 2.22.

2.3 APPROACH

In the previous chapter, examples have been provided of polymer membranes undergoing plasticization when exposed to CO_2 and large hydrocarbons like toluene and

n-hexane, due to high solubilities of these penetrants in the polymers. Natural gas typically contains numerous hydrocarbon compounds. Therefore, to determine the susceptibility of polymers to undergo plasticization in natural gas environments, it is important to estimate the solubility of natural gas components in the polymers being considered as membrane materials.

2.3.1 Hydrocarbons in Natural Gas and their Solubility in Hydrocarbon Polymers

The higher hydrocarbon content of natural gas is usually reported as a single cumulative value which includes all hydrocarbon compounds with 5 or more carbon atoms (*cf.* Table 1.1). This provides little knowledge of the size range of compounds present in the gas. However, detailed analysis of this heavy fraction of natural gas has revealed that it contains a host of large hydrocarbon compounds having as many as 15 or more carbon atoms per molecule [32]. Table 2.1 displays results of such an analysis of natural gas from a field in the Gulf of Thailand.

Reports of experimentally determined solubilities of large hydrocarbons in polymers, especially the strongly size-sieving ones considered for natural gas separations, are extremely rare due to the long times needed to measure solubility or diffusivity of large penetrants in such polymers [33,34]. However, in the absence of specific interactions between gas molecules and polymer chains, the logarithm of gas solubility in a polymer often increases linearly with measures of gas condensability like critical temperature, T_c, normal boiling point, T_b, or Lennard-Jones force constant (ε/k) [35-37]. The critical temperature, normal boiling point and the Lennard-Jones force constant,

however, are interrelated so that correlations of gas solubility with these properties are considered equivalent [38]. Figure 2.1 shows an example of gas solubility in low-density poly(ethylene) (LDPE) as a function of gas critical temperature. From the figure, a linear trendline describes the relationship between ln$S$ and T_c satisfactorily:

$$\ln S = a + b \times T_c \tag{2.23}$$

where a and b are adjustable constants. b, the slope of the above trendline, characterizes the increase in penetrant solubility in the polymer with increasing penetrant critical temperature. From the experimental data, *n*-pentane (T_c = 469.7 K) has a solubility of 24.9 cm^3(STP)/(cm^3·atm) in this polymer. If the heavy hydrocarbon fraction of natural gas consisted of hydrocarbons in this range of sizes and, therefore, condensabilities, they would have similar solubilities in this polymer. However, if the trendline in the figure is extrapolated to, for example, *n*-decane (T_c = 617.7 K), its estimated solubility would be more than an order of magnitude higher than that of *n*-pentane and three orders of magnitude higher than that of methane. Thus, large hydrocarbons can have very high solubilities in hydrocarbon polymers like LDPE, and as a result, can sorb into the polymer in appreciable amounts, even if they are present in low quantities in the gas stream.

The slope of the trendline, b, in Figure 2.1 is 0.019 K^{-1}. This is similar to the slope values for a wide range of hydrocarbon polymers (Table 2.2 provides a few examples). Interestingly, such an observation has been made in the study of gas solubility in liquids also. On the basis of solubility data of over 15 gases (including permanent gases, noble

gases, hydrocarbons and others like H_2S, SO_2 and NH_3) in 15 different organic liquids (with solubilities varying over 3 orders of magnitude), Korosy found that "the logarithm of solubility is nearly a linear function of the critical temperature of the gas and that the slope of these straight lines is about the same for all solvents" [39]. Since this linear relationship was seen to be valid for gases as different as helium and sulfur dioxide, Korosy concluded that "gas solubility is governed to a first approximation by 'physical' forces, while 'chemical affinity' only modifies their action to a small extent and probably causes the deviation of certain points from the straight lines" [39].

Gee has provided a theoretical framework to the observed correlation between gas solubility and gas condensability by considering gas solubility to be a hypothetical two-step process involving condensation of the gas to a liquid-like density followed by dilution of the gas in the polymer (*i.e.* mixing of gas molecules and polymer chains) [35]. His correlation in terms of the gas boiling point, modified using the Guldberg-Guye rule [36] relating boiling and critical temperatures, (*i.e.*, $T_b = 0.6 \times T_c$), is

$$\ln S = -(4.5 + \chi) + \left(\frac{0.6 \Delta S_{vap}}{RT} \right) T_c \tag{2.24}$$

where χ is the Flory-Huggins interaction parameter, ΔS_{vap} is the entropy of vaporization of the penetrant gas at the normal boiling point and has a value of 20 cal/(mol·K) according to Trouton's rule [35,40], R is the universal gas constant (1.987 cal/(mol·K)) and T is the absolute temperature. In eq 2.24, S has units of cm^3(STP)/(cm^3·atm).

Comparing eqs 2.23 and 2.24 provides a simple relation for the slope b when ln$S$ is described as a linear function of T_c,

$$b \cong \frac{6}{T} \tag{2.25}$$

This relation predicts a b slope value of 0.019 K^{-1} at 35 ^{o}C, as observed experimentally (*cf.* Figure 2.1 and Table 2.2).

Since the slope values are similar in a variety of hydrocarbon polymers (Table 2.2), the extent of higher hydrocarbon sorption relative to, for example, CO_2 or CH_4 is likely to be similar in these polymers. Thus, hydrocarbon polymers, in general, are likely to be susceptible to the plasticizing effects of higher hydrocarbons and, therefore, may not be promising membrane materials for removing CO_2 from natural gas.

2.3.2 Analysis of Fluorocarbon Solubility in Hydrocarbon Polymers

Studies of gas sorption in polymers have observed that fluorinated gases exhibit unexpectedly low solubility in hydrocarbon polymers. For example, in 1961, Michaels and Bixler reported that the solubility of sulfur hexafluoride in natural rubber and LDPE (amorphous basis) was much lower than expected based on the correlation between solubility and Lennard-Jones force constant [41]. Kamiya *et al.* have also made a similar observation for SF_6 solubility in PDMS [38]. Recently, it has been reported that perfluorinated gases like CF_4, C_2F_6 and C_3F_8 exhibit much lower solubility in hydrocarbon polymers like PDMS [38,42] and LDPE [38] than expected based on the

linear relationship between the logarithm of gas solubility and gas critical temperature (*cf.* Figure 2.2). This low solubility of perfluorocarbon gases in hydrocarbon polymers has been attributed to unfavorable interactions between the perfluorocarbon penetrants and the hydrocarbon matrix.

To understand the influence of interactions on the solubility behavior of perfluorinated gases in hydrocarbon polymers, it is instructive to analyze the data in Figure 2.2 by using the Flory-Huggins equation, which is often used to model gas sorption in uncrosslinked rubbery polymers. In the limit of infinite dilution, the Flory-Huggins equation (eq 2.11) can be reformulated as follows:*

$$S^{\infty} p_{sat} = \frac{22414}{\bar{V}_2 \exp(1+\chi)} \tag{2.26}$$

where S^{∞} in the gas solubility in the limit of infinite dilution (cm^3(STP)/(cm^3·atm)), p_{sat} is the penetrant vapor pressure (atm), $\bar{V}_2$ is the partial molar volume of the penetrant (cm^3/mol) and χ is the Flory-Huggins interaction parameter. 22,414 is a conversion factor (cm^3(STP)/mol). The term $S^{\infty}p_{sat}$ can be thought of as a condensability-normalized solubility within the scope of eq 2.26 and depends on the penetrant size ($\bar{V}_2$) and polymer-penetrant interactions (χ). Wong *et al.* pointed out that partial molar volumes often correlate linearly with gas critical volumes [43]. Therefore, a plot of condensability-normalized solubility as a function of penetrant critical volume should, to a first

approximation, decouple the effects of penetrant size and interactions on solubility. Such a plot of hydrocarbon and fluorocarbon penetrant solubility in PDMS is shown in Figure 2.3 [42].

From the figure, the condensability-normalized solubilities of both fluorocarbons and hydrocarbons decrease with increasing penetrant size, consistent with more energy of mixing required to open larger gaps in the polymer matrix to accommodate larger penetrants. However, at the same penetrant size, the $S^{\infty}p_{sat}$ values for fluorocarbons are significantly lower than those of the hydrocarbons, indicating that insertion of a fluorocarbon in a hydrocarbon matrix requires significantly more energy than insertion of a hydrocarbon molecule of similar size and condensability.

Direct calculations of the χ parameter using the Flory-Rehner equation for crosslinked polymers have shown that perfluorocarbons exhibit higher χ parameters than their hydrocarbon analogs in PDMS, thus indicating less favorable interactions between perfluorocarbons and PDMS [25]. Based on sorption results and conventional lattice fluid theory with a coordination number of 10, the separation of a single C_3H_8/PDMS segment pair requires 460 J/mol more energy than the separation of a C_3F_8/PDMS pair [25].

Low solubility of fluorocarbon gases has also been noted in hydrocarbon liquids. Hildebrand *et al.* reported the solubility of several permanent gases, hydrocarbon and fluorocarbon gases in cyclohexane at 25 ^{o}C [44]. Plotting sorbed gas mole fraction *vs.* the molal energy of vaporization (as a measure of penetrant condensability), Hildebrand observed that hydrocarbon and fluorocarbon gas solubilities followed different linear

---

* The Flory-Rehner equation (eq 2.12) used to describe sorption in crosslinked rubbery polymers like PDMS also gives a similar expression in the limit of infinite dilution.

trendlines with the hydrocarbon gas solubility being greater than the fluorocarbon solubility at the same condensability. Hildebrand attributed these results to differences in interaction energies of the hydrocarbon and fluorocarbon gases with the hydrocarbon liquid [44].

Further evidence of unfavorable hydrocarbon-fluorocarbon interactions in gas-liquid systems was obtained by Wilhelm and Battino [45] who reported solubility of CH_4 and its perfluorinated analog, CF_4, in benzene and hexafluorobenzene at 25 ^oC and 1 atm. The results are reproduced in Table 2.3. The table shows that CF_4 is more soluble than CH_4 in hexafluorobenzene. However, in the hydrocarbon solvent, benzene, CH_4 is significantly more soluble than CF_4, even though CF_4 has a higher critical temperature (the T_c of CF_4 is 227.6 K, as compared to 191.05 K for CH_4 [46]). Thus, hydrocarbon-fluorocarbon interactions suppress the solubility of the fluorinated gas in the hydrocarbon solvent to a markedly lower value than that of its lower-condensability hydrocarbon analog.

Interestingly, the effect of fluorocarbon-hydrocarbon interactions on the solution behavior (gas-polymer and liquid-liquid) of mixtures of these compounds is not adequately described by current theories, even though these theories provide a good description of hydrocarbon solutions and fluorocarbon solutions. For example, the regular solution theory, which is often used to describe solution behavior of non-polar non-electrolytes, is unable to predict the sizeable two phase liquid-liquid regions exhibited by the systems, C_7H_{16}-C_7F_{16}, C_5H_{12}-C_5F_{12} and C_4H_{10}-C_4F_{10} [47]. The failure of the geometric mean approximation, which is employed to enable prediction of mixture solution behavior from pure component properties, is the likely reason for the breakdown

of the theory [47]. Description of fluorocarbon gas solubility in the hydrocarbon-based polymer, PDMS, by the Sanchez-Lacombe model also requires an empirical adjustment to the geometric mean approximation that is used to describe unlike molecular interactions [48]. The theoretical treatment of fluorocarbon-hydrocarbon interactions is described in greater detail in Chapter 8.

2.3.3 Hydrocarbon Solubility in Perfluorinated Polymers

Since low fluorocarbon solubility in hydrocarbon polymers is ascribed to unfavorable interactions between hydrocarbon and fluorocarbon species, it is reasonable to expect the interaction to play a role in the sorption of hydrocarbons in fluorinated polymers and cause a reduction in hydrocarbon solubility in these polymers. Thus, perfluorinated polymers, which are completely fluorinated analogs of hydrocarbon polymers (called fluoropolymers, henceforth), should have low solubility for hydrocarbons and, therefore, be less likely to undergo plasticization due to hydrocarbons.

Hydrocarbon sorption in fluoropolymers has been studied. Merkel *et al.* report results of sorption of C1-C3 hydrocarbon and fluorocarbon gases in AF1600 and AF2400, which are glassy copolymers of tetrafluoroethylene (TFE) and 2,2-bistrifluoromethyl-4,5-difluoro-1,3-dioxole (BDD) containing 65% and 87% BDD, respectively [42]. In both fluoropolymers, the fluorinated penetrants are more soluble than their hydrocarbon analogs. However, unlike the case of PDMS, plots of condensability-normalized Henry's law coefficients *vs.* penetrant critical volume revealed no significant difference between the condensability-normalized solubilities of

fluorocarbon and hydrocarbon penetrants in AF2400, while only a small variation was seen in the case of AF1600. While these results in themselves are not very promising, these polymers have extremely high free volumes. AF1600 has a fractional free volume (FFV) of 0.30 while the FFV of AF2400 is 0.33 [42], as determined using Bondi's group contribution method [49]. These values are much higher than the FFV of conventional glassy polymers, which usually varies between 5 and 15% [50]. The large free volume of these polymers may provide easily accessible sorption sites for relatively nonspecific gas sorption. The small decrease in hydrocarbon sorption relative to fluorocarbon sorption in AF1600 is consistent with its FFV being lower than that of AF2400. The FFV of PDMS, determined using Bondi's group contribution method, is nearly half that of AF1600 [42] and is the likely reason for the larger contribution of the interaction effect on the overall sorption in that matrix (*cf.* Figure 2.3). Thus, it is possible that lower free volume fluoropolymers may exhibit a greater reduction in hydrocarbon solubility as compared to the solubility of the corresponding fluorocarbon analogs.

The approach taken in this fundamental study was to further investigate the interactions between hydrocarbons and fluorocarbons and their effect on gas transport in polymers. The objective was to assess the potential of low-hydrocarbon-solubility polymers as plasticization-resistant membranes for use in hydrocarbon-rich environments.

Table 2.1 Composition of a natural gas stream processed for CO_2 removal. The gas stream is a blend from 15 wells in the Pailin field in the Gulf of Thailand [32].

Compound	***Composition (mol %)***
CO_2	32.79
N_2	2.89
C_1	48.46
C_2	8.22
C_3	4.45
iC_4	1.22
nC_4	1.04
iC_5	0.40
nC_5	0.23
C_6 + benzene	0.18
C_7 + toluene	0.095
C_8 + xylenes	0.012
C_9	0.002
C_{10}	0.001
C_{11}	0.0009
C_{12}	0.0011
C_{13}	0.0001
C_{14}	0.0001
C_{15+}	0.0002

NOTE: "C_m" refers to hydrocarbon compounds containing "m" carbon atoms per molecule. The letters 'i' or 'n' preceding "C_m" refer to 'iso' and 'normal', respectively. Benzene, toluene and xylenes are grouped with other compounds having the same number of carbon atoms.

Table 2.2 Slope values for the correlation of gas solubility with critical temperature in rubbery and glassy polymers.

Classification	***Medium***	$b \times 10^3$ (K^{-1})
Rubbers	Natural rubber [41]	18 [a]
	Amorphous poly(ethylene) [41]	16 [a]
	Poly(butadiene) - hydrogenated [41]	17 [a]
	Poly(dimethylsiloxane) [38]	17 [b]
Glasses	Polysulfone [51]	17 [c]
	Poly(phenylene oxide) [52]	16 [d]
	Poly(ethylene terephthalate) [53]	19 [e]

[a] 25 ^{o}C and 1 atm

[b] 35 ^{o}C

[c] 35 ^{o}C and 10 atm for all gases except *n*-C_4H_{10}, which is at infinite dilution

[d] 35 ^{o}C and infinite dilution

[e] 24-45 ^{o}C and infinite dilution

Table 2.3 Solubility of CH_4 and CF_4 in liquid benzene and hexafluorobenzene at 25 ^oC and 1 atm [45].

Gas	***Solubility × 10^4 (mole fraction)***	
	C_6H_6	***C_6F_6***
CH_4	20.9	38.42
CF_4	5.75	45.61
CH_4/CF_4	3.6	0.84

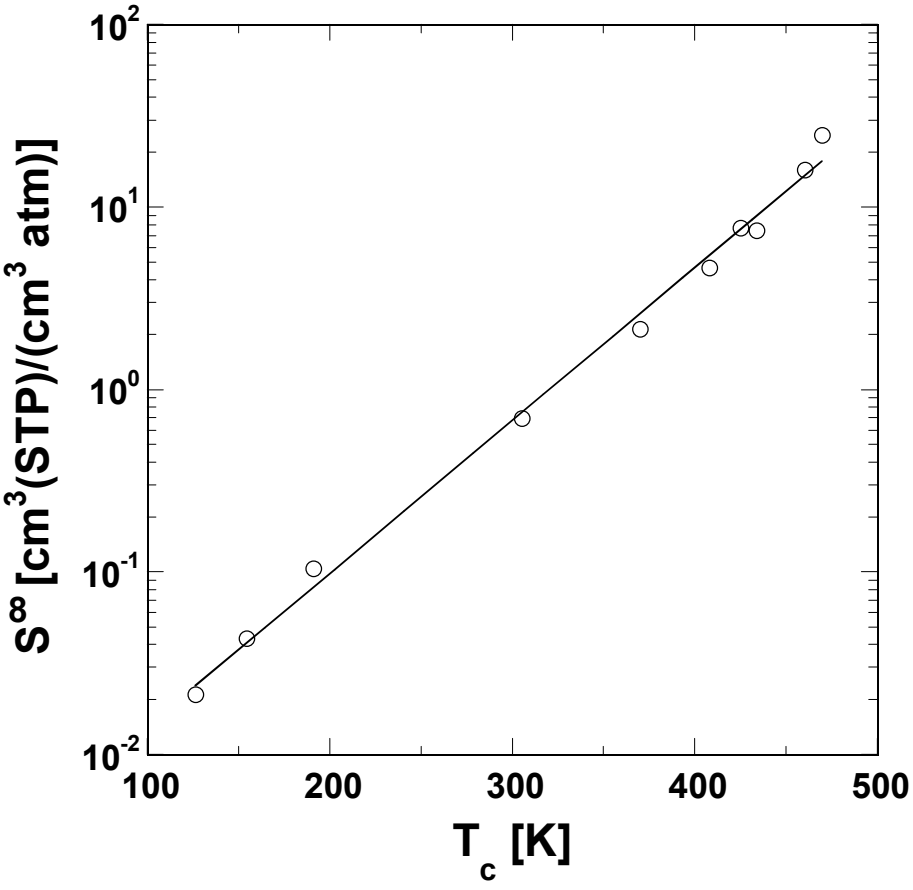

Figure 2.1: Infinite dilution solubility coefficients for permanent gases and hydrocarbons in low density poly(ethylene) [38]. The best fit line through the data is: $\ln(S^\infty\ [\text{cm}^3(\text{STP})/(\text{cm}^3\ \text{atm})]) = -6.17 + 0.019\ T_c\ [\text{K}]$.

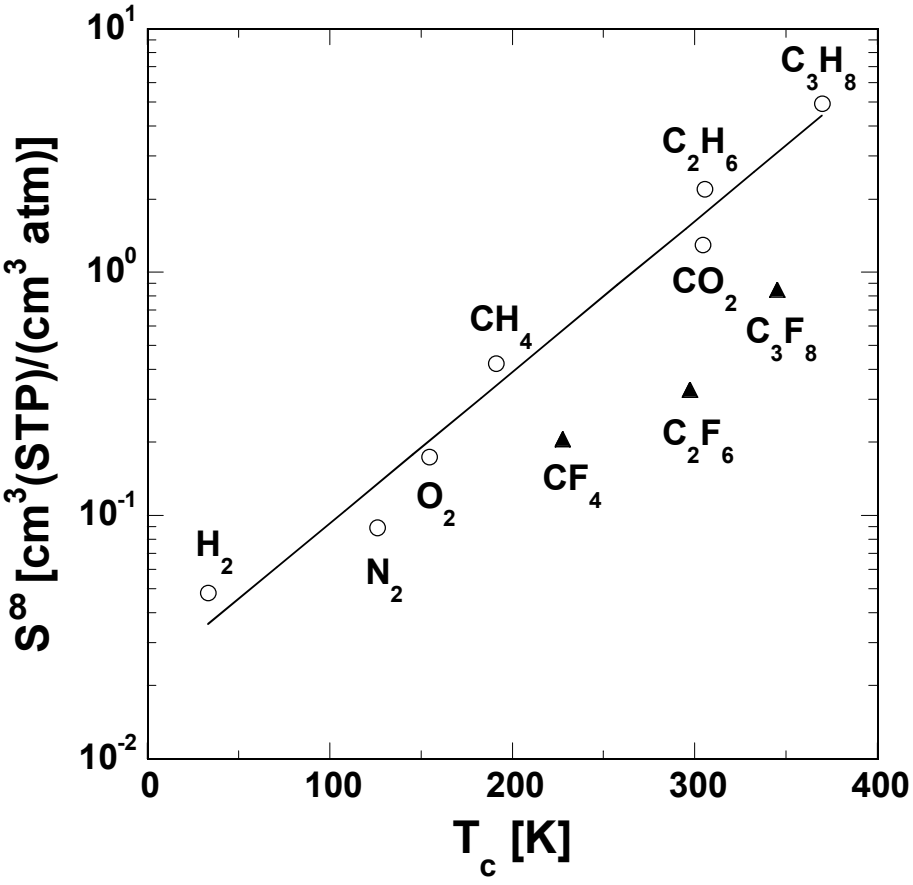

Figure 2.2: Infinite dilution solubility of permanent gases, hydrocarbon and fluorocarbon penetrants in poly(dimethylsiloxane) (PDMS) at 35 ^oC [42].

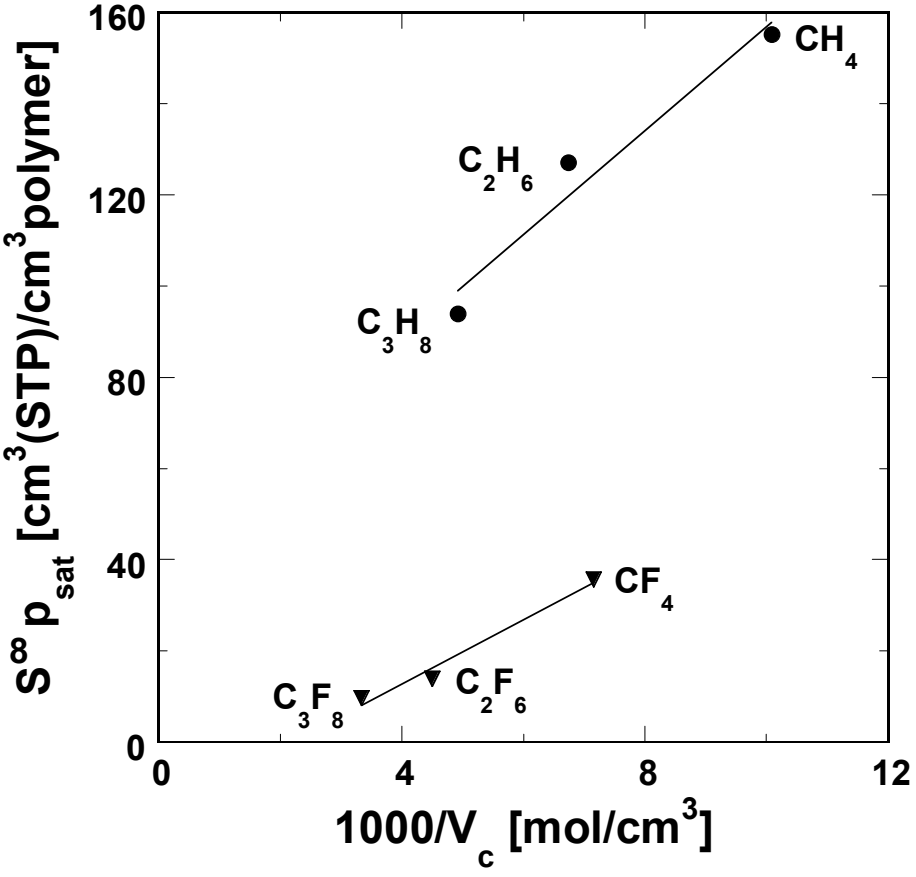

Figure 2.3: Condensability-normalized solubility of hydrocarbon and fluorocarbon penetrants in PDMS at 35 ^{o}C [42].

CHAPTER 3

Propane and Perfluoropropane Sorption and Transport in Poly(dimethylsiloxane) and Poly(1-trimethylsilyl-1-propyne)

3.1 SUMMARY

The effect of pressure on solubility and the influence of temperature on solubility, permeability and diffusivity of C_3F_8 and its hydrocarbon analog, C_3H_8, are reported in rubbery PDMS and glassy PTMSP. C_3F_8 solubility is lower than that of C_3H_8 in both polymers at all temperatures and pressures investigated. The isosteric enthalpy of mixing C_3F_8 with PDMS and PTMSP is higher than that of C_3H_8 due to less favorable polymer-fluorocarbon interactions in the case of C_3F_8, and it decreases with increasing C_3F_8 concentration. Assuming a coordination number of 10, the energy associated with mixing C_3F_8 molecules and PDMS segments is 4.5 kJ/mol more than that required to mix C_3H_8 molecules with PDMS segments, in the limit of infinite dilution. The isobaric activation energy of permeation (E_P) for C_3F_8 is positive for both polymers and that for C_3H_8 is negative in both polymers. This result is particularly interesting for PTMSP since all previous studies of activation energy of gas permeation in PTMSP report values that are near zero or negative; this study provides the first report of a positive E_P value in PTMSP. In PDMS, differences in both activation energy of diffusion (E_D) and enthalpy change on sorption contribute significantly to the difference in E_P values of C_3H_8 and C_3F_8. For PTMSP, the difference in E_P values for C_3F_8 and C_3H_8 stems mainly from a substantially larger E_D value for C_3F_8 than for C_3H_8.

3.2 INTRODUCTION

This report provides quantitative, experimental evidence of the less favorable interactions between fluorocarbon penetrants and hydrocarbon-based polymers that influence the energetics of gas sorption and transport. Perfluoropropane was selected as a model penetrant, and its sorption, diffusion and permeation properties are compared with those of its hydrocarbon analog, propane, in two very different hydrocarbon-based polymers, PDMS and PTMSP. PDMS is a rubbery polymer (its glass transition temperature, T_g, is -123 °C) [54]. As such, it presents a mobile, liquid-like environment to penetrant molecules. PTMSP, on the other hand, is a stiff chain, glassy polymer (T_g > 250 °C) exhibiting very poor chain packing in the solid state [55,56]. It is the most permeable polymer known, and it has the lowest density and highest fractional free volume of all known hydrocarbon-based polymers [57]. Permeability coefficients of N_2 and H_2 in these polymers are also provided because separation of PFCs from mixtures with these permanent gases have been the focus of industrial interest [58-66].

3.3 EXPERIMENTAL

3.3.1 Materials

PDMS composite membranes were used for pure gas permeation experiments. These membranes, composed of a filler-free PDMS film on a highly microporous support, were kindly provided by Dr. Ingo Pinnau of Membrane Technology and Research, Inc. (Menlo Park, CA). The PDMS was from Wacker Silicones Corp. (Adrian,

MI) and was crosslinked at 100 °C using a proprietary crosslinker/catalyst system supplied by them.

A dense filler-free PDMS film of thickness approximately 250 μm was used for the sorption measurements. Crosslinking was achieved using the same method described above. The crosslink density of this film was estimated to be 7.8×10^{-5} mol/cm^3 [67]. Since the film for the permeation measurements was crosslinked under the same conditions, it should have a similar crosslink density to that of the dense film.

PTMSP was kindly provided by Permea, Inc. (St. Louis, MO). Isotropic PTMSP films, approximately 50 μm thick, were prepared from a 2 wt % solution of the polymer in toluene according to the protocol described by Morisato *et al.* [68]. After casting and drying, the samples were stored in liquid methanol at ambient conditions to mitigate physical aging. The films were removed from methanol and dried at ambient conditions for 24 h before using them for experiments. These films were utilized for both sorption and permeation measurements.

The gases and vapors used in the permeation and sorption experiments had a purity of at least 99.5%. N_2 and H_2 were obtained from National Specialty Gases (Durham, NC) while C_3H_8 and C_3F_8 were purchased from Machine Welding (Raleigh, NC). All gases were used as received.

3.3.2 Characterization

Gas sorption experiments in PDMS were performed as described in section 2.2.1, in the following order: N_2, H_2, C_3H_8 and C_3F_8. For the last two gases, solubility was

measured at different temperatures in the order of increasing temperature, *i.e.*, 25 °C, 35 °C, 45 °C and then 55 °C. The order of gases and temperatures for PTMSP were also the same, except that sorption of H_2 in PTMSP was not measured.

Pure gas permeability coefficients were determined using a constant pressure/variable volume apparatus described in section 2.2.2. The upstream pressure was varied from 2 atm to 17.4 atm for N_2 and H_2 while for C_3H_8 and C_3F_8 it was kept constant at 2.36 atm. Permeability coefficients of the gases and vapors were determined in the following order: N_2, H_2, C_3H_8 and C_3F_8 where, for each gas, measurements at different temperatures were made in the order of increasing temperature. For PTMSP, to minimize conditioning effects, a fresh film was used for each gas. The variation in nitrogen permeability from film to film, at all temperatures measured, was less than 10%.

3.4 RESULTS AND DISCUSSION

3.4.1 Solubility

Sorption isotherms for nitrogen and hydrogen in PDMS at 35 °C are presented in Figure 3.1. The isotherms obey Henry's law, and our experimental data are in good agreement with previously published data for nitrogen sorption in PDMS at 35 °C [69]. From Figure 3.1, the ratio of nitrogen to hydrogen solubility is approximately 1.6. The value of this ratio in a wide variety of liquids lies between 1.2 and 2.2 [70]. For example, the N_2/H_2 solubility ratio is 1.4 in carbon disulfide, around 1.7 in alcohols and in the range 1.9-2.2 in hydrocarbon liquids at 25 ^oC and 1 atm [70]. Thus, the N_2/H_2 solubility

ratio lies in the same range as that in liquids, and this is one simple method for assuring that the data are reasonable, since this ratio is expected to be comparable among rubbery polymers and liquids.

Sorption isotherms for propane and perfluoropropane in PDMS at 25, 35, 45 and 55 °C are presented in Figures 3.2a and 3.2b, respectively. Perfluoropropane solubility in PDMS is enormously lower than that of propane. For example, at 35 °C and 3 atm the sorbed concentrations of C_3H_8 and C_3F_8 are 23 and 2.3 cm^3(STP)/(cm^3 polymer), respectively, a difference of one order of magnitude. For both penetrants, solubility decreases with increasing temperature at a given pressure, indicating that the sorption process is exothermic.

Propane sorption isotherms are convex to the pressure axis, which is consistent with the behavior of highly sorbing penetrants in rubbery polymers [11]. The curvature of the isotherms decreases with increasing temperature, suggesting a weaker dependence of solubility on pressure at higher temperatures. This is consistent with the findings of Shah *et al.*, who observed a decrease in the pressure dependence of propane solubility in PDMS as temperature increased [71]. They obtained an infinite dilution solubility of 6.45 cm^3(STP)/(cm^3 polymer·atm) at 35 °C, which is in excellent agreement with our value of 6.5 (± 0.06) cm^3(STP)/(cm^3 polymer·atm). However, if the propane sorption isotherms are plotted as a function of activity (*i.e.*, p/p_{sat}) instead of pressure (*cf.* Figure 3.2c), the four isotherms collapse to a single curve. This result suggests that the change in the curvature of the isotherms with temperature is a result of exploring a smaller activity range at higher temperatures, since the maximum pressure in these experiments is almost the same but the value of p_{sat} increases substantially with temperature.

Perfluoropropane sorption isotherms are linear (*cf.* Figure 3.2b). When the amount of perfluoropropane sorbed in PDMS is plotted against penetrant activity (*cf.* Figure 3.2d), which should account for variability in C_3F_8 condensability with temperature, the C_3F_8 sorbed concentration increases with temperature. This behavior is qualitatively unlike that of C_3H_8 and suggests less favorable interactions between C_3F_8 and the PDMS matrix than between C_3H_8 and PDMS.

As mentioned earlier, in the absence of specific interactions between penetrant molecules and the polymer matrix, gas solubility coefficients usually scale with measures of penetrant condensability such as critical temperature, T_c [11]. Such relationships often utilize solubility coefficients in the limit of zero pressure (called infinite dilution solubility, S^∞) to compare solubilities of penetrants on a consistent basis:

$$S^\infty = \lim_{p\to 0} S = \lim_{p\to 0} \frac{C}{p} \tag{3.1}$$

Suwandi and Stern observed a linear correlation of the logarithm of infinite dilution solubility, S^∞, with $(T_c/T)^2$ for a large number of penetrants in PDMS [72]. This result has been reproduced in Figure 3.3 (the numerical data have been tabulated previously [25]) along with the S^∞ values of propane and perfluoropropane determined in this study (filled symbols). The data for propane obey this correlation, but perfluoropropane solubility coefficients fall well below the trendline, consistent with a previous isothermal study of hydrocarbon and fluorocarbon solubility in PDMS [25].

This result suggests that effects other than condensability have a significant bearing on fluorocarbon sorption in this hydrocarbon polymer.

From sorption data such as those presented in Figures 3.2a and 3.2b, the effect of temperature on solubility can be determined. Solubility values from these figures, calculated either at constant penetrant pressure, or at a constant penetrant concentration in the polymer, can be fitted to the van't Hoff equation (eq 2.18) to obtain enthalpies of penetrant sorption. Thus, two enthalpies of sorption can be calculated *viz.*, the enthalpy of sorption at constant pressure (isobaric), ΔH_S^P, or the enthalpy of sorption at constant concentration (isosteric), ΔH_S^C. From eq 2.18 and the definition of solubility (eq 2.7),

$$\Delta H_S^P = -R\left[\frac{\partial \ln S}{\partial(1/T)}\right]_P = -R\left[\frac{\partial \ln C}{\partial(1/T)}\right]_P \tag{3.2}$$

$$\Delta H_S^C = -R\left[\frac{\partial \ln S}{\partial(1/T)}\right]_C = +R\left[\frac{\partial \ln p}{\partial(1/T)}\right]_P \tag{3.3}$$

In this document, ΔH_s will be used in equations which apply to both isosteric and isobaric enthalpies of sorption, while the superscripts, 'c' and 'p', respectively, will be used to denote the particular types of enthalpies when it is necessary to make this distinction.

Isosteric enthalpies of sorption were calculated for C_3H_8 and C_3F_8 in PDMS from the data in Figures 3.2a and 3.2b. Since sorption is typically viewed as a two-step process involving penetrant condensation from a gas-like density to a liquid-like density followed

by mixing condensed penetrant molecules with polymer segments, the enthalpy of sorption can be viewed as a sum of the enthalpy changes for these two steps [73]:

$$\Delta H_s = \Delta H_{cond} + \Delta H_m \tag{3.4}$$

where ΔH_{cond} and ΔH_m are the enthalpy changes associated with penetrant condensation and mixing, respectively [73]. To estimate ΔH_m, a value of ΔH_{cond} must be supplied. However, ΔH_{cond} varies somewhat over the temperature range of study. For example, ΔH_{cond} for C_3H_8 and C_3F_8 changes by 2.7 and 4.5 kJ/mol, respectively, over the temperature range investigated. For the present calculation, ΔH_{cond} values have been taken at 40 ^oC, which is the midpoint of the experimental temperature range. The ΔH_{cond} values are –13.6 kJ/mol and -12.7 kJ/mol, for C_3H_8 and C_3F_8, respectively, at this temperature [74]. These values were used in eq 3.4 to calculate the isosteric enthalpy of mixing in PDMS, and the results are presented in Figure 3.4a. Basing the calculation of ΔH_m on the ΔH_{cond} value at 40 °C is an arbitrary choice, and the absolute values of ΔH_m in Figure 3.4a will vary somewhat depending on the value of ΔH_{cond} used. However, there is no qualitative change in the order of the data presented in Figure 3.4a or its dependence on concentration if other reasonable reference temperatures are used for determining ΔH_{cond}, so the discussion and conclusions below are not affected by this choice.

As indicated in Figure 3.4a, the enthalpy of mixing C_3F_8 with PDMS segments is much greater than that of C_3H_8. For example, at infinite dilution the enthalpies of mixing for C_3F_8 and C_3H_8 are 2.5 kJ/mol and –2.8 kJ/mol, respectively. In both cases, the enthalpy of mixing decreases with concentration, implying that the process of mixing becomes more favorable in the presence of greater amounts of penetrant. Typically, if the polymer matrix and the penetrant molecules are chemically dissimilar and do not have specific interactions with each other, interactions among penetrant molecules are more favorable than those between penetrant molecules and polymer chains. At low penetrant concentrations, mixing these penetrant molecules with the polymer is a less favorable process than at higher concentrations. As penetrant concentration increases, the environment into which the penetrant is dissolving becomes more like that of the penetrant, and the mixing process becomes more favorable. The enthalpy of mixing of propane depends much less on penetrant concentration than that of perfluoropropane. This result is reasonable since, from a structural viewpoint, propane and PDMS are much more similar than perfluoropropane and PDMS.

The difference in interaction energy of PDMS with perfluoropropane and propane can be estimated from polymer-polymer, penetrant-penetrant and polymer-penetrant interaction energies. Based on the regular solution and Flory-Huggins theories [25]:

$$z(\Gamma_{FP}-\Gamma_{HP}) = \frac{RT}{N_A}[(\chi_F-\chi_H)-\frac{1}{RT}(\Delta H_{condH}-\Delta H_{condF})] \qquad (3.5)$$

where Γ_{FP} is the potential energy required to separate a perfluoropropane molecule and a PDMS segment to infinite distance, Γ_{HP} is the potential energy required to separate a propane molecule and a PDMS segment to infinite distance, z is the coordination number, N_A is Avogadro's number, χ_F and χ_H are the Flory-Huggins interaction parameters for perfluoropropane and propane, respectively, and, ΔH_{condF} and ΔH_{condH} are the molar enthalpies of condensation of perfluoropropane and propane, respectively. The product $z(\Gamma_{FP} - \Gamma_{HP})$ is the difference in potential energy associated with inserting a C_3F_8 molecule and a C_3H_8 molecule in PDMS. Also,

$$\Delta H_m = RT\chi(1-\phi_2) \tag{3.6}$$

where ϕ_2 is the penetrant volume fraction (which is <<1 in this study) [24]. Combining eqs 3.5 and 3.6 yields:

$$\begin{aligned} N_A z(\Gamma_{FP}-\Gamma_{HP}) &= (\Delta H_{mF}-\Delta H_{mH})-(\Delta H_{condH}-\Delta H_{condF}) \\ &= \Delta H_{sF}^{C}-\Delta H_{sH}^{C} \end{aligned} \tag{3.7}$$

where ΔH_{sF}^{C} and ΔH_{sH}^{C} are the isosteric enthalpies of mixing the fluorocarbon and hydrocarbon penetrants, respectively, with the polymer segments. The left hand side of eq 3.7 is the difference in energy associated with inserting a mole of C_3F_8 molecules and a mole of C_3H_8 molecules in PDMS.

Figure 3.4b presents the calculated difference in potential energy associated with inserting C_3F_8 molecules and C_3H_8 molecules in PDMS. In the limit of infinite dilution, this difference is 4.5 kJ/mol while at the highest concentration considered, 3 cm^3(STP)/(cm^3 polymer), it is 1.2 kJ/mol. The result at infinite dilution is in excellent agreement with that previously estimated from isothermal sorption data (4.6 kJ/mol at infinite dilution) [25].

A nitrogen sorption isotherm in PTMSP at 35 °C is presented in Figure 3.5 along with previously published data for comparison [75]. Our data are in good agreement with the literature data. Sorption isotherms for C_3H_8 and C_3F_8 in PTMSP at 25, 35 and 45 °C are presented in Figures 3.6a and 3.6b, respectively. The isotherms are concave to the pressure axis, which is typical for gas sorption in glassy polymers [11]. There is a substantial difference in the solubilities of the hydrocarbon and fluorocarbon analogs, with propane being more soluble in PTMSP at all temperatures and pressures tested. As noted previously [57], this difference in hydrocarbon and perfluorocarbon solubilities is smaller in high free volume PTMSP than in liquid-like PDMS. For example, at 35 °C and 3 atm, the sorbed concentrations of C_3H_8 and C_3F_8 in PTMSP are 68 and 26 cm^3(STP)/(cm^3 polymer), respectively, which is significantly smaller than the order of magnitude difference observed in PDMS.

Isosteric enthalpies of sorption were calculated for C_3H_8 and C_3F_8 in PTMSP from the data in Figures 3.6(a-b). The enthalpies of condensation for C_3H_8 (-14 kJ/mol) and C_3F_8 (-13.4 kJ/mol) were taken at 35 ^oC, the midpoint of the experimental temperature range [74]. The isosteric enthalpies of mixing in PTMSP were then calculated from eq

3.4 and are presented in Figure 3.7a as a function of penetrant concentration. Similar to PDMS, the enthalpy of mixing of C_3F_8 in PTMSP is generally higher than that of C_3H_8 in PTMSP. However, unlike PDMS, the enthalpy of mixing of the two penetrants show opposite trends in PTMSP; the enthalpy of mixing C_3F_8 with PTMSP decreases with concentration while the enthalpy of mixing C_3H_8 with PTMSP increases with concentration.

The trend of the enthalpy of mixing of propane can be rationalized by considering the additional mode of sorption available in glassy polymers, *i.e.*, the Langmuir microvoids. A glassy polymer such as PTMSP contains non-equilibrium microvoids (so-called Langmuir sites) dispersed throughout the equilibrium matrix. These microvoids represent sorption sites that, from an energetic perspective, are easily accessible to penetrant molecules. At low penetrant concentrations, the microvoids are relatively unoccupied and can accommodate penetrant molecules with little or no distortion (*i.e.*, swelling) of the polymer matrix. As penetrant concentration in the polymer increases, these sites become progressively more saturated, resulting in a larger fraction of the sorption occurring in the densified regions of the polymer (*i.e.*, the so-called Henry's law region). Penetrant sorption in the Henry's law region is energetically more expensive than sorption in a Langmuir microvoid, since this process involves the creation of a gap large enough to accommodate the penetrant (*i.e.*, the polymer swells [76]). Thus, the enthalpy of mixing increases with concentration. At high concentrations, it reaches a limiting value determined by the enthalpy of sorption of the penetrant in the densified matrix. A similar trend has been reported for CO_2 sorption in a high barrier, glassy polymer, poly(ethylene terephthalate) [77].

The concentration dependence of the enthalpy of mixing of perfluoropropane in PTMSP is similar to that in PDMS. This result suggests that the less favorable interactions between the fluorinated penetrant and the hydrocarbon matrix are more important than the dual mode effects in determining sorption energetics.

An interesting example of mixing behavior that follows the same logic is displayed in Figure 3.7b for isosteric enthalpies of mixing C_3H_8 and C_3F_8 with a perfluorinated copolymer, AF2400 [78]. In this case, the penetrants encounter a fluorinated environment, and the concentration dependence of the enthalpies of mixing as well as their relative magnitudes reflect this fact. Propane has a less exothermic enthalpy of mixing, and ΔH_m decreases with concentration, both of which signify less favorable polymer-penetrant interactions. On the other hand, the concentration dependence of perfluoropropane's enthalpy of mixing suggests that the dual mode sorption effect is the dominant factor affecting the energetics of the dissolution process.

3.4.2 Permeability

The permeability of PDMS to nitrogen and hydrogen as a function of the pressure difference across the polymer film at 25, 35, 45 and 55 °C are shown in Figures 3.8a and 3.8b respectively. The permeability of both penetrants increases with increasing temperature at a given pressure, indicating a positive activation energy of permeation. This result is typical for the permeation of supercritical gases in PDMS. For example, Bixler and Sweeting [79] reported an E_P value for nitrogen in PDMS of 10.9 kJ/mol, which is close to the value of 9.3 kJ/mol obtained from the data in Figure 3.8a.

Figures 3.9a and 3.9b present the effect of temperature on the permeability of PDMS to C_3H_8 and C_3F_8, respectively, at an upstream pressure of 2.36 atm. The data can be fitted to the Arrhenius equation (eq 2.16) and the activation energy of permeation, E_P, can be calculated. Since the permeability values are at a constant upstream pressure, the E_P value thus calculated is an isobaric (*i.e.*, constant pressure) activation energy of permeation. In a similar fashion, isobaric enthalpies of sorption can be calculated for the two penetrants at a pressure of 2.36 atm, from eq 3.2 and the data in Figures 3.2a and 3.2b. The calculated values are presented in Table 3.1. The errors in the table have been calculated by the method of propagation of errors [80]. These E_P and ΔH_S^p values have been used to calculate E_D values according to eq 2.19. As indicated earlier, the use of eq 2.19 is subject to restrictions on the concentration or pressure dependence of the permeability, solubility and diffusion coefficients. However, since the permeability data have been measured at a single pressure, it is not possible to evaluate the pressure (or concentration) dependence of the permeability coefficients. Therefore, the activation energy of diffusion has been calculated by assuming the validity of eq 2.19, as is practically always done in the literature.

Usually, the permeability of relatively condensable gases in PDMS decreases with increasing temperature (*i.e.*, E_P is negative) [27]. This is because, in weakly size-sieving PDMS, the solubility of condensable gases decreases with increasing temperature more rapidly than diffusion coefficients increase (*i.e.*, $|\Delta H_S| > E_D$). The propane data in PDMS are consistent with this trend. However, perfluoropropane displays markedly different behavior. Its permeability coefficient increases with temperature (*cf.* Figure 3.9b),

indicating a positive E_P value. From Table 3.1, the different effect of temperature on the permeation behavior of the C_3 analogs is related to differences in both the dissolution and diffusion of these penetrants. Larger penetrants require more energy to execute a diffusive jump in a polymer matrix than smaller penetrants [81]. In this regard, perfluoropropane is substantially larger than its hydrocarbon analog. The critical volumes of C_3F_8 and C_3H_8 are 300 cm^3/mol and 203 cm^3/mol, respectively. Consequently, the activation energy of diffusion is much larger for C_3F_8 (16 kJ/mol) than for C_3H_8 (7 kJ/mol). Additionally, a difference in polymer-penetrant interactions contributes to the difference in the temperature dependence of permeability of C_3F_8 and C_3H_8. From Table 3.1, the magnitude of the isobaric enthalpy of sorption is lower for C_3F_8 than for C_3H_8. Since the enthalpies of condensation for C_3F_8 and C_3H_8 are similar (-12.7 kJ/mol and -13.6 kJ/mol, respectively, at 40 ^oC [74]), mixing propane with PDMS is more favorable than mixing perfluoropropane with PDMS. The combination of less favorable mixing and hindered diffusion causes C_3F_8 to have a substantially larger activation energy of permeation than C_3H_8 in PDMS.

Figures 3.10a and 3.10b present N_2 and H_2 permeability in PTMSP as a function of temperature and pressure. For these penetrants, permeability coefficients decrease with increasing temperature, which is opposite to the behavior in PDMS. Figures 3.11a and 3.11b present Arrenhius plots of C_3H_8 and C_3F_8 permeability coefficients, respectively, in PTMSP at 2.36 atm. For C_3H_8, permeability increases as temperature decreases, which is qualitatively similar to the trend in PDMS. On the other hand, C_3F_8 permeability decreases as temperature decreases, and this is the first report of permeability coefficients decreasing with decreasing temperature in PTMSP. Isobaric activation energies of

permeation for these penetrants are tabulated in Table 3.1 along with enthalpies of sorption and calculated activation energies of diffusion. Similar to PDMS, E_P for C_3F_8 in PTMSP is positive and opposite in sign to that of propane. This result reflects the larger size of perfluoropropane (larger E_D) and its less favorable interactions with PTMSP (larger ΔH_m and, therefore, more positive ΔH_S relative to propane). The relative contributions of these two effects to the difference in E_P between C_3H_8 and C_3F_8 in PTMSP are shown in Table 3.1. For PTMSP, the difference in C_3H_8 and C_3F_8 activation energies of permeation (15 kJ/mol) is mostly due to the large difference in E_D values (13 kJ/mol) with a small contribution from the ΔH_S difference (2 kJ/mol). Thus, for PTMSP, it is primarily the difference in penetrant size and the associated effect on the diffusion process that causes the dramatic difference in C_3 analog transport properties. In contrast, in PDMS the difference in E_P values between C_3H_8 and C_3F_8 (16 kJ/mol) is due to nearly equal contributions from the difference in E_D (9 kJ/mol) and ΔH_S (7 kJ/mol). This result suggests that hydrocarbon-fluorocarbon interactions have a stronger effect on penetrant transport properties in liquid-like PDMS than in high-free-volume, glassy PTMSP.

The unusual nature of C_3F_8's positive activation energy of permeation in PTMSP is highlighted in Figure 3.12, which presents E_P values as a function of penetrant critical temperature for this polymer. The data of Masuda *et al.* [82] are included in Figure 3.12 for comparison. Excluding our data for C_3F_8, E_P values in PTMSP are negative for all penetrants and decrease (*i.e.*, increase in absolute value) with increasing penetrant critical temperature. This behavior is consistent with a solubility selective polymer, where E_P is

significantly influenced by ΔH_S (because $|\Delta H_S| > E_D$) and where the enthalpy of sorption decreases with increasing penetrant condensability (T_c). The activation energy of permeation for C_3F_8 deviates substantially from the empirical trendline through the other penetrants. In fact, based on C_3F_8's critical temperature and the best fit line through the rest of the data, it's expected E_P value would be -9.8 kJ/mol as compared to the measured value of 7 kJ/mol. As mentioned previously, this difference appears to be primarily due to C_3F_8's large size and its effect on the diffusion process.

It has been suggested that PTMSP contains a network of quasi-permanent, interconnected free volume elements spanning the polymer through which the majority of penetrant transport occurs [83,84]. Transport in these interconnected free volume elements may be similar to that in zeolites, where the critical penetrant diameter, or the smallest size window through which a given molecule can fit, governs the transport. Transport through such interconnected free volume elements should be an energetically inexpensive process compared to transport through the densified polymer matrix. The kinetic diameter of C_3F_8 (5.4 $\mathring{A}$) is much larger than that of C_3H_8 (4.3 $\mathring{A}$) [85]. Thus, it is possible that C_3F_8 is larger than the critical free volume element diameter for transport in the interconnected free volume elements, which may restrict its access to this energetically inexpensive mode of transport.

3.5 CONCLUSIONS

C_3F_8 solubility is lower than that of its hydrocarbon analog, C_3H_8, in both PDMS and PTMSP due to less favorable polymer-fluorocarbon interactions as indicated by a

higher ΔH_m for the fluorocarbon as well as a decrease in ΔH_m with increasing penetrant concentration. Unlike PDMS, ΔH_m of C_3H_8 in PTMSP increases with penetrant concentration, which is due to the different energy requirements for dissolution in the two types of sorption sites present in a glassy polymer *viz.*, the Langmuir sites and the Henry's law sites.

The activation energy of permeation for C_3F_8 is positive and opposite in sign to that of C_3H_8 in both polymers. This is the first report of a penetrant having a positive activation energy of permeation in PTMSP. In PDMS, the difference in E_P values is due to the difference in penetrant sizes as well as the difference in polymer-penetrant interactions. For PTMSP, however, it is primarily the larger size of C_3F_8 and its associated effect on diffusion that is responsible for the difference in E_P values. Thus, polymer-penetrant interactions have more of an effect on gas transport properties in liquid-like PDMS than in high-free-volume, glassy PTMSP.

Table 3.1 Activation energies of permeation and diffusion, and enthalpy of sorption at 2.36 atm (*i.e.*, isobaric) for C_3H_8 and C_3F_8 in PDMS and PTMSP.

Polymer	***Penetrant***	E_P ***(kJ/mol)***	ΔH_S^p ***(kJ/mol)***	E_D ***(kJ/mol)***
PDMS	C_3H_8	-13 ± 1.2	-20 ± 0.2	7 ± 1.2
PDMS	C_3F_8	3 ± 3	-13 ± 1.8	16 ± 3
PTMSP	C_3H_8	-8 ± 1.2	-9 ± 0.7	1 ± 1.4
PTMSP	C_3F_8	7 ± 4.0	-7 ± 2.0	14 ± 4.5

Note: E_P, ΔH_S and E_D values have been calculated using eqs 2.16, 2.18 and 2.19, respectively.

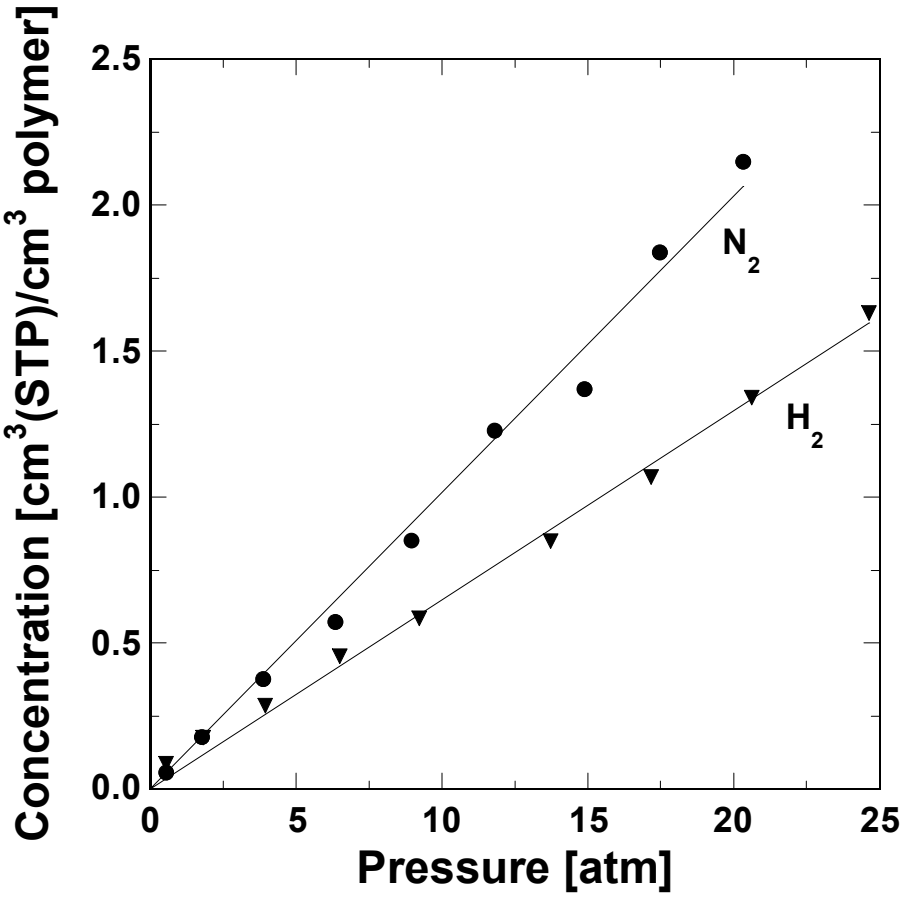

Figure 3.1: N_2 and H_2 sorption in PDMS at 35 °C.

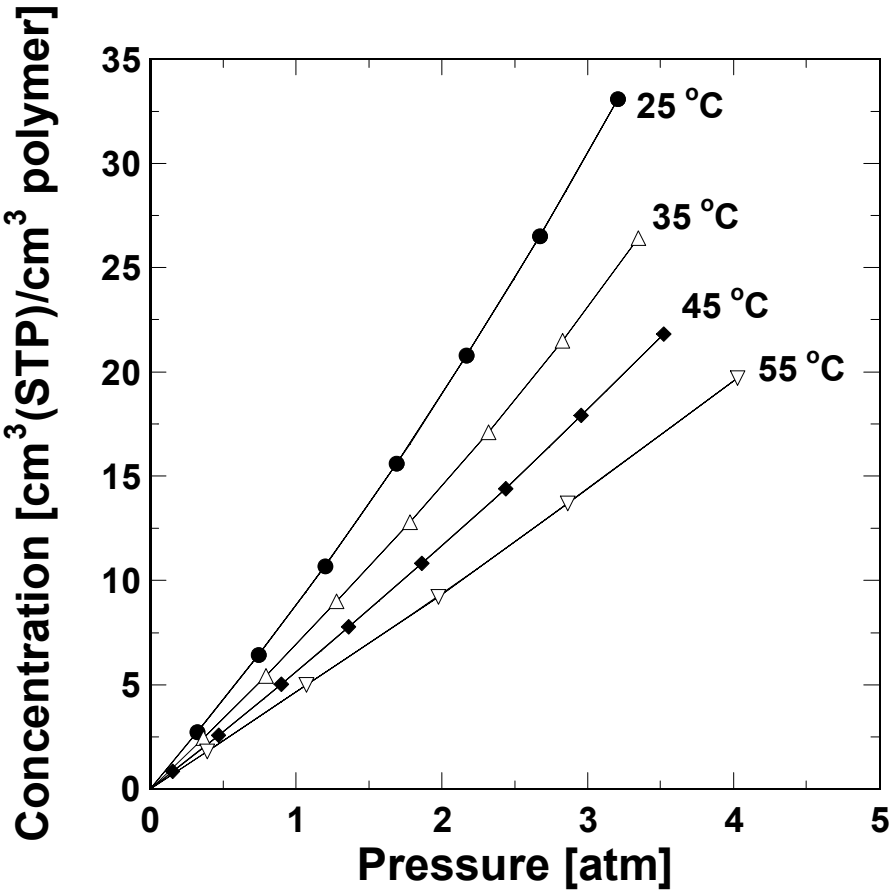

Figure 3.2a: C_3H_8 sorption in PDMS as a function of temperature.

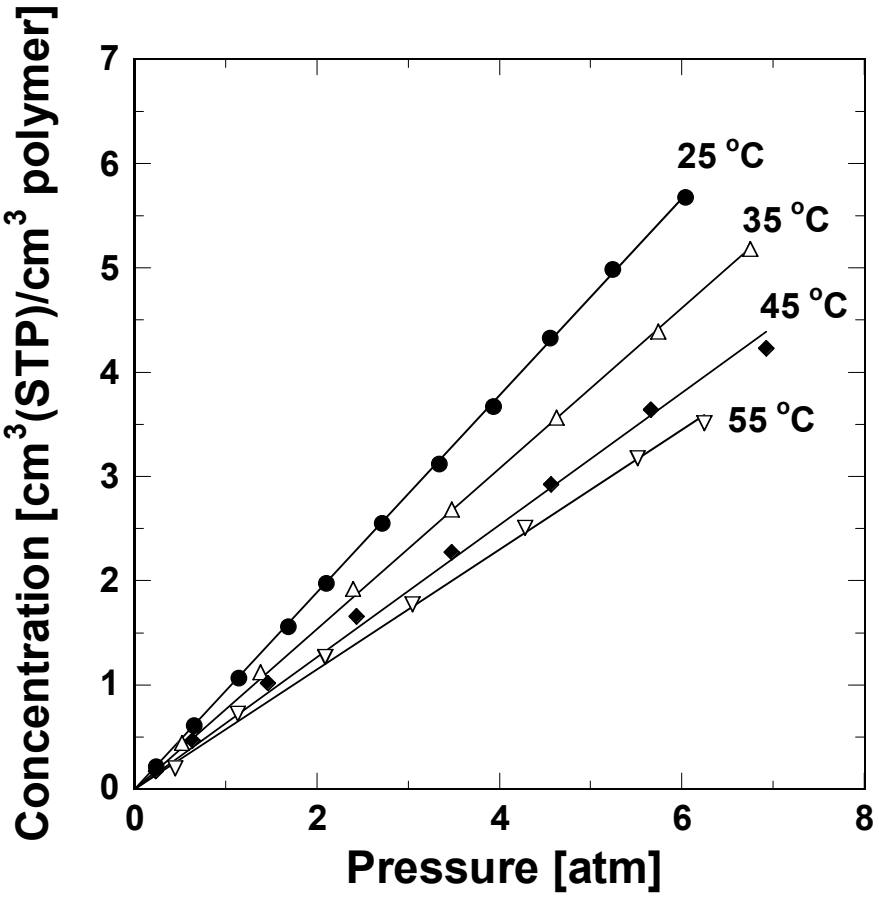

Figure 3.2b: C_3F_8 sorption in PDMS as a function of temperature.

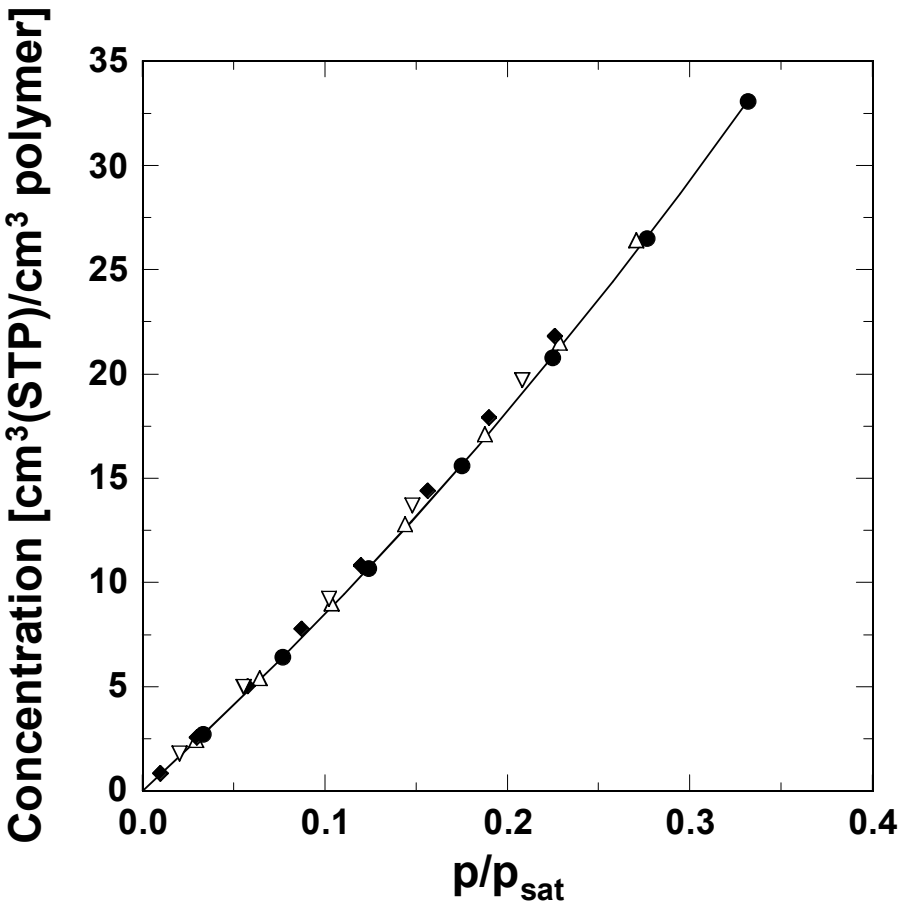

Figure 3.2c: C_3H_8 sorption in PDMS as a function of penetrant activity (p/p_{sat}) at four temperatures: (●) 25 °C, (Δ) 35 °C, (♦) 45 °C, and (∇) 55 °C. p_{sat} values are from the correlations in Appendix A of Reid *et al* [46].

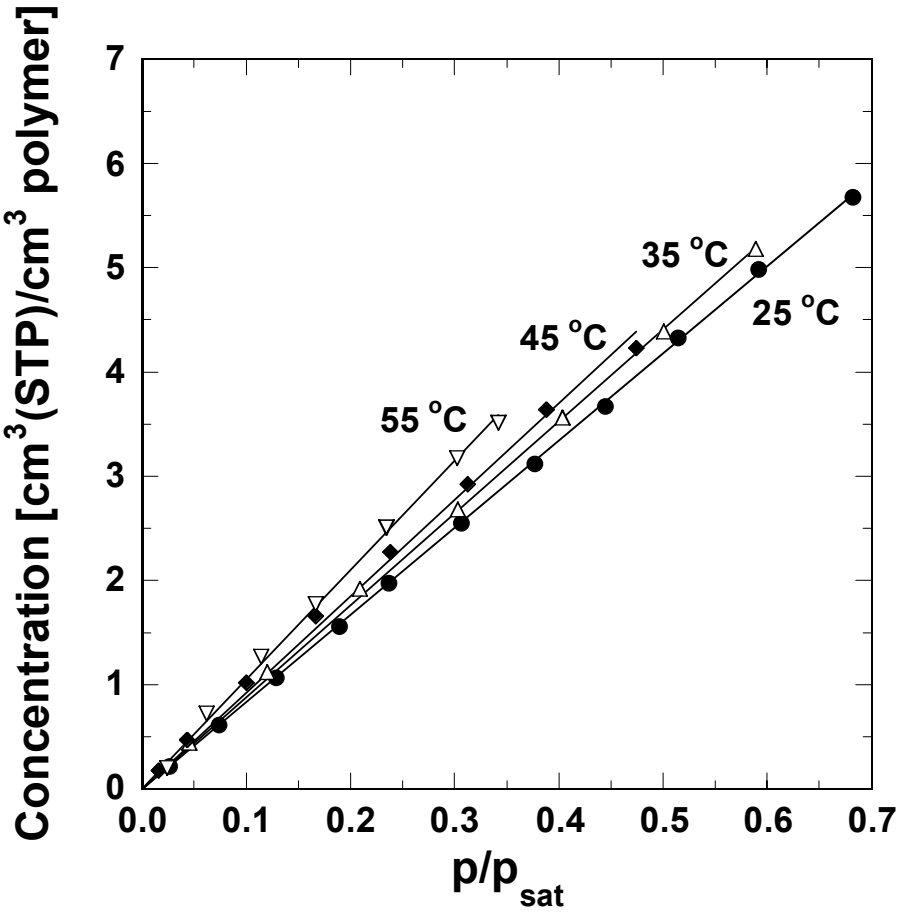

Figure 3.2d: C_3F_8 sorption in PDMS as a function of penetrant activity (p/p_{sat}) at four temperatures (●) 25 °C, (▽) 35 °C, (♦) 45 °C, and (Δ) 55 °C. p_{sat} values are from the correlations in Appendix A of Reid *et al* [46].

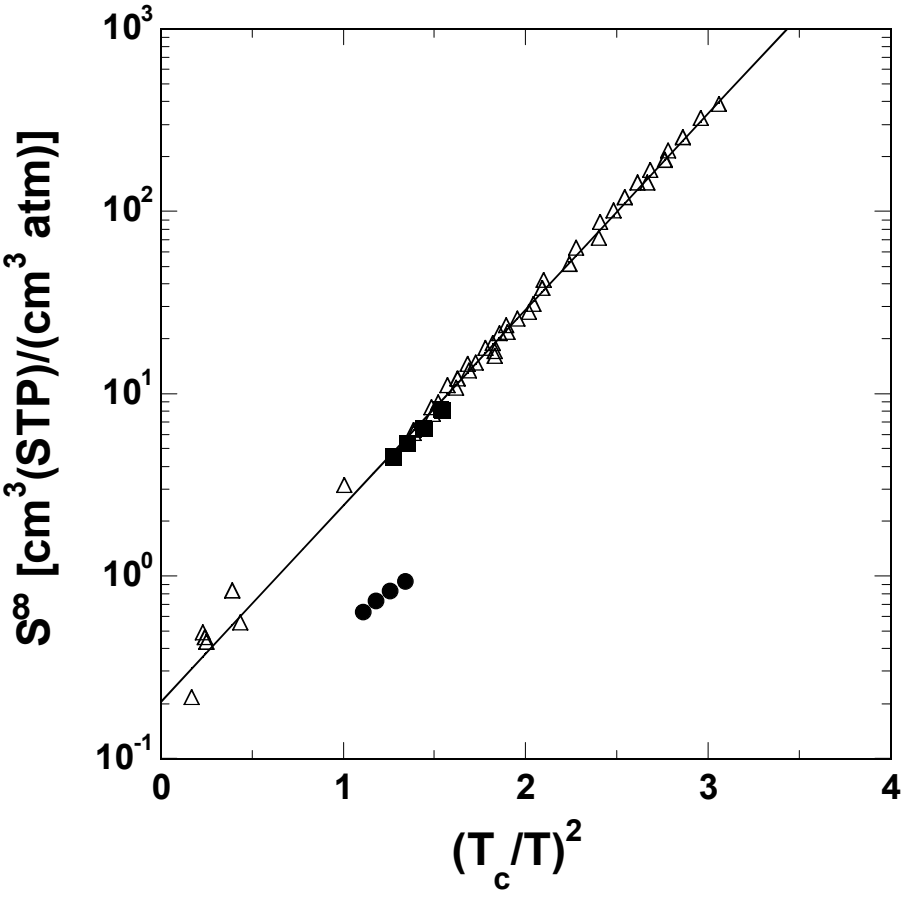

Figure 3.3: Correlation of infinite dilution solubility, S^{∞}, in PDMS with reduced critical temperature. (■) = propane data of this study, (●) = perfluoropropane data of this study, (Δ) = data of Suwandi and Stern [72], Barrer *et al.* [86] and Robb [87]. The correlation line is:

$$S_o\,[cm^3(STP)/(cm^3\,atm)] = 0.0245\times 10^{1.075\left(T_c/T\right)^2}$$

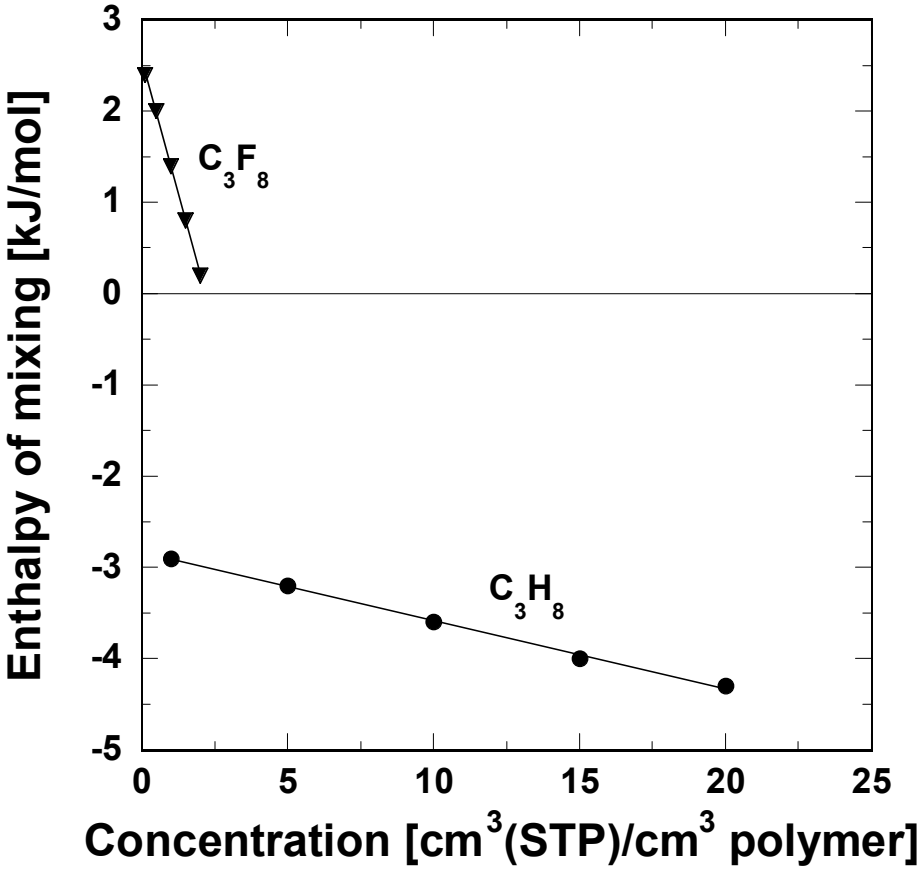

Figure 3.4a: Isosteric enthalpy of mixing of C_3H_8 and C_3F_8 in PDMS.

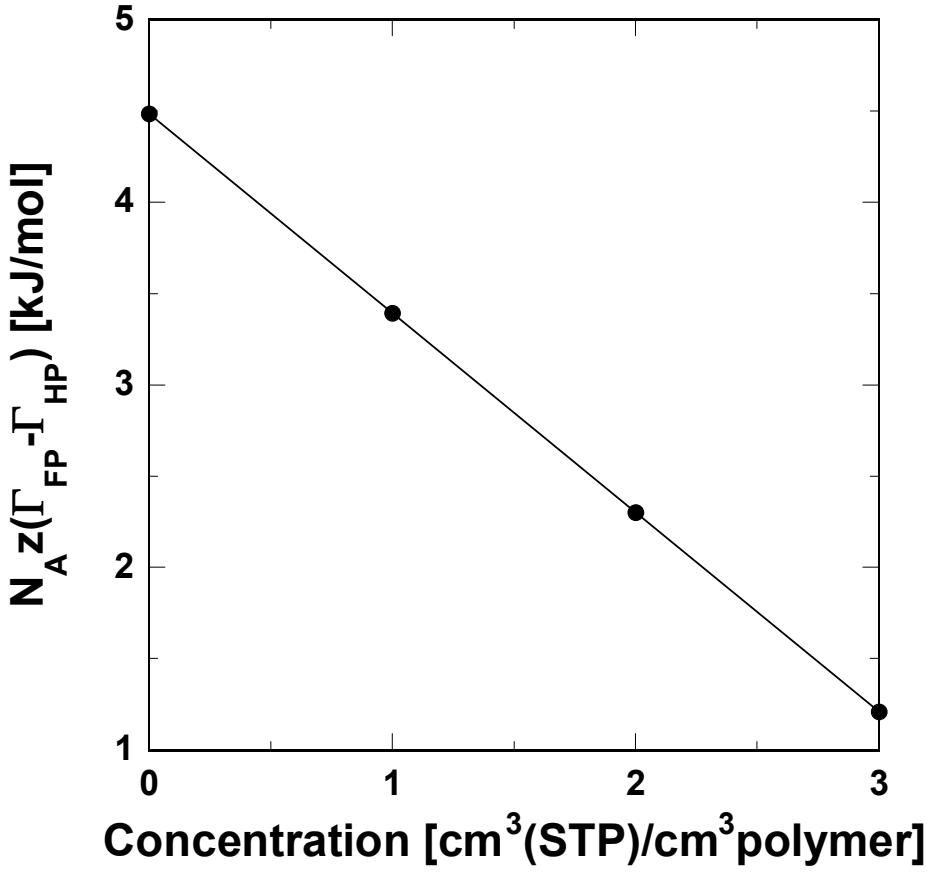

Figure 3.4b: Difference in potential energies associated with insertion of C_3F_8 and C_3H_8 in PDMS.

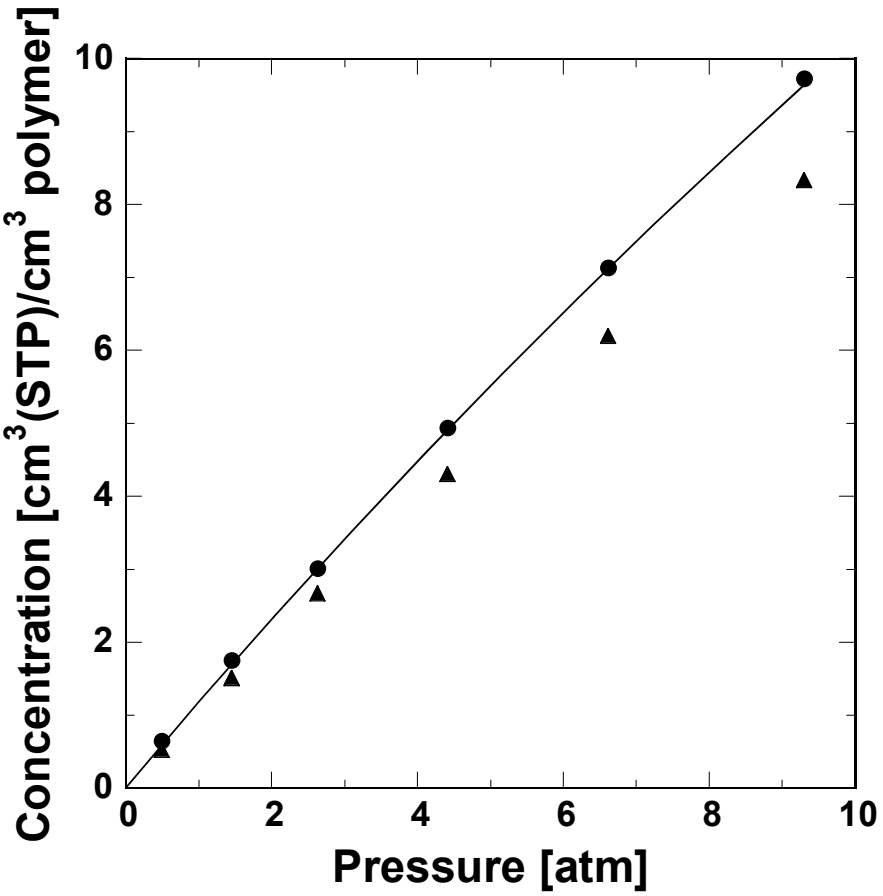

Figure 3.5: N_2 sorption in PTMSP at 35 °C. Data of Ichiraku *et al.* [75] (▲) are provided for comparison.

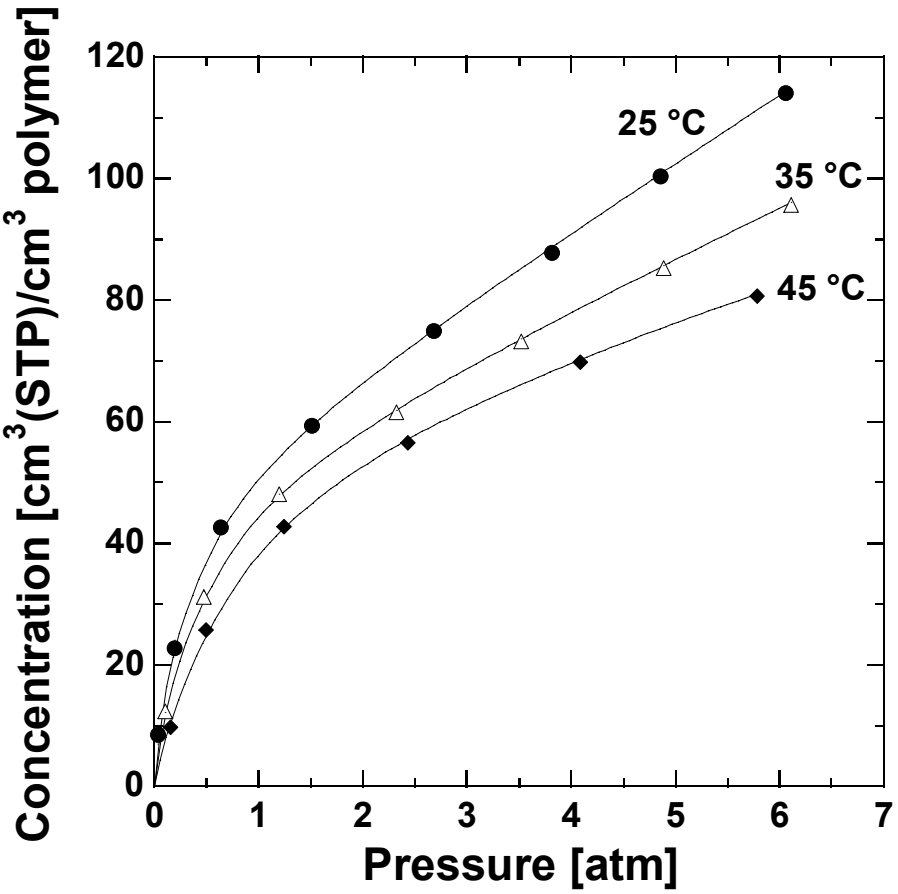

Figure 3.6a: C_3H_8 sorption in PTMSP as a function of temperature.

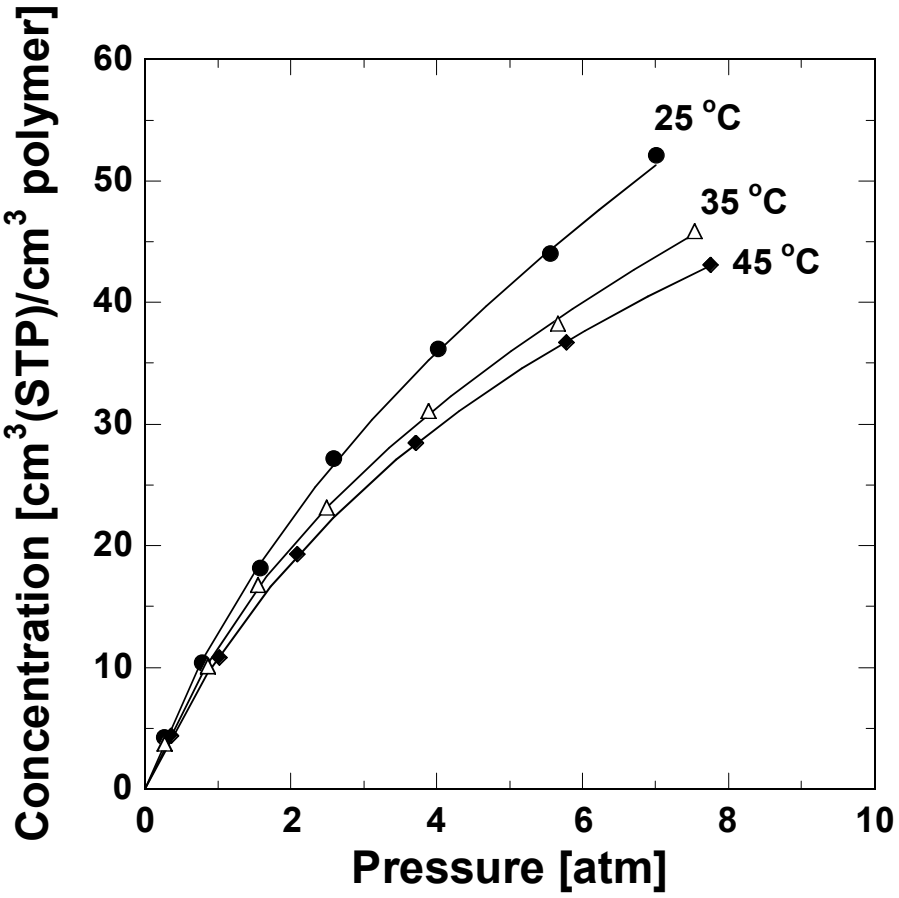

Figure 3.6b: C_3F_8 sorption in PTMSP as a function of temperature.

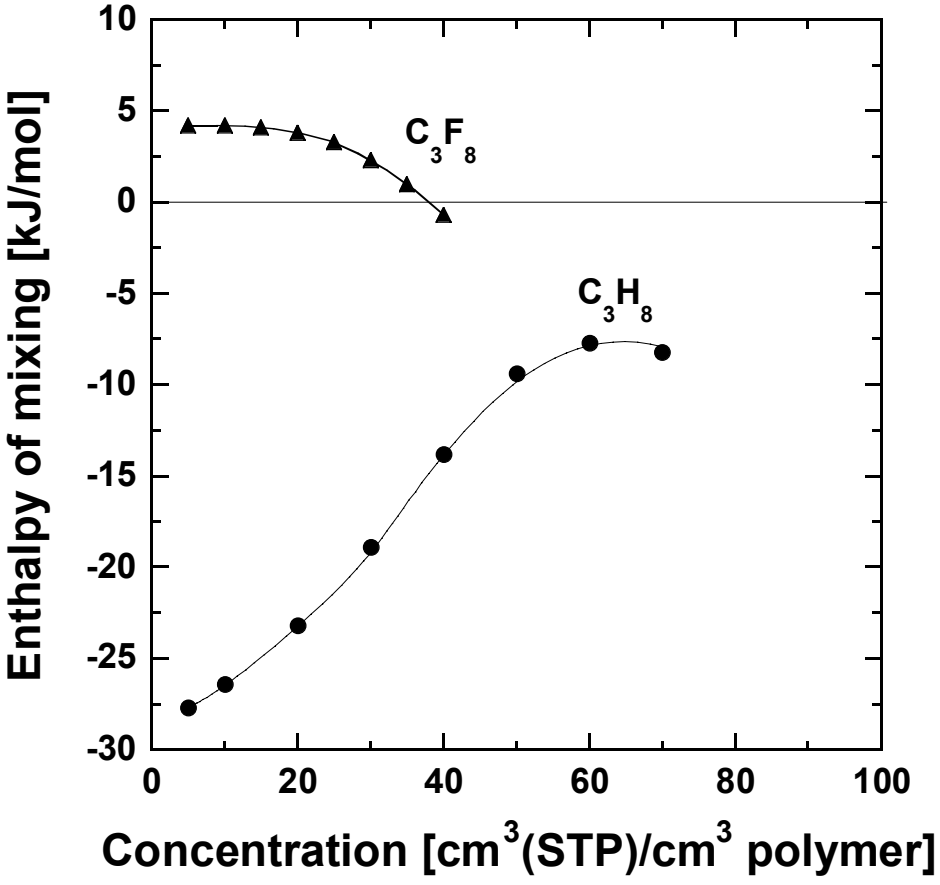

Figure 3.7a: Isosteric enthalpy of mixing of C_3H_8 and C_3F_8 in PTMSP.

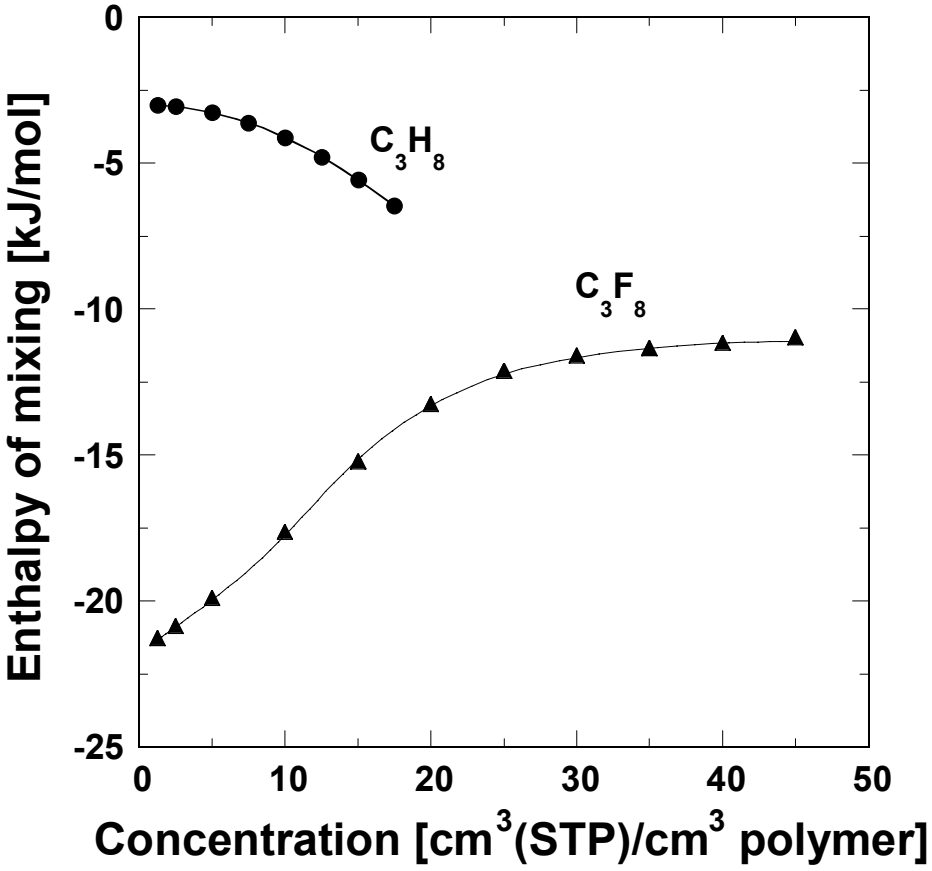

Figure 3.7b: Isosteric enthalpy of mixing of C_3H_8 and C_3F_8 in AF2400 [78].

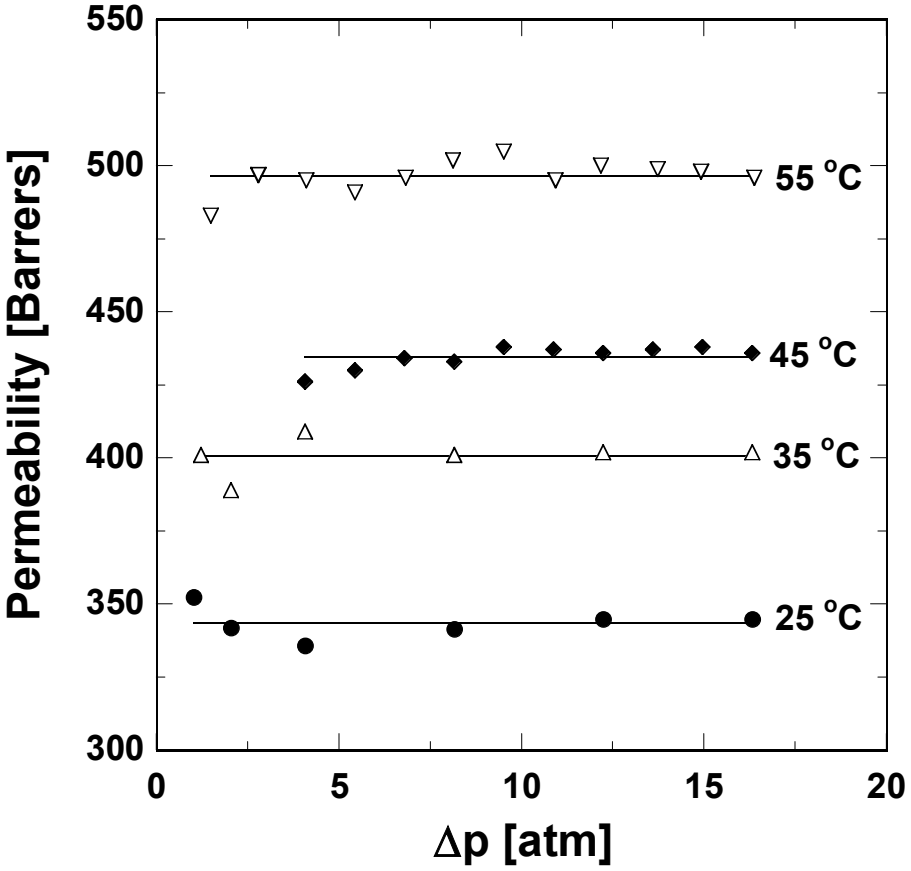

Figure 3.8a: N_2 permeation in PDMS as a function of temperature and pressure difference across the membrane. The downstream pressure is 1 atm.

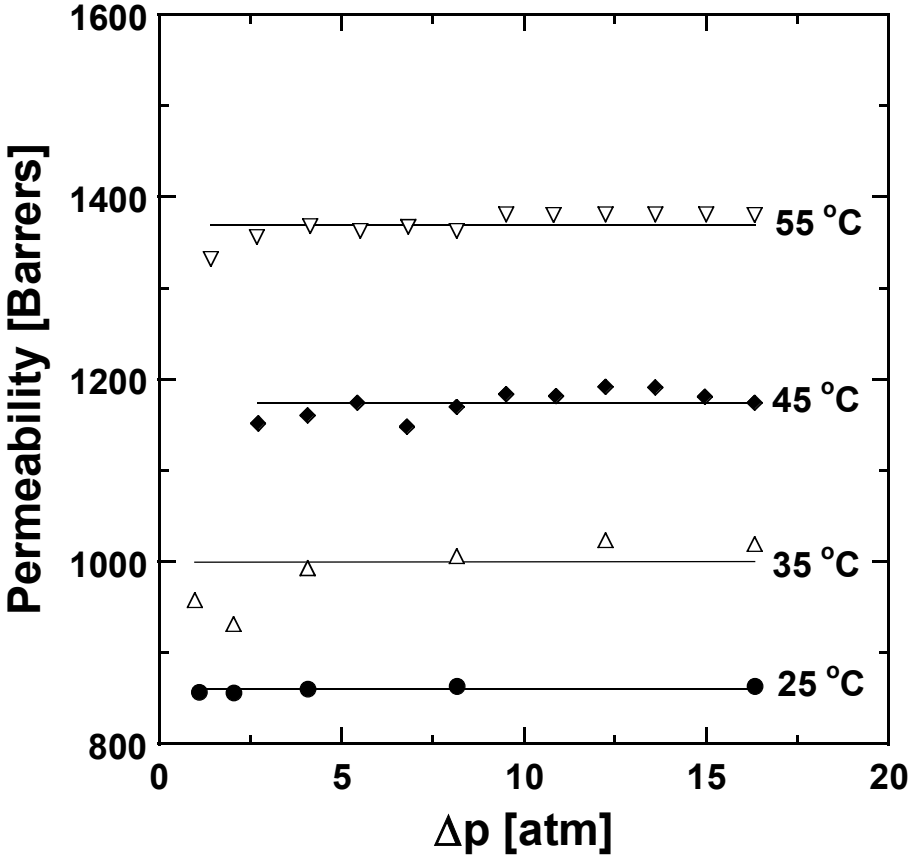

Figure 3.8b: H_2 permeation in PDMS as a function of temperature and pressure difference across the membrane. The downstream pressure is 1 atm.

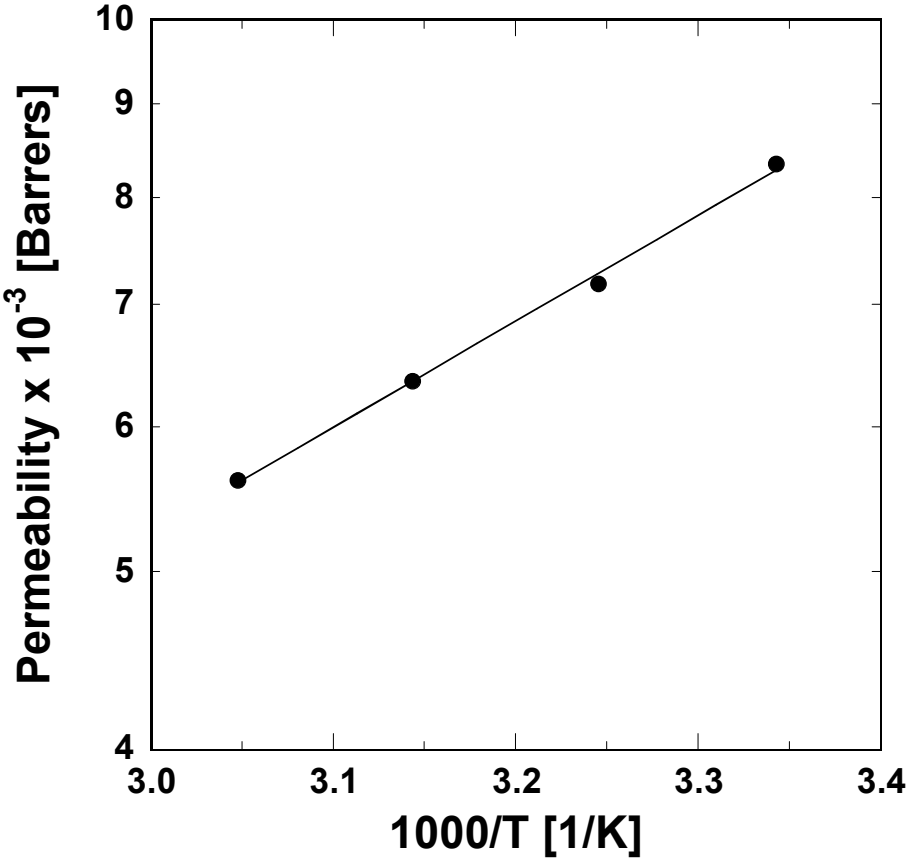

Figure 3.9a: Effect of temperature on C_3H_8 permeation in PDMS at 2.36 atm upstream pressure and 1 atm downstream pressure.

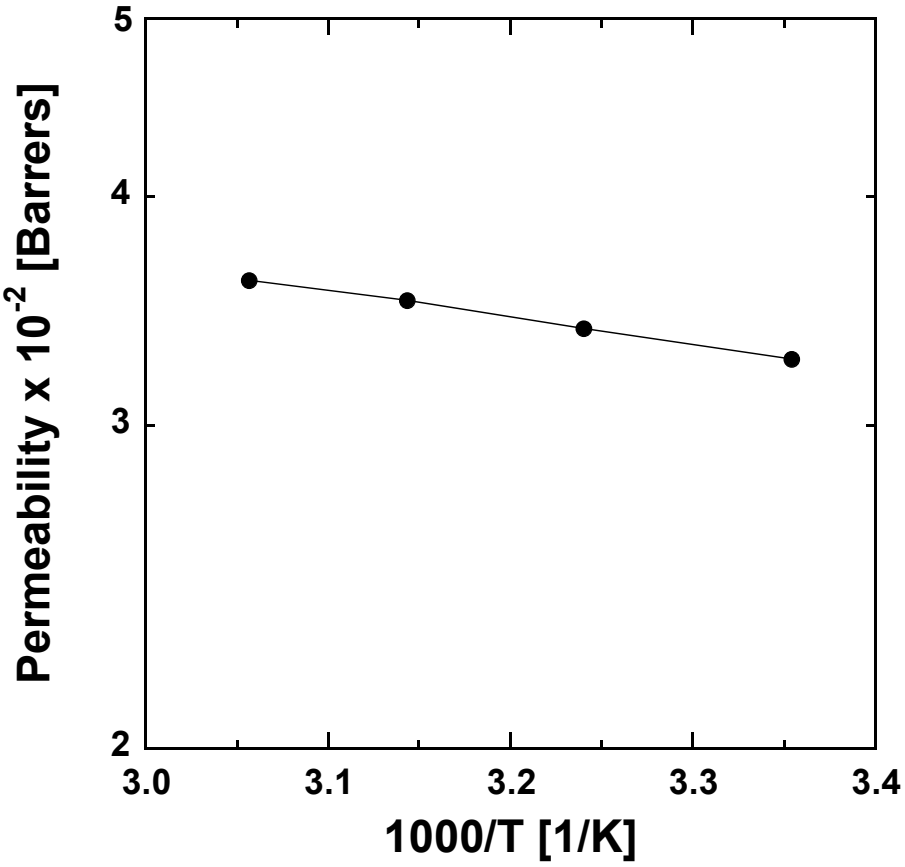

Figure 3.9b: Effect of temperature on C_3F_8 permeation in PDMS at 2.36 atm upstream pressure and 1 atm downstream pressure.

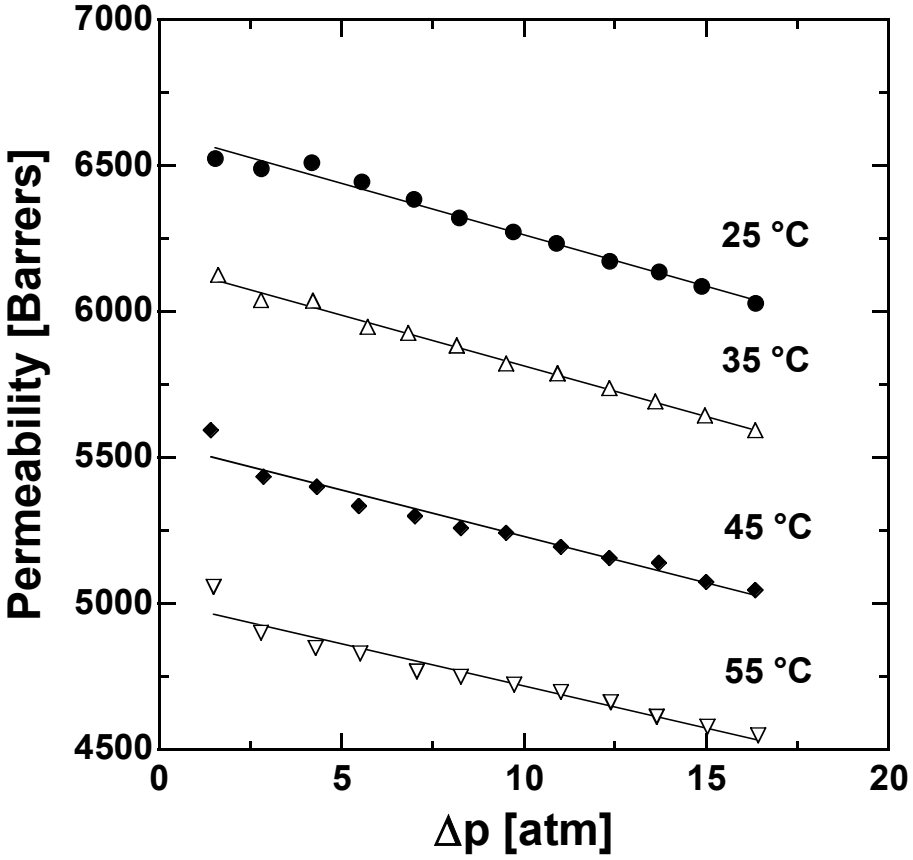

Figure 3.10a: N_2 permeation in PTMSP as a function of temperature and pressure difference across the membrane. The downstream pressure is 1 atm.

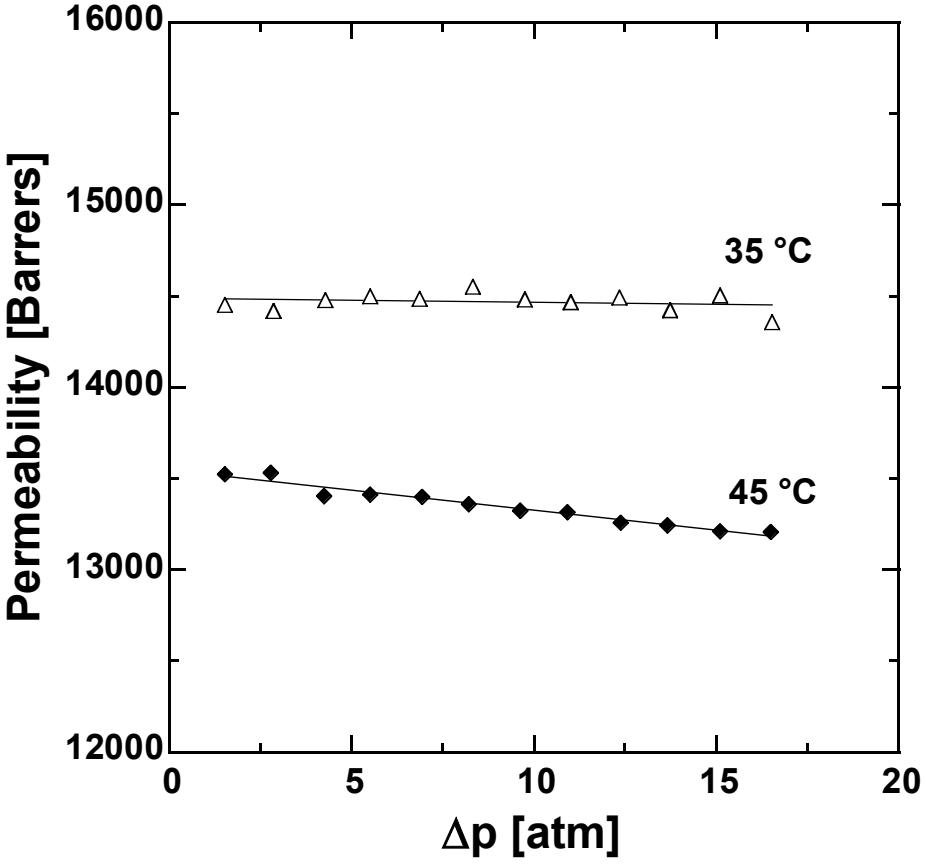

Figure 3.10b:H_2 permeation in PTMSP as a function of temperature and pressure difference across the membrane. The downstream pressure is 1 atm.

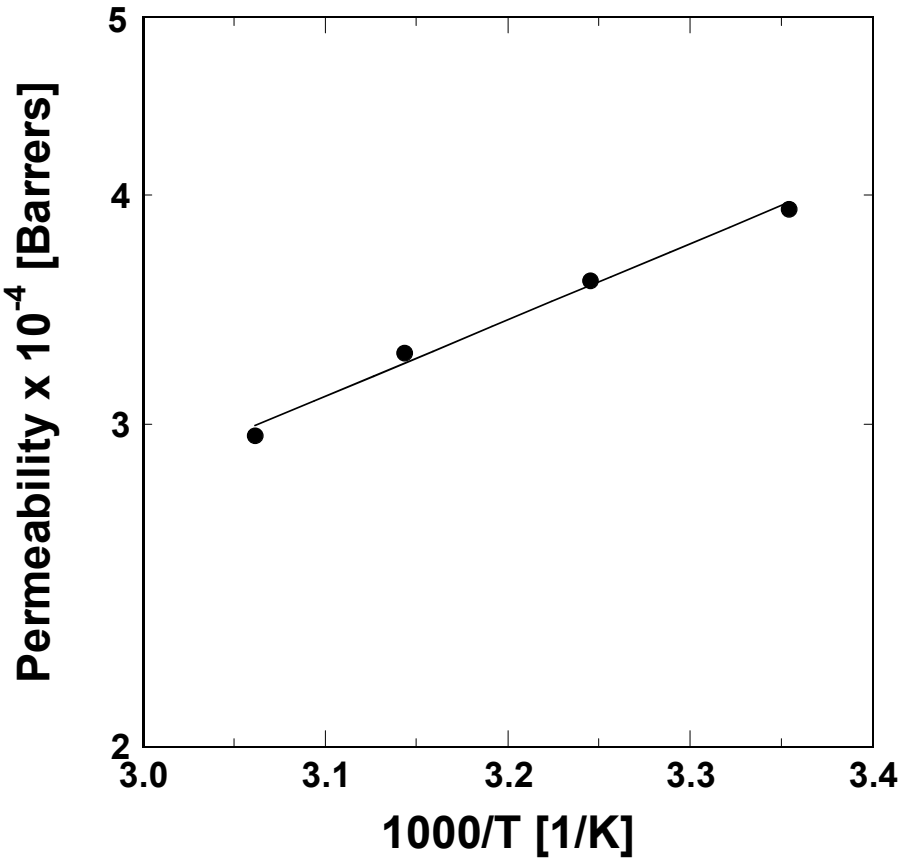

Figure 3.11a: Effect of temperature on C_3H_8 permeation in PTMSP at 2.36 atm upstream pressure and 1 atm downstream pressure.

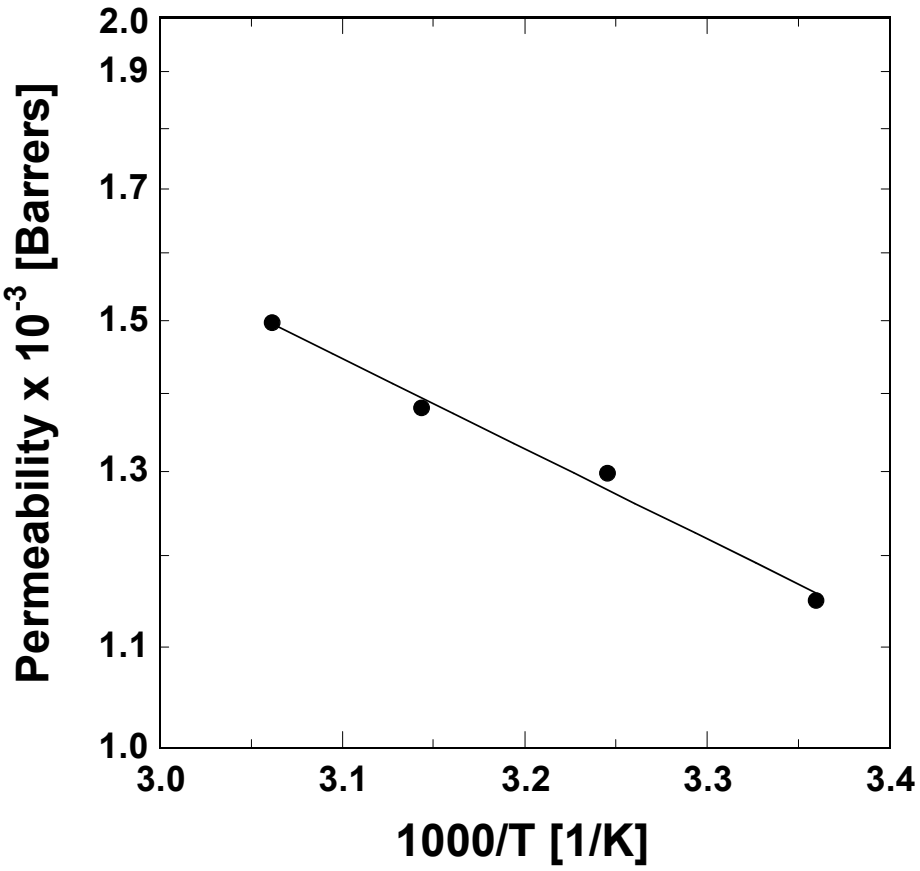

Figure 3.11b:Effect of temperature on C_3F_8 permeation in PTMSP at 2.36 atm upstream pressure and 1 atm downstream pressure.

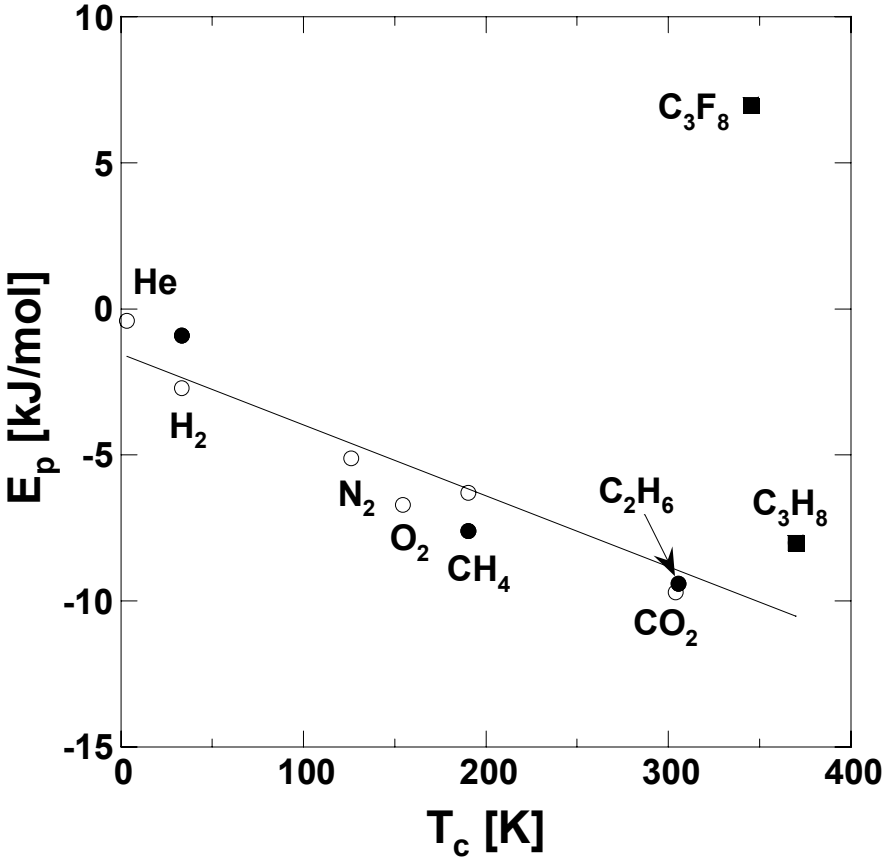

Figure 3.12: Activation energy of permeation of various penetrants in PTMSP. (•) = data from Masuda *et al.* [82]; (o) = unpublished data of T. C. Merkel and Z. He from Membrane Technology and Research, Inc. (Menlo Park, CA); (■) = data from this study. The straight-line in the figure is the least-square fit to the data for all the penetrants except C_3F_8 and is given by: E_P [kJ/mol] = $-1.52 - 0.024 \times T_c$ [K].

CHAPTER 4

Gas and Vapor Sorption and Transport in Poly(tetrafluoroethylene-co-perfluoromethyl vinyl ether)

4.1 SUMMARY

Solubilities of N_2, CO_2, C1-C3 saturated hydrocarbons and their corresponding fluorocarbon analogs and permeabilities of N_2, O_2, CO_2 and C1-C3 saturated hydrocarbons at 35 ^oC are reported in an amorphous, random, rubbery copolymer composed of 50.7 mol % tetrafluoroethylene and 49.3 mol % perfluoromethyl vinyl ether, TFE/PMVE49. Solubilities of hydrocarbon penetrants in this fluoropolymer are lower than those of their corresponding fluorocarbon analogs due to less favorable interactions of the fluorinated polymer with the hydrocarbon penetrants than with the fluorocarbon penetrants. While linear correlations between the natural logarithm of hydrocarbon gas solubility and penetrant critical temperature in hydrocarbon polymers often have slope values of about 0.019 K^{-1} at 35 ^oC, this fluoropolymer has a much lower slope value, 0.011 K^{-1}. Hydrocarbon/nitrogen permeability selectivity is much lower in TFE/PMVE49 than in hydrocarbon-based rubbery polymers like PDMS. This effect is, to a very large extent, a result of hydrocarbon solubility suppression in the fluoropolymer, due to less favorable hydrocarbon-fluorocarbon interactions.

4.2 INTRODUCTION

In the previous chapter, interactions of hydrocarbon polymers with fluorocarbon penetrants were less favorable than interactions with hydrocarbon penetrants. The effect of these interactions on gas transport properties was greater in the low free volume rubbery polymer, PDMS, than in high free volume, glassy PTMSP. If the interactions between fluorocarbons and hydrocarbons are weaker in general than those between two hydrocarbons, then one might expect low hydrocarbon solubility in fluoropolymers. To explore this hypothesis, we present sorption data for C1-C3, C5 and C6 alkanes and C1-C3 saturated fluorocarbons in a rubbery, fluorinated, random copolymer containing 50.7 mol % tetrafluoroethylene (TFE) and 49.3 mol % perfluoromethyl vinyl ether (PMVE), called TFE/PMVE49. The sorption results show the effect of hydrocarbon-fluorocarbon interactions on the slope of the linear relationship between ln$S$ and T_c (eq 2.23). N_2, CO_2 and C1-C3 hydrocarbon permeabilities in this polymer are also reported. The effect of hydrocarbon-fluorocarbon interactions on hydrocarbon permeabilities in this polymer is discussed.

4.3 EXPERIMENTAL

4.3.1 Materials

TFE/PMVE49 was kindly provided by Dr. Mike Coughlin of DuPont-Dow Elastomers (Wilmington, DE). The chemical structure of this perfluoroelastomer is shown in Figure 4.1. Isotropic dense films of this polymer were prepared from a 2%

(w/v) solution (*i.e.*, 2 g of polymer per 100 cm^3 of solvent) in a volatile, fluorinated solvent, PF5060 (3M, Minneapolis, MN). The films were dried at ambient conditions. The polymer film density was determined to be 1.992 ± 0.005 g/cm^3 which agrees with the value of 2.0 g/cm^3 provided by the company.

N_2, CO_2, CH_4 and C_2H_6 were obtained from National Specialty Gases (Raleigh, NC) and Matheson TriGas (Austin, TX), CF_4 and C_2F_6 from Scott Specialty Gases (Durham, NC) and Matheson TriGas (Austin, TX), and C_3H_8 and C_3F_8 from Machine and Welding (Raleigh, NC) and Matheson TriGas (Austin, TX). All gases had a purity of at least 99.5% and were used as received.

4.3.2 Characterization

Pure gas sorption experiments were performed as described in section 2.2.1, in the order N_2, CO_2, CH_4, CF_4, C_2H_6, C_3H_8, C_2F_6 and C_3F_8. N_2 sorption was also measured after each of the other penetrants to determine whether the polymer film had undergone significant structural changes during the sorption process. Sorption experiments were continued only after the N_2 sorption isotherm matched the initially measured values.

Pure gas permeability coefficients were measured at 35 ^oC as a function of upstream pressure, in a constant volume/variable pressure apparatus described in section 2.2.2. After measurement of each penetrant, N_2 permeation was measured at 4.4 atm upstream pressure. Further permeation measurements with other penetrants were performed only after the N_2 permeability matched the originally measured value.

4.4 RESULTS AND DISCUSSION

4.4.1 Sorption

Figures 4.2(a-d) present sorption isotherms of N_2, CO_2, and C1-C3 saturated hydrocarbon and fluorocarbon penetrants in TFE/PMVE49 at 35 ^{o}C. The isotherms for the lighter, low sorbing gases are linear while the higher sorbing penetrants exhibit isotherms that are convex to the pressure axis. This is consistent with the generally expected nature of gas and vapor sorption isotherms in rubbery polymers [81]. Comparison of fluorocarbon and hydrocarbon gas/vapor sorption isotherms (Figures 4.2(b-d)) reveals that the hydrocarbon penetrants sorb less than their fluorocarbon analogs in TFE/PMVE49, which is consistent with previous reports of sorption in perfluorinated polymer matrices [88]. For the C1 penetrants, this trend is not unexpected because CF_4 has a higher critical temperature than CH_4 (*cf.* the Appendix at the end of this dissertation) and, therefore, CF_4 is expected to be more soluble than CH_4 on the basis of the ln$S$-T_c relationship. However, C_2H_6 and C_3H_8 have higher critical temperatures than C_2F_6 and C_3F_8, respectively, thus indicating that factors other than condensability are also influencing the sorption process.

Figure 4.3 presents the condensability-normalized infinite dilution solubility as a function of inverse penetrant critical volume. As discussed in section 2.3.2, presenting the data in this fashion helps separate the three principal factors governing penetrant sorption in a polymer: (i) penetrant condensability, (ii) penetrant size and (iii) polymer-penetrant interactions. From Figure 4.3, condensability-normalized solubilities of both fluorocarbons and hydrocarbons decrease with increasing penetrant size, consistent with

more energy being required to open larger gaps in the polymer matrix to accommodate larger penetrants. However, at the same penetrant critical volume, hydrocarbon penetrants have a lower condensability-normalized solubility than fluorocarbon penetrants. On this basis, interactions between the hydrocarbon penetrants and the fluoropolymer are less favorable than those between the fluorinated penetrants and the fluoropolymer. This observation agrees with the report of lower fluorocarbon solubility in the hydrocarbon rubbery polymer, PDMS, due to hydrocarbon-fluorocarbon interactions.

Figure 4.4 presents infinite dilution solubility coefficients of N_2, C1-C3, C5 and C6 linear alkanes in TFE/PMVE49 as a function of critical temperature. As discussed earlier, gas solubility in polymers correlates well with measures of penetrant condensability such as critical temperature. The slope of a linear relation between ln$S$ and T_c is expected to have a value of 0.019 K^{-1} at 35 ^oC, based on theoretical considerations (eqs 2.24 - 2.25), and experimentally obtained data for a wide variety of polymers also provide best fit slope values within a narrow range around this value (*cf.* Table 2.2). However, the least squares best fit straight line to the data in Figure 4.4 has a significantly lower slope value (0.011 K^{-1}). Therefore, with increasing condensability, hydrocarbon solubility in TFE/PMVE49 increases much less than in typical hydrocarbon polymers such as those in Table 2.2. Such a difference in slopes is also seen for fluorocarbon gas sorption in hydrocarbon polymers like PDMS and low density poly(ethylene) (LDPE) (*cf.* Figures 4.5(a-b)). Gee's correlation, in its present form (eq 2.24), does not predict this difference in slope at constant temperature. However, eq 2.24 assumes that the polymer-penetrant interaction parameter, χ, varies negligibly from penetrant to penetrant and, therefore, can be assigned a constant value. Experimental

results of gas sorption in polymers show that χ can vary significantly among penetrants of the same chemical family sorbing in a polymer. Figures 4.6a and 4.6b present χ values of hydrocarbon and fluorocarbon linear alkanes in PDMS and LDPE [38]. From these figures, in both hydrocarbon polymers, the fluorocarbon penetrants have higher χ values than the hydrocarbons at the same critical temperature due, presumably, to less favorable interactions of fluorocarbons with the hydrocarbon polymers. Also, the χ parameter shows much more variation with increasing carbon number in the fluorocarbon family than in the hydrocarbon family. One way to modify Gee's correlation is to take account of the observed variation in χ with penetrant condensability within a family of penetrants. From Figures 4.6(a-b), the dependence of χ on penetrant critical temperature is linear and can be empirically described as:

$$\chi = \chi_0 + \chi_1 \times T_C \tag{4.1}$$

where χ_0 and χ_1 are adjustable constants. χ_0 and χ_1 are determined from the linear best fit trendline to experimental χ values as a function of T_c within a family of penetrants (*e.g.*, hydrocarbons, fluorocarbons *etc.*). Gee's correlation (eq 2.24) can be modified by using eq 4.1 as follows:

$$\ln S = -(4.5 + \chi_0) + \left(\frac{6}{T} - \chi_1\right) T_c \tag{4.2}$$

The best-fit values of the adjustable parameters, χ_0 and χ_1, for hydrocarbon and fluorocarbons in PDMS and LDPE and for hydrocarbon sorption in TFE/PMVE49 are listed in Table 4.1. From Table 4.1, taking account of the empirical dependence of χ on Tc brings the predicted slope in agreement with the slope obtained by fitting the experimental solubility data for these polymers.

The lower slope for hydrocarbons in TFE/PMVE49 also implies that, for extremely large hydrocarbons, the differences in hydrocarbon solubility between this polymer and a polymer with a slope value around 0.019 K^{-1} can be very large. One example of this is shown in Figure 4.7, which compares the ln$S$-T_c relationship of polysulfone, a commercial membrane polymer which has a slope value of 0.017 K^{-1}, with that of TFE/PMVE49. If the trendlines in the figure are assumed to be valid beyond the range of presently available experimental data, then for a very large hydrocarbon like *n*-decane, having a critical temperature of 617.7 K, the difference in solubility in the two polymers is estimated to be over an order of magnitude, with the fluoropolymer exhibiting lower solubility. Polymers like TFE/PMVE49, which have low hydrocarbon solubility, may be less susceptible to plasticization in hydrocarbon environments than hydrocarbon-based polymers, and they may, therefore, provide more stable membranes for applications such as olefin/paraffin separation and natural gas purification [89-91].

4.4.2 Permeability

The permeabilities of N_2, O_2, CO_2 and C1-C3 hydrocarbon alkanes in TFE/PMVE49 at 35 ^oC are presented in Figure 4.8. N_2, O_2 and CH_4 exhibit constant

permeabilities at all upstream pressures tested, while the permeabilities of CO_2, C_2H_6 and C_3H_8 increase with increasing upstream pressure. This is consistent with the behavior of permanent gases and higher condensability penetrants in other rubbery polymers, *e.g.*, PDMS [25]. However, the selectivities of PDMS for hydrocarbons over a permanent gas like N_2 are much higher than in TFE/PMVE49. Table 4.2 shows the ratios of hydrocarbon to N_2 selectivity values, calculated from infinite dilution permeabilities, in these two polymers. The ratio of infinite dilution solubility selectivities and diffusivity selectivities are also shown to demonstrate the source of the difference in overall selectivity in the two polymers. The diffusivity selectivities were calculated from infinite dilution diffusion coefficients determined from eq 2.6 and infinite dilution permeability and solubility values (from Figures 4.4 and 4.8). From Table 4.2, solubility selectivity differences play a major role in the overall hydrocarbon/N_2 selectivity differences in the two polymers. For example, propane/N_2 selectivity is more than an order of magnitude higher in PDMS than in TFE/PMVE49 due to nearly an order of magnitude difference in the solubility selectivity. The propane/N_2 diffusivity selectivity of TFE/PMVE49 is only a third lower than that of PDMS. Thus, the suppression of hydrocarbon solubility in the fluoropolymer, due to weak hydrocarbon-fluorocarbon interactions, plays a major role in influencing gas transport through the polymer.

The CO_2/CH_4 pure gas selectivity of TFE/PMVE49 is approximately 6 at infinite dilution conditions. Also, CO_2 permeability increases with increasing pressure, suggesting the possibility of plasticization. This will reduce the size selectivity of the membrane, and hence its mixed-gas selectivity at higher pressures is likely to be lower.

4.4.3 Diffusivity

Infinite dilution diffusion coefficients of gases in TFE/PMVE49 are presented in Figure 4.9 as a function of penetrant critical volume. Diffusion coefficients of gases in a rubbery polymer (PDMS) and a typical glassy polymer (polysulfone) are also presented to compare the size-sieving abilities of TFE/PMVE49 with commercial gas and vapor separation membrane materials. Membranes for CO_2/CH_4 separation derive their separation ability, in large part, from strong size-sieving abilities. From Figure 4.9, diffusion coefficients in polysulfone decrease by nearly six orders of magnitude from helium (V_c = 57.4 cm^3/mol) to *n*-butane (V_c = 255 cm^3/mol), while in PDMS, the decrease in diffusion coefficients is only about 2 orders of magnitude over the same penetrant range. Thus, polysulfone has a much greater size sieving ability and this translates into high selectivities for smaller gas molecules over larger gas molecules. In contrast, PDMS is actually more permeable to larger penetrants like ethane and propane than permanent gases like nitrogen, because the high solubility of these condensable penetrants as compared to permanent gas solubility overshadows the moderate size-selectivity of this rubbery polymer. From the figure, the size-sieving ability or diffusivity selectivity of TFE/PMVE49 is closer to that of rubbery PDMS than the glassy polysulfone.

The variation of diffusion coefficients with critical volume (a measure of penetrant size) is usually described by the empirical equation [92]:

$$D = \frac{\tau}{V_c^{\eta}} \tag{4.3}$$

where τ and η are adjustable parameters. η provides a measure of the rate of decrease of diffusion coefficients with increasing penetrant size; the higher the value of η, the greater the diffusivity selectivity of the polymer. From Figure 4.9, the η values of PDMS and polysulfone are 2.3 and 8.4, respectively, indicating the much greater size-sieving ability of polysulfone. TFE/PMVE49 has an η value of 2.9 ($\pm$ 0.1), based on the best-fit trendline through the data in Figure 4.9, which is much lower than the η value of polysulfone. Glassy fluoropolymers may provide greater diffusivity selectivity and hence overall selectivity for CO_2/CH_4 separation. Higher CO_2/CH_4 selectivity, coupled with low hydrocarbon solubility due to fluorocarbon-hydrocarbon interactions, may provide stable, high performance membrane materials for CO_2 removal from natural gas.

4.5 CONCLUSIONS

C1-C3 hydrocarbons exhibit lower sorption in TFE/PMVE49 than their corresponding fluorocarbon analogs due to less favorable interactions of the fluorinated polymer matrix with the hydrocarbon penetrants than with the fluorocarbon penetrants. The slope of the linear correlation between natural logarithm of gas solubility and gas critical temperature is 0.011 K^{-1}, which is much lower than that exhibited by other polymers as well as that expected on the basis of a thermodynamic model by Gee. The lower slope is a consequence of hydrocarbon solubility suppression due to fluorocarbon-

hydrocarbon interactions and is predicted satisfactorily by a modified form of Gee's correlation, which takes into account the variability in χ among penetrants within the same family of compounds, *e.g.*, hydrocarbon linear alkanes. The hydrocarbon-fluorocarbon interactions play a major role in influencing hydrocarbon penetrant permeation through this fluoropolymer. TFE/PMVE49 has a size-sieving ability that is closer to rubbery polymers like PDMS than glassy polymers like polysulfone.

Table 4.1 Comparison of slope of ln$S$-T_c trendlines for gas sorption in polymers with theoretical predictions from eqs 2.25 and 4.2.

Polymer	***Penetrant***	χ_0	χ_1	***Original slope*** [a] ***(eq 2.25)***	***Modified slope (eq 4.2)***	***Slope from experimental data***
PDMS	Hydrocarbons	-0.20	0.0015	0.020	0.0185	0.018
	Fluorocarbons	-0.27	0.007	0.020	0.013	0.013
LDPE	Hydrocarbons	0.99	-0.0001	0.020	0.020	0.019
	Fluorocarbons	0.59	0.011	0.020	0.009	0.009
TFE/PMVE49	Hydrocarbons	-1.39 ± 0.02	0.0077 ± 0.0001	0.019	0.0113	0.011 ± 0.0003

[a] T = 35 ^{o}C for TFE/PMVE49 data and 25 ^{o}C for the remaining data.

Table 4.2 Hydrocarbon/nitrogen permselectivity, solubility selectivity and diffusivity selectivity in PDMS[25] and TFE/PMVE49 at 35 ^{o}C.

Hydrocarbon	***TFE/PMVE49***			***PDMS***		
	P/P(N_2)	***S/S(N_2)***	***D/D(N_2)***	***P/P(N_2)***	***S/S(N_2)***	***D/D(N_2)***
CH_4	0.56	1.7	0.33	3.0	4.7	0.64
C_2H_6	0.71	3.6	0.20	8.3	24	0.34
C_3H_8	0.72	6.1	0.12	10.3	56	0.18

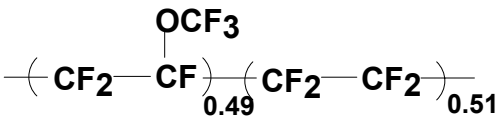

Figure 4.1: Chemical structure of TFE/PMVE49.

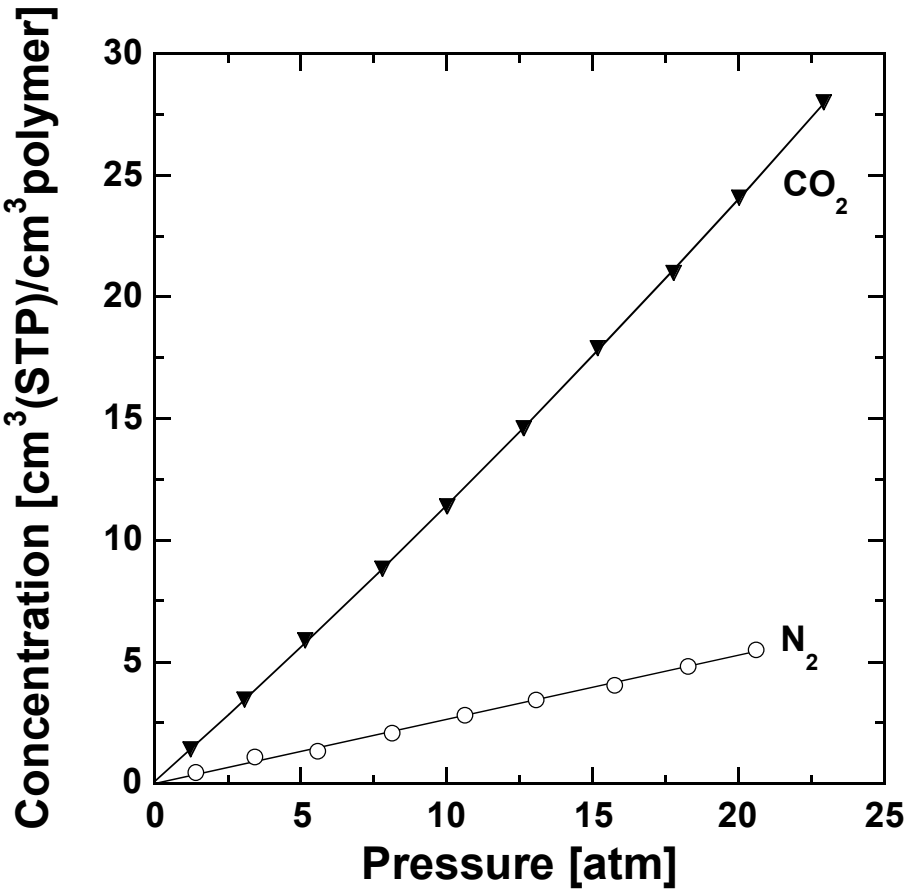

Figure 4.2a: Sorption isotherms of N_2 and CO_2 in TFE/PMVE49 at 35 ^{o}C.

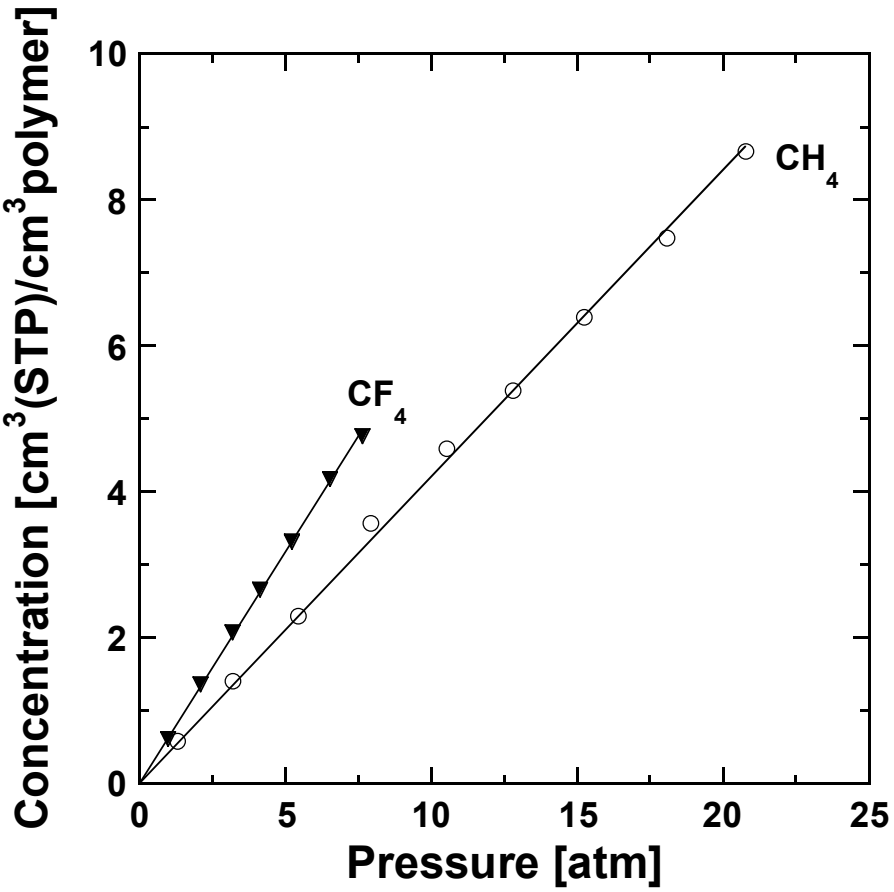

Figure 4.2b: Sorption isotherms of CH_4 and CF_4 in TFE/PMVE49 at 35 ^{o}C.

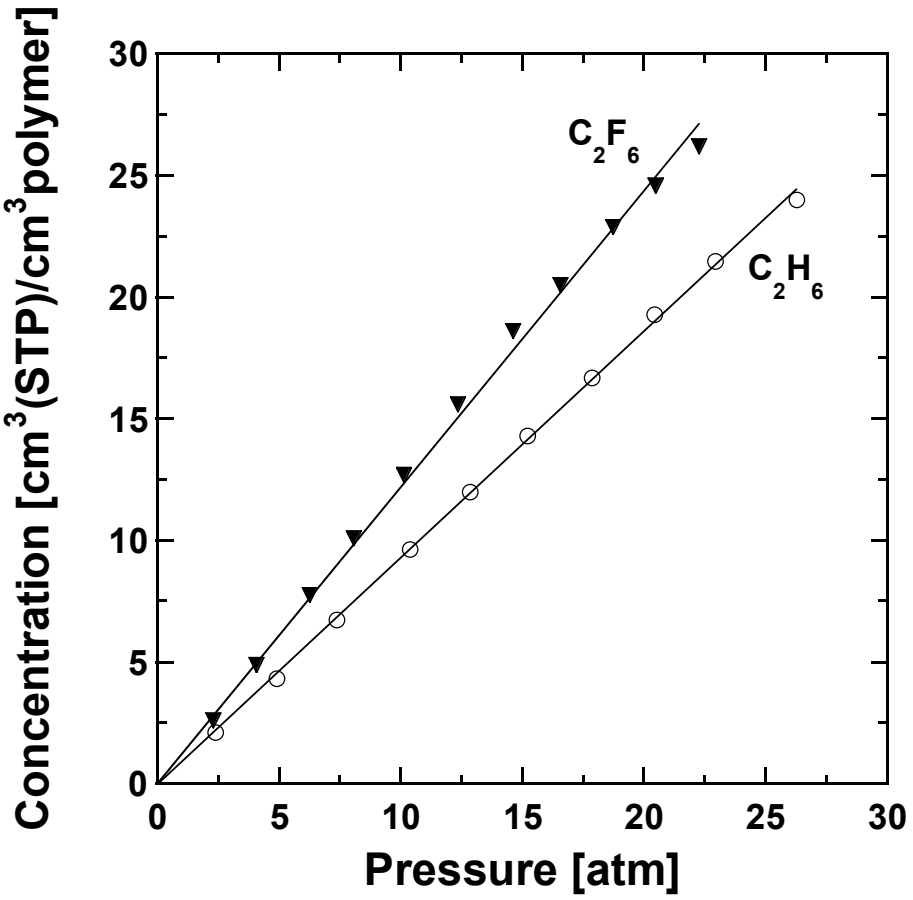

Figure 4.2c: Sorption isotherms of C_2H_6 and C_2F_6 in TFE/PMVE49 at 35 ^oC.

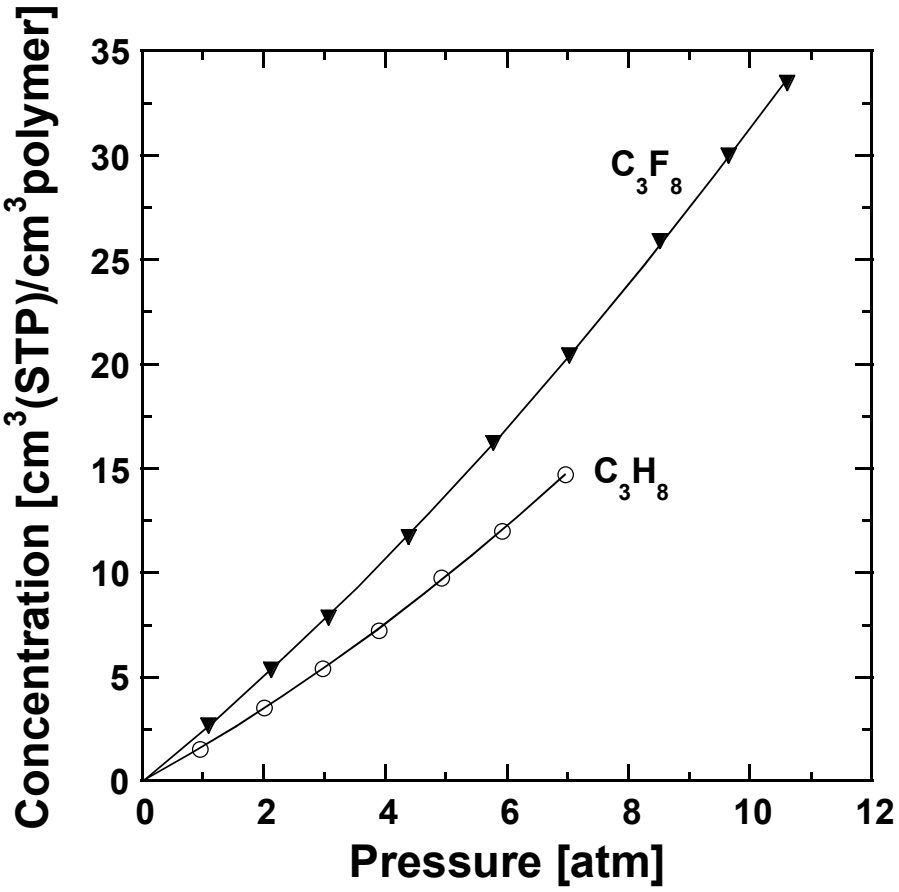

Figure 4.2d: Sorption isotherms of C_3H_8 and C_3F_8 in TFE/PMVE49 at 35 ^oC.

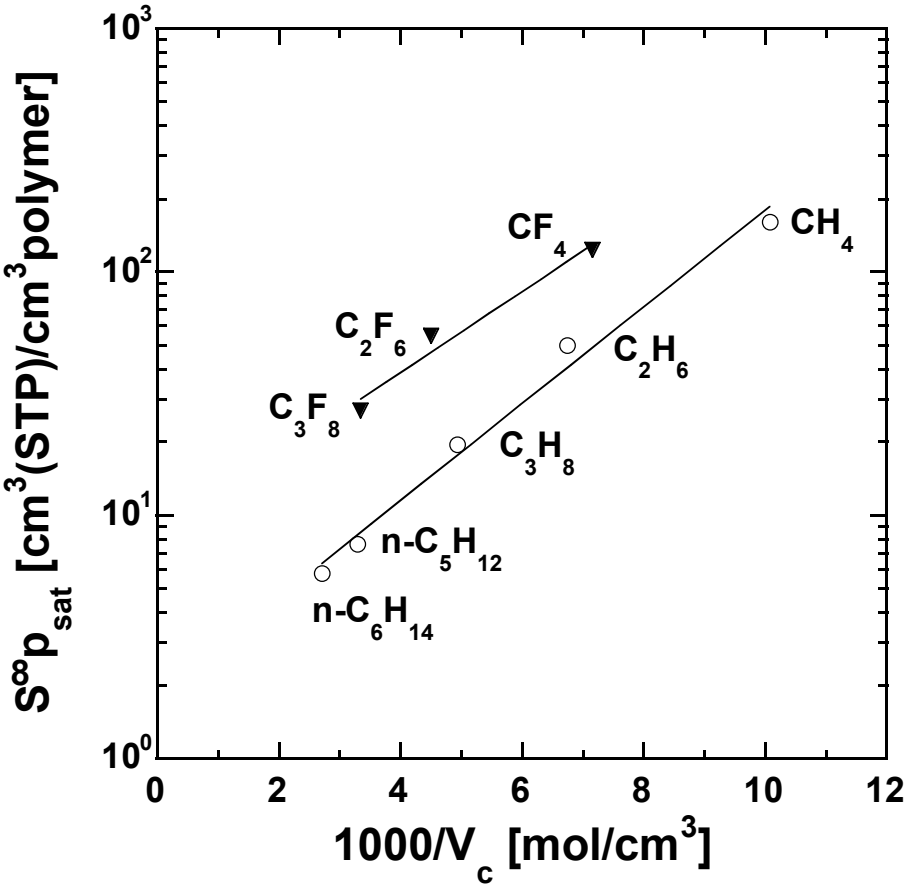

Figure 4.3: Condensability-normalized infinite dilution solubility of hydrocarbon and fluorocarbon penetrants in TFE/PMVE49 at 35 ^oC.

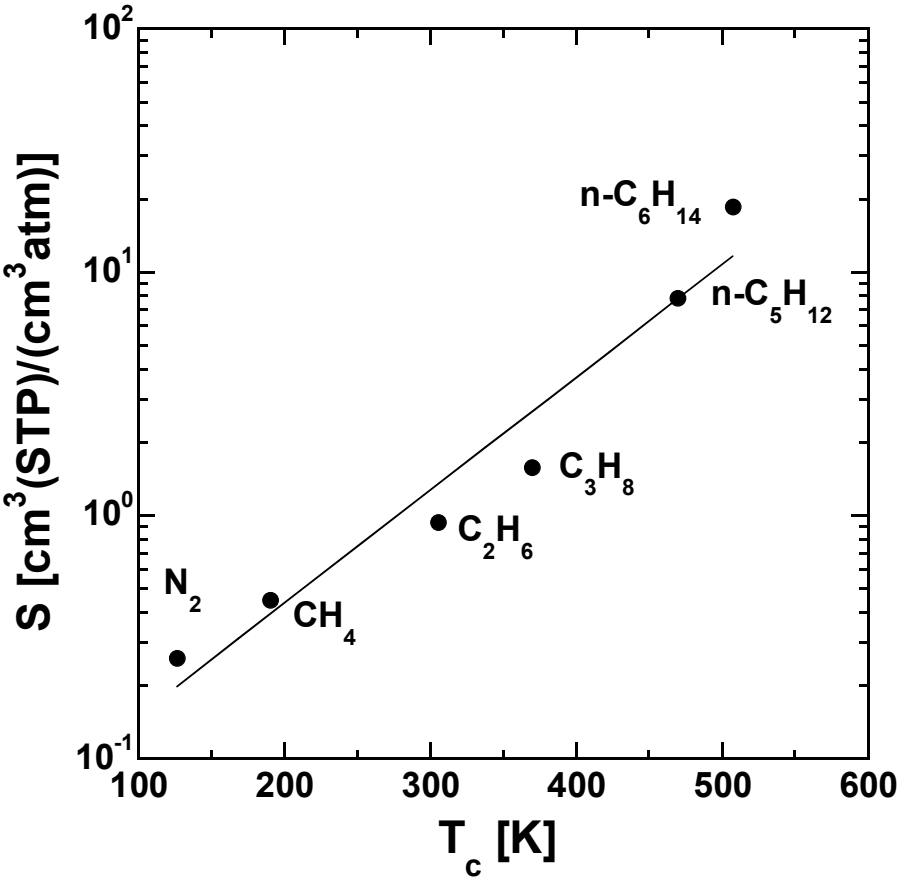

Figure 4.4: Infinite dilution solubility of N_2 and C1-C3 hydrocarbons in TFE/PMVE49 at 35 ^{o}C as a function of penetrant critical temperature. The best fit trendline through the experimental data has the equation: $\ln(S\ [\mathrm{cm}^3(\mathrm{STP})/(\mathrm{cm}^3\ \mathrm{atm})]) = -2.96 + 0.011 T_c\ [\mathrm{K}]$.

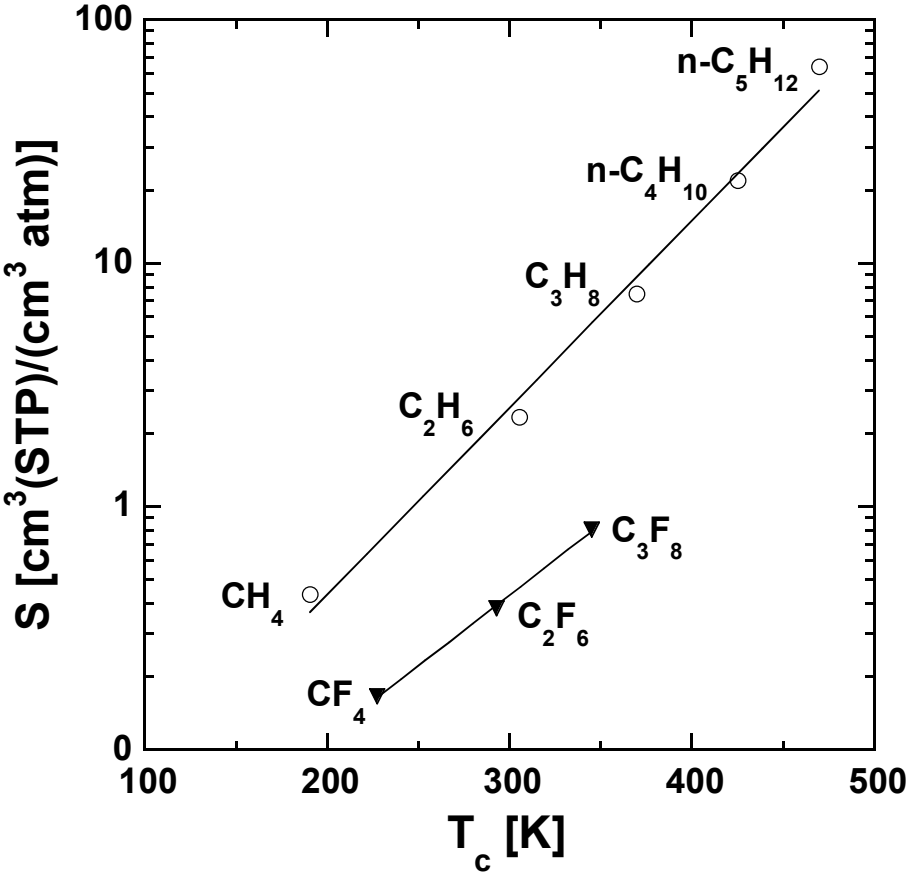

Figure 4.5a: Infinite dilution solubility coefficients of C1-C5 linear alkanes and C1-C3 fluorocarbons in PDMS at 25 °C as a function of penetrant critical temperature. The best fit trendlines through the experimental data have the equations: $\ln(S\ [\mathrm{cm}^3(\mathrm{STP})/(\mathrm{cm}^3\ \mathrm{atm})]) = -4.37 + 0.018T_c\ [\mathrm{K}]$ for the hydrocarbons and $\ln(S\ [\mathrm{cm}^3(\mathrm{STP})/(\mathrm{cm}^3\ \mathrm{atm})]) = -4.85 + 0.013T_c\ [\mathrm{K}]$ for the fluorocarbons [38].

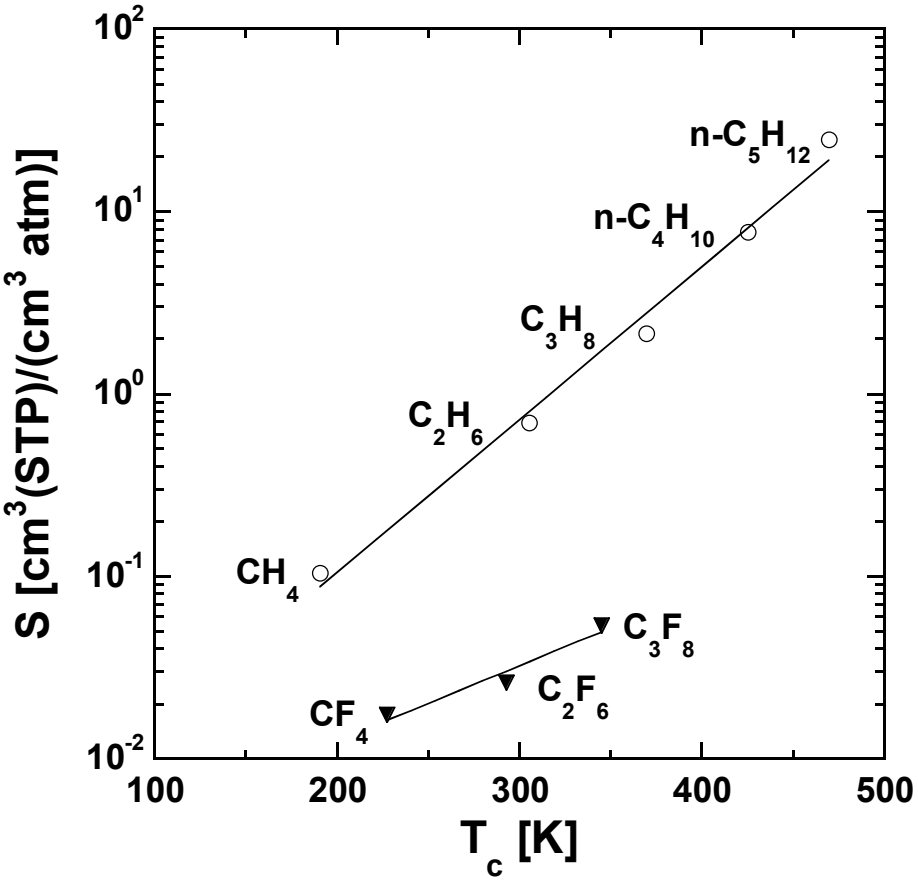

Figure 4.5b: Infinite dilution solubility coefficients of C1-C5 linear alkanes and C1-C3 fluorocarbons in LDPE at 25 °C as a function of penetrant critical temperature. The best fit trendlines through the experimental data have the equations: $\ln(S\ [\mathrm{cm}^3(\mathrm{STP})/(\mathrm{cm}^3\ \mathrm{atm})]) = -6.12 + 0.019T_c\ [\mathrm{K}]$ for the hydrocarbons and $\ln(S\ [\mathrm{cm}^3(\mathrm{STP})/(\mathrm{cm}^3\ \mathrm{atm})]) = -6.27 + 0.009T_c\ [\mathrm{K}]$ for the fluorocarbons [38].

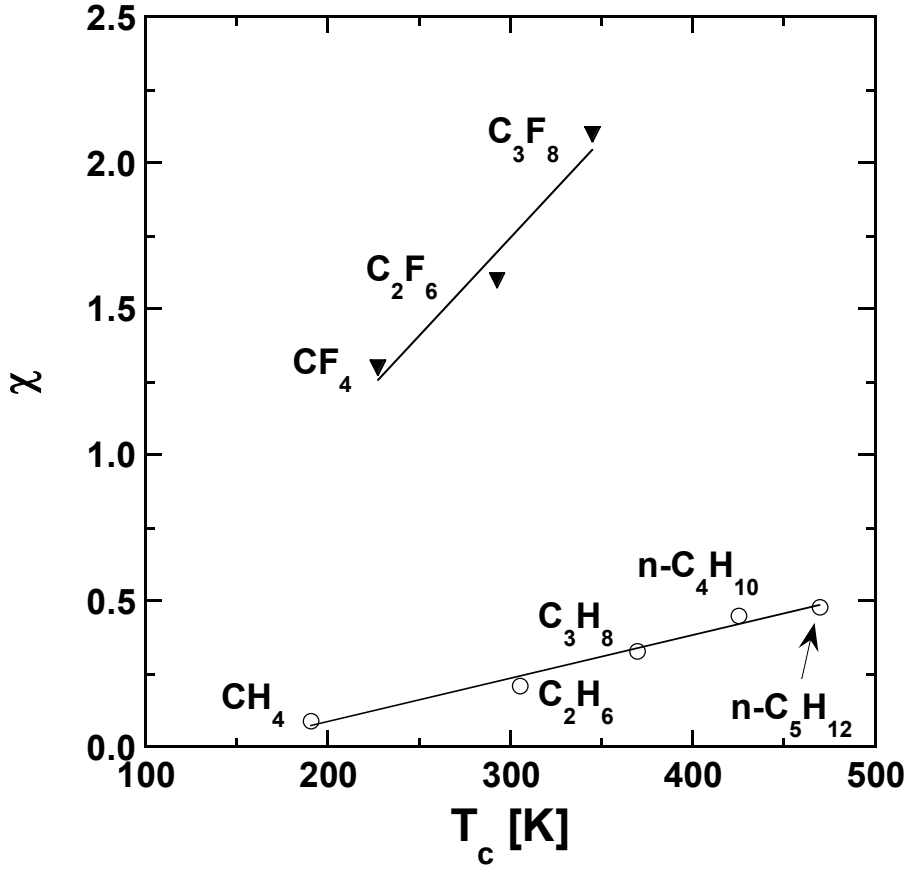

Figure 4.6a: χ values of C1-C5 linear alkanes and C1-C3 fluorocarbons in PDMS at 25 ^{o}C as a function of penetrant critical temperature. The best fit trendlines through the experimental data have the equations: $\chi = -0.2 + 0.0015T_c$ [K] for the hydrocarbons and $\chi = -0.27 + 0.007T_c$ [K] for the fluorocarbons [38].

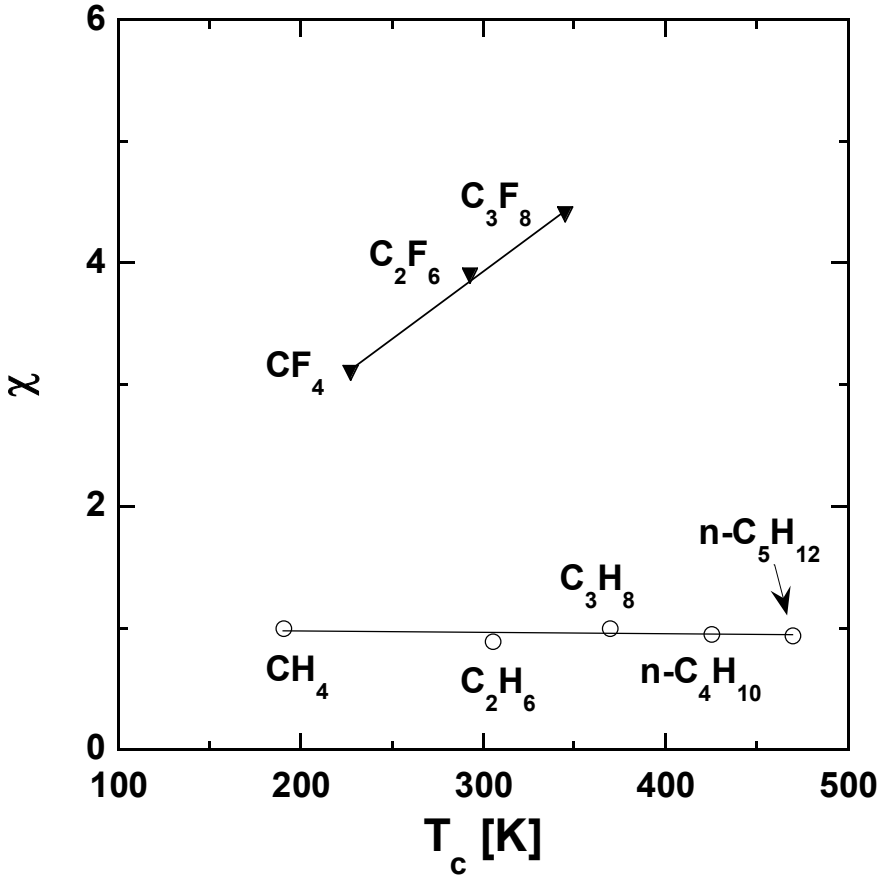

Figure 4.6b: χ values of C1-C5 linear alkanes and C1-C3 fluorocarbons in LDPE at 25 ^{o}C as a function of penetrant critical temperature. The best fit trendlines through the experimental data have the equations: $\chi = 0.99 - 0.0001T_c$ [K] for the hydrocarbons and $\chi = 0.59 + 0.011T_c$ [K] for the fluorocarbons [38].

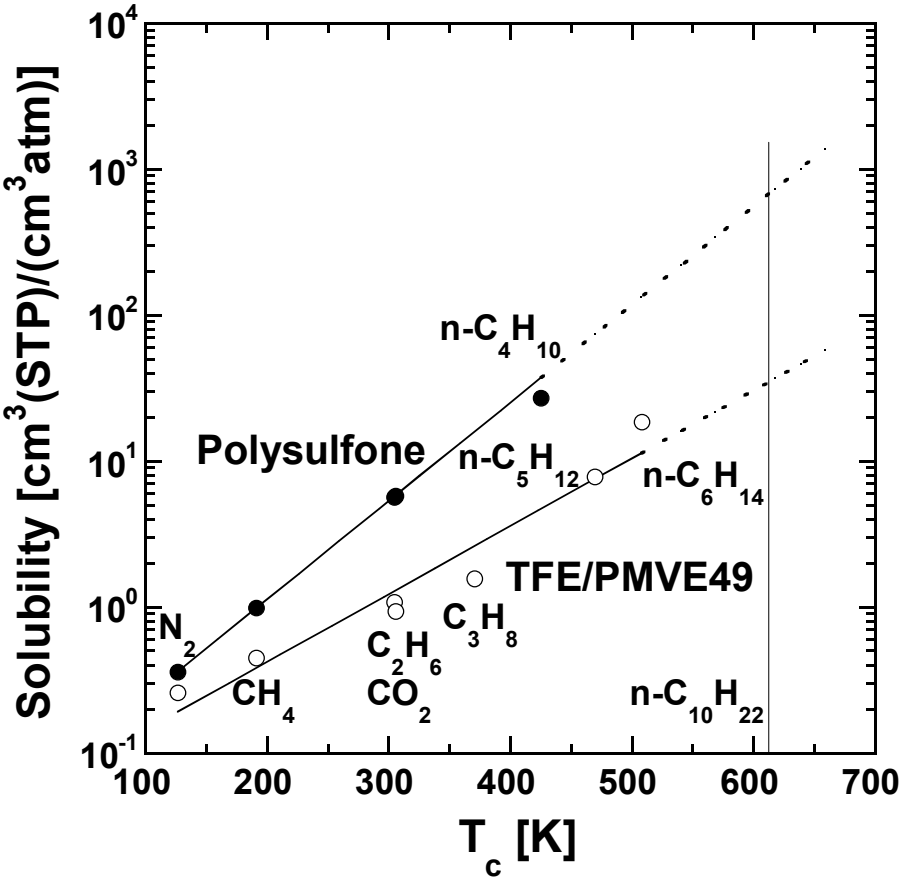

Figure 4.7: Solubility of N_2 and C1-C6 hydrocarbons in polysulfone [51] and TFE/PMVE49 at 35 °C as a function of penetrant critical temperature. Polysulfone data are at 10 atm except for *n*-C_4H_{10} which is at infinite dilution. Data for TFE/PMVE49 have been extrapolated to infinite dilution conditions. The vertical line at a T_c value of 617.7 K corresponds to the critical temperature of *n*-decane.

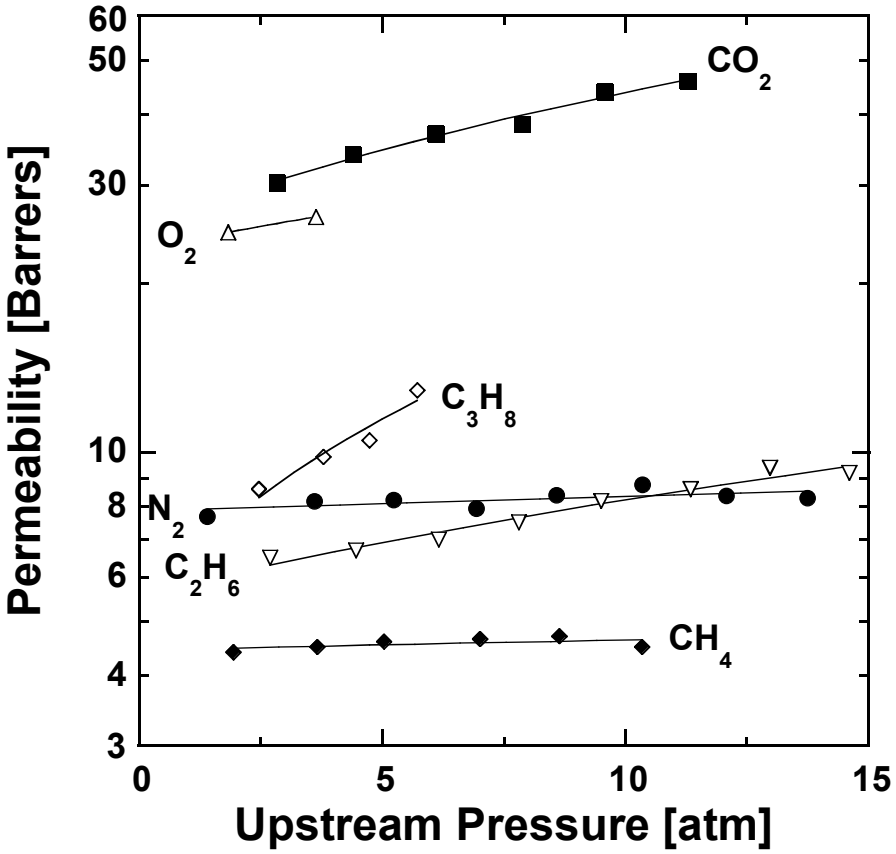

Figure 4.8: Permeabilities of N_2, O_2, CO_2 and C1-C3 saturated hydrocarbons in TFE/PMVE49 at 35 ^{o}C.

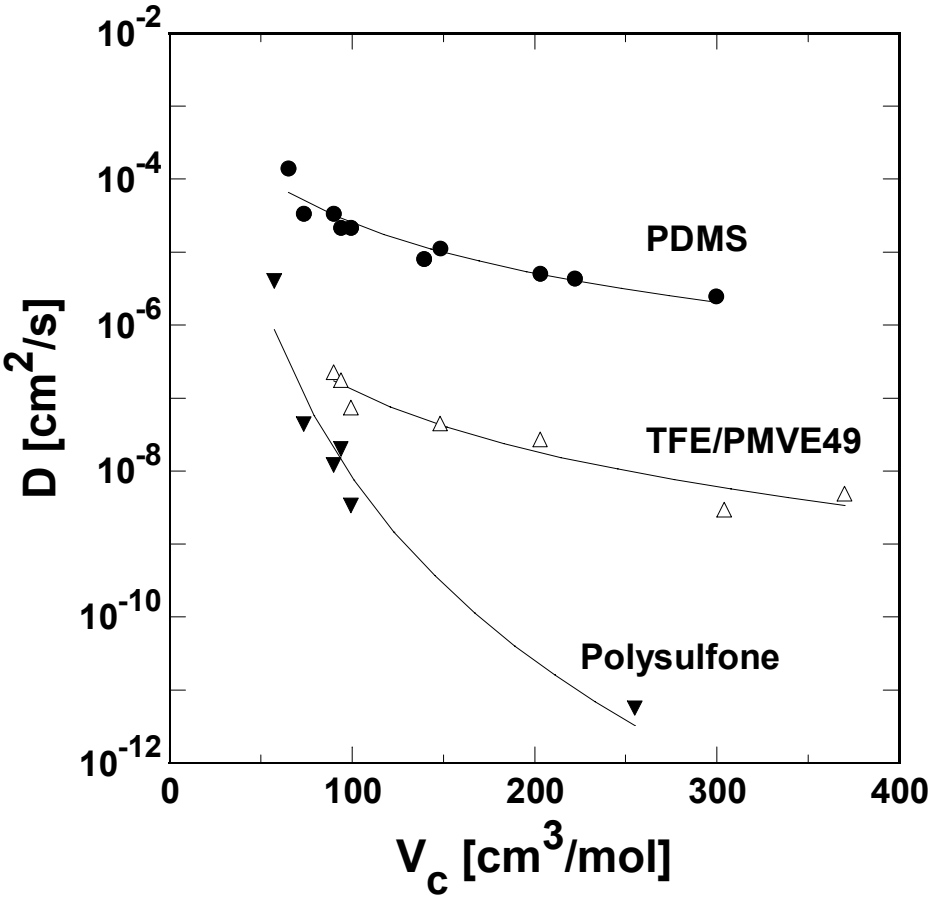

Figure 4.9: Comparison of the variation of infinite dilution diffusion coefficients with penetrant critical volume in TFE/PMVE49 with that in a typical rubbery (PDMS) [25] and glassy (polysulfone) polymer [51,93-95]. The trendlines in the figure satisfy eq 4.3, where η is a measure of the size-sieving ability or size-selectivity of the polymer to penetrants. The best-fit values of η in the plot are: PDMS: 2.3; Polysulfone: 8.4; TFE/PMVE49: 2.9 ± 0.1.

CHAPTER 5

Gas and Vapor Sorption and Transport in Poly(2,2,4-trifluoro-5-trifluoromethoxy-1,3-dioxole-*co*- tetrafluoroethylene)

5.1 SUMMARY

The solubilities of N_2, CO_2, CH_4, C_2H_6, C_3H_8 and C_3F_8 and permeabilities of N_2, O_2, CO_2, CH_4, C_2H_6, and C_3H_8 were determined in a glassy, amorphous fluoropolymer prepared from 80 mol % 2,2,4-trifluoro-5-trifluoromethoxy-1,3-dioxole (TTD) and 20 mol % tetrafluoroethylene (TFE), commercially known as Hyflon AD 80. This polymer exhibits lower increases in hydrocarbon gas and vapor solubility with increasing penetrant critical temperature than conventional hydrocarbon polymers. Based on a best fit of the natural logarithm of solubility versus critical temperature, Hyflon AD 80 should have much lower solubility for high molar mass hydrocarbon compounds (*e.g.*, *n*-decane) than conventional hydrocarbon polymers. Pure gas CO_2/CH_4 separation properties of this polymer are comparable with those of some hydrocarbon polymers considered for natural gas purification. When exposed to a feed stream containing a mixture of CO_2 and CH_4, the polymer exhibits a CO_2 permeability of approximately 250 Barrers and a CO_2/CH_4 mixed-gas selectivity of 10.6 at 1.6 atm CO_2 partial pressure. The mixed gas selectivity decreases minimally as CO_2 partial pressure increases to 10.6 atm. The mixed gas selectivity is also maintained when moderate amounts of toluene and *n*-hexane are present in the CO_2-CH_4 feed stream. Diffusion coefficients, calculated from pure gas permeability and solubility coefficients, suggest membrane plasticization at higher pressures of CO_2 and C_2H_6. The polymer also exhibits reversible hysteresis in C_3H_8 permeability with pressure.

5.2 INTRODUCTION

In the previous chapter, the fluoropolymer, TFE/PMVE49, was seen to have low solubility for hydrocarbon compounds, as desired in our strategy for achieving plasticization-resistant membranes for CO_2 removal from natural gas. However, the size sieving ability of this rubbery polymer was much lower than that of conventional glassy polymers that exhibit high selectivities for CO_2/CH_4 separation. Glassy fluoropolymers may have higher CO_2/CH_4 selectivities and also exhibit low solubility for hydrocarbon compounds.

Gas transport properties of high-free-volume, glassy fluoropolymers have been studied [78,88]. However, these polymers exhibit low CO_2/CH_4 selectivities. For example, at 35 ^oC and low to moderate pressures (up to 10 atm), the pure gas CO_2/CH_4 selectivities of AF1600 and AF2400 are 6.2 and 5.6, respectively [78,88]. A lower free volume glassy polymer would be expected to possess greater size-sieving ability and, therefore, greater CO_2/CH_4 selectivity. Also, gas molecules sorbing into a lower free volume matrix may find themselves, on average, in closer proximity to polymer chains in a dense polymer matrix and, therefore, experience stronger interactions with the surrounding polymer than they would in a high free volume material. Thus, it is of interest to study hydrocarbon solubility in a lower free volume fluoropolymer and compare it with that in higher free volume fluoropolymers and in hydrocarbon polymers. With these objectives in mind, we report gas solubility, permeability and diffusivity of N_2, CO_2 and C1-C3 hydrocarbons as well as C_3F_8 solubility in a low free volume, glassy, amorphous copolymer composed of 80 mol % 2,2,4-trifluoro-5-trifluoromethoxy-1,3-

dioxole (TTD) and 20 mol % tetrafluoroethylene (TFE), commercially known as Hyflon AD 80. The structure of Hyflon AD 80 is presented in Figure 5.1a [96]. This polymer has a glass transition temperature of 134 °C and a FFV of 0.197, which was estimated using Bondi's group contribution method and the reported density value of 1.918 g/cm^3 [49]. Gas sorption and transport properties of this fluoropolymer are compared with those of Teflon AF1600 and AF2400, a structurally similar family of high free volume, glassy fluoropolymers, whose chemical structures are depicted in Figure 5.1b. While permeabilities of H_2, N_2, O_2, CO_2 and CH_4 have been reported earlier for Hyflon AD 80 [97], we could not find reports of solubility or the pressure dependence of permeability or solubility in this polymer. Additionally, diffusion coefficients of gas molecules in this polymer have not been reported. The pure-gas-based CO_2/CH_4 separation performance of Hyflon AD 60, a copolymer containing 60 mol % TTD and 80 mol % TFE, is also reported.

5.3 EXPERIMENTAL

5.3.1 Materials

Hyflon AD 60 and Hyflon AD 80 were purchased from the Ausimont Company (Thorofare, NJ), now Solvay Solexis. Uniform, isotropic films with thicknesses ranging from 35 to 90 μm were cast from 2% (w/v) solution (*i.e.*, 2 g of polymer per 100 cm^3 of solvent) in PF5060, a perfluorinated, volatile solvent from 3M (St. Paul, MN). The films were dried at ambient conditions for 2-3 days and then utilized for sorption and

permeation measurements. The pure gases and vapors used in the experiments had a purity of at least 99.5%. N_2, O_2, CO_2, CH_4 and C_2H_6 were obtained from National Specialty Gases (Durham, NC) and Matheson TriGas (Austin, TX). C_3H_8 and C_3F_8 were purchased from Machine and Welding (Raleigh, NC) and Matheson TriGas (Austin, TX). A gas mixture containing 20% CO_2 in CH_4 and another containing 10% CO_2, 50 ppm toluene and 500 ppm *n*-hexane in CH_4 (primary standards with analyses provided) were purchased from MG Industries (Wilmington, DE) for the mixed-gas permeation experiments. All gases were used as received.

5.3.2 Characterization

Sorption experiments were performed as described in section 2.2.1, in the following order: N_2, CO_2, CH_4, C_2H_6, C_3H_8 and C_3F_8. A N_2 sorption experiment was also performed after each of the other penetrants to ensure that the polymer film had not undergone significant sorption hysteresis during the experiments. Isotherms for subsequent penetrants were measured only after the N_2 isotherm matched the initially measured isotherm.

Pure gas permeability coefficients for N_2, O_2 and CO_2 were determined using a constant pressure/variable volume apparatus and pure gas permeability coefficients of the hydrocarbons, CH_4, C_2H_6 and C_3H_8, were measured in a constant volume/variable pressure apparatus. Both experimental systems are described in section 2.2.2.

Mixed gas CO_2 and CH_4 permeabilities and CO_2/CH_4 selectivity of Hyflon AD 80 were measured in a constant volume/variable pressure permeation apparatus described in

section 2.2.3. The CO_2-CH_4 feed pressure was 8 - 53.2 atm, while for the hydrocarbon-containing feed, it was set at 35 atm.

5.4 RESULTS AND DISCUSSION

5.4.1 Solubility

Figure 5.2 presents gas sorption isotherms in Hyflon AD 80 at 35 ^{o}C. Except for C_3F_8, which is the most soluble penetrant at high pressures, all isotherms are concave to the pressure axis, which is characteristic of gas sorption in glassy polymers at low to moderate pressures [11]. The infinite dilution solubilities of these gases increase in the order:

$$N_2 < CH_4 < CO_2 \approx C_2H_6 < C_3F_8 < C_3H_8$$

This is also the order of increasing gas critical temperature and, hence, gas condensability. C_3F_8 solubility, while lower than that of C_3H_8 at very low pressures, rises above that of C_3H_8 at higher pressures (*cf.* Figure 5.3). At low pressures, sorption in a glassy polymer occurs preferentially in the frozen microvoids that constitute the non-equilibrium excess free volume of glassy polymers [26]. Molecules sorbing into these pre-existing microvoids at low pressure experience weaker interactions with the polymer matrix than those sorbing into more dense regions of the polymer where a gap must be created to accommodate the penetrant. Therefore, sorption at low pressures is likely to be strongly influenced by penetrant condensability and weakly influenced by interactions with the glassy polymer. This hypothesis is consistent with higher sorption of C_3H_8 at

lower pressures. At higher pressures, interactions with the polymer have a more pronounced effect on solubility as penetrant molecules sorb increasingly into more densified regions of the polymer. Due to its chemical similarity with the polymer, C_3F_8 enjoys more favorable interactions with this fluoropolymer than does C_3H_8, and this better chemical affinity for the polymer is consistent with C_3F_8 solubility exceeding that of C_3H_8 at higher pressures.

Table 5.1 compares the ratio of propane to nitrogen solubility in several hydrocarbon-rich media with that in a perfluorinated liquid and two fluoropolymers. Propane solubility is approximately 65-130 times larger than nitrogen solubility in the hydrocarbon liquids and polymers. In stark contrast, in the perfluorinated liquid, perfluoro-*n*-heptane, the rubbery polymer, TFE/PMVE49, and the high-free-volume, glassy fluoropolymers, AF2400 (fractional free volume, FFV=0.33) and AF1600 (FFV=0.30), propane solubility is only about 5-20 times higher than nitrogen solubility. Since nitrogen is not expected to experience specific interactions with these media, the significant reduction in propane to nitrogen solubility ratio results from dramatically lower than expected propane solubility in the perfluorinated media. From Table 5.1, the ratio of C_3H_8 to N_2 solubility in Hyflon AD 80 at infinite dilution conditions is approximately 6, which is 2.5-3.5 times lower than in the high free volume, glassy fluoropolymers, AF1600 and AF2400, and about 16 times lower than that in poly(ethylene). Thus, the lower free volume glassy fluoropolymer displays much lower sorption for hydrocarbon penetrants, such as C_3H_8, relative to N_2, than higher free volume glassy fluoropolymers or hydrocarbon polymers. While the influence of differences in chemical structure among the fluoropolymers on solubility cannot be ruled out, it is

interesting that C_3H_8/N_2 solubility ratio decreases systematically as fractional free volume decreases among the glassy fluoropolymers (*cf.* Table 5.1). Also, with increasing penetrant pressure, the C_3H_8/N_2 solubility ratio decreases for each glassy fluoropolymer as penetrants sorb to a greater extent into the densified regions of the polymer (*cf.* Figure 5.4). The high free volume AF materials, which have large Langmuir microvoid capacities, exhibit a more significant decrease than that of the lower free volume Hyflon AD 80.

As mentioned earlier, the natural logarithm of gas solubility in polymers often increases linearly with an increase in gas critical temperature, and the slopes of the best fit trendline for many hydrocarbon rubbery polymers, glassy polymers and liquids lie in a narrow range around 0.019 K^{-1} at 35 ^oC (*cf.* Table 2.2). Figure 5.5 shows the correlation between gas solubility and penetrant critical temperature in Hyflon AD 80 at infinite dilution conditions and compares it with data for a typical hydrocarbon-based membrane polymer, polysulfone [51]. The figure also displays infinite dilution gas solubility data in AF1600 [88].

From Figure 5.5, permanent gases such as N_2 and O_2 appear to exhibit higher sorption in the two fluoropolymers than in polysulfone. Permanent gas solubility is often higher in fluorinated media than in their hydrocarbon analogs [45], and fluorinated liquids have been considered as additives to increase the oxygen solubility of blood substitutes, in part, because of their high O_2 sorption capacity [98]. This higher sorption capacity for permanent gases in fluorinated liquids is thought to be predominantly due to the structure of the fluid, with attractive intermolecular forces playing a minor role [99]. Fluorine atoms attached to the carbon backbone of fluorocarbons are larger than the

hydrogen atoms on analogous hydrocarbon chains. It is hypothesized that the larger fluorine atoms influence the molecular scale packing in fluorocarbons in such a way that more large-sized cavities are formed in fluorocarbon liquids than in hydrocarbon liquids [99]. These larger cavities enhance the ability of the fluorocarbon liquid to dissolve significant quantities of gases [99]. This hypothesis also explains the lower boiling points of fluorinated compounds [98]. Also, perfluorinated liquids have lower cohesive energy densities (CED) than their hydrocarbon analogs. For example, the CED of perfluoro-*n*-heptane (*n*-C_7F_{16}) is 36.25 cal/cm^3 as compared to 55.3 cal/cm^3 for *n*-heptane [74]. Similarly, the CED values for perfluorobenzene and benzene are 68.5 and 83.7 cal/cm^3, respectively [74]. Lower cohesive energy density also contributes to increased gas sorption [11]. It is not unreasonable to expect the existence of these effects in fluoropolymers. Thus, higher nitrogen solubility in fluoropolymers is expected to be primarily due to polymer properties like free volume distribution and low CED than due to any specific interactions with the permanent gases.

Following the above reasoning, the solubility of larger penetrants such as hydrocarbons should also be correspondingly higher in fluoropolymers. However, as noted above, the solubility ratio of propane to that of nitrogen is much less in perfluorinated media due to specific interactions between hydrocarbons and fluorocarbons which suppress hydrocarbon solubility in these materials. In fact, the solubility of larger, more condensable hydrocarbon gases increases less rapidly with increasing critical temperature in fluoropolymers than in hydrocarbon polymers. That is, the slope of the best fit trendline of the natural logarithm of solubility versus critical temperature is much lower in fluoropolymers than in hydrocarbon-based materials. (*cf.*

Tables 2.2 and 5.2). From Table 2.2, polysulfone has a best fit slope value of 0.017 K^{-1}, which is similar to that of most hydrocarbon polymers [100]. However, from Table 5.2, AF1600 has a significantly lower slope of 0.011 K^{-1} despite having much higher fractional free volume than polysulfone. Hyflon AD 80 has an even lower slope of 0.007 K^{-1} (± 0.0003 K^{-1}). Liquid perfluoro-*n*-heptane (*n*-C_7F_{16}) has a slope of 0.0105 K^{-1} [101].

The lower slope for Hyflon AD 80 at infinite dilution indicates a greater suppression of hydrocarbon solubility in this fluoropolymer than in AF1600. As mentioned earlier, gas solubility in glassy polymers at very low pressures is assumed to occur primarily in Langmuir microvoids frozen into the polymer matrix due to the non-equilibrium nature of the polymer. Sorption in these pre-existing gaps depends strongly on penetrant condensability, which is constant for a given penetrant at fixed temperature and pressure. In such cases, infinite dilution solubility of a penetrant in different polymers should be influenced, primarily, by differences in available non-equilibrium free volume for sorption and interactions between the penetrant and the polymer chains. These fluoropolymers, while structurally quite similar, do have chemical structure differences that might contribute to differences in penetrant solubility, and systematic material sets are not available to definitively decouple free volume effects from chemical structure effects. However, from Table 5.2, the systematic change in slope with fluoropolymer fractional free volume is intriguing, and it raises the possibility of a significant effect of available non-equilibrium excess free volume on the infinite dilution solubility. At higher pressures, sorption occurs in the denser, less energetically accessible regions of the polymer matrix, where penetrant molecules and polymer segments are expected to be closer, and greater solubility suppression might be observed at these

pressures than at infinite dilution. From Table 5.3, the slopes of the solubility correlation for Teflon AF at 5 atm are lower than at infinite dilution, which is consistent with the above reasoning. The decrease in slope is more pronounced for higher free volume polymers due to their larger Langmuir sorption capacity. For Hyflon AD 80, the slope value at high pressure is very close to that at infinite dilution.

If the trendlines in Figure 5.5 are extrapolated beyond the range of presently available experimental data, a large hydrocarbon like *n*-decane (T_c = 617.7 K) [46] would have approximately 6 times lower solubility in AF1600 than in polysulfone. Also, Hyflon AD 80 is estimated to sorb about 60 times less *n*-decane than polysulfone and about 10 times less than AF1600. Due to inherently low solubility for such large hydrocarbons, low free volume fluoropolymers may be more resistant to plasticization caused by sorption of these compounds into the polymer matrix. However, more experimental mixed gas permeation studies of a variety of fluoropolymers are required to understand the full extent to which this hypothesis might be valid.

5.4.2 Permeability

Figure 5.6 displays the permeability of Hyflon AD 80 to N_2, O_2, CO_2, CH_4, and C_2H_6 as a function of pressure difference across the membrane up to 20 atm at 35 ^oC. The penetrant permeabilities decrease as size increases:

$$CO_2 > O_2 > N_2 > CH_4 > C_2H_6$$

These permeability coefficients, measured in dense films, are 2-3 times lower than those reported by Arcella *et al.* in a composite membrane of this polymer on a PVDF support [97]. The source of this discrepancy is not known, although it can be challenging to measure the effective thickness in a composite membrane, and the influence of substructure resistance in Arcella *et al*.'s data was not reported [97]. From Figure 5.6, the permeabilities of N_2 and O_2 are independent of pressure while CH_4 permeability decreases with increasing pressure. In contrast, the permeabilities of CO_2 and C_2H_6 increase somewhat at higher pressures. Permanent gases and low-condensability penetrants typically exhibit constant or decreasing permeabilities with increasing penetrant pressure in glassy polymers, due to the dual modes of sorption and transport available in these materials [11]. Also, at high gas pressures or penetrant activities, penetrants can plasticize the polymer matrix, which increases their permeabilities at higher pressures [11].

C_3H_8 permeability in Hyflon AD 80 is presented in Figure 5.7. Multiple measurements were made at each pressure over a period of 1-2 days before increasing the upstream pressure. At the highest pressure, a considerable difference in permeability was measured on successive days, as shown in the figure. Then, the upstream pressure was decreased and measurements were made in a similar fashion. After measuring permeability at the lowest pressure, the polymer film was left in the permeation cell for 6 days before the final measurement was made. The polymer exhibits considerably higher permeability values in the decreasing-pressure cycle than that measured in the increasing-pressure cycle. This hysteresis effect is a likely result of alterations in the glassy polymer matrix due to exposure to high activity penetrants and has been previously observed in

other glassy polymers [102,103]. During the increasing-pressure cycle, the penetrant causes subtle perturbations in chain packing conformations and also increases packing defect size in the matrix [102]. These alterations persist in glassy polymers due to low mobility of polymer chain segments below their glass transition temperature. As seen from Figure 5.7, in this specific example, the polymer returns to its original permeability within 6 days, which is a relatively short duration compared to previous reports in other glassy, hydrocarbon-based polymers [102,103].

Figure 5.8 compares the CO_2/CH_4 separation performance, based on pure gas permeation experiments, of Hyflon AD 60 and Hyflon AD 80 at 35 °C and 4.4 atm upstream pressure with three hydrocarbon-based polymers with attractive separation properties for CO_2 removal from natural gas [4]. The figure also shows the separation performance of TFE/PMVE49, AF2400 and AF1600. The upper bound line denotes the best properties achieved to date by polymers considered for this separation [104]. Hyflon AD 60 and Hyflon AD 80 are approximately one order of magnitude more permeable to CO_2 than the hydrocarbon-based polymers. But their CO_2/CH_4 selectivity is 2-3 times lower. However, Hyflon AD 60 and 80 lie approximately the same distance from the upper bound line as the hydrocarbon polymers, so it appears to be an encouraging start for this materials design concept.

Systematic structure-property studies have shown that polymers with greater chain rigidity and sufficient chain spacing have better combinations of permeability and selectivity for gas separations [105]. Polymers meeting these requirements usually have significant aromatic character and bulky groups on the chain [9,106]. In this respect, the structure of Hyflon AD 80 more closely resembles that of aliphatic polymers that do not

have attractive gas separation properties. This observation suggests a potential opportunity to considerably improve the materials performance of fluorinated polymers via systematic structure-property studies.

5.4.3 Mixed-Gas Permeability

CO_2-CH_4 mixed-gas permeation properties of Hyflon AD 80 were determined using a feed gas mixture containing 20% CO_2 in CH_4 at 35 ^oC and 8–53.2 atm total pressure. The separation performance of the film is recorded in Table 5.3. The film exhibited a CO_2 permeability of approximately 250 Barrers and a CO_2/CH_4 mixture selectivity of 10.6 at 8.2 atm feed pressure. Upon increasing pressure to 53.2 atm, the CO_2 permeability increased slightly to 280 Barrers, while the mixed gas CO_2/CH_4 selectivity decreased slightly to 8.7. Thus, this material exhibits a minor decrease in selectivity at CO_2 partial pressures up to 10.6 atm. This result is in striking contrast to the dramatic decrease in selectivity with increasing CO_2 partial pressure in high-performance hydrocarbon-based polyimide materials [16,20]. For example, CO_2/CH_4 selectivity of an aromatic polyimide (6FDA-mPD) decreases from 58 under pure gas conditions to approximately 4 in a 50:50 gas mixture at about 17.5 atm total pressure [20]. White *et al.* report that the CO_2/CH_4 selectivity of another aromatic polyimide (6FDA-DMB) decreases from 33 in pure gas measurements (20.4 atm CH_4, 6.8 atm CO_2, 22 ^oC), to 19 in mixed gas measurements (10% CO_2 in CH_4, 68 atm total pressure, 22 ^oC) [16].

From Figure 5.2, CO_2 concentration in Hyflon AD 80 is only about 15 cm^3(STP)/cm^3 at 10 atm. CO_2 concentration in the 6FDA polyimide family is reported to be much higher [9,107]. While we could not find CO_2 concentrations in the 6FDA polyimides mentioned above, the reported CO_2 concentrations in other 6FDA polyimides is in excess of 30 cm^3(STP)/cm^3 at 10 atm [9,107]. This difference in CO_2 solubilities between the fluoropolymer and the polyimides is consistent with the greater CO_2-induced plasticization resistance of Hyflon AD 80.

The polymer film was also exposed to a feed stream containing 10% CO_2, 50 ppm toluene and 500 ppm *n*-hexane in CH_4 at 35 ^oC and 35 atm total pressure. This gas stream has a dew point in the range of -29 to -40 ^oC, depending on the equation of state used to estimate the dew point. In comparison, natural gas at field conditions has a dew point of -20 ^oC, when it is fed to a membrane module for CO_2 removal. Thus, the gas mixture has a comparable but somewhat lower dew point to that experienced in industrial environments. When exposed to this gas mixture, the polymer exhibited a CO_2 permeability of about 270 Barrers and a CO_2/CH_4 selectivity of 10.6 after 3 hours. These values remained constant after 22 hours of exposure to this feed mixture. Thus, the polymer exhibited undetectable hydrocarbon-induced plasticization in the presence of moderate concentrations of model higher hydrocarbons in the feed stream.

5.4.4 Diffusivity

Effective diffusion coefficients of N_2, CO_2, CH_4, and C_2H_6 as a function of pressure in Hyflon AD 80 are presented in Figure 5.9. The values were calculated using

eq 2.15. From the figure, the diffusivities of N_2 and CH_4 are independent of penetrant concentration in the polymer. Effective diffusion coefficient for the more condensable gases, CO_2 and C_2H_6, increases with penetrant concentration at higher pressures, indicating plasticization. The diffusion coefficients decrease with increasing penetrant size, in agreement with the trend in permeability coefficients. As mentioned earlier, the variation of diffusion coefficients with critical volume (a measure of penetrant size) is usually described by eq 4.3, where η provides a measure of the rate of decrease of diffusion coefficients with increasing penetrant size; the higher the value of η, the greater the diffusivity selectivity of the polymer. Figure 5.10 compares the diffusivity selectivity or size-sieving ability of Hyflon AD 80 with that of a typical rubbery (PDMS) and glassy (polysulfone) polymer. The glassy polymer, polysulfone, exhibits a greater decrease in the diffusion coefficient with increase in penetrant size than rubbery PDMS; it has an η value of 8.4 compared to only 2.3 for PDMS. Thus, the glassy polymer is able to separate molecules better based on their size differences. Hyflon AD 80 has an η value of approximately 6, thus exhibiting a much stronger size-sieving ability than rubbery PDMS, but slightly lower than the aromatic, glassy polymer, polysulfone. As mentioned before, high performance polymers for this application usually have very strong size-sieving abilities and significant aromatic character. Thus, designing fluoropolymers with greater size-sieving abilities might lead to better separation performance membranes for CO_2 removal from natural gas.

5.5 CONCLUSIONS

Hyflon AD 80 exhibits a much lower slope in the correlation of natural logarithm of hydrocarbon solubility and penetrant critical temperature than hydrocarbon-based polymers and even high free volume fluoropolymers like AF1600. Thus, this polymer may have inherently lower solubility for large hydrocarbon compounds than hydrocarbon polymers and, therefore, may exhibit greater resistance to plasticization by these compounds than conventional hydrocarbon-based membrane polymers. Permanent gas and light hydrocarbon permeabilities in this polymer decrease with increasing penetrant size, following the same trend as the diffusion coefficients. In CO_2-CH_4 mixed-gas permeation experiments where the feed gas partial pressure of CO_2 was as high as 10.6 atm, the polymer exhibited relatively little CO_2-induced plasticization. The polymer also showed excellent plasticization resistance to moderate concentrations of toluene and *n*-hexane in the CO_2-CH_4 gas stream. There is some evidence of plasticization of this polymer by pure CO_2 and C_2H_6 at higher pressures, based on the increase in diffusion coefficients with concentration. The polymer exhibits significant hysteresis of C_3H_8 permeability, indicating long-lived disturbances of the polymer matrix upon exposure to high activity propane.

Table 5.1 Ratio of propane to nitrogen solubility coefficients in hydrocarbon and fluorocarbon media.

Classification	***Medium***	***Fractional Free Volume***	***Solubility Selectivity C_3H_8/N_2***
Hydrocarbons	*n*-C_7H_{16} [101]	0.31	99 [c]
	Poly(1-trimethylsilyl-1-propyne) [57]	0.29	64 [d]
	c-C_6H_{12} [44]	0.28	130 [c]
	C_6H_6 [44]	0.27	89 [c]
	Poly(ethylene) [41]	0.22 [b]	96 [e]
	Natural rubber [41]	0.22 [b]	89 [e]
	Poly(butadiene)-hydrogenated [41]	0.19 [b]	83 [e]
	Poly(dimethylsiloxane) [38]	0.16	68 [f]
Fluorocarbons	AF2400 [88]	0.33	22 [d]
	n-C_7F_{16} [101]	0.31	18.5 [c]
	AF1600 [88]	0.30	15 [d]
	TFE/PMVE49	0.22	5.1 [d]
	Hyflon AD 80	0.197	6 [d]

[a] calculated using Bondi's group contribution method [49].
[b] calculated using an amorphous phase specific volume of 1.171 cm^3/g [41].
[c] 1 atm and 25 ^oC.
[d] infinite dilution and 35 ^oC.
[e] for completely amorphous polymer at 25 ^oC.
[f] infinite dilution and 25 ^oC.

Table 5.2 Slope of the correlation of the natural logarithm of solubility versus penetrant critical temperature in the Teflon AF materials [88] and in Hyflon AD 80 at 35 ^{o}C.

Polymer	***Fractional Free Volume***	***Slope, $b \times 10^3$ (K^{-1})***	
		p = 0 atm	***p = 5 atm***
AF2400	0.33	12.5	9
AF1600	0.30	11	8
Hyflon AD 80	0.197	7 ± 0.3	6 ± 0.3

Table 5.3 Mixed gas performance of Hyflon AD 80 at 35 ^{o}C when exposed to a feed stream of 20% CO_2 in CH_4.

Total feed pressure (atm)	***CO_2 Permeability (Barrer)***	***CO_2/CH_4 Selectivity***
8.2	257	10.6
14.3	266	10.3
21.0	286	10.2
35.0	276	9.3
53.2	281	8.7

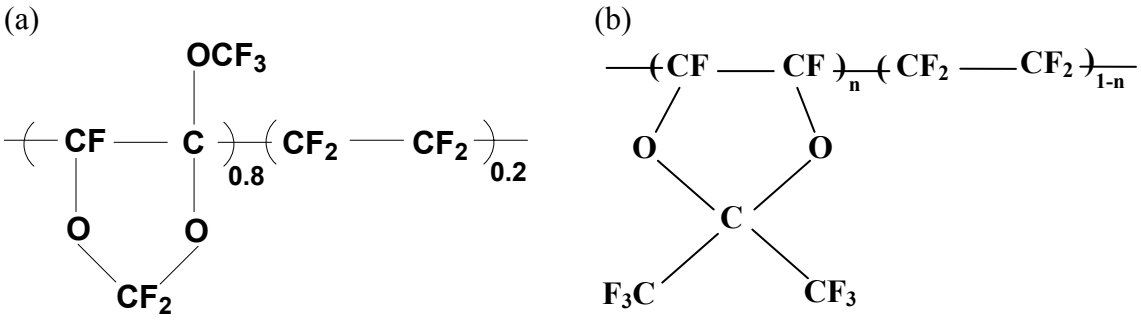

Figure 5.1: Chemical structure of (a) Hyflon AD 80 and (b) Teflon AF polymers. n=0.65 for AF1600 and n=0.87 for AF2400.

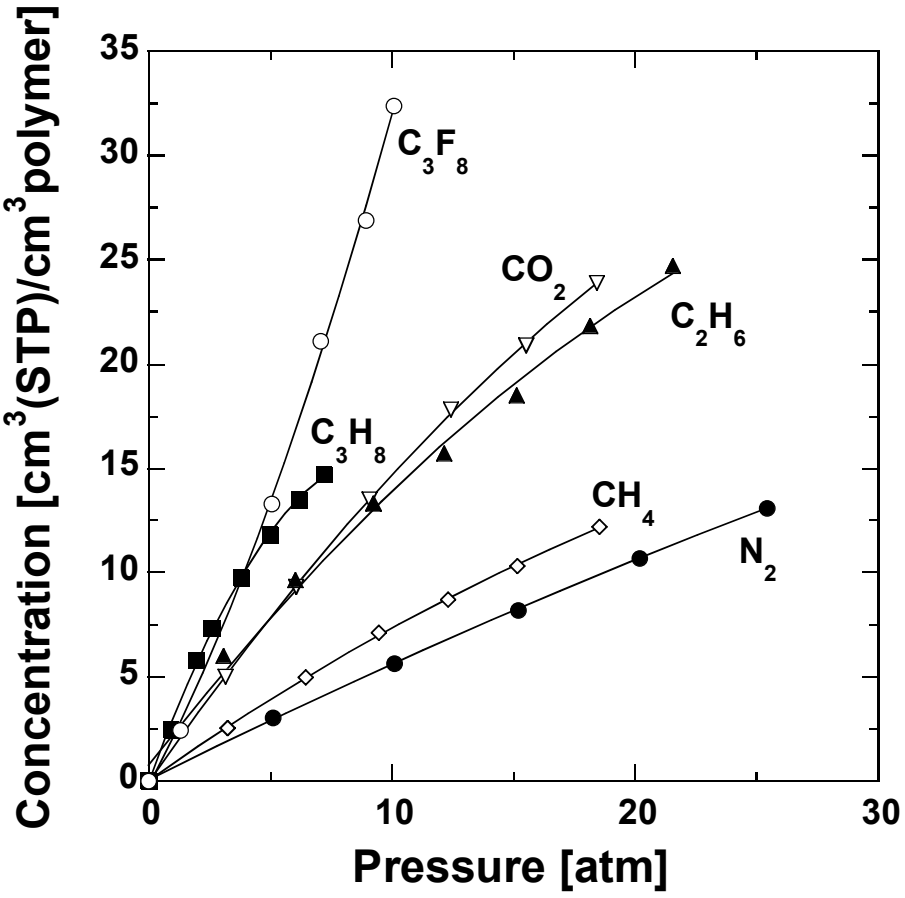

Figure 5.2: Sorption isotherms of N_2, CO_2, C1-C3 hydrocarbons and C_3F_8 in Hyflon AD 80 at 35 ^{o}C.

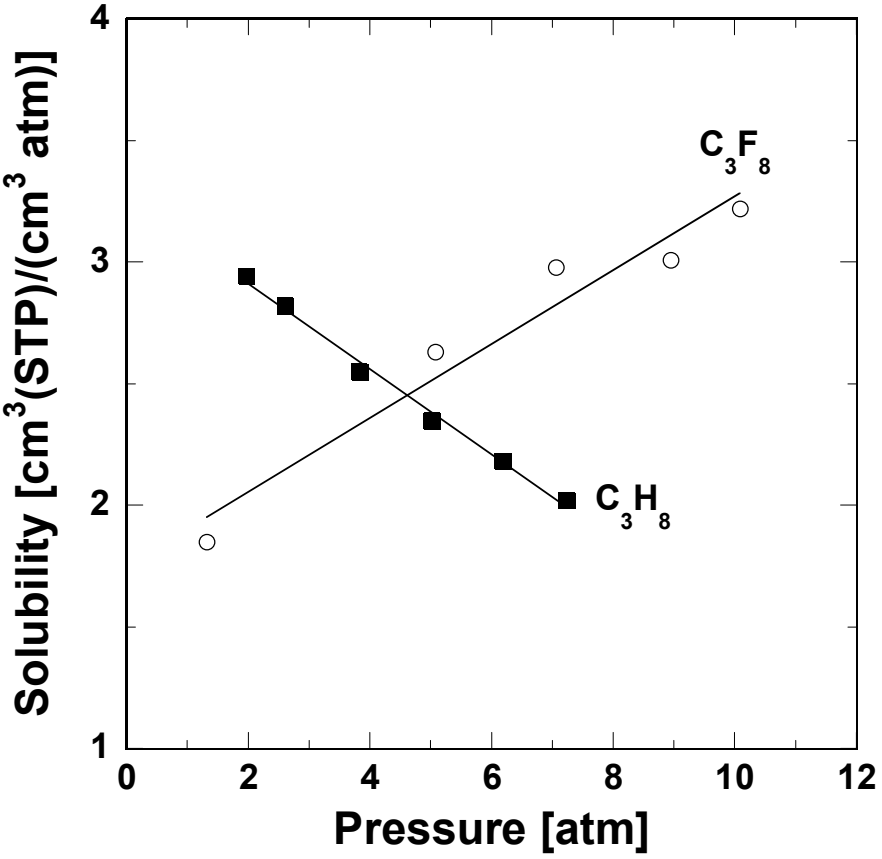

Figure 5.3: Comparison of C_3H_8 (■) and C_3F_8 (○) solubility in Hyflon AD 80 at 35 ^oC as a function of pressure.

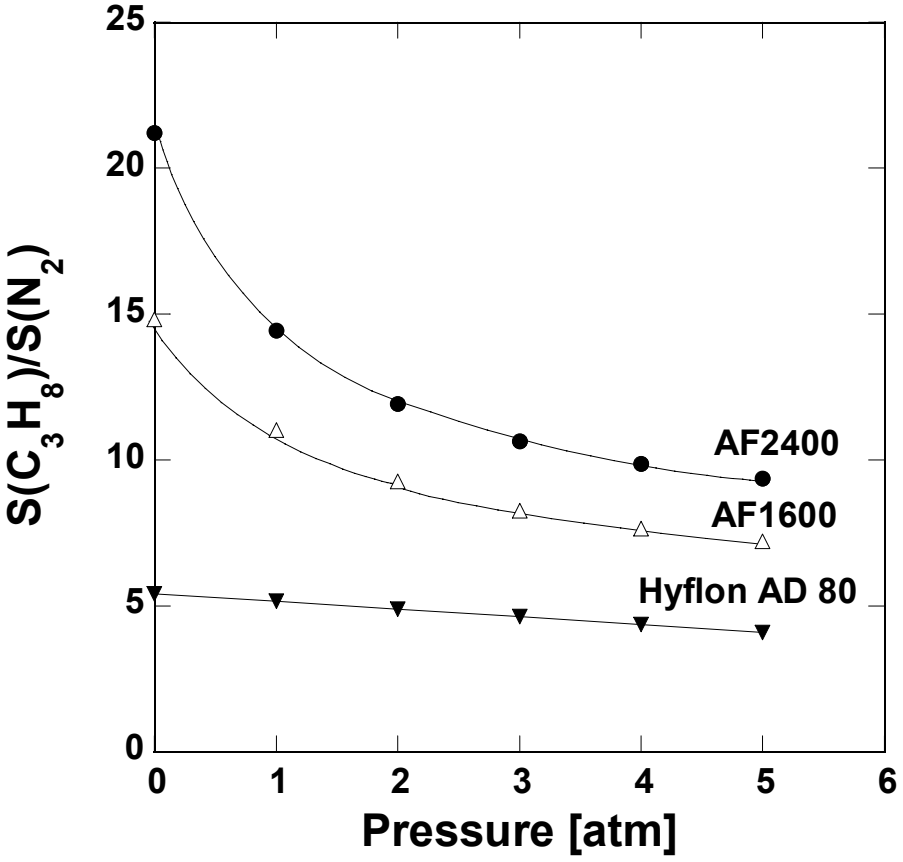

Figure 5.4: Variation of C_3H_8/N_2 solubility ratio with pressure for Teflon AF polymers [88] and Hyflon AD 80 at 35 ^{o}C.

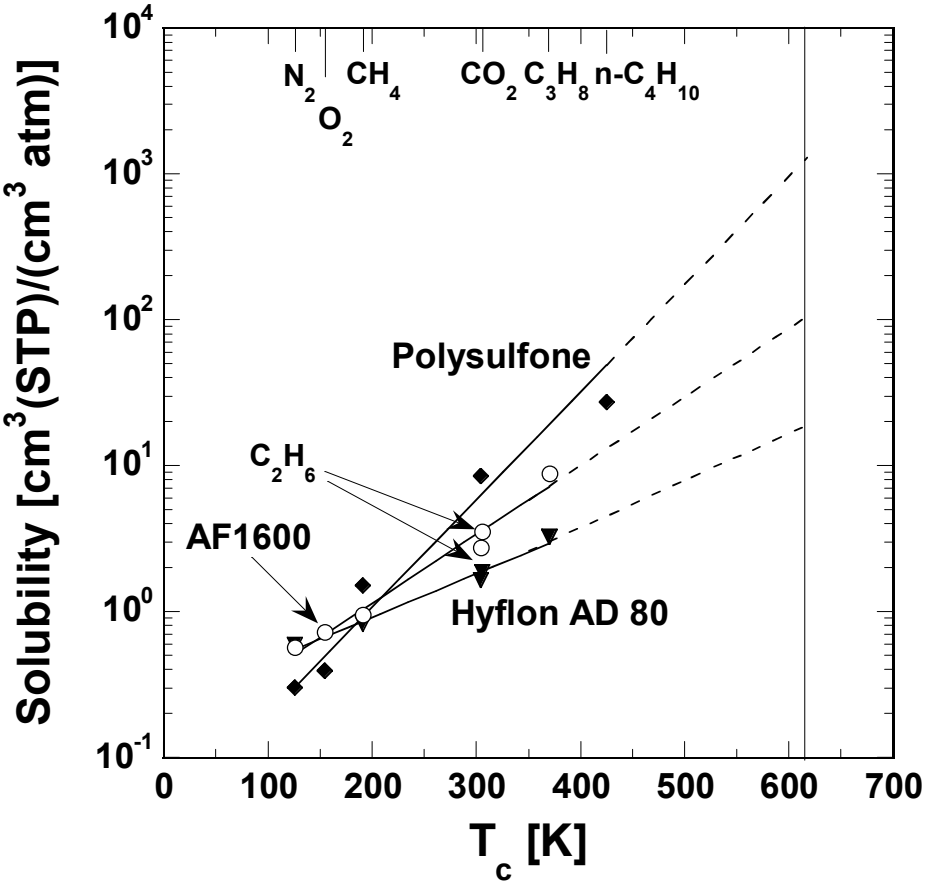

Figure 5.5: Correlation between gas solubility and critical temperature in polysulfone [51], AF1600 [88] and Hyflon AD 80 at 35 ^{o}C. Polysulfone data are at 10 atm except for *n*-C_4H_{10} which is at infinite dilution. Data for the other two polymers have been extrapolated to infinite dilution conditions. The vertical line at a T_c value of 617.7 K corresponds to the critical temperature of *n*-decane.

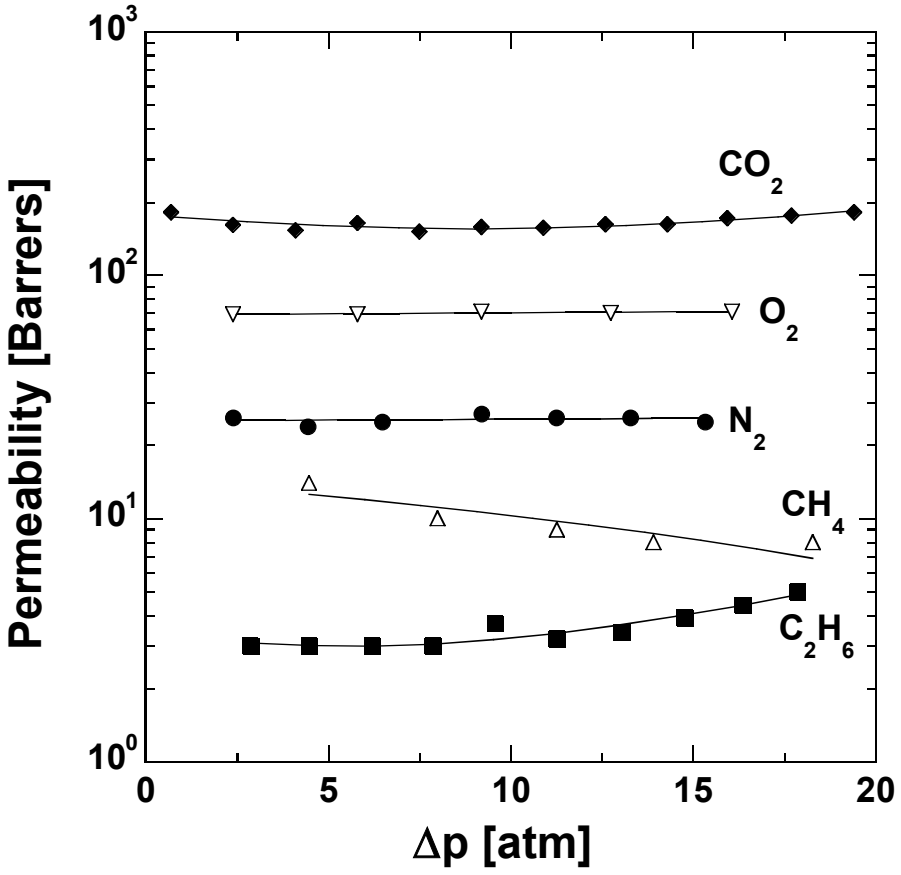

Figure 5.6: Permeability of N_2, O_2, CO_2, CH_4 and C_2H_6 in Hyflon AD 80 at 35 ^oC as a function of pressure difference across the membrane.

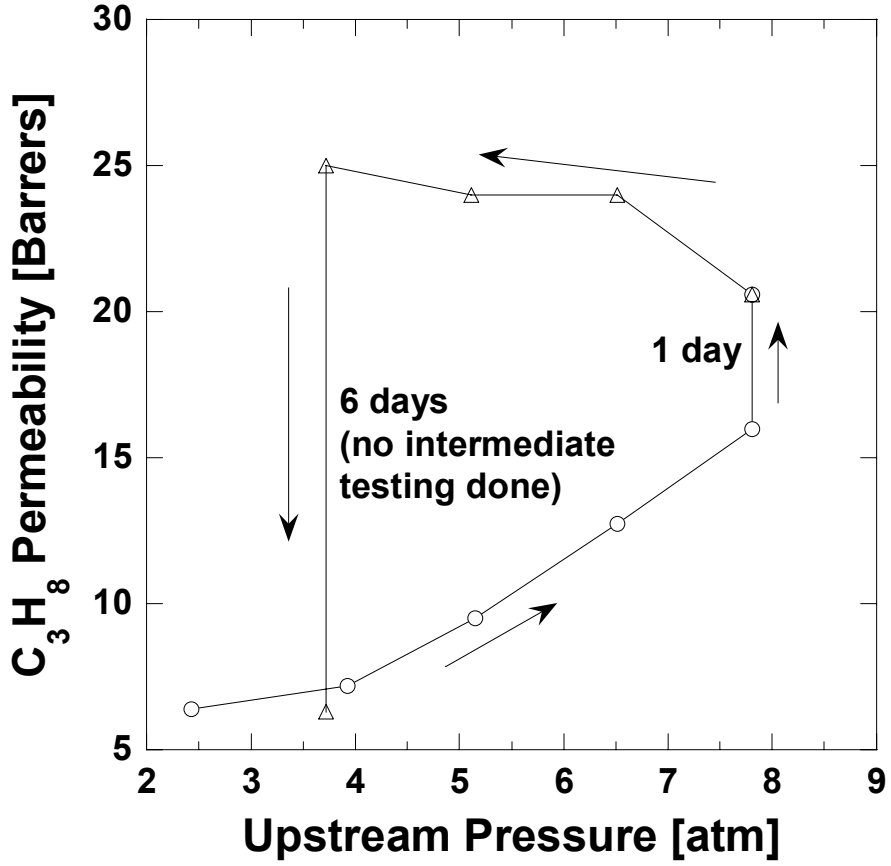

Figure 5.7: C_3H_8 permeability with increasing (○) and decreasing (Δ) pressure in Hyflon AD 80 at 35 ^oC. Arrows indicate the order of testing.

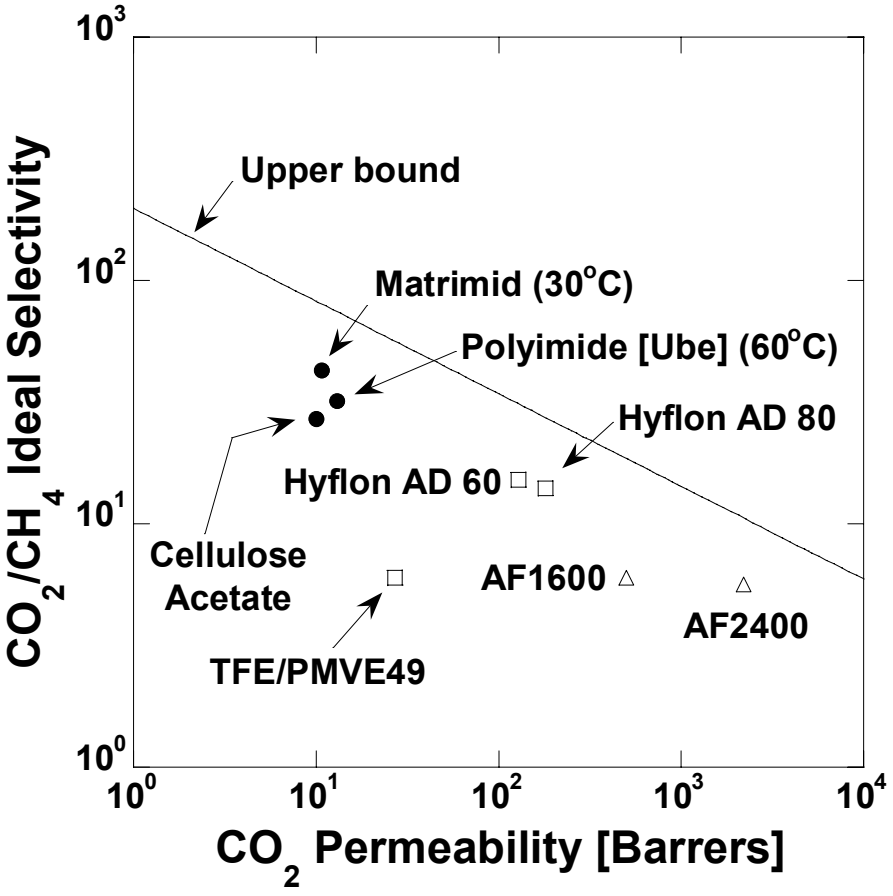

Figure 5.8: Comparison of CO_2/CH_4 separation performance of TFE/PMVE49, Hyflon AD 60 and Hyflon AD 80 (□) based on pure gas permeabilities with select hydrocarbon polymers (●) [4] and high free volume fluoropolymers (Δ) [78,88]. Temperature=35 °C, unless mentioned otherwise.

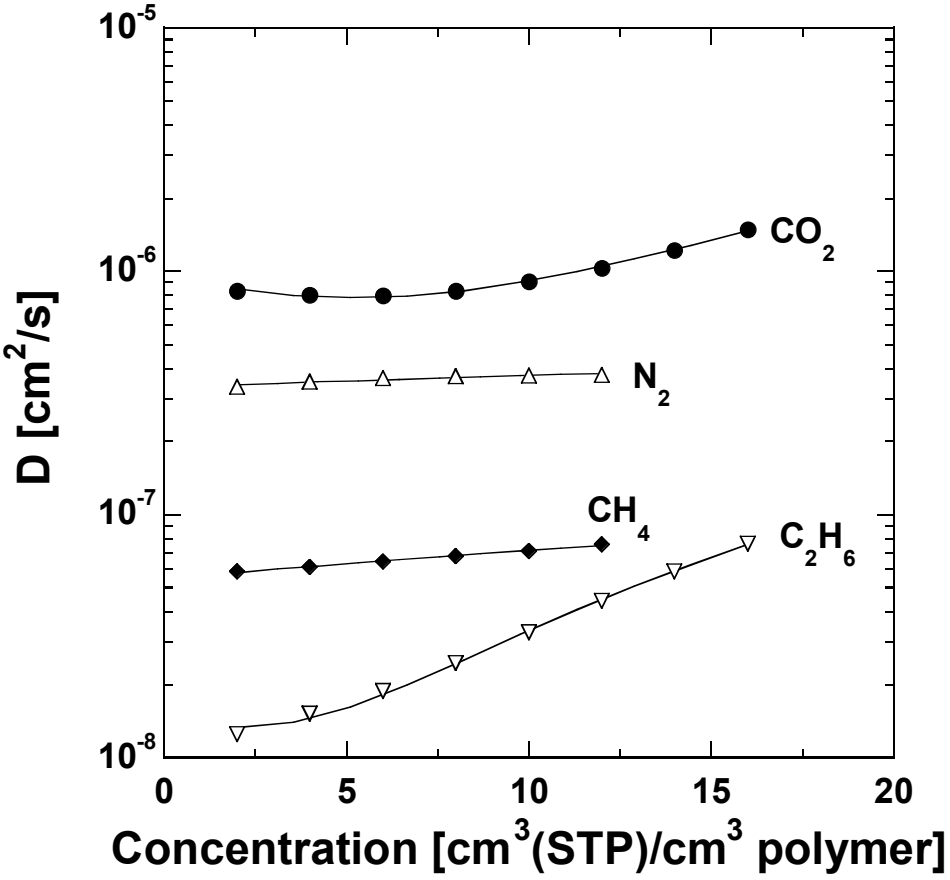

Figure 5.9: Effective diffusion coefficients of N_2, CO_2, CH_4 and C_2H_6 in Hyflon AD 80 as a function of upstream penetrant concentration in the polymer at 35 ^{o}C.

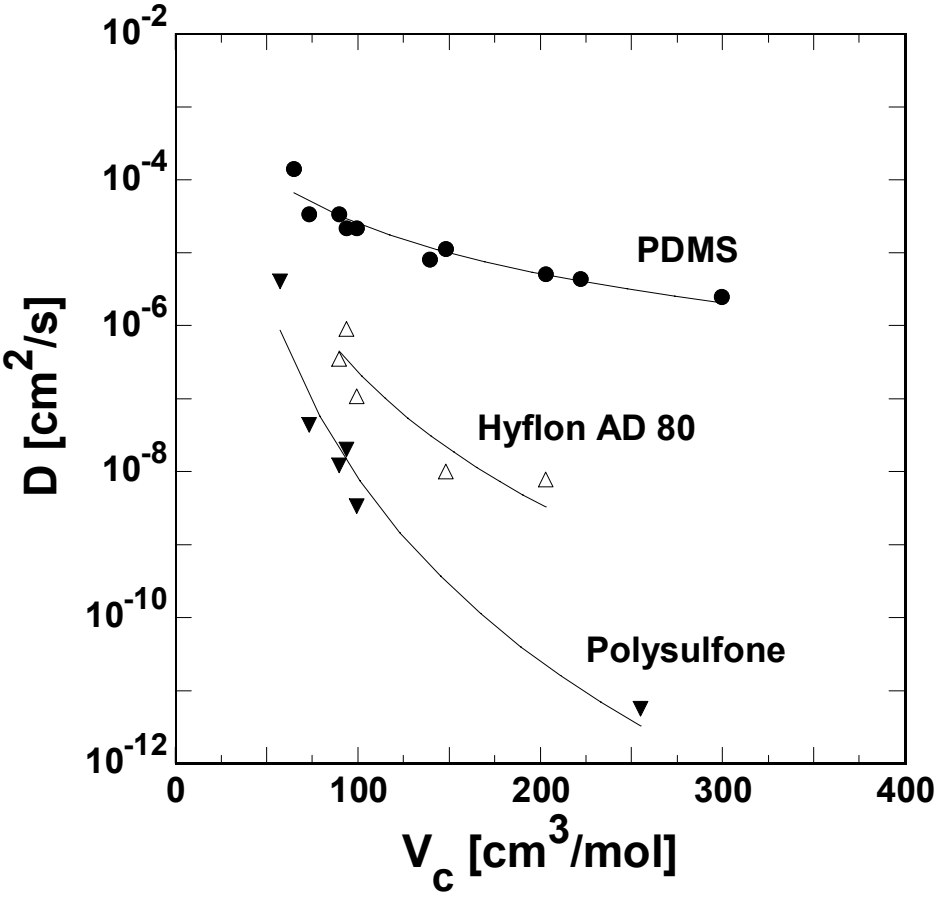

Figure 5.10: Comparison of the variation of infinite dilution diffusion coefficients with penetrant critical volume in Hyflon AD 80 with that in a typical rubbery (PDMS) [25] and glassy (polysulfone) polymer [51,93-95]. The trendlines in the figure satisfy the eq 4.3, where η is a measure of the size sieving ability or size-selectivity of the polymer to penetrants. The best-fit values of η in the plot are: PDMS: 2.3; Polysulfone: 8.4; Hyflon AD 80: 6.0 ± 0.6.

CHAPTER 6

Fluoropolymer-Hydrocarbon Polymer Composite Membranes for Carbon Dioxide Removal from Natural Gas

---

Reproduced in part with permission from R. S. Prabhakar and B. D. Freeman, Fluoropolymer-Hydrocarbon Polymer Composite Membranes for Natural Gas Separation, in I. Pinnau and B. D. Freeman (Eds.), Advanced Materials for Membrane Separations, Vol. 876, American Chemical Society, Washington, DC, 2004, pp. 106-128.

6.1 SUMMARY

A simple model is presented to evaluate the conditions under which coating a hydrocarbon-based polymer membrane with a fluoropolymer could reduce the sorption of higher hydrocarbons into the hydrocarbon polymer, thereby protecting the hydrocarbon polymer from plasticization by these compounds. Based on this analysis, an effective plasticization-resistant coating should have a lower ratio of higher hydrocarbon to CO_2 solubility than that of the hydrocarbon polymer and be as strongly size-sieving as possible. Model cases are presented to illustrate the possibilities and limitations of this approach.

6.2 INTRODUCTION

In the previous chapter, the gas separation properties and plasticization-resistance of Hyflon AD 80 have been reported for CO_2 removal from natural gas. While this polymer shows relatively stable gas separation properties, it's intrinsic selectivity is not as high as the ideal selectivities of engineered hydrocarbon polymer membranes. Systematic structure-property studies that have produced high performance hydrocarbon-based membranes may be a potential, though long-term, option to produce high performance, stable, fluoropolymer membranes. A shorter-term strategy may be to use fluoropolymers as plasticization-resistant coatings on existing hydrocarbon membranes for CO_2 removal from natural gas. This approach might lower the effective higher-hydrocarbon partial pressure to which the underlying hydrocarbon polymer layer is exposed, thereby reducing plasticization.

The coatings strategy outlined above has obvious tradeoffs. The fluoropolymer coating would reduce gas flux due to the extra mass transfer resistance that it imposes on all penetrants. In addition, the composite membrane selectivity could be adversely affected if the selectivity of the coating layer was less than that of the hydrocarbon layer. In this chapter, a theoretical analysis is used to assess the ability of a fluoropolymer coating to reduce the exposure of an underlying hydrocarbon membrane to higher hydrocarbons and the penalty associated with having an extra resistance to mass transfer. A complete derivation of the model is presented and the possibilities and limitations of this approach are discussed with the aid of model cases.

6.3 PROBLEM DEFINITION

Figure 6.1a presents the cross section of a hydrocarbon polymer membrane of thickness l^{HP} used for removing CO_2 from natural gas. The membrane is exposed, on its upstream side, to higher hydrocarbons having a partial pressure of $p_{up,HC}$ [#]. Figure 6.1b shows a cartoon of the proposed approach of applying a fluoropolymer layer on the hydrocarbon polymer. In this scenario, the overcoated hydrocarbon polymer membrane is now exposed to a hydrocarbon partial pressure, p^*_{HC}, which is lower than the upstream partial pressure of the hydrocarbon, $p_{up,HC}$, due in part to low solubility and diffusivity of the higher hydrocarbon in the fluoropolymer coating. The objective is to use the fluoropolymer coating to achieve a large reduction in p^*_{HC} relative to $p_{up,HC}$ with a minimal loss in CO_2 flux and CO_2/CH_4 selectivity provided by the original hydrocarbon membrane. Mathematically, these criteria can be expressed as:

$$\left(\frac{p^*}{p_{up}}\right)_{HC} \to 0, \quad while \quad \left(\frac{N^C}{N}\right)_{CO_2} \to 1 \quad and \quad \left(\frac{\alpha^C}{\alpha}\right)_{CO_2/CH_4} \to 1 \qquad (6.1)$$

where N and α are the membrane gas flux and selectivity, respectively, and the subscript HC refers to higher hydrocarbons (*e.g.*, hexane, octane, decane, aromatic compounds, *etc*.). The composite membrane properties are denoted by a superscript 'C'.

[#] The subscript 'HC' stands for hydrocarbon and will be used later to indicate the name of the specific higher hydrocarbon under consideration.

6.4 ANALYSIS

6.4.1 Flux Condition

From Figure 6.1b, at steady state, the flux of a gas, A, through the composite membrane is the same as that through each polymer layer of the composite, and is given by:

$$N_A^C = \frac{P_A^{COAT}(p_{up,A} - p_A^*)}{l^{COAT}} = \frac{P_A^{HP}(p_A^* - p_{down,A})}{l^{HP}} = \frac{P_A^C(p_{up,A} - p_{down,A})}{l^C} \qquad (6.2)$$

where the superscript 'COAT' refers to the fluoropolymer coating layer while 'HP' refers to the hydrocarbon polymer layer. This equation sets the hypothetical interfacial partial pressure of the penetrant, p_A^*, equal in the two polymers at the polymer-polymer interface, which is equivalent to equating chemical potential of the penetrant in the two polymers at the interface. Eq 6.2 can be recast as follows:

$$N_A^C = \frac{\left(p_{up,A} - p_{down,A}\right)}{\left(\frac{l}{P_A}\right)^{COAT} + \left(\frac{l}{P_A}\right)^{HP}} \qquad (6.3)$$

The ratio of the membrane thickness to its gas permeability coefficient represents the mass transfer resistance of the membrane layer to permeation of gas A. From eqs 2.1 and 6.3, the flux condition in eq 6.1 becomes:

$$\left(\frac{N^C}{N}\right)_{CO_2} = \frac{\left(\frac{l}{P_{CO_2}}\right)^{HP}}{\left(\frac{l}{P_{CO_2}}\right)^{COAT} + \left(\frac{l}{P_{CO_2}}\right)^{HP}} \to 1 \tag{6.4}$$

which implies that the fluoropolymer coating layer resistance to CO_2 transport should be as low as possible to maintain CO_2 flux in the composite membrane as close as possible to that in the uncoated polymer:

$$\frac{\left(\frac{l}{P_{CO_2}}\right)^{COAT}}{\left(\frac{l}{P_{CO_2}}\right)^{HP}} \to 0 \tag{6.5}$$

6.4.2 Partial Pressure Condition

From eq 6.2,

$$p_A^* = p_{up,A} - N_A^C \left(\frac{l}{P_A}\right)^{COAT} \tag{6.6}$$

Substituting the expression for N_A^c from eq 6.3 and assuming that the downstream penetrant partial pressure is negligible relative to the upstream penetrant partial pressure, the partial pressure condition of eq 6.1 can be rewritten as

$$\left(\frac{p^*}{p_{up}}\right)_{HC} = \frac{\left(\frac{l}{P_{HC}}\right)^{HP}}{\left(\frac{l}{P_{HC}}\right)^{COAT} + \left(\frac{l}{P_{HC}}\right)^{HP}} \to 0 \tag{6.7}$$

which implies that the resistance of the coating layer to higher hydrocarbon transport should be as large as possible:

$$\frac{\left(\frac{l}{P_{HC}}\right)^{COAT}}{\left(\frac{l}{P_{HC}}\right)^{HP}} \to \infty \tag{6.8}$$

Eqs 6.5 and 6.8 may be combined to yield the following expression:

$$\frac{\left(\frac{P_{CO_2}}{P_{HC}}\right)^{COAT}}{\left(\frac{P_{CO_2}}{P_{HC}}\right)^{HP}} \to \infty \tag{6.9}$$

Equation 6.9 depends only on the permeation properties of the materials used in the coating and hydrocarbon polymer separating layer, so it can be used to provide materials selection guidelines. Using the solution diffusion model (eq 2.6) and the

solubility and diffusivity correlations in eqs 2.23 and 4.3, respectively, the above condition can be expressed as:

$$\exp[(b^{HP} - b^{COAT})(T_{c_{HC}} - T_{c_{CO_2}})]\left(\frac{V_{c_{HC}}}{V_{c_{CO_2}}}\right)^{\eta^{COAT} - \eta^{HP}} \rightarrow \infty \left(>>1\right) \qquad (6.10)$$

From a practical viewpoint, this condition is modified to the inequality shown in parenthesis in eq 6.10 with the understanding that the higher the value of the left hand side of the inequality, the better will be the performance of the composite membrane. As higher hydrocarbon critical temperatures and critical volumes are greater than those of CO_2, this inequality is satisfied when:

$$b^{HP} > b^{COAT} \; and \quad \eta^{COAT} > \eta^{HP} \qquad (6.11)$$

Based on these conditions, for optimal performance, the fluoropolymer coating should have a lower ratio of higher hydrocarbon to CO_2 solubility and a higher size-selectivity than the hydrocarbon polymer. In other words, ideally, the coating material should pose a large resistance to higher hydrocarbon permeation. The conditions in eq 6.11 provide guidelines for appropriate materials selection of the coating material to achieve a large reduction in the higher hydrocarbon partial pressure to which the hydrocarbon membrane is exposed without a large sacrifice in membrane flux.

Analysis of the condition on CO_2/CH_4 selectivity is presented in section 6.8 at the end of this chapter. The analysis highlights the tradeoff between maintaining high CO_2/CH_4 selectivity while minimizing the transport of higher hydrocarbons to the hydrocarbon membrane. Based on these results, with existing fluoropolymer membranes, which do not have exceptionally high CO_2/CH_4 selectivity, CO_2/CH_4 selectivity will be reduced by overcoating a hydrocarbon polymer to protect it from higher hydrocarbons. However, as will be seen from the model cases, if the conditions of eq 6.11 are satisfied, the selectivity loss can be quite small.

6.5 MODEL CASES

The validity of the materials selection guidelines in eq 6.11 was tested by contrasting the performance of two fluoropolymer-coated hydrocarbon membranes, one that satisfies the conditions in eq 6.11 and one that does not. The two hydrocarbon polymers were ethyl cellulose and polysulfone. The transport properties of the hydrocarbon polymers were obtained from literature [51,54,93-95] and are displayed in Figures 6.2 and 6.3. The data in the two figures are for He, N_2, O_2, CO_2 and hydrocarbon penetrants up to C_3H_8 or C_4H_{10}, depending on the polymer.

Hyflon AD 80 served as the coating layer for both composite membranes. The infinite dilution solubility and diffusions coefficients of N_2, CO_2, CH_4, C_2H_6 and C_3H_8 in this polymer were obtained from Figures 5.5 and 5.10, and are reproduced in Figures 6.2 and 6.3, respectively. The experimental conditions of these data are not representative of those that might be experienced by a membrane being used to treat natural gas.

However, we did not have sufficient mixed gas solubility and permeability (and therefore, diffusivity) data at high pressure to enable a more realistic study. The results presented here using low pressure pure gas experimental data are therefore only qualitatively indicative of the benefits and tradeoffs of the proposed approach.

The data in Figures 6.2 and 6.3 were used to find least-square best fit values of the coefficients a, b, τ and η in eqs 2.23 and 4.3. The best fit values are tabulated in Table 6.1. Solubility and diffusivity values for higher hydrocarbons were obtained by extrapolation using these equations and the critical properties of the penetrants (*cf.* the Appendix at the end of this dissertation for critical properties).

For both composite membranes, the slope of the trendline of infinite dilution solubility coefficients with T_c (*i.e.* the value of b) of the fluoropolymer is much less than that of the hydrocarbon polymer, thus satisfying the first inequality in eq 6.11 (*cf.* Figure 6.2 and Table 6.1). However, the size sieving ability of polysulfone (*i.e.* the value of η) is much greater than that of Hyflon AD 80, while ethyl cellulose is less strongly size sieving than Hyflon AD 80 (*cf.* Figure 6.3 and Table 6.1). Thus, the ethyl cellulose/Hyflon AD 80 membrane satisfies both inequalities in eq 6.11 while the polysulfone/Hyflon AD 80 membrane does not.

The 3 ratios in eq 6.1 were calculated for 4 linear alkanes and for fluorocarbon coating-to-hydrocarbon membrane thickness ratios, $\left(l^{COAT}/l^{HP}\right)$, ranging from 0.05 to 5. This range was chosen to obtain a wide variation in values for $\left(p^*/p_{up}\right)_{HC}$ values. The results are shown in Figures 6.4 and 6.5 for polysulfone/Hyflon AD 80 and ethyl cellulose/Hyflon AD 80, respectively.

6.6 RESULTS AND DISCUSSION

Figures 6.4 and 6.5 present the tradeoff between reducing partial pressure of C2, C3, C8 and C10 saturated linear hydrocarbons at the polymer-polymer interface and maintaining high CO_2 permeability and CO_2/CH_4 selectivity for polysulfone/Hyflon AD 80 and ethyl cellulose/Hyflon AD 80 composite membranes, respectively. The ordinates show the ratio of CO_2 flux through the composite membrane to that through the original hydrocarbon membrane and the ratio of CO_2/CH_4 selectivity of the composite relative to that of the original membrane.

Figure 6.4 shows that the reduction of hydrocarbon partial pressure at the polysulfone/Hyflon AD 80 interface comes at the expense of a significant drop in CO_2 flux (throughput) and CO_2/CH_4 selectivity (purity). For example, a 15% reduction in C_3H_8 partial pressure at the interface is accompanied by a 25% loss in flux and a loss of more than 15% in CO_2/CH_4 selectivity. Also, as hydrocarbon penetrant size increases, the tradeoff becomes more unfavorable. The same losses in flux and CO_2/CH_4 selectivity mentioned above yield only an 11% reduction in *n*-$C_{10}H_{22}$ partial pressure at the hydrocarbon polymer-fluoropolymer interface.

In contrast, for the ethyl cellulose/Hyflon AD 80 membrane (*cf.* Figure 6.5), a large reduction in hydrocarbon penetrant partial pressure at the interface can be obtained with only moderate decreases in CO_2 flux and CO_2/CH_4 selectivity. For example, at 25% loss in CO_2 flux, the interface partial pressure of propane is reduced by 70%, which is a much greater reduction than the 15% reduction in interfacial partial pressure achieved in

the polysulfone/Hyflon AD 80 membrane for this penetrant. Also, the associated loss in CO_2/CH_4 selectivity is only about 4% for the ethyl cellulose/Hyflon AD 80 membrane. Interestingly, the tradeoff between interfacial partial pressure reduction and flux and selectivity losses becomes more favorable with increasing penetrant size, which is opposite to the case of polysulfone/Hyflon AD 80. Thus, a coating that reduces CO_2 flux by 25% and CO_2/CH_4 selectivity by 4% provides over 95% reduction in *n*-C_8H_{18} and *n*-$C_{10}H_{22}$ interfacial partial pressures.

The poor predicted performance of the Hyflon AD 80 coating on polysulfone relative to that on ethyl cellulose results from the unfavorable mismatch in size sieving ability for the polysulfone/Hyflon AD 80 composite membrane. Polysulfone is far more size sieving than Hyflon AD 80, so the critical volume term in eq 6.10 is less than unity for higher hydrocarbons, and its value decreases progressively with increasing hydrocarbon contaminant size. Figure 6.6 shows the value of the expression in eq 6.10 for the two composite membranes as a function of hydrocarbon penetrant critical volume. With increasing hydrocarbon penetrant size, the condition of eq 6.10 becomes progressively better satisfied for the ethyl cellulose containing membrane while it worsens for the polysulfone/Hyflon AD 80 composite.

In summary, a hydrocarbon-fluorocarbon composite polymer membrane satisfying the conditions of eq 6.11 could, in principle, achieve large reductions in interfacial partial pressure of higher hydrocarbon penetrants without a large sacrifice in flux and selectivity. Therefore, this approach might be useful for addressing the issue of plasticization of hydrocarbon membranes used in natural gas separations. However, it must be stressed that the model cases presented above are based on pure gas permeation

properties determined under laboratory conditions and hence are, at best, only qualitatively suggestive of the potential benefits. The actual performance benefits can be analyzed only with the help of mixture permeation properties determined at process conditions, and such data are currently quite rare in the open literature. Also, if a fluoropolymer were available that was considerably more strongly size sieving than conventional hydrocarbon-based polymers, one might eliminate the hydrocarbon polymer membrane entirely.

6.7 CONCLUSIONS

A model is presented for using a lipophobic fluoropolymer coating on a hydrocarbon membrane to mitigate plasticization of the hydrocarbon membrane due to sorption of higher hydrocarbon contaminants in natural gas. Fluoropolymers can have much lower solubility values for higher hydrocarbons than hydrocarbon-based polymers, and the model calculations suggest that, under certain circumstances, this property may be exploited to reduce the exposure of the hydrocarbon polymer in the composite membrane to higher hydrocarbons. However, fluoropolymers reported to date in the open literature have only modest size-selectivities. Therefore, moderately size-sieving hydrocarbon polymers (*e.g.*, ethyl cellulose, cellulose acetate, *etc*.) might benefit more from this approach than more strongly size-sieving materials (*e.g.*, polysulfones, polyimides, *etc*.) To provide effective plasticization resistance to the latter polymers, more strongly size-sieving fluoropolymers may need to be developed.

6.8 APPENDIX: ANALYSIS OF SELECTIVITY CONDITION

The CO_2/CH_4 selectivity condition in eq 6.1 is:

$$\left(\frac{\alpha^C}{\alpha}\right)_{CO_2/CH_4} \geq 1 \tag{6.12}$$

which can be written as follows:

$$\left(\frac{P_{CO_2}}{P_{CH_4}}\right)^C \left(\frac{P_{CH_4}}{P_{CO_2}}\right)^{HP} \geq 1 \tag{6.13}$$

Introducing the thicknesses of the hydrocarbon polymer membrane and the composite membrane into eq 6.13 converts the permeabilities into mass transfer resistances:

$$\frac{\left(\frac{l}{P_{CH_4}}\right)^C \left(\frac{l}{P_{CO_2}}\right)^{HP}}{\left(\frac{l}{P_{CO_2}}\right)^C \left(\frac{l}{P_{CH_4}}\right)^{HP}} \geq 1 \tag{6.14}$$

Expressing the composite membrane resistances in terms of the resistances of the individual layers in the composite (*cf.* eq 6.3) and simplifying the resulting expression yields the following:

$$\frac{\left(1+\frac{l^{COAT}}{l^{HP}}\frac{P^{HP}_{CH_4}}{P^{COAT}_{CH_4}}\right)}{\left(1+\frac{l^{COAT}}{l^{HP}}\frac{P^{HP}_{CO_2}}{P^{COAT}_{CO_2}}\right)} \geq 1 \tag{6.15}$$

This condition implies that:

$$\left(\frac{P_{CO_2}}{P_{CH_4}}\right)^{COAT} \geq \left(\frac{P_{CO_2}}{P_{CH_4}}\right)^{HP} \tag{6.16}$$

Using eqs 2.6, 2.23 and 4.3 in the above expression gives the condition that ideal materials should meet to satisfy the selectivity constraint in eq 6.12:

$$\exp[(b^{COAT}-b^{HP})(T_{c_{CO_2}}-T_{c_{CH_4}})]\left(\frac{V_{c_{CH_4}}}{V_{c_{CO_2}}}\right)^{\eta^{COAT}-\eta^{HP}} \geq 1 \tag{6.17}$$

Table 6.1 Parameter values for polysulfone, ethyl cellulose and Hyflon AD 80.

Polymer	***a*** $[cm^3(STP)/(cm^3 \cdot atm)]$	***b*** (K^{-1})	τ^a $[(cm^2/s)\cdot(cm^3/mol)^{\eta}]$	η (-)
Polysulfone	0.0511	0.017	4.79×10^8	8.37
Ethyl cellulose	0.0148	0.017	1.48×10^3	5.03
Hyflon AD 80	0.1936	0.007	2.34×10^5	6.09

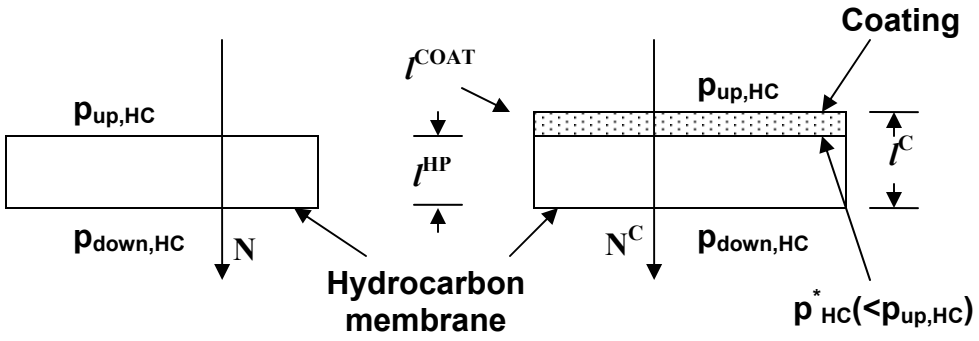

(a) Hydrocarbon polymer membrane **(b) Composite membrane**

Figure 6.1: Schematic diagram of (a) a hydrocarbon polymer membrane and (b) a composite membrane. The subscript 'HC' denotes hydrocarbon gas.

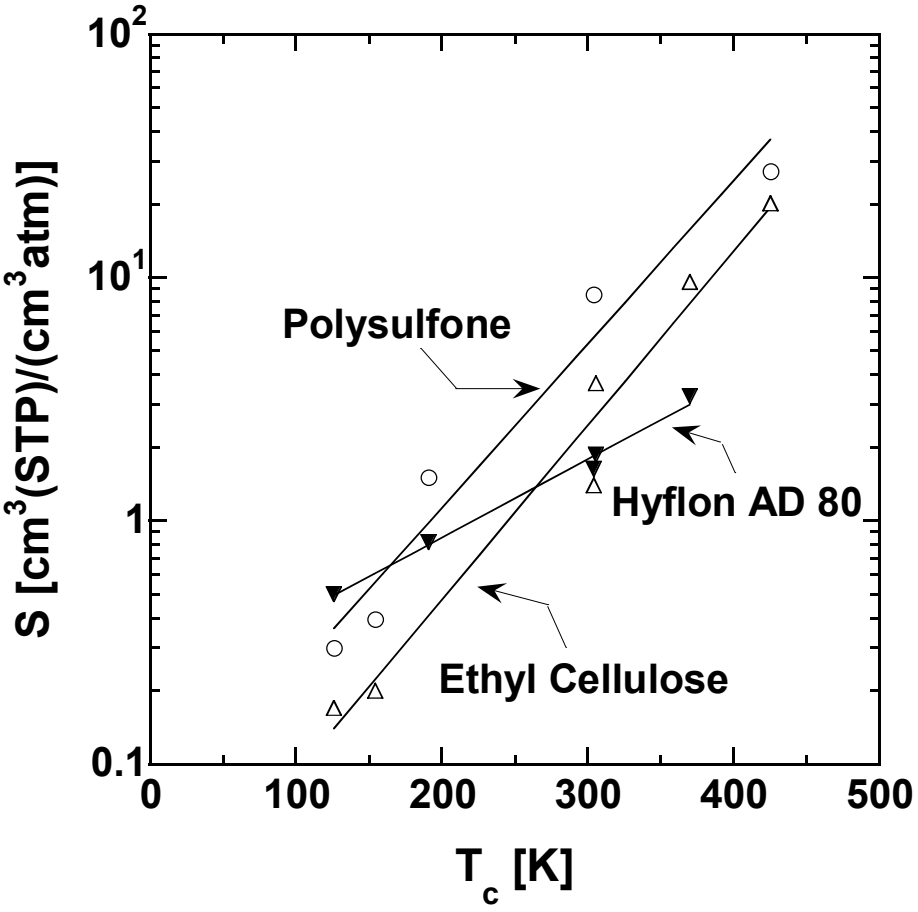

Figure 6.2: Infinite dilution solubility coefficients in polysulfone (o) [51], ethyl cellulose (Δ) [54] and Hyflon AD 80 (▼) at 35 °C as a function of penetrant critical temperature.

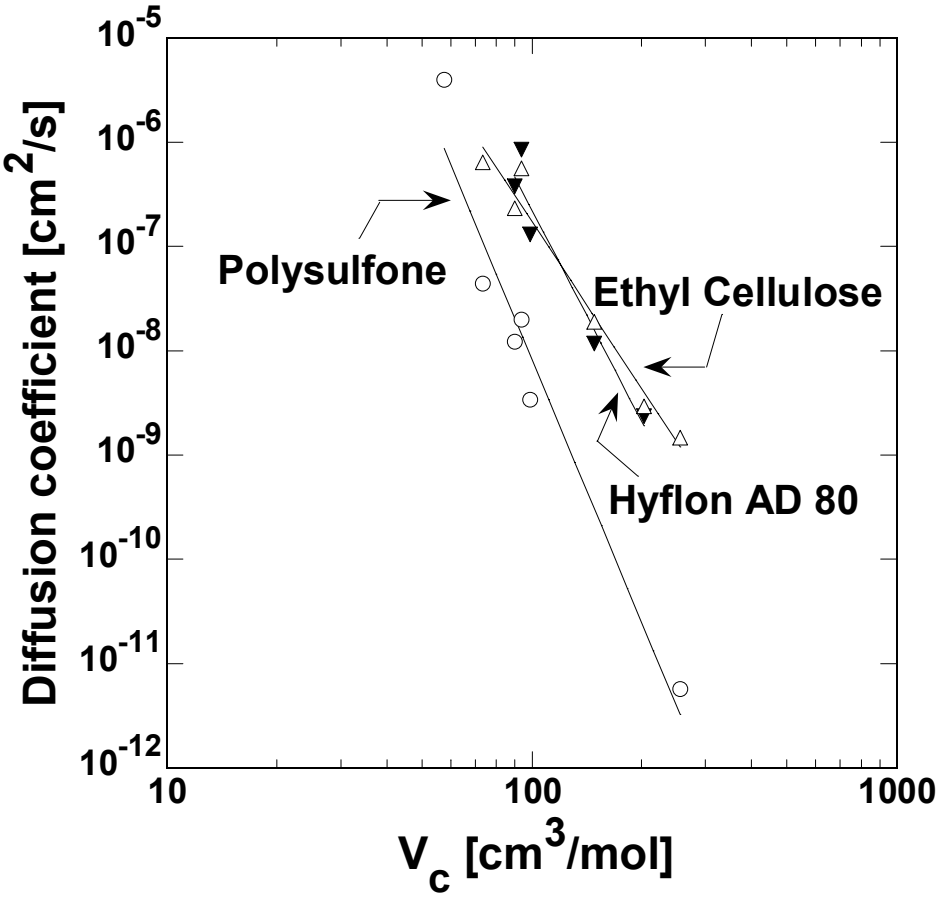

Figure 6.3: Infinite dilution diffusion coefficients in polysulfone (o) [92], ethyl cellulose (Δ) [54] and Hyflon AD 80 (▼) at 35 °C as a function of penetrant critical volume.

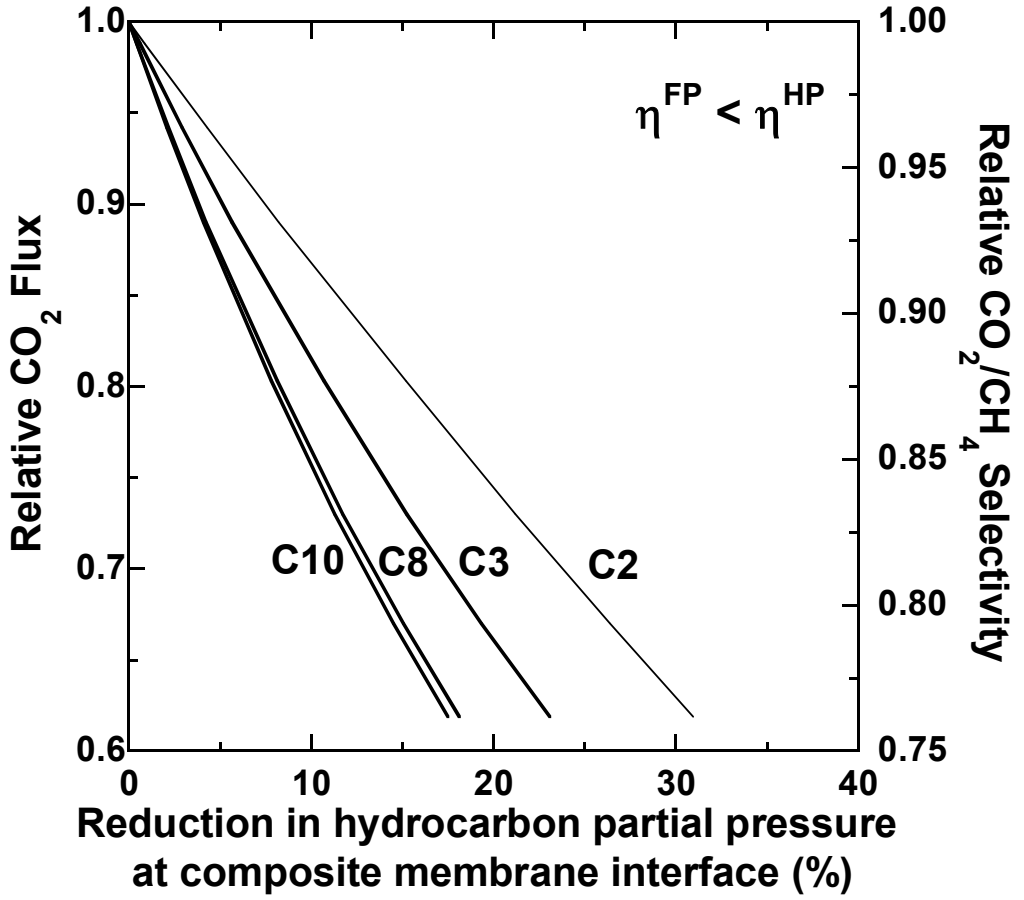

Figure 6.4: Tradeoff between partial pressure reduction of C2, C3, C8 and C10 linear alkanes at the polysulfone/Hyflon AD 80 composite membrane interface and loss in CO_2 flux and CO_2/CH_4 permselectivity. The two y-axes have been so plotted that each of the curves in the figure corresponds to values on both axes.

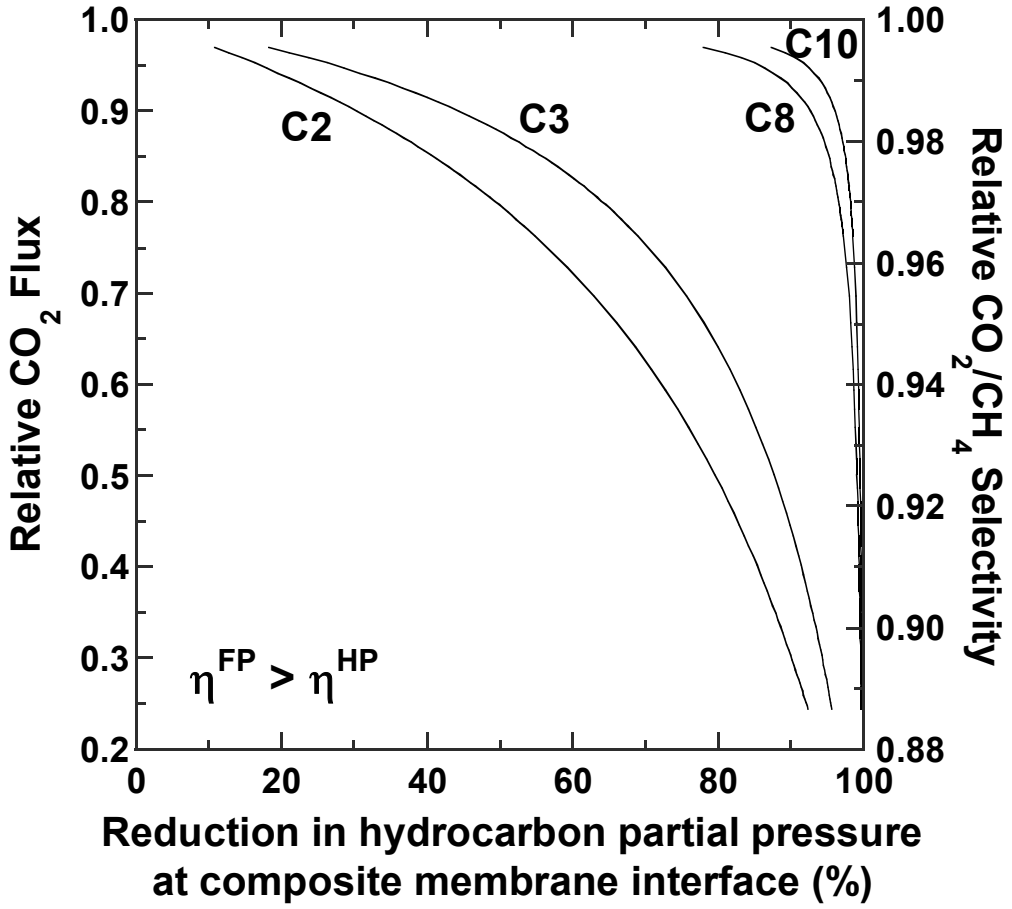

Figure 6.5: Tradeoff between partial pressure reduction of C2, C3, C8 and C10 linear alkanes at the ethyl cellulose/Hyflon AD 80 composite membrane interface and loss in CO_2 flux and CO_2/CH_4 permselectivity. The two y-axes have been so plotted that each of the curves in the figure corresponds to values on both axes.

$$\frac{e^{[(b^{HP}-b^{COAT})(T_{c_{HC}}-T_{c_{CO_2}})]}}{\left(\frac{V_{c_{CO_2}}}{V_{c_{HP}}}\right)^{\eta^{COAT}-\eta^{HP}}}$$

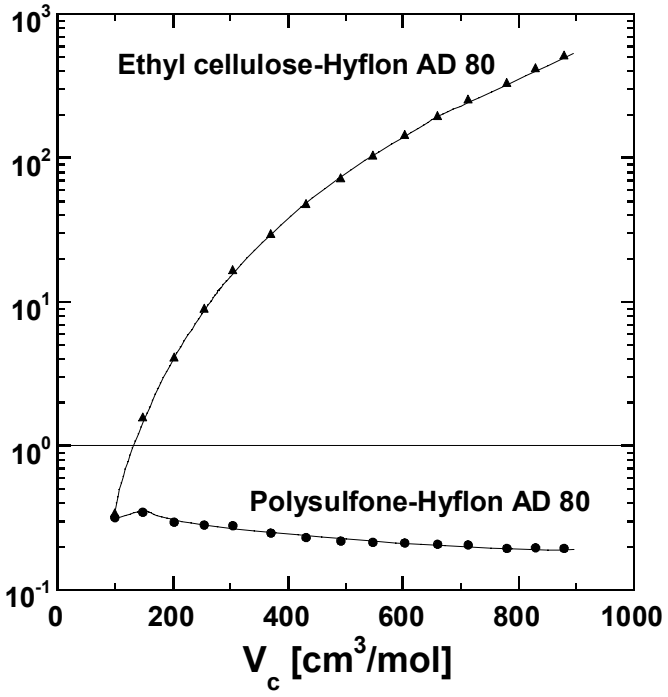

Figure 6.6: Comparison of the value of the expression in eq 6.10 for the two composite membranes as a function of critical volume of C1 to C15 linear alkanes.

CHAPTER 7

Model for Concentration and Temperature Dependence of Permeability in Rubbery Polymers

7.1 SUMMARY

A model describing the concentration and temperature dependence of gas and vapor permeability in rubbery polymers is presented. Solubility and permeability of propane in PDMS, a commercially used vapor separation membrane material, were determined over a wide range of temperatures and pressures to test the model. The model describes propane permeability in PDMS with an average error of 8.2%. The model also accurately predicts a decrease in propane permeability in PDMS with decreasing permeate pressure, at fixed feed pressure. The model is also tested satisfactorily using literature data for transport of condensable penetrants in PDMS and poly(ethylene).

7.2 INTRODUCTION

The permeability of permanent gases in polymers at a fixed temperature is very often constant at low to moderate pressures. The temperature dependence of the permeability coefficient over limited temperature ranges away from polymer thermal transitions can usually be described satisfactorily by an Arrhenius-type equation [11] (*cf.* eq 2.16). Thus, permeabilities measured over a range of temperatures at fixed feed and permeate pressures are sufficient to fit eq 2.16. This equation can then be used to predict permeability coefficients at different temperatures and pressures which might be of interest for the design of a membrane separation system.

However, as seen from the data in Chapters 3, 4 and 5, the solubility and/or diffusion coefficients of condensable penetrants depend, often strongly, on penetrant concentration in the polymer. Such condensable penetrants are increasingly being encountered in newer separations such as organic vapor removal from industrial vent-gas streams, hydrocarbon vapor separation from hydrogen in refineries and hydrocarbon dewpointing of natural gas [25,33,67,72,108-112]. For such penetrants, the permeability coefficient also depends on penetrant concentration and, hence, on temperature as well as feed and permeate pressures. In such cases, permeability coefficient estimates are required at each combination of pressures and temperature being considered for the membrane system. Experimental determination of permeability coefficients at all operating conditions of interest can be a prohibitive task. Therefore, a theoretical framework that can guide the estimation of permeability coefficients as a function of

these processing conditions using a limited amount of experimental data could be useful for designing membrane systems.

The objective of this study has been to develop a rational framework to guide the estimation of permeability at conditions away from those where experimental data are available, especially when permeability is a function of both temperature and pressure. The focus is on modeling the transport of gases and vapors in rubbery polymers since such materials are being used in applications where permeability is a strong function of both temperature as well as upstream and downstream pressure. The model is based on fundamental and well-accepted principles of gas solubility in rubbery polymers, activated Fickian diffusion of small molecules in polymers, and a judicious use of reasonable empirical approximations in cases where available theory does not provide a straight forward and simple element for the model. In all cases, pure gas permeability and sorption data are used to test the model because: (i) there are no systematic experimental studies of gas mixture sorption and permeation properties in rubbery polymers that would permit reasonable validation of a model that included such effects, and (ii) available experience from industrial sources suggests that, for many of the applications mentioned above, mixture effects have less impact on permeability than temperature and pressure.

The following section describes the existing background information and presents the conventional framework for interpreting the temperature and pressure dependence of permeability. It also illustrates the shortcomings of the conventional approach when permeability is a strong function of penetrant concentration in the polymer. Then, the basis for the new model is presented and the relevant equations are derived. Finally, the model is compared with experimental data.

7.3 BACKGROUND

Predicting the effect of pressure and temperature on permeability coefficients is often done by a simple extension of eq 2.16 (*cf.* Figures 7.1(a-d)). Permeability coefficients are first determined experimentally over a range of feed pressures and temperatures, usually at fixed permeate pressure (Figure 7.1a). From these data, permeability values are obtained at fixed feed pressure (*i.e.*, p_1, p_2, p_3 and p_4 in Figure 7.1a), often by interpolation, and over the entire temperature range. These values are used to obtain P_o and E_P values by a least-squares fit of eq 2.16 (Figure 7.1b). By repeating this process at different feed pressures, the values of E_P and P_o can be determined over a range of feed pressures (*cf.* Figures 7.1(c-d)). Eq 2.16 can then be used, along with the best-fit values of the adjustable constants, to estimate gas permeability at various combinations of feed pressure and temperature.

The above methodology has several drawbacks. It requires many empirical adjustable constants to fit eq 2.16 using the graphical method outlined in Figure 7.1. Also, these parameters may have little or no physical significance, which can sharply compromise the ability to estimate permeability coefficients beyond the temperature and pressure window that has been explored experimentally. Finally, this methodology cannot account for the effect of changes in permeate pressure on the permeability coefficient. So, if a membrane was operated at a permeate pressure other than that for which experimental data are available, and if permeability is sensitive to permeate pressure, then this method fails to provide a pathway for rational extrapolation of the data. Therefore, a

method circumventing these disadvantages and providing predictions of the concentration and temperature dependence of gas and vapor permeability in polymers based on limited experimental data would be useful. As a first step in this direction, we describe a model which yields algebraic expressions to describe the effect of temperature and feed as well as permeate pressure on pure gas permeability coefficients. This model requires very few fitting parameters. The utility of the model and its capabilities are demonstrated by correlating data from the literature and from our laboratory for the transport of organic vapors in rubbery polymers.

PDMS was chosen as the model polymer because it is used commercially as a vapor separation membrane material [4]. The permeability and solubility of a condensable hydrocarbon, propane, were measured over a wide range of (feed) pressures and temperatures to obtain data for testing the model. Permeability measurements were also performed at two different permeate pressures to study the effect of changes in permeate pressure on vapor permeability in this polymer. These data were utilized to test the capability of the model for predicting the effect of change in permeate pressure on vapor permeability. The model has also been tested with data from literature for the transport of halothane, a commercial anesthetic, in PDMS and for several organic compounds in poly(ethylene). The main selection criterion for data was the availability of both solubility and permeability coefficients for the penetrant in the polymer as a function of pressure and temperature. Detailed information about the model cases is recorded in Table 7.1.

7.4 THEORY

Eq 2.6 is widely used to calculate gas transport properties of membranes and gas flux in membrane-based separation processes. However, this equation is based on several assumptions like constant diffusion coefficient and applicability of Henry's law or negligible permeate pressure, as discussed in section 2.1.1. If the diffusion coefficient is a function of penetrant concentration and temperature, then an appropriate form of this function must be chosen and substituted in eq 2.3 to determine the permeability coefficient.

The temperature dependence of the diffusion coefficient is typically well-described by the activated diffusion model of Arrhenius [113] (eq 2.17). Interestingly, it has been observed that D_o and E_D in this equation are not independent. Using diffusivity data for light gases in several rubbery polymers over the temperature range from 17 to 50 ^oC, van Amerongen found that [114]:

$$\ln D_o = A\frac{E_D}{R} - B \tag{7.1}$$

where A has a value of 0.0023 K^{-1} and B is 9.7 when D_o has units of cm^2/s. This equation is the "linear free energy relationship". Barrer used a slightly different expression to describe the relationship between D_o and E_D [115],

$$\ln D_o = A'\frac{E_D}{RT} - B' \tag{7.2}$$

Barrer utilized van Amerongen's data [114], as well as diffusivity of permanent gases and light hydrocarbons over different temperature ranges in several rubbery polymers [115,116], to obtain best fit values for A' and B'. The reported values are 0.64 for A' and 8.3 for B', when D_o has units of cm^2/s. While eq 7.2 appears to be a more general form of eq 7.1, it leads to an apparent inconsistency. If eq 7.2 is substituted in eq 2.17, one obtains,

$$D = e^{-B'} \exp\left(\frac{(A'-1)E_D}{RT}\right) \tag{7.3}$$

Eq 7.3 implies that a plot of the natural logarithm of D versus $1/T$ should result in a fixed intercept of ($-B'$), irrespective of the value of E_D, or for that matter, the gas and the polymer. This is contradictory to the linear free energy relationship and is obviously not the case [114-116]. The equation proposed by van Amerongen does not suffer from this issue, as can be seen by substituting eq 7.1 into eq 2.17:

$$D = e^{A\frac{E_D}{R}-B} \exp\left(\frac{-E_D}{RT}\right) \tag{7.4}$$

From eq 7.4, a plot of the natural logarithm of D versus $1/T$ results in an intercept which depends on E_D as described by the linear free energy relationship. Eq 7.1 is, therefore, chosen as a more consistent form of the empirical linear free energy relationship.

Figure 7.2 presents the least square best fit form of eq 7.1 to experimental data from several sources to demonstrate the correlation between D_o and E_D [50,114-119]. These data include the original data utilized by van Amerongen and Barrer as well as more recent reports of D_o and E_D values for diffusion in rubbery polymers. Eq 7.1 fits the data well with A and B values of 2.0×10^{-3} K^{-1} and 8.3, respectively (Figure 7.2), when D_o is expressed in cm^2/s, which are very similar to the values obtained by van Amerongen almost 60 years ago. These updated values of the fitting parameters are used in the model for the temperature and concentration dependence of permeability.

Rearranging eq 7.4, one obtains:

$$D = e^{-B} \exp\left(\alpha E_D\right) \tag{7.5}$$

where

$$\alpha = \frac{1}{R}\left(A - \frac{1}{T}\right) \tag{7.6}$$

7.4.1 Concentration Dependence of the Diffusion Coefficient

Penetrant diffusion coefficients in rubbery polymers typically increase with increasing penetrant concentration in the polymer [25,33,67,72,109,111,112]. In many cases, the following simple model is used to describe this concentration dependence [26,109,111,120]:

$$D = \varepsilon e^{\lambda C} \tag{7.7}$$

where ε and λ are adjustable constants and C is penetrant concentration in the polymer. Some reports use penetrant volume fraction [110,111] or penetrant activity [112], instead of concentration, in eq 7.7.

Free volume theory is often invoked to explain the concentration dependence of diffusivity as described in eq 7.7. In the free volume model, D is given by [121]:

$$D = M \exp\left(-\frac{N}{v_f}\right) \tag{7.8}$$

where M and N are adjustable constants and v_f is the volume fraction of the free volume of the polymer (called free volume, henceforth). The free volume of the polymer is often expressed as a function of three thermodynamic variables: temperature, T, hydrostatic pressure, p, applied to the penetrant-polymer system, and penetrant concentration in the polymer, which is usually expressed as the penetrant volume fraction in the polymer, φ [122]:

$$v_f\left(T, p, \phi\right) = v_{fs}\left(T_s, p_s, 0\right) + \alpha'\left(T - T_s\right) - \beta'\left(p - p_s\right) + \gamma'\phi \tag{7.9}$$

where $v_{fs}(T_s,p_s,0)$ is the free volume of the pure polymer at some reference temperature, T_s, and pressure, p_s, and α', β' and γ' are adjustable constants. α' and β' are often set to the polymer's thermal expansion coefficient and compressibility, respectively.

This model (eqs 7.8-7.9) has many parameters that need to be determined by independent experiments or estimated by data-fitting techniques. Also, Rogers *et al.* have shown that at low sorbed concentrations, the above model degenerates (via a Taylor series expansion) to the empirical model (eq 7.7) [112]. From a practical standpoint, for the development of the model in this study, eq 7.7 is advantageous due to its simplicity.

From eqs 7.5 and 7.6, D is a function of E_D and T. Therefore, the concentration dependence of the diffusion coefficient must arise due to a concentration dependence of E_D. Comparing eqs 7.5 and 7.7, an exponential dependence of the diffusion coefficient on concentration requires a linear dependence of the activation energy on concentration. Thus, as a first approximation,

$$E_D = E_D^o\left(1 - kC\right) \tag{7.10}$$

where $E_D{}^o$ is the activation energy of diffusion in the infinite dilution limit and k is an adjustable constant that describes the effect of penetrant concentration in the polymer on the activation energy of diffusion. From eqs 2.3, 7.5, 7.6 and 7.10,

$$P = \frac{e^{-B}}{p_2 - p_1}\frac{e^{\alpha E_{D2}} - e^{\alpha E_{D1}}}{-\alpha E_D^o k} \tag{7.11}$$

where

$$E_{Dn} = E_D^o(1 - k\,C_n), \quad n = 1, 2 \tag{7.12}$$

where subscripts 1 and 2 refer to the downstream and upstream faces of the membrane, respectively. Eq 7.11 incorporates the concentration dependence of the diffusion coefficient and also explicitly describes the effect of permeate pressure, p_1, on the permeability coefficient.

Eq 7.11 requires concentration values at the pressures and temperature at which the permeability coefficients are to be calculated. Therefore, an appropriate sorption model is needed to calculate the penetrant concentration values required in eq 7.11. The cases in this study correspond to condensable vapor sorption and transport in rubbery polymers. Therefore, the Flory-Huggins model (eq. 2.11) is utilized to describe penetrant sorption in these cases. For crosslinked rubbers like PDMS, one might also consider the Flory-Rehner model (eq 2.12), which accounts for the influence of crosslinks on the penetrant free energy in the polymer. However, from a practical viewpoint, such effects are often quite small for the industrial examples mentioned earlier, so we have used the simpler Flory-Huggins model in this development.

In the Flory-Huggins equation, the χ parameter describes the interaction between the penetrant and the polymer and is hence a function of temperature, T [123]. In some cases, this parameter also varies with penetrant concentration in the polymer [25]. The concentration dependence is normally described adequately by a power series [54]. Although many forms have been proposed to describe the temperature and concentration

dependence of χ [54], in this work, these two dependencies have been empirically combined into a single equation as follows:

$$\chi = \chi_a + \frac{\chi_b}{T} + \chi_c\left(1-\phi_2\right) \tag{7.13}$$

where χ_a, χ_b and χ_c are adjustable constants. The need for a temperature or concentration dependence of χ for a particular penetrant-polymer pair can be determined by performing an F-test on the results obtained by fitting sorption data to the Flory-Huggins equation with different number of adjustable constants in eq 7.13 [80].

7.5 EXPERIMENTAL

7.5.1 Materials

PDMS films were prepared from an isooctane solution of 40 wt % Dehesive® 940A silicone (Wacker Silicones Corporation, Adrian, MI). As supplied by the manufacturer, the Dehesive® 940A silicone product is a viscous 30 wt % silicone gum in naphtha solvent. Before casting, the proprietary Crosslinker V24/Catalyst OL system provided by Wacker Silicones Corporation was added to the polymer solution. The films were made by pouring the polymer solution into a casting ring supported by a glass plate. The cast films were dried slowly at ambient conditions for 4 days. They were then placed in an oven at 110 °C for 30 min to remove residual solvent and to fully crosslink the polymer. After cooling to room temperature, the crosslinked films were easily

removed from the casting ring and glass plate. Finally, the films were washed with *n*-heptane in a soxhlet extractor for 3 days to remove impurities (*i.e.*, unreacted crosslinker and catalyst). The resulting PDMS films were transparent and rubbery and were not tacky. Film thicknesses were determined with a digital micrometer readable to ±1 μm and were 220 μm for the permeation samples. The density of the PDMS films was 0.99 g/cm^3, and their crosslink density was approximately 4.93×10^{-4} mol/cm^3.

Chemical grade propane of purity 99% was purchased from Matheson TriGas (Austin, TX) and was used as received.

7.5.2 Characterization

Propane solubility coefficients were determined using a high-pressure barometric apparatus as described in section 2.2.1. The sorption experiments were performed in the following order: 35 °C, 55 °C, 20 °C and 0 °C. The maximum pressure was 3.4 to 8.3 atm depending on the temperature.

Pure gas propane permeability coefficients at a permeate pressure of 1 atm were determined using a constant pressure/variable volume apparatus as described in section 2.2.2. The upstream pressure was varied from a minimum of 1.1 – 1.7 atm to a maximum of 1.95 – 8.5 atm, depending on the temperature. Permeability coefficients were determined in the order of decreasing temperature, *i.e.*, 55°C to -20 °C.

Pure gas permeability coefficients at a permeate pressure of 0 atm were measured in a constant volume/variable pressure apparatus, which is also described in section 2.2.2.

The upstream pressure was varied from 1.3 atm to 2.3 atm. The downstream side was maintained below 10 mm Hg.

7.6 EXPERIMENTAL RESULTS

Figure 7.3 displays sorption isotherms of propane in PDMS from 0 to 55 ^{o}C. The isotherms are convex to the pressure axis, which is typical for sorption of condensable penetrants in rubbery polymers [11]. The curvature of the isotherms decreases with increasing temperature, suggesting a weaker dependence of solubility on pressure at higher temperatures. This is consistent with the findings of Shah *et al.* [71] who observed a decrease in the pressure dependence of propane solubility in PDMS as temperature increased. Shah *et al.* report infinite dilution propane solubilities of 6.45 and 4.04 cm^3(STP)/(cm^3·atm) at 35 and 55 ^{o}C, respectively. Our values (6.5 and 4.2 cm^3(STP)/(cm^3·atm), respectively) are in excellent agreement with theirs.

Figure 7.4 displays permeability coefficients for propane in PDMS as a function of upstream pressure over the temperature range -20 to 55 ^{o}C. The downstream pressure was 1 atm. Propane permeability increases with decreasing temperature at any given pressure. This is consistent with previous observations of the temperature dependence of propane permeability in PDMS [27]. Stern *et al.* obtained a propane permeability of 8,580 Barrers at 35 ^{o}C in the limit of negligible pressure drop across the membrane [27], which is in reasonable agreement with the value of about 6,500 Barrers obtained in this study under the same temperature and pressure conditions.

7.7 MODEL-FITTING PROCEDURE

As indicated in section 7.4, the Flory-Huggins equation was used to describe penetrant sorption and calculate penetrant concentration values for fitting the permeability model (eq 7.11). Eq 7.13 was used to describe the temperature and concentration dependence of the χ parameter in the Flory-Huggins equation. The values of the adjustable constants in eq 7.13 and the quality of the fits are reported in Table 7.2. The model fit is shown as the smooth curves through the data points in Figure 7.3 for propane in PDMS and it is in excellent agreement with the experimental data.

The permeability model (eq 7.11) contains 2 adjustable constants, E_D^o and k. In addition, B is treated as an adjustable constant, despite its best-fit value determined from Figure 7.2, due to the scatter in the data points around the best-fit linear trendline in Figure 7.2. Best-fit values of these parameters are determined by a non-linear least-squares fit to experimental permeability data over a range of pressures and temperatures, and they are listed in Table 7.3 for all penetrant-polymer pairs in this study. The smooth curves in Figure 7.4 represent fits of the model to the propane-PDMS data using the parameters in Table 7.3. The fits are, in most cases, within the experimental uncertainty of the data.

7.8 RESULTS AND DISCUSSION

7.8.1 Propane in PDMS

From Figure 7.3 and Table 7.2, the Flory-Huggins equation provides an excellent description of propane sorption in PDMS with a concentration and temperature dependent χ parameter. Penetrant concentration values from this equation and experimental permeability data from Figure 7.4 were used to fit the permeability model in Eq 7.11. The best fit values of the adjustable constants, E_D^o, k and B, are listed in Table 7.3. The quality of the resulting fit can be judged from Figures 7.4 and 7.5a. From Table 7.3, the best-fit value for E_D^o is 11.3 kJ/mol. This compares well with the E_D value of 11.8 kJ/mol reported by Stern *et al.*, based on diffusivity values in the infinite dilution limit over the temperature range 10 – 55 ^oC [27]. The best-fit value of B obtained from the fitting procedure with the current data set is 10.2, which is higher than the value of 8.3 given by the best-fit trendline in Figure 7.2. However, using our E_D^o and B values in eq 7.1, the calculated D_o value is 5.6×10^{-4} cm^2/s, which is close to the value of 9×10^{-4} cm^2/s reported by Stern *et al*. [27].

7.8.2 Halothane in PDMS

Halothane ($CF_3CHClBr$) solubility and permeability data are presented in Figures 7.6 and 7.7, respectively [72]. Halothane sorption in PDMS is adequately modeled by the Flory-Huggins equation with a constant χ parameter (Table 7.2 and Figure 7.6). The best-fit values of the adjustable constants of eq 7.11 for this penetrant-polymer pair are

reported in Table 7.3. With these parameters, the permeability data can be described with less than 10% error (except for one point), as shown in Figure 7.5b, which is probably the limit of the experimental measurements. The best-fit E_D^o value is 15 kJ/mol, which is in excellent agreement with the E_D value of 14.8 kJ/mol calculated by Suwandi and Stern [72] from the same data set, in the infinite dilution limit, by using eq 2.17. Similar to the case of propane transport in PDMS, the B value for this penetrant in PDMS is 10.6, which is higher than the best-fit value of 8.3 estimated from the data in Figure 7.2. Thus, PDMS seems to obey the linear free energy relationship with a B value that is higher than that reported for other polymers. This can also be seen from Figure 7.2, where the points depicting penetrant transport in PDMS (solid symbols) are seen to lie at the outer fringes of the data scatter in the figure. The fundamental basis for this discrepancy is not known.

7.8.3 Various Organic Vapors in Poly(ethylene)

Methyl bromide, isobutylene and *n*-hexane sorption isotherms in poly(ethylene) (PE) are presented in Figures 7.8(a-c) [112]. Sorption of *n*-hexane and isobutylene in PE is very well described by the Flory-Huggins model with a temperature dependent χ parameter, while methyl bromide sorption requires a concentration and temperature dependent χ parameter (*cf.* Table 7.2). The permeability coefficients of the three penetrants in PE are shown in Figures 7.9(a-c) [112]. Eq 7.11 could predict permeabilities for the 3 penetrants in PE with less than 10% error for practically all of the data, with the best-fit values reported in Table 7.3 (*cf.* Figures 7.5(c-e)). From this Table, B values for the 3 penetrants in this polymer are much closer to the best-fit value of 8.3

(from Figure 7.2), than the B values for PDMS. E_D values for these penetrant-polymer pairs could not be found in the literature, for comparison. However, diffusion coefficients of penetrants in polymers typically decrease with increasing penetrant size [92]. Diffusion coefficients often scale with penetrant critical volume, V_c, as mentioned previously (eq 4.3). From eqs 2.17 and 4.3, E_D is expected to have a logarithmic dependence on V_c. Figure 7.10 presents E_D values of several penetrants in PE [54] as well as the E_D^o values of the three penetrants in this study. A logarithmic trendline provides a good correlation between E_D and V_c for these penetrants in PE.

The above examples show that the model (eq 7.11) can describe concentration and temperature dependent permeability data well with very few fitting parameters. Also, estimates of the values of two of the parameters, E_D^o and B, can be obtained from their values for other penetrants in the same polymer and by utilizing correlations between activation energy of diffusion and penetrant size. These can then be used to provide rough estimates of permeabilities, as a first approximation, in the absence of any experimental permeability values.

7.8.4 Effect of Permeate Pressure on Permeability

For penetrants having a concentration dependent permeability, variation in both feed and permeate pressures can change the permeability because both pressures affect penetrant concentration in the polymer. For example, Figure 7.11 shows predictions (solid lines) of the model (eq 7.11) for propane permeability in PDMS at -10 ^oC and two different permeate pressures, using the best-fit values in Table 7.3. (Permeability data at

-10 °C were not used to determine these best-fit values.) The model predicts that permeability decreases as downstream pressure decreases. At the highest upstream pressure (2.36 atm), propane permeability is predicted to decrease by 24% on decreasing the downstream pressure from 1 atm to 0 atm. This prediction is of interest because decreasing the downstream pressure at fixed upstream pressure may be used to increase the driving force for permeation and, hence, gas flux through a membrane. In the current example, at the highest feed pressure, the driving force is increased by 73.5% as the downstream pressure decreases from 1 atm to vacuum. The standard model, as given by eq 2.16, would predict a constant permeability coefficient with change in permeate pressure. Thus, eq 2.1 would predict a 73.5% increase in flux. However, experimentally, and according to the new model, flux only increases by 32% due to the decrease in permeability with decreasing permeate pressure. Thus, the new model is able to predict the effect of permeate pressure on permeability coefficients and therefore provides more reliable values of permeability for design calculations.

7.9 CONCLUSIONS

Propane solubility in PDMS increases with decreasing temperature, and the sorption isotherms are well-described by the Flory-Huggins equation with a concentration and temperature dependent χ parameter. Propane permeability increases with decreasing temperature in PDMS, and is well-described by the model presented in this chapter. Propane permeability decreases with decreasing permeate pressure, and both the magnitude and direction of this permeability change are captured by the model. The

model also provides a good description of halothane permeability in PDMS and various organic vapors in PE. The model requires few adjustable constants and may be useful as a first step to provide a rational framework for estimating permeability coefficients in rubbery polymers at operating conditions that are not in the range of those used to acquire experimental data.

Table 7.1 Solubility and permeability data sources.

Penetrant	***Polymer***	***Solubility Data***			***Permeability Data***			***Reference***
		Temperature Range (^oC)	***Number of Isotherms***	***Total number of points***	***Temperature Range (^oC)***	***Number of Isotherms***	***Total number of points***	
Propane	PDMS	0 – 55	4	65	-20 – 55	5	45	this study
Halothane *	PDMS	21 – 50	6	35	17 – 60	5	27	[72]
Methyl Bromide	PE	0 – 30	2	11	0 – 30	2	8	[112]
Isobutylene	PE	-8 – 30	3	8	-8 – 30	3	8	[112]
n-hexane	PE	0 – 30	2	10	0 - 30	2	7	[112]

* The chemical formula of Halothane is $CF_3CHClBr$.

Table 7.2 Model parameters for solubility data.

Penetrant	***Polymer***	***Adjustable constants from equation 7.13***			***Error in Model Prediction (%)*** [a]		
		χ_a	χ_b ***(K)***	χ_c	***Average***	***Standard deviation***	***Maximum***
Propane	PDMS	-0.64	518	-0.97	1.9	1.6	8.9
Halothane	PDMS	0.52	-	-	3.6	2.4	8.6
Methyl bromide	PE	-5.97	863	5.11	1.3	1.1	3.2
Isobutylene	PE	-2.38	1159	-	1.2	1.2	3.5
n-hexane	PE	-0.63	603	-	2.3	1.7	4.5

[a] Percentage error in model prediction (for each data point) = $\left|\frac{C_{model} - C_{expt}}{C_{expt}}\right| \times 100$. The magnitude and variation of prediction errors of individual experimental points are characterized by the average, maximum and standard deviation of these error values.

Table 7.3 Model parameters for permeability data.

Penetrant	***Polymer***	***Adjustable constants from equations 7.11 and 7.12***		
		E_D^o ***(kJ/mol)***	$k \times 10^3$ ***(cm^3/cm^3(STP))***	***b***
Propane	PDMS	11.3	5.35	10.2
Halothane	PDMS	15	0.10	10.6
Methyl bromide	PE	55	7.45	7.6
Isobutylene	PE	53	19.5	8.6
n-hexane	PE	59	14.85	7.8

(a)

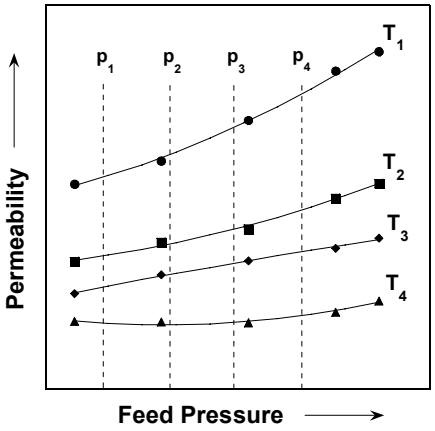

Permeate pressure - constant

(b)

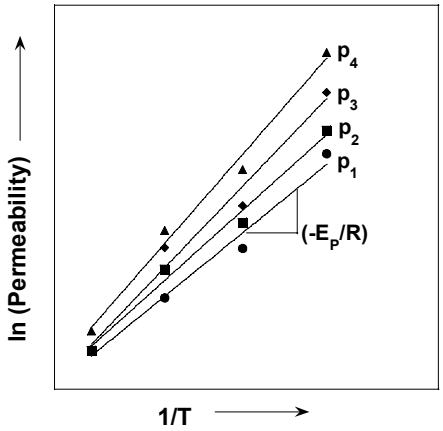

Minimum requirement: 2 fitting parameters per line, 3 lines to provide 3 points for figures (c) and (d).

(c)

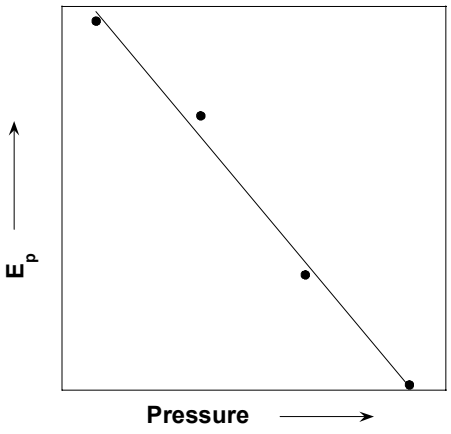

Minimum requirement: 2 fitting parameters, 3 points

(d)

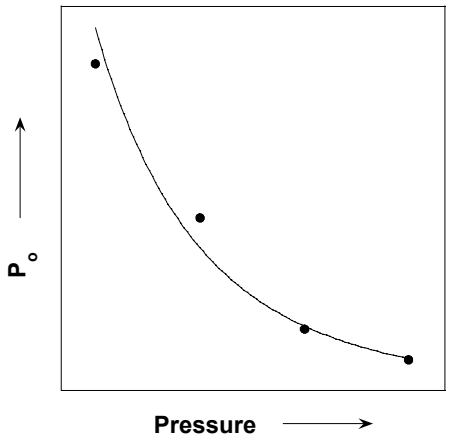

Minimum requirement: 2 fitting parameters, 3 points

Figure 7.1: Cartoon illustrating the graphical technique for using eq 2.16 to describe pressure and temperature dependent penetrant permeability in a polymer. The experimentally measured permeabilities are shown in figure (a). These data are re-plotted, at fixed feed pressures, in figure (b) to determine the adjustable parameters, E_D and P_o, from the slope and intercept of the best-fit trendline through the data. The values of these parameters at different pressures are then plotted in figures (c) and (d), respectively. The pressure dependence of these two parameters are then determined from figures (c) and (d). This graphical method requires at least 10 fitting parameters: 6 for figure (b) and 2 each for figures (c) and (d).

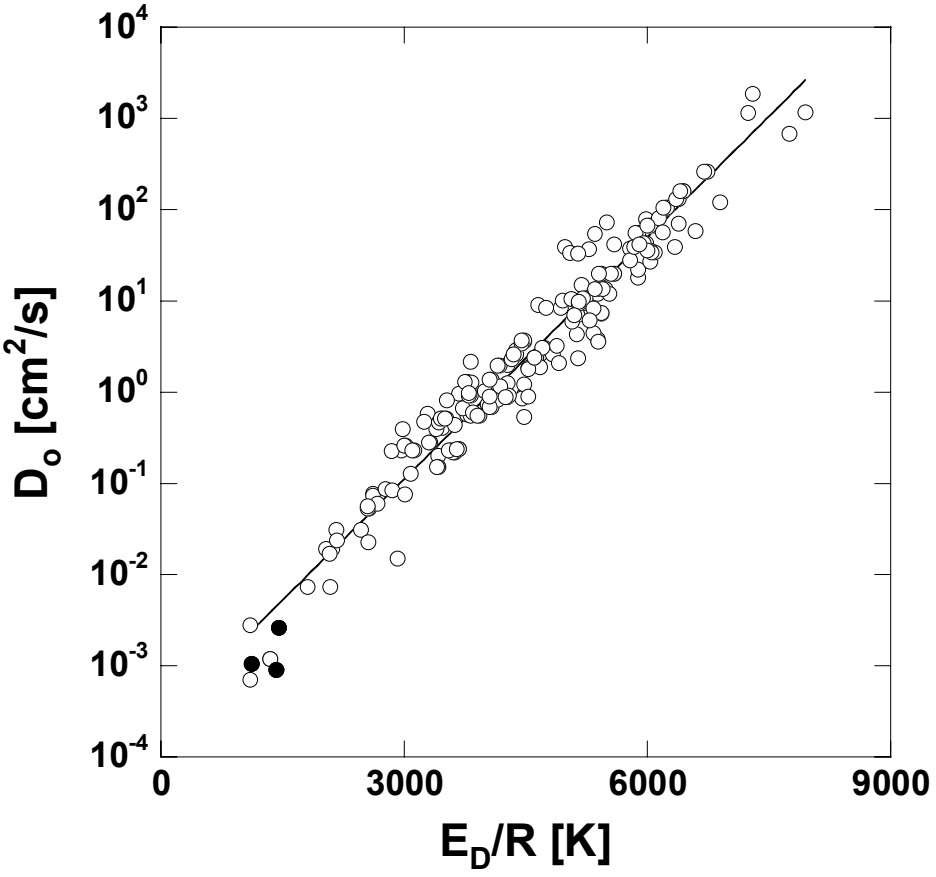

Figure 7.2: Linear free energy relationship based on data for transport of permanent gases and hydrocarbons in several rubbery polymers [50,114-119]. The least square best-fit line in the figure has the equation: $\ln(D_o[\text{cm}^2/\text{s}]) = 2.0\times10^{-3}\ E_D/R\ [\text{K}] - 8.3$. The filled symbols indicate points corresponding to PDMS, and they have been included in determining the constants of the linear free energy relationship.

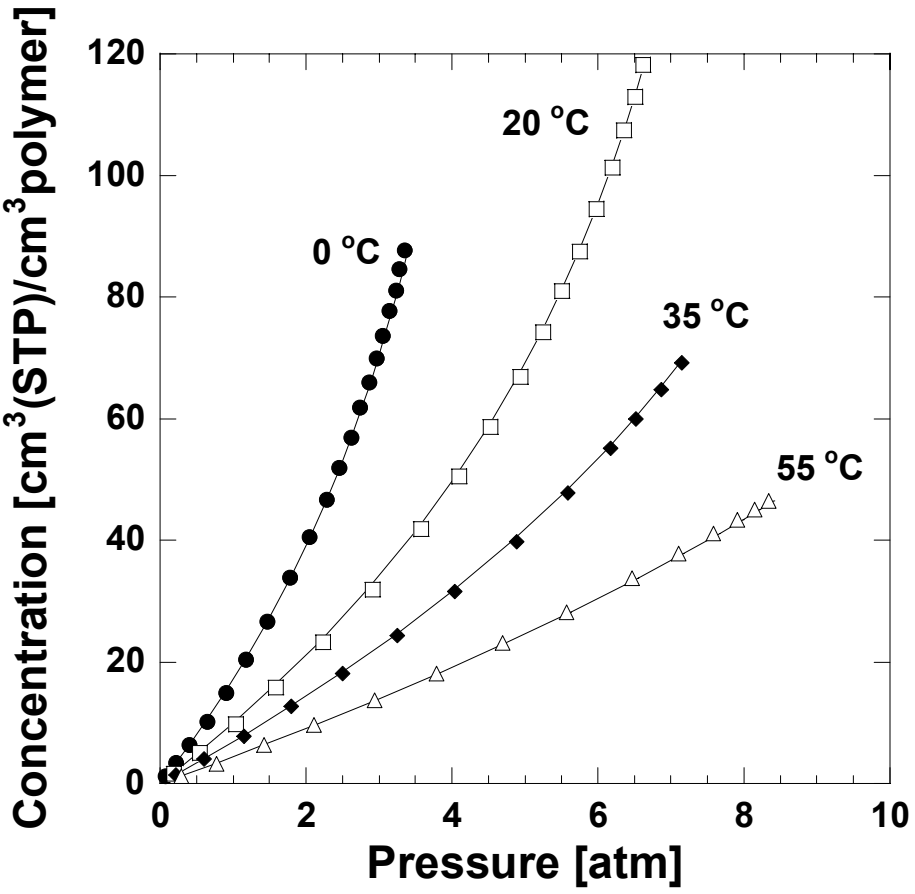

Figure 7.3: Sorption isotherms of propane in PDMS at 0 – 55 °C. The lines represent Flory-Huggins fits to the experimental data based on the adjustable constants in Table 7.2.

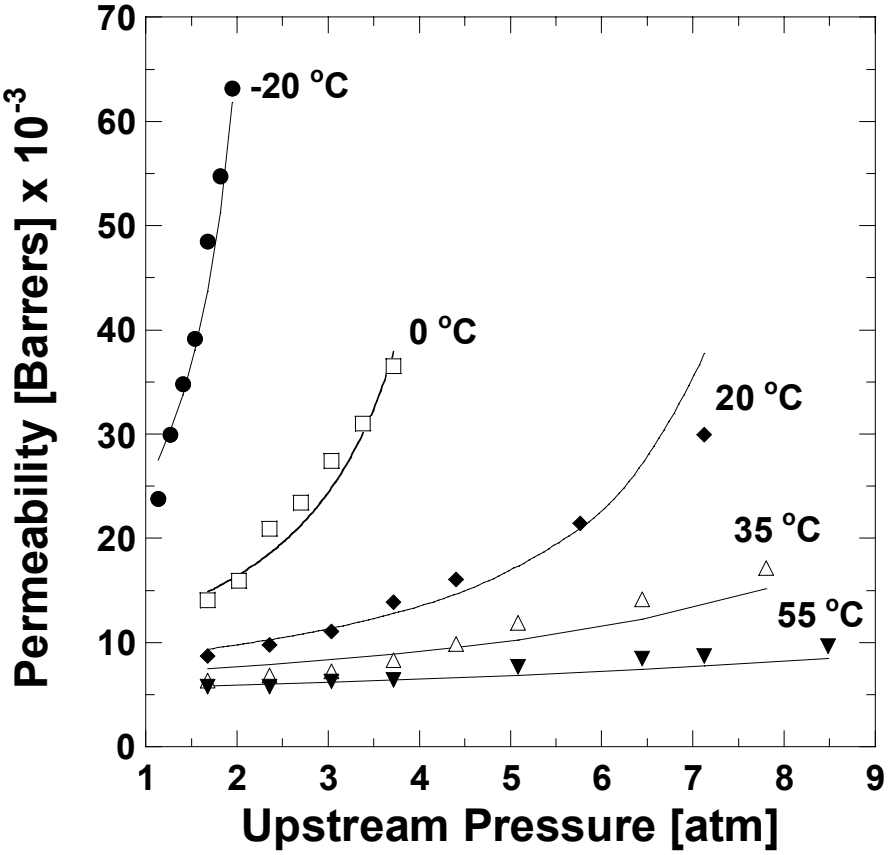

Figure 7.4: Permeability coefficients of propane in PDMS at -20 °C to 55 °C. The lines represent model fits to the experimental data based on the adjustable constants in Table 7.3.

(a) Propane in PDMS

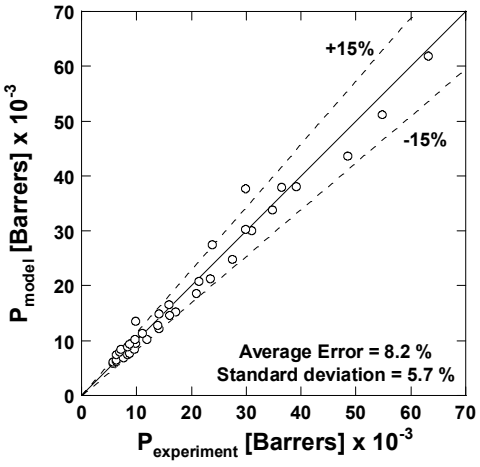

(b) Halothane in PDMS

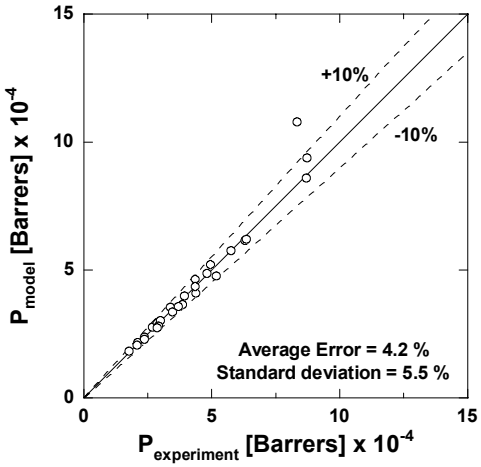

(c) Methyl bromide in Poly(ethylene)

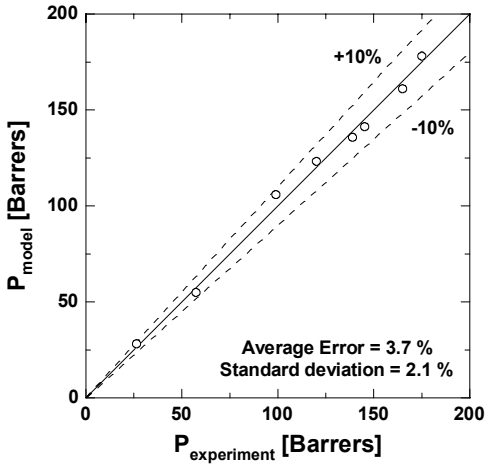

(d) Isobutylene in Poly(ethylene)

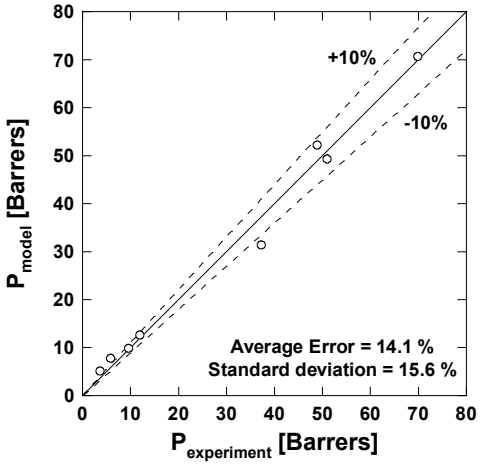

(e) *n*-hexane in Poly(ethylene)

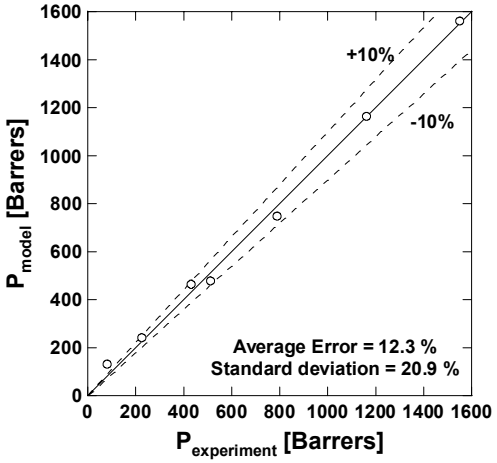

Figure 7.5: Quality of fit.

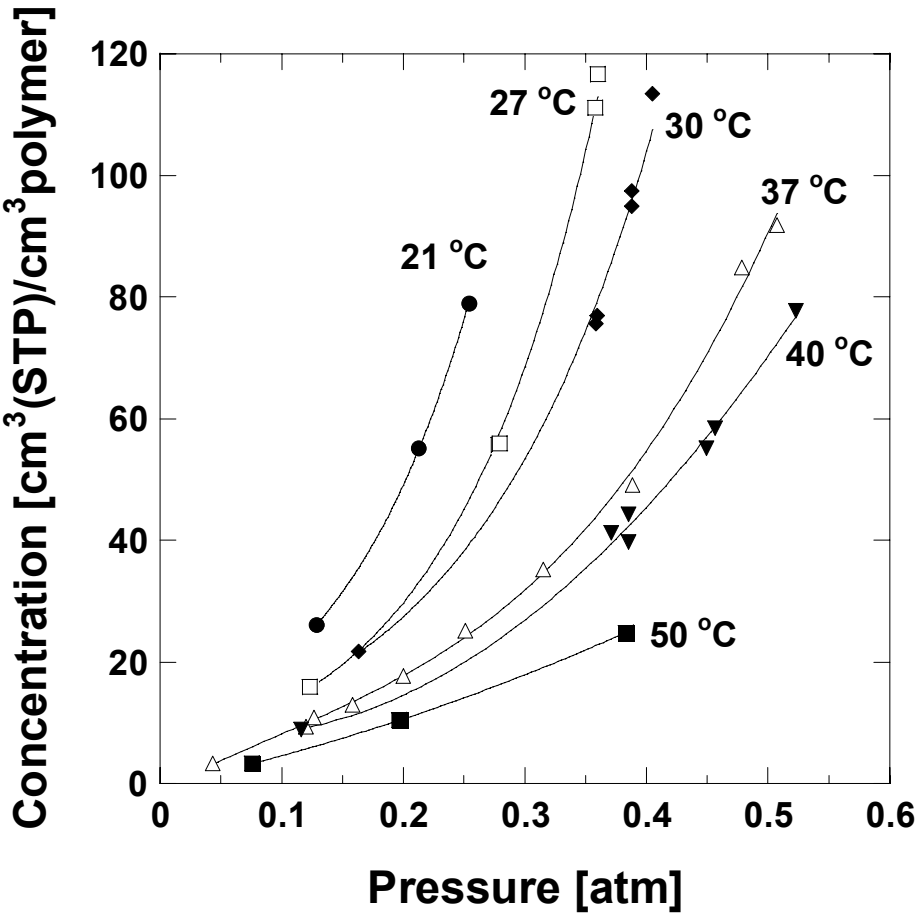

Figure 7.6: Halothane sorption isotherms in PDMS at 21 – 50 °C [72]. The lines represent Flory-Huggins fits to the experimental data based on the adjustable constants in Table 7.2.

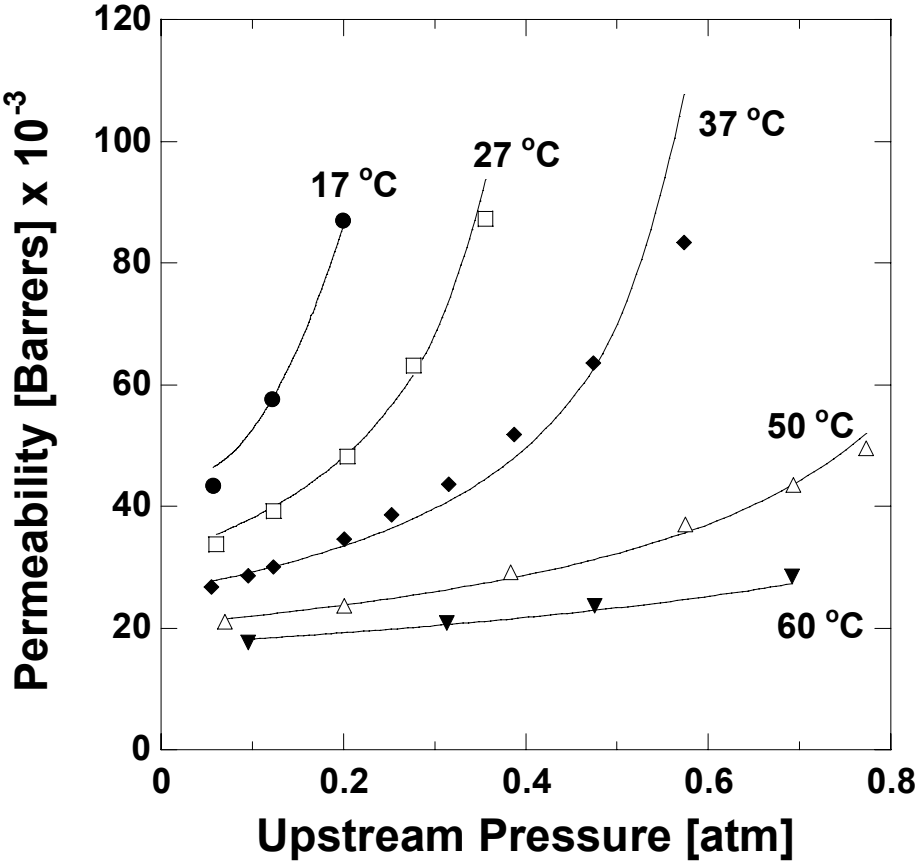

Figure 7.7: Permeability coefficients of halothane in PDMS at $17 - 60\ ^{o}C$ [72]. The lines represent model fits to the experimental data based on the adjustable constants in Table 7.3.

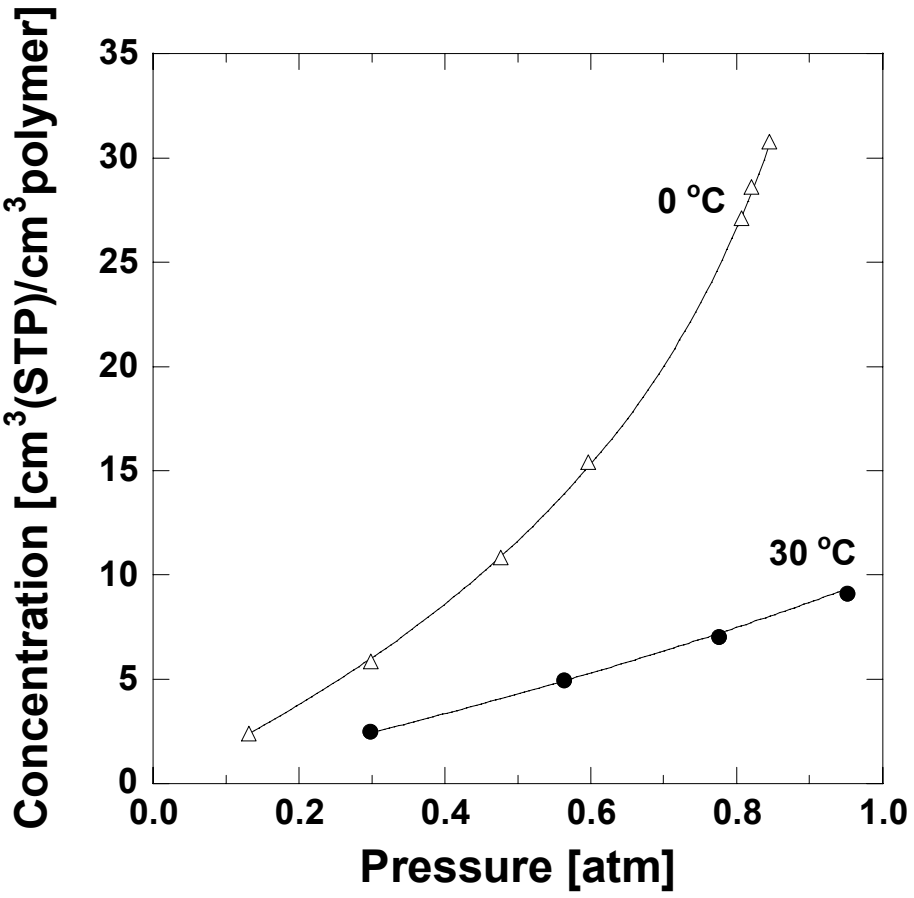

Figure 7.8a: Sorption isotherms of methyl bromide in poly(ethylene) [112]. The lines represent Flory-Huggins fits to the experimental data based on the adjustable constants in Table 7.2.

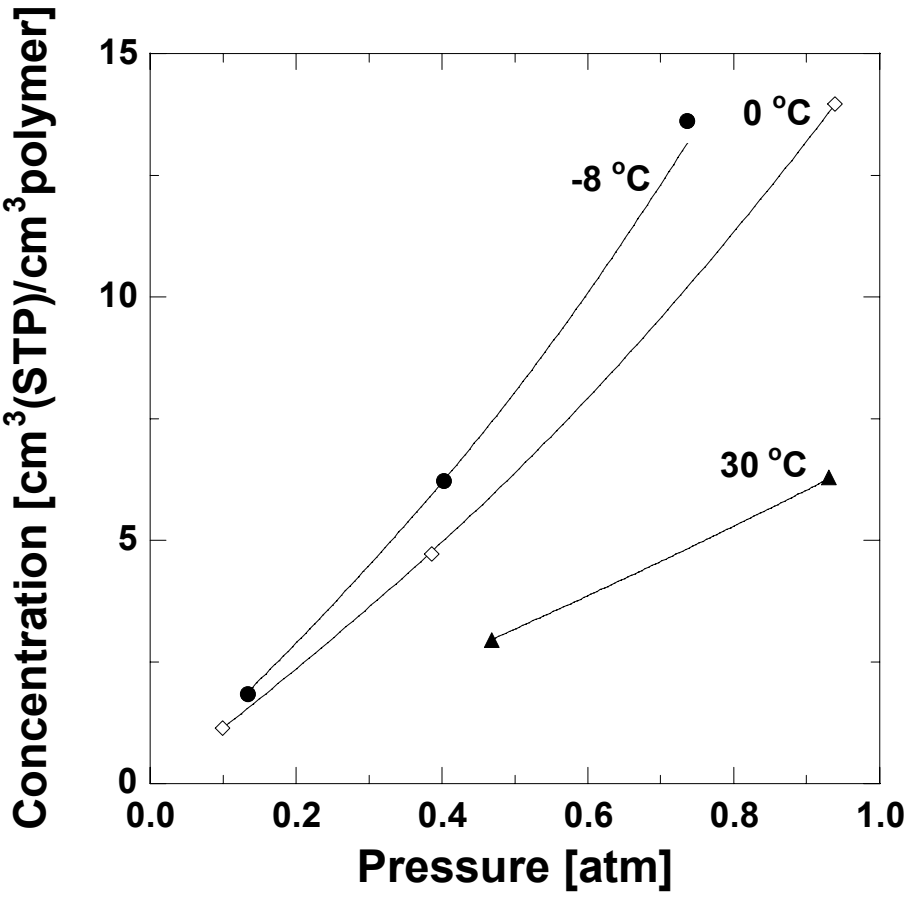

Figure 7.8b: Sorption isotherms of isobutylene in poly(ethylene) [112]. The lines represent Flory-Huggins fits to the experimental data based on the adjustable constants in Table 7.2.

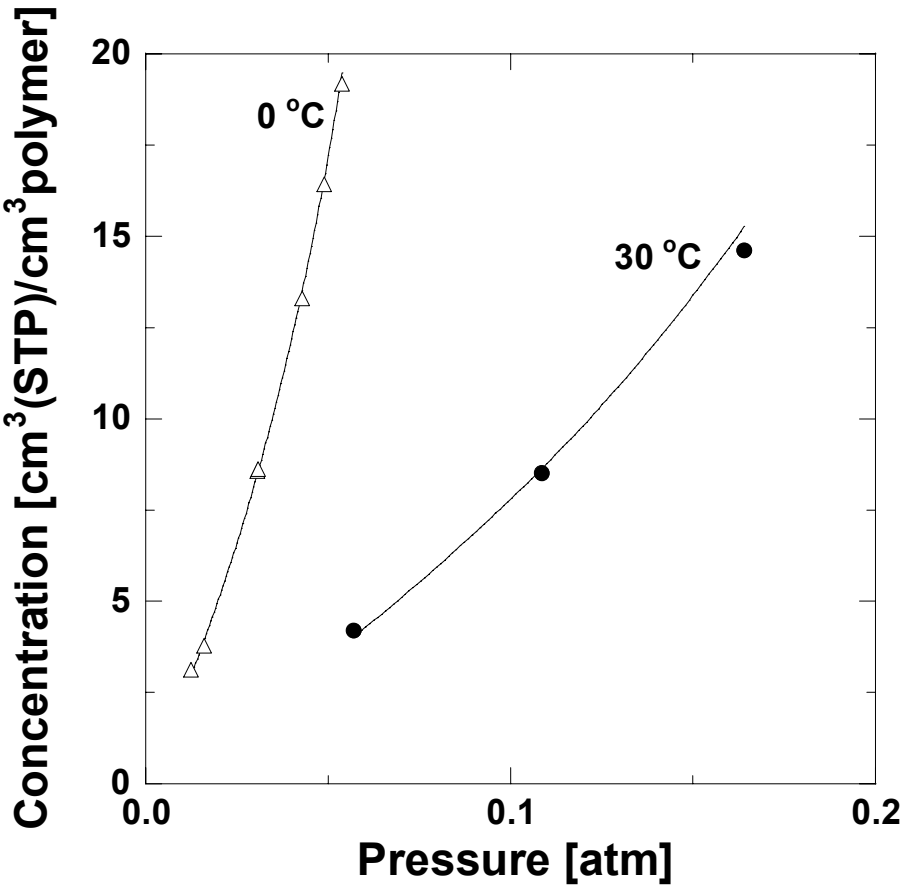

Figure 7.8c: Sorption isotherms of *n*-hexane in poly(ethylene) [112]. The lines represent Flory-Huggins fits to the experimental data based on the adjustable constants in Table 7.2.

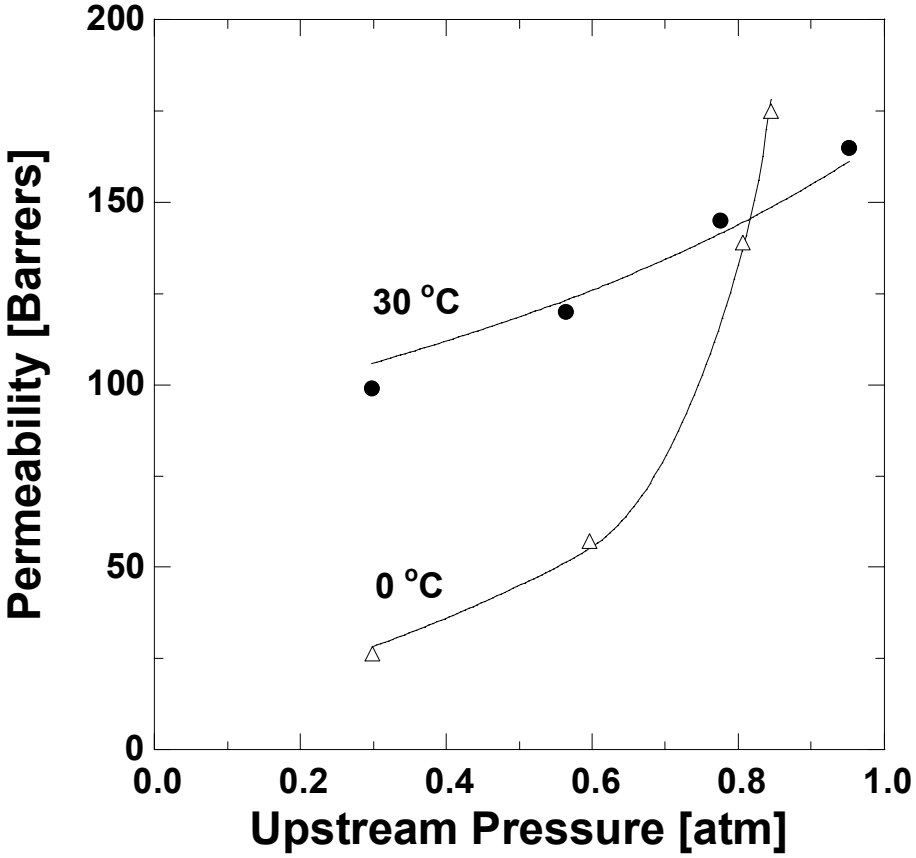

Figure 7.9a: Permeability coefficients of methyl bromide in poly(ethylene) [112]. The lines represent model fits to the experimental data based on the adjustable constants in Table 7.3.

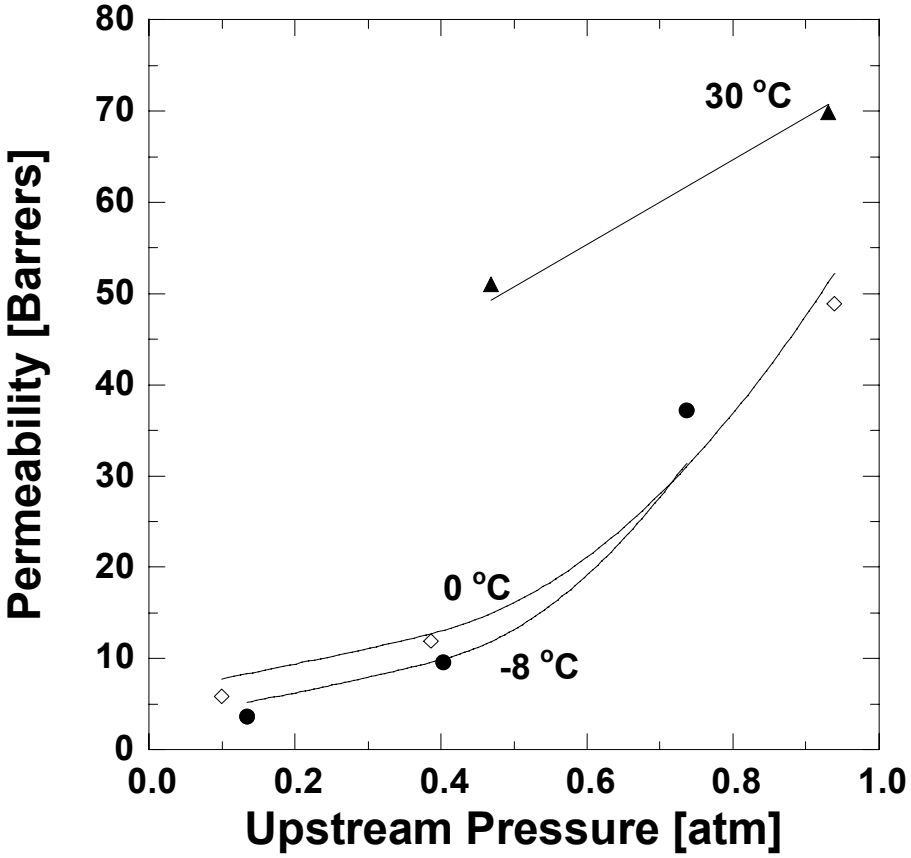

Figure 7.9b: Permeability coefficients of isobutylene in poly(ethylene) [112]. The lines represent model fits to the experimental data based on the adjustable constants in Table 7.3.

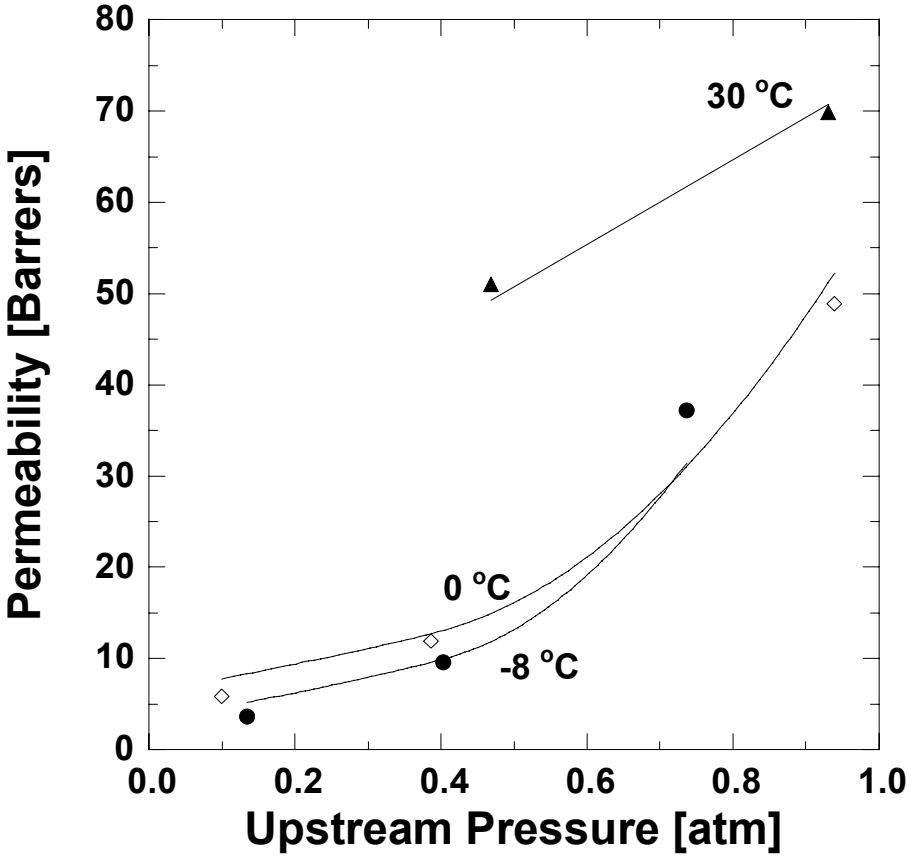

Figure 7.9c: Permeability coefficients of *n*-hexane in poly(ethylene) [112]. The lines represent model fits to the experimental data based on the adjustable constants in Table 7.3.

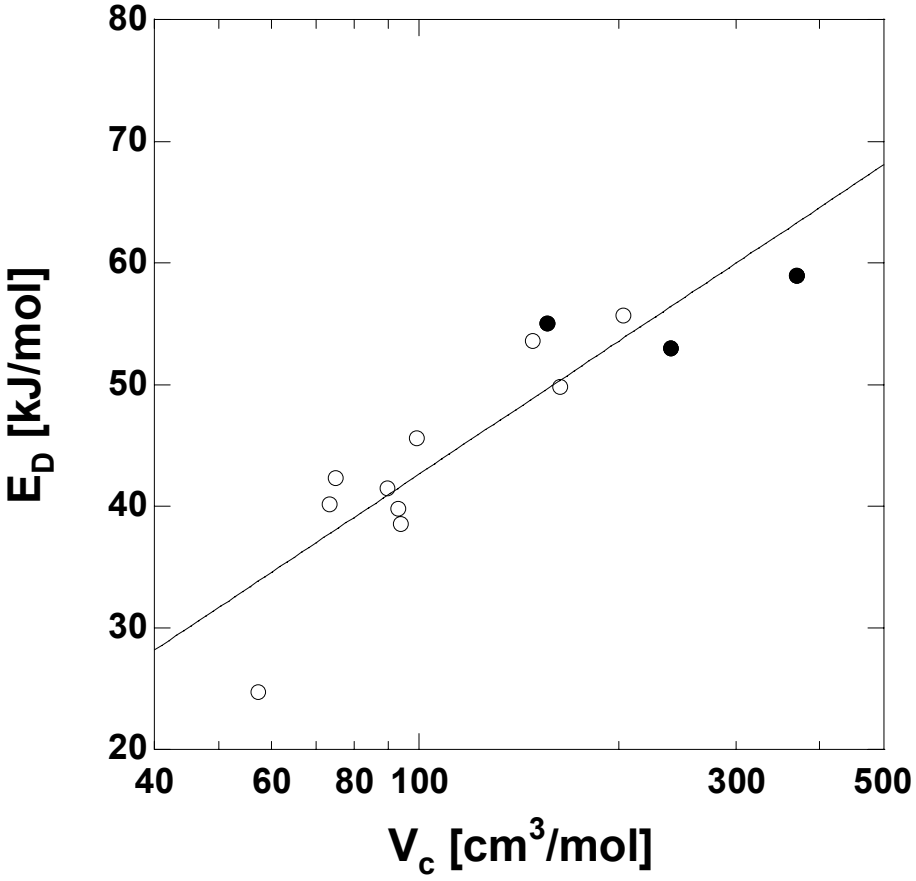

Figure 7.10: Correlation of the activation energy of diffusion of penetrants in poly(ethylene) with penetrant critical volume. The unfilled symbols are literature data [54], and the filled symbols are E_D^o values for methyl bromide, isobutylene and *n*-hexane calculated from the new model. The solid line is fitted to all the data and has the equation: E_D[kJ/mol] = 36.4 × log(V_c[cm^3/mol]) – 30.2.

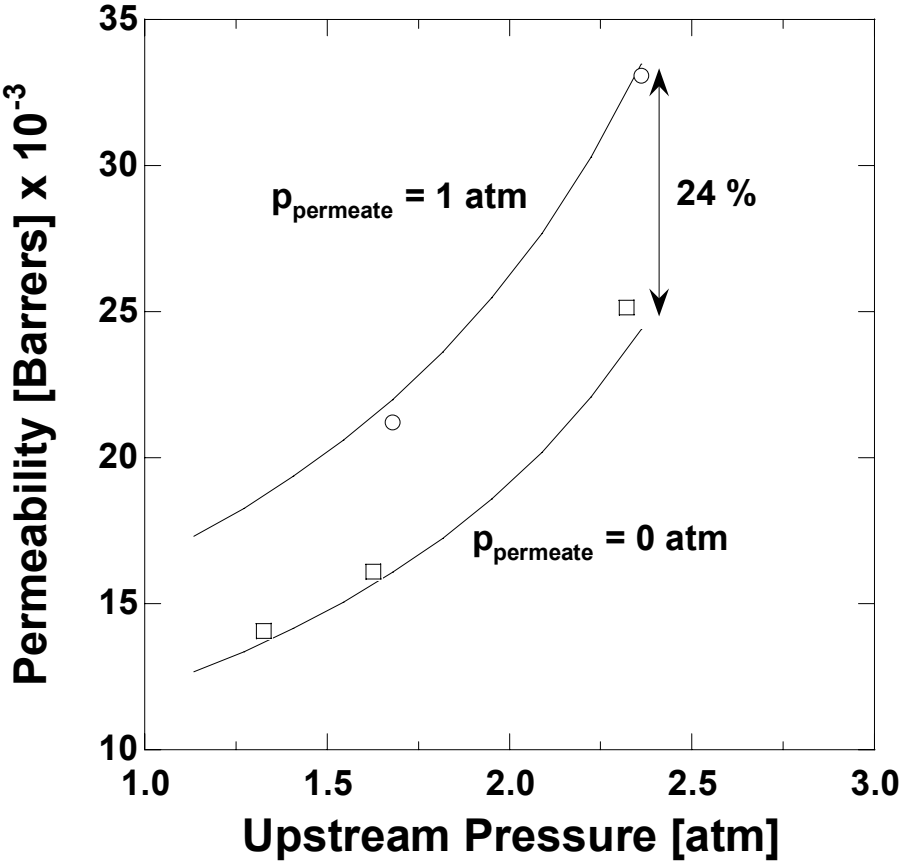

Figure 7.11: Effect of permeate pressure on the permeability of propane in PDMS at -10 ^{o}C. The solid lines depict the model prediction based on best-fit values from Table 7.3. The open symbols are experimentally measured permeabilities at downstream pressures of 1 atm (○) and 0 atm (□). These permeability data were not used in determining the best-fit values of the model.

CHAPTER 8

Fluorocarbon-Hydrocarbon Interactions

8.1 SUMMARY

The unusual hydrocarbon solubility properties of fluorocarbons are well known, but, so far, no theory has fully explained the underlying molecular phenomena responsible for these properties. This chapter presents an overview of the most promising approaches that have been attempted and reviews the current state of knowledge in this field.

8.2 INTRODUCTION

Hydrocarbons and fluorocarbons fall under the category of non-polar, non-electrolytes and, therefore, their mixture behavior is expected to conform to predictions of the regular solution theory. Fluorocarbon-fluorocarbon mixtures and hydrocarbon-hydrocarbon mixtures obey the regular solution theory to a reasonable extent in most cases, but the behavior of fluorocarbon-hydrocarbon mixtures is often at odds with the predictions of regular solution theory [47,124]. For example, the systems C_7H_{16}-C_7F_{16}, C_5H_{12}-C_5F_{12} and C_4H_{10}-C_4F_{10} show sizeable two phase liquid-liquid regions, while theoretical predictions indicate that they should be miscible [47]. In addition, many hydrocarbon-fluorocarbon solutions exhibit abnormally large enthalpies of mixing and volume expansions on mixing, properties that are mutually consistent, but at variance with predictions of regular solution theory [125].

The anomalous behavior of hydrocarbon-fluorocarbon solutions attracted significant scientific interest in the 1940s and 1950s [126-133]. Extensive experimental data were reported on fluorocarbon-containing solutions, and several theories were proposed to account for the observed deviations from regular solution theory. In a critical review of these theories, Scott suggested that the failure of the geometric mean approximation, which is used to describe interactions between unlike molecules (hydrocarbons and fluorocarbons, in this case), was the most likely reason for the inability of regular solution theory to describe hydrocarbon-fluorocarbon solution behavior [47].

8.3 FAILURE OF THE GEOMETRIC MEAN APPROXIMATION

Regular solution theory predicts the behavior of mixtures based upon properties of the pure components and mixing rules to describe unlike molecular interactions [44]. For example, the Lennard-Jones 6-12 potential function is often used to describe the intermolecular potential energy, Γ_{ii}, for a pair of spherically symmetric, neutral molecules of type *i* [134],

$$\Gamma_{ii} = 4\varepsilon_{ii}\left[\left(\frac{\sigma_{ii}}{r}\right)^{12} - \left(\frac{\sigma_{ii}}{r}\right)^{6}\right] \tag{8.1}$$

where σ_{ii} is the intermolecular separation at zero potential energy, ε_{ii} is the minimum interaction energy, which corresponds to equilibrium separation, and *r* is the center-to-center distance between the two molecules. The interaction potential between 2 unlike molecules *i* and *j*, Γ_{ij}, is assumed to have the same functional form, with σ_{ij} being the arithmetic mean (the 'Lorentz' rule) and ε_{ij} being the geometric mean (the 'Berthelot' rule) of the pure substance parameter values [135]:

$$\sigma_{ij} = \frac{\left(\sigma_{ii} + \sigma_{jj}\right)}{2} \tag{8.2}$$

and

$$\varepsilon_{ij} = \sqrt{\varepsilon_{ii}\varepsilon_{jj}} \tag{8.3}$$

Scott observed that the geometric mean approximation (eq 8.3) systematically overestimates the interaction energy between hydrocarbon and fluorocarbon molecules [47]. He suggested that two factors, arising from differences in molecular properties, may be responsible for the failure of the geometric mean approximation to predict hydrocarbon-fluorocarbon mixture behavior because these factors violate assumptions inherent in the geometric mean approximation [47].

(i) Difference in Ionization Potentials between Fluorocarbons and Hydrocarbons

The London equation for the attractive energy due to dispersion forces between two spherically symmetric, non-polar molecules *i* and *j*, Γ_{ij}^{D}, is [136,137]:

$$\Gamma_{ij}^{D} = -\frac{3\alpha_i\alpha_j}{2r^6}\left(\frac{I_i I_j}{I_i + I_j}\right) \tag{8.4}$$

where α_i is the polarizability of molecule *i*, and I_i is its ionization potential. The center-to-center distance between the molecules is *r*. If the ionization potentials of the molecules are equal, then the London dispersion force potential between unlike molecules is given by the geometric mean rule. This can be seen by considering the product of the interaction energies for pairs of like molecules. From eq 8.4,

$$\Gamma_{ii}^{D}\Gamma_{jj}^{D}=\left[-\frac{3\alpha_i\alpha_i}{2r^6}\left(\frac{I_iI_i}{I_i+I_i}\right)\right]\left[-\frac{3\alpha_j\alpha_j}{2r^6}\left(\frac{I_jI_j}{I_j+I_j}\right)\right] \tag{8.5}$$

Therefore,

$$\sqrt{\Gamma_{ii}^{D}\Gamma_{jj}^{D}}=\left[-\frac{3\alpha_i\alpha_j}{2r^6}\left(\frac{\sqrt{I_iI_j}}{2}\right)\right] \tag{8.6}$$

where the negative root is chosen on the right hand side of the equation since the interaction potential is attractive in nature. If I_j is equal to I_i, then from eq 8.4,

$$\Gamma_{ij}^{D}=\left[-\frac{3\alpha_i\alpha_j}{2r^6}\left(\frac{I_i^2}{I_i+I_i}\right)\right]=\left[-\frac{3\alpha_i\alpha_j}{2r^6}\left(\frac{I_i}{2}\right)\right] \tag{8.7}$$

Comparing eqs 8.6 and 8.7 yields:

$$\Gamma_{ij}^{D}=\sqrt{\Gamma_{ii}^{D}\Gamma_{jj}^{D}} \tag{8.8}$$

if I_j is equal to I_i in eq 8.6.

Normally, the polarizabilities of two substances differ by much more than their ionization potentials, so the assumption of equal ionization potentials introduces little error. Table 8.1 presents polarizabilities and ionization potentials of saturated, linear hydrocarbon and fluorocarbon penetrants. With increasing carbon number in the

hydrocarbon series or in the fluorocarbon series, the polarizability values vary to a much larger extent than the ionization potentials. For example, the difference between the ionization potentials of CH_4 and *n*-C_4H_{10} is about 25%, while the polarizability of *n*-C_4H_{10} is more than 3 times that of CH_4. However, the ionization potentials of the fluorocarbons (15-18 e.v.) are much higher than those of the hydrocarbons (10-13 e.v.). As a result, differences in ionization potentials between hydrocarbons and their fluorocarbon analogs are comparable to differences in their polarizabilities. For example, from Table 1, the ionization potential of *n*-C_4F_{10} is about 70% higher than that of *n*-C_4H_{10} while the polarizability of this fluorocarbon is 50% higher than its hydrocarbon analog.

Large differences in ionization potentials can lead to significant deviations in calculated thermodynamic properties from those obtained using the geometric mean approximation. For example, in the regular solution theory, the enthalpy of mixing two non-polar, non-electrolytes, *i* and *j*, is related to the cohesive energy density of the pure substances, c_{ii} and c_{jj}, and of the mixture, c_{ij}, by the term K [47]:

$$K = c_{ii} + c_{jj} - 2c_{ij} \tag{8.9}$$

If the geometric mean approximation ($c_{ij} = \sqrt{c_{ii}c_{jj}}$) is applied, then:

$$K = \left(\sqrt{c_{ii}} - \sqrt{c_{jj}}\right)^2 = \left(\delta_i - \delta_j\right)^2 \tag{8.10}$$

where δ is the solubility parameter, which is defined as the square root of the cohesive energy density ($\delta_i \equiv \sqrt{c_{ii}}$) [44]. Eq 8.10 is a result of the geometric mean approximation and, therefore, the equality of ionization potentials. If, however, the difference in ionization potentials is taken into account in the intermolecular potential function by using, for example, the Lennard Jones potential with the attractive component described by the London equation, then K is modified [47]:

$$K = \left(\delta_i - \delta_j\right)^2 \left[1 + \frac{2\delta_i\delta_j}{\left(\delta_i - \delta_j\right)^2}\left(1 - f_I f_\sigma\right)\right] \tag{8.11}$$

where

$$f_I = \frac{2\sqrt{I_i I_j}}{I_i + I_j} \tag{8.12}$$

and

$$f_\sigma = \left[\frac{2\sqrt{\sigma_{ii}\sigma_{jj}}}{\left(\sigma_{ii} + \sigma_{jj}\right)}\right]^3 \tag{8.13}$$

Using a semi-empirical method to estimate ionization potentials of fluorocarbons and hydrocarbons, Reed calculated f_I and f_σ values for *n*-C_4F_{10}/*n*-C_4H_{10} mixtures. From this calculation, f_I and f_σ are 0.9666 and 0.9944, respectively [138]. Using these values,

the second term in the square brackets of eq 8.11 has a value of about 2.5 (solubility parameters for *n*-butane and its perfluorinated analog are 7.4 and 6.2 $(cal/cm^3)^{0.5}$, respectively, at 259.95 K [130]). As a result, the modified expression in K has a value of 5 cal/cm^3, as compared to 1.44 cal/cm^3 from the original expression (eq 8.10). The value of K calculated from free energy of mixing values obtained from vapor-liquid mixing measurements is 7.7 cal/cm^3 and thus the modified expression (eq 8.11) explains a large part of the discrepancy between the experimental observations and predictions based on the geometric mean approximation [47,130]. Interestingly, a seemingly small correction due to ionization potential differences (*i.e.*, $(1 - f_I f\sigma) \approx 0.04$) explains a large portion of the observed discrepancy. This correction becomes even more important in predicting observed properties such as solubility because solubility varies exponentially with enthalpy (*cf.* eq 2.18). Thus, accounting for the significant differences in ionization potentials of hydrocarbons and fluorocarbons can provide better agreement between observed results and regular solution theory predictions, at least for the case of *n*-C_4F_{10}/*n*-C_4H_{10} mixtures. However, there are mixtures having differences in ionization potentials between component molecules as large as those between hydrocarbons and fluorocarbons, but these mixtures obey regular solution theory without taking into account differences in ionization potentials. For example, from Table 8.1, the difference in ionization potentials of fluorocarbons and compounds like benzene, carbon tetrachloride and iodine are as large as, or even larger than those between fluorocarbons and aliphatic hydrocarbons. However, solutions of these compounds with fluorocarbons obey regular solution theory, which implies that differences in ionization potentials

between molecules in a mixture cannot consistently account for observed differences in solution thermodynamic properties [47].

(ii) Non-central Force Fields

A recognized oversimplification in the treatment of intermolecular forces is the assumption of a spherically symmetric force potential located on the central atom in a molecule [47]. This assumption is strictly valid only for monoatomic substances (*e.g.*, He, Ne *etc.*), and can, at best, be extended to substances like methane where the electronic distribution is nearly spherically symmetric around the carbon nucleus [47]. For larger, more complex molecules, Hamann *et al.* showed that the assumption of central force fields is often not valid, even if the molecules are nearly spherical [139]. They calculated interactions between a monoatomic gas, A, and a hypothetical tetrahedral molecule, AA_4, by modeling the tetrahedral molecule as consisting of point forces centered at the position of each atom. To the approximation that the weak forces between hydrogen atoms can be ignored, this model can be considered to be a reasonable description of interactions in methane – neo-pentane mixtures. Each atom, A, was modeled using a Lennard-Jones 6-12 potential, and interactions of a molecule with other molecules (A or AA_4) were calculated by summing over all pairs of interactions, averaged over all orientations of the molecules. The mixture interaction results were then fitted to the Lennard-Jones potential, and the results are shown in Table 8.2. The first 2 rows of the table present the σ and ε values for interactions between like molecules, A-A and AA_4-AA_4. These values are normalized by the σ and ε values for A-A interactions. The 3rd row presents σ and ε values for interactions between A and AA_4 calculated using

the arithmetic and geometric mean mixing rules, respectively (*cf.*, eqs 8.2 and 8.3). The final row presents results from the calculations of Hamann *et al.* according to the procedure described above. From the table, $\sigma_{A\text{-}AA4}$(model) is quite close to the arithmetic mean of the pure component σ values, but $\varepsilon_{A\text{-}AA4}$(model) is appreciably less than the geometric mean of the pure component ε values [139]. Thus, description of the potential field of the mixture by summing over individual atomic interactions does not match that obtained from the geometric mean approximation for ε. This discrepancy exposes another shortcoming of the geometric mean approximation when applied to certain mixtures. However, the above explanation is not unique to fluorocarbon-hydrocarbon mixtures. Also, this explanation incorrectly predicts the qualitative behavior of some hydrocarbon-fluorocarbon mixtures [47].

8.4 EMPIRICAL MODIFICATIONS TO THE GEOMETRIC MEAN APPROXIMATION

The inadequacy of the geometric mean approximation to describe unlike molecular interactions in some cases has led to empirical modifications of this mixing rule for modeling the thermodynamic properties of mixtures. Hildebrand used eq 8.11 with an arbitrary adjustable constant, l_{12}, in place of the term $(1 - f_1 f_\sigma)$ to model the excess Gibbs free energy, ΔG^E, of methane-tetrafluoromethane mixtures at 110.5 K [44]:

$$\Delta G^E = \left(x_1 v_1 + x_2 v_2\right)\phi_1\phi_2\left(\delta_1 - \delta_2\right)^2\left[1 + l_{12}\frac{2\delta_1\delta_2}{\left(\delta_1 - \delta_2\right)^2}\right] \tag{8.14}$$

where x_i, v_i and ϕ_i are the mole fraction, molar volume and volume fraction of component i, respectively, in the mixture. Figure 8.1 presents experimental data for excess Gibbs free energy for methane-tetrafluoromethane mixtures as well as model predictions with $l_{12} = 0$ (*i.e.*, using the geometric mean approximation) and $l_{12} = 0.07$. The experimental excess Gibbs free energy can be modeled well with $l_{12} = 0.07$, while the theoretical prediction using the geometric mean approximation deviates substantially from the experimental data. Thus, a small change in the value of l_{12} provides a large improvement in predicting solution behavior. This trend is especially true for mixtures where the solubility parameters of the solution components are quite close to each other. For the above example, the solubility parameters of methane and tetrafluoromethane at 110.5 K are 7.2 and 8.0 $(\text{cal/cm}^3)^{0.5}$, as determined from enthalpy of vaporization and liquid molar volume values at that temperature [74]. With these solubility parameter values, the second term in the square brackets of eq 8.14 has a value of about 12.6 (when $l_{12} = 0.07$). Thus, even low l_{12} values can be very significant and result in large differences in thermodynamic property predictions as seen from Figure 8.1.

Another empirical modification of the geometric mean approximation is shown below:

$$\varepsilon_{12} = \left(1 - k_{12}\right)\sqrt{\varepsilon_{11}\varepsilon_{22}} \tag{8.15}$$

where k_{12} is an empirical coefficient [44]. Dantzler-Siebert and Knobler used this modified mixing rule in the Kihara potential to model small molecule hydrocarbon-

fluorocarbon mixture behavior [140]. They observed that interactions between hydrocarbons and fluorocarbons were 10% weaker than those predicted by the geometric mean (*i.e.*, $k_{12} = 0.10$) [140].

Empirical corrections of the geometric mean approximation have also been shown to improve the description of fluorocarbon gas solubility in hydrocarbon-based polymers and *vice versa*. Based on the modeling of polymer-penetrant interactions using equations of state, De Angelis *et al.* showed that a reduction in the unlike molecular interaction of about 10% was required to accurately model solubility in hydrocarbon-fluorocarbon gas-polymer systems [48,141]. For example, Figure 8.2a shows experimental C_2F_6 sorption data in PDMS. The characteristic pressure of the binary mixture in the Sanchez-Lacombe equation, P_{12}^*, is calculated as [48]:

$$P_{12}^* = \psi\sqrt{P_1^* P_2^*} \tag{8.16}$$

where P_i^* is the characteristic pressure of component *i*, and ψ is an empirical mixing parameter that corrects for deviations of P_{12}^* from the geometric mean approximation value. When ψ is unity, P_{12}^* is given by the geometric mean of the pure component values. Using this equation with ψ=1, C_2F_6 solubility in PDMS is over-predicted by a factor of about 9 (*cf.* Figure 8.2a) [48]. A ψ value of 0.863 was required to fit the experimental sorption data to the Sanchez-Lacombe model [48]. In contrast, C_2H_6 solubility in PDMS could be predicted with a ψ value of 0.963 (*cf.* Figure 8.2b) [48]. Similarly, in the high free volume, glassy fluoropolymers, AF1600 and AF2400, ψ had to

be reduced to about 0.9 in the non-equilibrium lattice fluid model, which is based on the Sanchez-Lacombe model, to describe C_2H_6 sorption in these fluoropolymers satisfactorily (*cf.* Figure 8.3a) [141]. However, as shown in Figure 8.3b, with ψ equal to unity, a good fit of the model to experimental C_2F_6 sorption data in these two fluoropolymers was obtained [141]. Thus, fluorocarbon gas solubility in fluoropolymers and hydrocarbon gas solubility in hydrocarbon-based polymers could be described with little or no deviation from the geometric mean approximation. However, fluorocarbon gas solubility in hydrocarbon-based polymers or hydrocarbon gas solubility in fluoropolymers requires a significant (approximately 10%) correction to the geometric mean estimates of the interaction energies. Interestingly, the 10% reduction in interaction energy, relative to that suggested by the geometric mean rule, observed in these gas-polymer systems is strikingly similar to that observed by Hildebrand [44] and Dantzler-Siebert and Knobler [140] in small molecule systems, suggesting that the molecular phenomena at work here are rather general in nature.

8.5 COMPUTER SIMULATION

The empirical modifications described above do not provide a molecular explanation for the weaker-than-expected interactions between hydrocarbon and fluorocarbons. In an attempt to address this issue, Song *et al.* recently used state-of-the-art computer simulation to calculate, from first principles, thermodynamic properties (*e.g.*, second virial coefficients) of methane/perfluoromethane mixtures [142]. They employed the recently-developed all atom optimized potentials for liquid simulations

(OPLS-AA) potential energy model and used the geometric mean approximation to model interactions between alkanes and perfluoroalkanes. The objective was to determine whether the subtleties of molecular geometry and molecular charge distribution incorporated in the OPLS-AA potential would account for the apparent departure from the geometric mean approximation in calculating interaction energies between fluorocarbon and hydrocarbon molecules. Surprisingly, these refined models of molecular structure and electron distribution could not describe experimental second virial coefficients of mixing methane and perfluoromethane even though the models provided accurate predictions of the thermodynamic properties of the pure components. The model calculations and experimental data could only be brought into concordance if the interaction energy between a methane molecule and a perfluoromethane molecule was reduced to a value 10% lower than that suggested by the geometric mean approximation [142]. Because mixture thermodynamic properties such as solubility depend exponentially on these interaction energies, small deviations in interaction energies yield large effects in observed properties (*cf.* Figure 8.2a). After exploring many combinations of mixing rules and examining in detail the various contributions to the potential model, Song *et al.* concluded "At this point, it must be admitted that the origins of the weaker-than-expected interactions between perfluoroalkanes and alkanes remain a mystery." [142].

Table 8.1 Polarizabilities and ionization potentials of selected compounds.

Penetrant	***Polarizability*** **(× 10^{-24} cm^3)**	***Ionization Potential*** **(e.v.)**
CH_4	2.6 [143]	13.1 [47]
n-C_4H_{10}	8.3 [143]	10.3 [138]
n-C_5H_{12}	10.0 [143]	10.6 [143]
CF_4	3.9 [144]	16-18 [47]
n-C_4F_{10}	12.7 [144]	17.4 [138]
n-C_5F_{12}	18.3 [144]	15.8 [140]
C_6H_6	-	9.2 [47]
I_2	-	9.7 [47]
CCl_4	-	11.0 [47]

Table 8.2 Calculations of interactions between hypothetical monoatomic and polyatomic substances [139].

Interactions	***i***	***j***	σ_{ij}/σ_{AA}	$\varepsilon_{ij}/\varepsilon_{AA}$
A-A	A	A	1.00	1.00
AA_4-AA_4	AA_4	AA_4	1.74	2.64
A-AA_4 (mixing rules)	A	AA_4	1.37	1.62
A-AA_4 (model)	A	AA_4	1.375	1.53

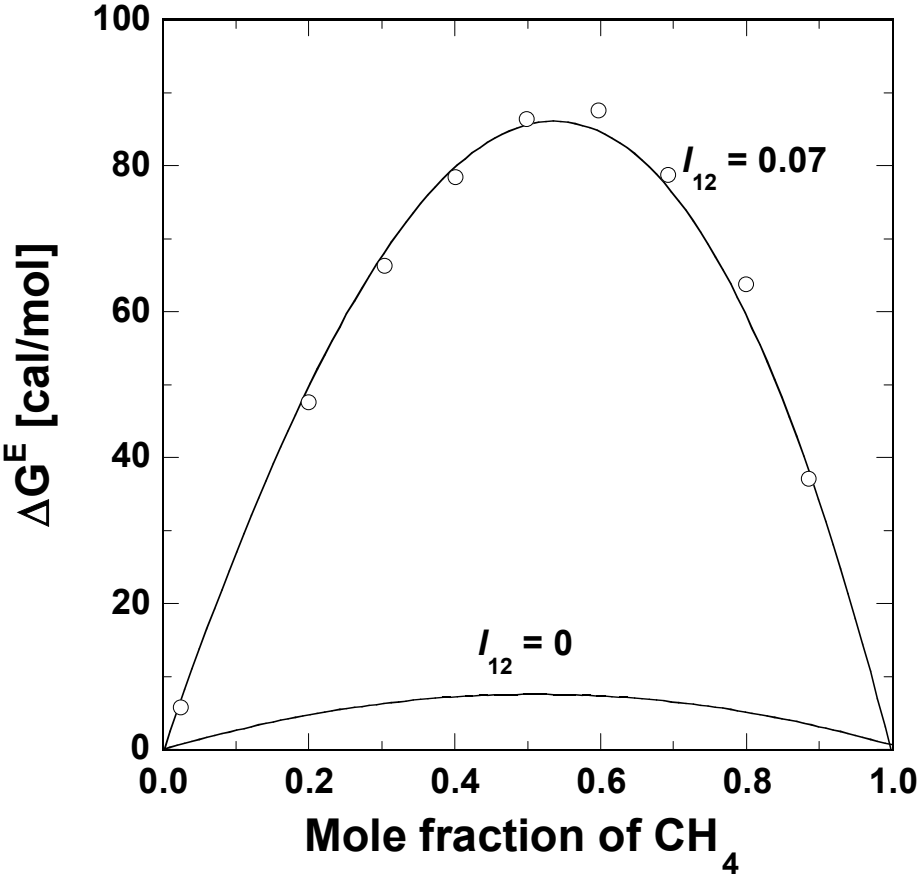

Figure 8.1: Excess Gibbs free energy for the methane-tetrafluoromethane system at 110.5 K [44].

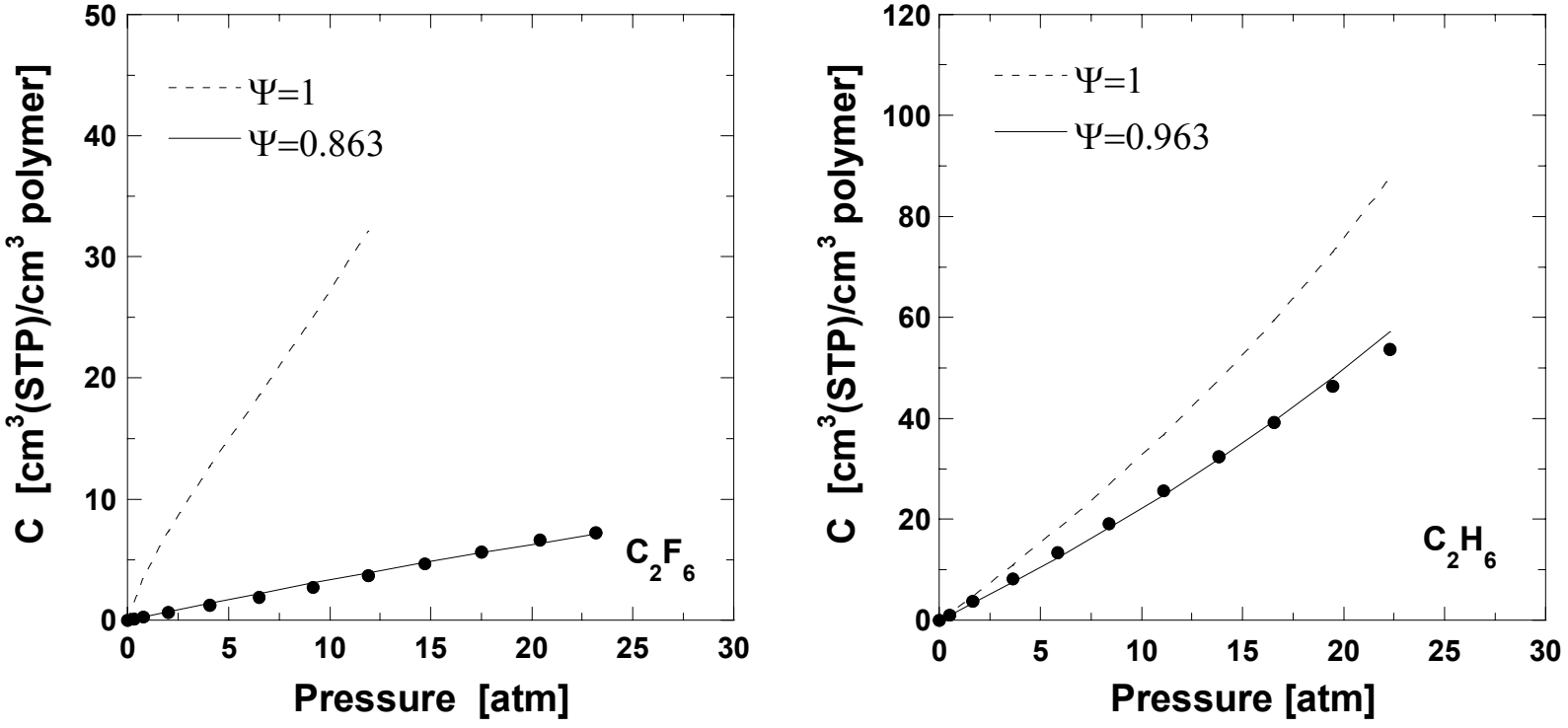

(a) (b)

Figure 8.2: Comparison of experimental and predicted sorption isotherms at 35 °C of (a) C_2F_6 and (b) C_2H_6 in PDMS using the Sanchez-Lacombe model with ψ=1 (dashed line) and ψ adjusted (solid line) [48].

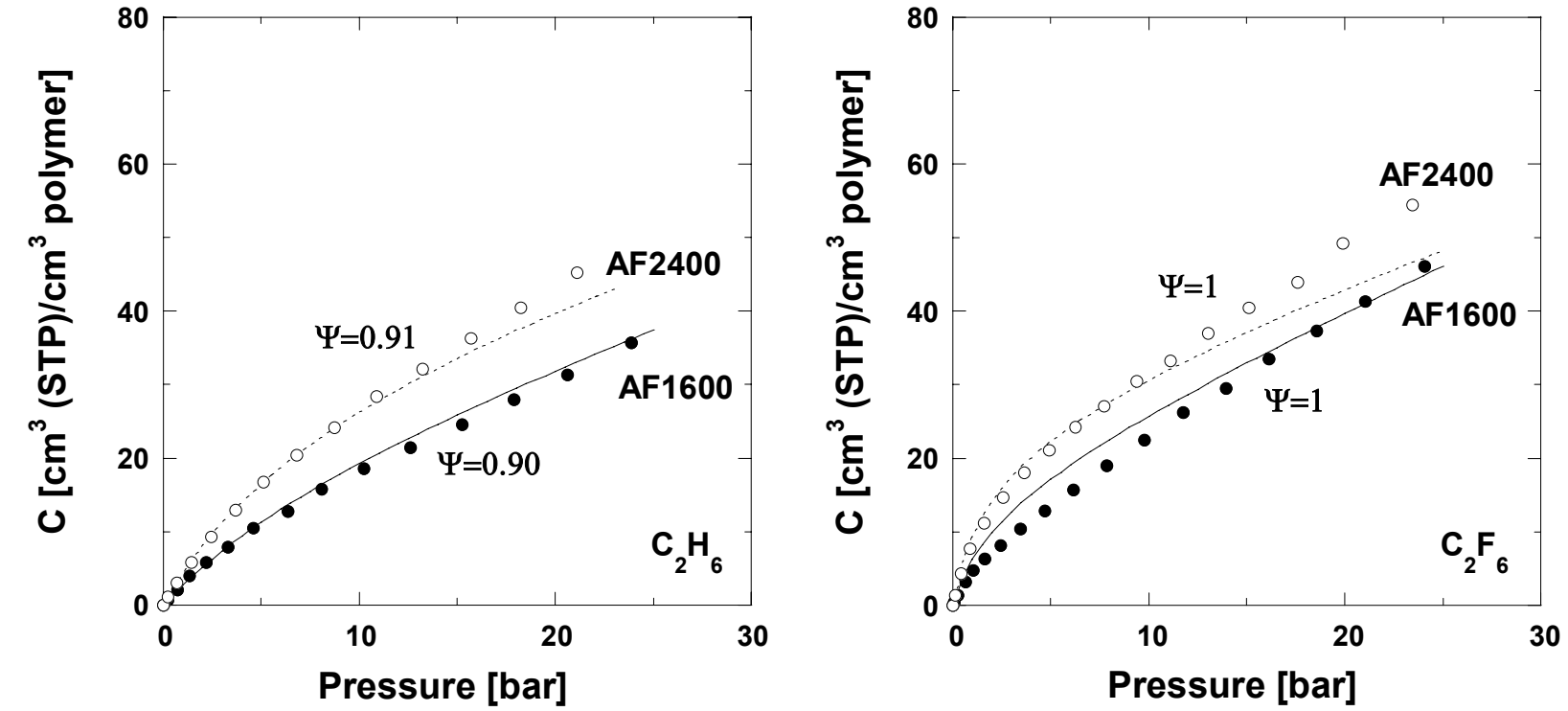

Figure 8.3: Comparison of experimental and predicted sorption isotherms at 35 °C of (a) C_2H_6 and (b) C_2F_6 in AF1600 and AF2400 using the non-equilibrium lattice fluid (NELF) model [141]. The solid and dotted lines represent NELF model fits to the experimental data for penetrant sorption in AF1600 and AF2400, respectively.

CHAPTER 9

Conclusions and Recommendations

9.1 INTRODUCTION

The aim of this study was to investigate the potential of using low-hydrocarbon-solubility polymers as plasticization-resistant membrane materials for CO_2 removal from natural gas. To the extent that gas solubility in the polymer influences the degree of plasticization, lower hydrocarbon solubility can result in greater resistance of the polymer to plasticization by hydrocarbon compounds.

9.2 CONCLUSIONS

Sorption of propane and perfluoropropane in PDMS and PTMSP revealed that the energetics of fluorocarbon gas sorption in the hydrocarbon polymers was less favorable than hydrocarbon gas sorption in these polymers. This phenomenon was a result of less favorable interactions between hydrocarbon and fluorocarbon species, as evidenced by a more positive enthalpy of mixing, than between hydrocarbons themselves. The effect of these interactions on gas permeation through the polymers was more pronounced in the rubbery polymers, PDMS, than in the high-free-volume glassy polymer, PTMSP. Interestingly, perfluoropropane exhibited a positive activation energy of permeation in PTMSP, mainly due to its large molecular size and hence high activation energy of diffusion.

The less favorable hydrocarbon-fluorocarbon interactions also resulted in expectedly lower solubility of hydrocarbon penetrants, as compared to their fluorinated analogs, in fluoropolymers like rubbery TFE/PMVE49 and low-free-volume glassy,

Hyflon AD 80. The extent of solubility suppression in Hyflon AD 80 was greater than in higher free volume fluoropolymers like AF1600 and AF2400. As compared to hydrocarbon polymers, the fluoropolymers showed lower increases in hydrocarbon solubility with increasing penetrant condensability than most hydrocarbon polymers. This property is expected to result in substantially lower solubility of higher hydrocarbons in fluoropolymers than in typical hydrocarbon polymers. The lower free volume glassy polymer, Hyflon AD 80, showed greater suppression of hydrocarbon solubility with increasing penetrant condensability than the Teflon AF materials.

Pure gas CO_2/CH_4 selectivities of Hyflon AD 60 and Hyflon AD 80 were higher than those of the rubbery or the high free volume glassy fluoropolymers mentioned above. But, these selectivity values were not as high as the intrinsic ideal selectivities of high performance hydrocarbon polymers developed for CO_2 removal from natural gas. However, both the Hyflon polymers exhibited significantly greater CO_2 permeabilities than the high performance hydrocarbon polymers.

When exposed to a mixture of 20% CO_2 in CH_4, Hyflon AD 80 showed minimal decrease in separation performance up to 53.2 atm total pressure, thus exhibiting greater performance stability in mixed-gas environments than many hydrocarbon polymers. When moderate amounts of higher hydrocarbons like toluene and *n*-hexane were added to the feed gas stream, there was no detectable change in CO_2/CH_4 selectivity of Hyflon AD 80 at 35 atm total pressure.

Analysis of the strategy of using fluoropolymers as plasticization-resistant coatings on hydrocarbon polymers provided materials selection guidelines for choosing appropriate materials to coat hydrocarbon membranes. The guidelines required the

fluoropolymer to have a lower ratio of higher hydrocarbon to CO_2 solubility, which is usually satisfied quite easily by fluoropolymers. However, the guidelines also required the fluoropolymer coating to have a comparable or higher size-selectivity than the hydrocarbon polymer. This latter criterion was seen to be more decisive in the choice of coating material for a hydrocarbon polymer.

Transport of condensable penetrants such as large hydrocarbons through polymers is often a function of penetrant concentration inside the polymer. In such cases, gas permeability, which is usually viewed as an intrinsic property of the polymer, becomes a function of membrane operating conditions. A model to rationally describe effects of operating conditions on gas permeability in rubbery polymers was described and tested satisfactorily with experimental data on pure propane transport in PDMS and literature reports for penetrant transport in PDMS and poly(ethylene). The model also accurately predicts a decrease in propane permeability in PDMS with decreasing permeate pressure, at fixed feed pressure. The model requires few adjustable constants and may be useful as a first step to provide a rational framework for estimating permeability coefficients in rubbery polymers at operating conditions that are not in the range of those used to acquire experimental data.

9.3 RECOMMENDATIONS FOR FUTURE WORK

Field conditions in natural gas separations affect membrane performance in ways not normally observed in typical laboratory experiments performed with pure gases at near ambient temperatures and pressures. Thus, fundamental structure-property studies

aimed at improving membrane permeability and ideal selectivity are not sufficient in themselves to provide high performance membranes for industrial conditions. However, due to the relative ease of performing experiments at typical laboratory conditions, industrially-relevant issues such as membrane plasticization are often addressed by performing physical or chemical modifications to the best performing materials obtained from structure-property studies. The present study has attempted to deviate from this paradigm and incorporate considerations of plasticization resistance into the core materials design strategy. This study has demonstrated the potential of fluoropolymers as plasticization-resistant membranes for CO_2 removal from natural gas through experimental characterization of commercial fluoropolymers. The next step in this direction is to perform a systematic structure-property study of fluoropolymers, along the lines of previous studies on hydrocarbon polymers, to develop fluoropolymers with better separation properties.

Systematic structure property studies on hydrocarbon polymers have shown that achieving the twin objectives of higher free volume in the membrane and higher polymer chain rigidity is the key for obtaining high performance membrane materials. Such polymers have significant aromatic character and bulky side groups. Therefore, it is quite likely that systematic structure-property studies on fluoropolymers will lead to aromatic fluoropolymers. However, current, commercially-available fluoropolymers resemble aliphatic hydrocarbon polymers. Also, perfluorinated aromatic monomers are not widely available and the chemistry of aromatic fluoropolymer synthesis is probably not straightforward, as can be concluded from the lack of commercial aromatic fluoropolymers. Therefore, other techniques may have to be used to obtain aromatic

fluoropolymers. One such technique is to fluorinate aromatic hydrocarbons by dissolving them in a liquid solvent and bubbling a gaseous mixture of fluorine and nitrogen through the solution [145]. This technique can potentially provide a variety of aromatic fluoropolymers with systematic variations in polymer structure to perform a fundamental structure-property study. Such a study can provide high performance membranes that possess greater plasticization resistance in hydrocarbon environments. Determination of membrane plasticization resistance should be an integral element of this study.

The strategy of plasticization-resistant fluoropolymer coatings on hydrocarbon polymers was analyzed using pure gas permeabilities in polymers. To evaluate the true benefits of this technique, a systematic set of mixed-gas experiments need be performed on hydrocarbon polymers and on fluorocarbon-hydrocarbon composite membranes. These experiments should be performed with well-characterized model natural gas mixtures (which usually contain carbon dioxide and hydrocarbons like toluene and *n*-hexane, in addition to methane) at pressures high enough to plasticize the hydrocarbon polymer. For the purposes of laboratory experiments, the composite membranes can be obtained by simply placing the fluoropolymer on the hydrocarbon polymer inside the high pressure permeation cell. This study will provide valuable insights into the potential of using fluoropolymers as coatings to protect hydrocarbon polymers from plasticization.

The model developed for predicting pure gas permeability in rubbery polymers can be extended to prediction of mixed-gas permeabilities and also to transport in glassy polymers. The extension to mixed-gas permeation will require insight into the dependence of a penetrant's diffusion coefficient on its concentration inside the polymer as well as the concentration of co-permeating species in the polymer. This dependence is

expected to be application-specific and dependent on the gas or vapor under consideration. For example, based on simple considerations, the permeation of methane through a rubbery polymer can be affected by co-permeation of carbon dioxide at moderate pressures because carbon dioxide is likely to plasticize the rubbery polymer at these pressures. Thus, methane diffusion may be dependent on carbon dioxide concentration in the polymer or total gas concentration in the polymer. In contrast, carbon dioxide permeability may not show much dependence on methane concentration in the polymer as methane usually does not affect the polymer packing and chain mobility in a significant way.

Extension of the model to permeation in glassy polymers will require the use of a sorption model like the dual mode model, instead of the Flory Huggins model, to calculate gas concentration in the polymer. Also, the dependence of the diffusion coefficient on concentration may be different from that in rubbery polymers. This dependence can be determined from literature reports of gas transport properties in polymers as a function of pressure and temperature. Careful determination of gas or vapor permeation in a glassy polymer over a wide range of temperatures and pressures would provide valuable data to test this model. The model can be extended to mixed-gas permeation in glassy polymers along the same lines as described above for rubbery polymers.

Appendix

CRITICAL PROPERTIES OF SELECTED COMPOUNDS [46,74].

Penetrant	***Critical Volume*** ***(cm^3/mol)***	***Critical Temperature*** ***(K)***	***Penetrant***	***Critical Volume*** ***(cm^3/mol)***	***Critical Temperature*** ***(K)***
He	57.4	5.19	*n*-C_8H_{18}	492	568.8
H_2	65.1	33.24	*n*-C_9H_{20}	548	594.6
O_2	73.4	154.58	*n*-$C_{10}H_{22}$	603	617.7
N_2	89.8	126.2	*n*-$C_{11}H_{24}$	660	638.8
CO_2	93.9	304.2	*n*-$C_{12}H_{26}$	713	658.2
CH_4	99.2	191.05	*n*-$C_{13}H_{28}$	780	676
C_2H_6	148.3	305.35	*n*-$C_{14}H_{30}$	830	693
C_3H_8	203	369.95	*n*-$C_{15}H_{32}$	880	707
n-C_4H_{10}	255	425.2	CF_4	139.6	227.6
n-C_5H_{12}	304	469.7	C_2F_6	222	293
n-C_6H_{14}	370	507.5	C_3F_8	299.8	345.1
n-C_7H_{16}	432	540.3			

Bibliography

[1] http://www.iclei.org/efacts/natgas.htm.

[2] International Energy Outlook 2003, Energy Information Administration of the Department of Energy, US Government, Washington, DC (2003).

[3] J. G. Speight, Gas Processing: Environmental Aspects and Methods, Butterworth Heinemann, 1993, p. 124.

[4] R. W. Baker, Membrane Technology and Applications, McGraw-Hill, New York, 2000.

[5] R. E. Babcock, R. W. Spillman, C. S. Goddin and T. E. Cooley, Natural Gas Cleanup: A Comparison of Membrane and Amine Treatment Processes, Ener. Prog., 8 (1988) 135-142.

[6] T. E. Cooley and W. L. Dethloff, Field Tests Show Membrane Processing Attractive, Chem. Engr. Prog., October (1985) 45-50.

[7] F. J. C. Fournie and J. P. Agostini, Permeation Membranes Can Efficiently Replace Conventional Gas Treatment Processes, J. Petro. Technol., June (1987) 707-712.

[8] R. W. Spillman, Economics of Gas Separation Membranes, Chem. Engr. Prog., January (1989) 41-62.

[9] S. A. Stern, Polymers for Gas Separations: The Next Decade, J. Membr. Sci., 94 (1994) 1-65.

[10] W. J. Koros and R. T. Chern, Separation of Gaseous Mixtures Using Polymer Membranes, in R. W. Rousseau (Ed.), Handbook of Separation Process Technology, John Wiley & Sons, New York, 1987, pp. 862-953.

[11] K. Ghosal and B. D. Freeman, Gas Separation Using Polymer Membranes: An Overview, Polym. Adv. Technol., 5 (1993) 673-697.

[12] J. K. Sears and J. R. Darby, The Technology of Plasticizers, John Wiley and Sons, New York, 1982.

[13] A. R. Berens, Transport of Organic Vapors and Liquids in Poly(vinylchloride), Makromol. Chem. Macromol. Symp., 29 (1989) 95-108.

[14] A. R. Berens, Transport of Plasticizing Penetrants in Glassy Polymers, in W. J. Koros (Ed.), Barrier Polymers and Structures, Vol. 423, American Chemical Society, Washington DC, 1990, pp. 92-110.

[15] S. Y. Lee and B. S. Minhas, Effect of Gas Composition and Pressure on Permeation through Cellulose Acetate Membranes, Membrane Materials and Processes, Vol. 84, AIChE Symposium Series, Washington, DC, 1988, pp. 93-101.

[16] L. S. White, T. A. Blinka, H. A. Kloczewski and I.-F. Wang, Properties of a Polyimide Gas Separation Membrane in Natural Gas Streams, J. Membr. Sci., 103 (1995) 73-82.

[17] A. Bos, I. G. M. Punt, M. Wessling and H. Strathmann, Suppression of CO_2-Plasticization by Semiinterpenetrating Polymer Network Formation, J. Polym. Sci. Part B. Polym. Phys., 36 (1998) 1547-1556.

[18] A. Bos, I. Punt, H. Strathmann and M. Wessling, Suppression of Gas Separation Membrane Plasticization by Homogeneous Polymer Blending, AIChE J., 47 (2001) 1088-1093.

[19] A. Bos, I. G. M. Punt, M. Wessling and H. Strathmann, Plasticization-resistant Glassy Polyimide Membranes for CO_2/CH_4 Separations, Sep. Purif. Technol., 14 (1998) 27-39.

[20] C. Staudt-Bickel and W. J. Koros, Improvement of CO_2/CH_4 Separation Characteristics of Polyimides by Chemical Crosslinking, J. Membr. Sci., 155 (1999) 145-154.

[21] J. D. Wind, C. Staudt-Bickel, D. R. Paul and W. J. Koros, The Effects of Crosslinking Chemistry on CO_2 Plasticization of Polyimide Gas Separation Membranes, Industrial and Engineering Chemistry Research, 41 (2002) 6139-6148.

[22] J. D. Wind, C. Staudt-Bickel, D. R. Paul and W. J. Koros, Solid-state Crosslinking of Polyimide Membranes for Carbon Dioxide Plasticization Reduction, Macromolecules, 36 (2003) 1882-1888.

[23] R. B. Bird, W. E. Stewart and E. N. Lightfoot, Transport Phenomena, John Wiley & Sons, Inc., New York, 1960.

[24] P. Flory, Principles of Polymer Chemistry, Cornell University Press, Ithaca, NY, 1953.

[25] T. C. Merkel, V. I. Bondar, K. Nagai, B. D. Freeman and I. Pinnau, Gas Sorption, Diffusion and Permeation in Poly(dimethylsiloxane), J. Polym. Sci. Part B. Polym. Phys., 38 (2000) 415-434.

[26] R. M. Barrer, J. A. Barrie and J. Slater, Sorption and Diffusion in Ethyl Cellulose. Part III. Comparison between Ethyl Cellulose and Rubber, J. Polym. Sci., 27 (1958) 177-197.

[27] S. A. Stern, V. M. Shah and B. J. Hardy, Structure-Permeability Relationships in Silicone Polymers, J. Polym. Sci. Part B. Polym. Phys., 25 (1987) 1263-1298.

[28] V. I. Bondar, B. D. Freeman and I. Pinnau, Gas Sorption and Characterization of Poly(ether-b-amide) Segmented Block Copolymers, J. Polym. Sci. Part B. Polym. Phys., 37 (1999) 2463-2475.

[29] S. A. Stern, P. J. Gareis, T. F. Sinclair and P. H. Mohr, Performance of a Versatile Variable-Volume Permeability Cell. Comparison of Gas Permeability Measurements by the Variable-Volume and Variable-Pressure Methods, J. Appl. Polym. Sci., 7 (1963) 2035-2051.

[30] R. M. Felder and G. S. Huvard, Permeation, Diffusion and Sorption of Gases and Vapors, in R. A. Fava (Ed.), Methods of Experimental Physics, Methods of Experimental Physics, Vol. 16 Part C, Academic Press, New York, 1980, pp. 315-377.

[31] K. C. O'Brien, W. J. Koros and T. A. Barbari, A New Technique for the Measurement of Multicomponent Gas Transport through Polymeric Films, J. Membr. Sci., 29 (1986) 229-238.

[32] C. T. Ratcliffe, A. Diaz, C. Nopasit and G. Munoz, Laurence Reid Gas Conditioning Conference, Norman, OK, 1999, pp. 118-140.

[33] S. V. Dixon-Garrett, K. Nagai and B. D. Freeman, Ethylbenzene Solubility, Diffusivity, and Permeability in Poly(dimethylsiloxane), J. Polym. Sci. Part B. Polym. Phys., 38 (2000) 1461-1473.

[34] S. V. Dixon-Garrett, K. Nagai and B. D. Freeman, Sorption, Diffusion and Permeation of Ethylbenzene in Poly(1-trimethylsilyl-1-propyne), J. Polym. Sci. Part B. Polym. Phys., 38 (2000) 1078-1089.

[35] G. Gee, Some Thermodynamic Properties of High Polymers and their Molecular Interpretation, Quart. Rev. (London), 1 (1947) 265-298.

[36] R. M. Barrer and G. Skirrow, Transport and Equilibrium Phenomena in Gas-Elastomer Systems. II. Equilibrium Phenomena, J. Polym. Sci., 3 (1948) 564-575.

[37] G. J. van Amerongen, Diffusion in Elastomers, Rubber Chemistry and Technology, 37 (1964) 1065-1152.

[38] Y. Kamiya, Y. Naito, K. Terada and K. Mizoguchi, Volumetric Properties and Interaction Parameters of Dissolved Gases in Poly(dimethylsiloxane) and Polyethylene, Macromolecules, 33 (2000) 3111-3119.

[39] F. Korosy, Two Rules Concerning Solubility of Gases and Crude Data on Solubility of Krypton, Trans. Faraday Soc., 33 (1937) 416-425.

[40] R. M. Felder and R. W. Rousseau, Elementary Principles of Chemical Processes, 2nd ed., John Wiley and Sons, New York, 1986.

[41] A. S. Michaels and H. J. Bixler, Solubility of Gases in Polyethylene, J. Polym. Sci., 50 (1961) 393-412.

[42] T. C. Merkel, V. Bondar, K. Nagai and B. D. Freeman, Hydrocarbon and Perfluorocarbon Gas Sorption in Poly(dimethylsiloxane), Poly(1-trimethylsilyl-1-propyne), and Copolymers of Tetrafluoroethylene and 2,2-Bis(trifluoromethyl)-4,5-difluoro-1,3-dioxole, Macromolecules, 32 (1999) 370-374.

[43] B. Wong, Z. Zhang and Y. P. Handa, High-Precision Gravimetric Technique for Determining the Solubility and Diffusivity of Gases in Polymers, J. Polym. Sci. Part B. Polym. Phys., 36 (1998) 2025-2032.

[44] J. H. Hildebrand, J. M. Prausnitz and R. L. Scott, Regular and Related Solutions, Van Nostrand Reinhold Company, New York, 1970.

[45] E. Wilhelm and R. Battino, The Solubility of Gases in Liquids 4. Calculations of Gas Solubilities in Hexafluorobenzene and Benzene, J. Chem. Thermody., 3 (1971) 761-768.

[46] R. C. Reid, J. M. Prausnitz and B. E. Poling, The Properties of Gases and Liquids, 4th ed., McGraw-Hill, New York, 1987.

[47] R. L. Scott, The Anomalous Behavior of Fluorocarbon Solutions, J. Phys. Chem., 62 (1958) 136-145.

[48] M.-G. De Angelis, T. C. Merkel, V. I. Bondar, B. D. Freeman, F. Doghieri and G. C. Sarti, Hydrocarbon and Fluorocarbon Solubility and Dilation in Poly(dimethylsiloxane): Comparison of Experimental Data with Predictions of the Sanchez-Lacombe Equation of State, J. Polym. Sci. Part B. Polym. Phys., 37 (1999) 3011-3026.

[49] A. Bondi, Physical Properties of Molecular Crystals, Liquids and Glasses, Wiley, New York, 1968.

[50] D. W. van Krevelen, Properties of Polymers: Their Correlation with Chemical Structure; their Numerical Estimation and Prediction from Additive Group Contributions, 3rd ed., Elsevier, Amsterdam, 1990.

[51] K. Ghosal, R. Y. Chern, B. D. Freeman and R. Savariar, The Effect of Aryl Nitration on Gas Sorption and Permeation in Polysulfone, J. Polym. Sci. Part B. Polym. Phys., 33 (1995) 657-666.

[52] K. Toi, G. Morel and D. R. Paul, Gas Sorption and Transport in Poly(phenylene oxide) and Comparisons with Other Glassy Polymers, J. Appl. Polym. Sci., 27 (1982) 2997-3005.

[53] G. E. Serad, B. D. Freeman, M. E. Stewart and A. J. Hill, Gas and Vapor Sorption and Diffusion in Poly(ethylene terephthalate), Polymer, 42 (2001) 6929-6943.

[54] J. Brandrup, E. H. Immergut and E. A. Grulke, Polymer Handbook, 4th ed., Wiley Interscience, New York, 1999.

[55] T. Masuda, E. Isobe and T. Higashimura, Polymerization of 1-(Trimethylsilyl)-1-propyne by Halides of Niobium(V) and Tantalum(V) and Polymer Properties, Macromolecules, 18 (1985) 841-845.

[56] K. Nagai, T. Masuda, T. Nakagawa, B. D. Freeman and I. Pinnau, Poly(1-trimethylsilyl-1-propyne) and Related Polymers: Synthesis, Properties and Functions, Prog. Polym. Sci., 26 (2001) 721-798.

[57] T. C. Merkel, V. Bondar, K. Nagai and B. D. Freeman, Sorption and Transport of Hydrocarbon and Perfluorocarbon Gases in Poly(1-trimethylsilyl-1-propyne), J. Polym. Sci. Part B. Polym. Phys., 38 (2000) 273-296.

[58] J. G. Wijmans and R. W. Baker, Refrigeration Process with Purge and Recovery of Refrigerant, US Patent 5,044,166 (1991).

[59] I. Chernyakov, T. H. Hsiung, A. Schwarz and J. H. Yang, Fluorochemical Recovery and Recycle Using Membranes, US Patent 5,730,779 (1998).

[60] Y. Li, J. E. Paganessi, D. Vassallo and G. K. Fleming, Process and System for Separation and Recovery of Perfluorocompound Gases, US Patent 5,785,741 (1998).

[61] I. Pinnau, J. G. Wijmans, Z. He, S. Goakey and R. W. Baker, Process for Recovering Semiconductor Industry Cleaning Compounds, US Patent 5,779,763 (1998).

[62] Y. Li, Process for Recovering CF_4 and C_2F_6 from a Gas, US Patent 5,814,127 (1998).

[63] Y. Li, J. E. Paganessi, D. Vassallo and G. K. Fleming, Process and System for Separation and Recovery of Perfluorocompound Gases, US Patent 5,919,285 (1999).

[64] Y. Li, Process for Recovering CF_4 and C_2F_6 from Vent Gases of an Aluminum Production Cell, US Patent 5,968,334 (1999).

[65] W. Ji, D. Shen, R. Jain, A. I. Shirley, A. M. Athalye and P. J. Sadkowski, Method of Processing Semiconductor Manufacturing Exhaust Gases, US Patent 6,017,382 (2000).

[66] I. Chernyakov, T. H. Hsiung, A. Schwarz and J. H. Yang, Recovery of Perfluorinated Compounds from the Exhaust of Semiconductor Fabs with Recycle of Vacuum Pump Diluent, US Patent 6,032,484 (2000).

[67] A. Singh, B. D. Freeman and I. Pinnau, Pure and Mixed Gas Acetone/Nitrogen Permeation Properties of Polydimethylsiloxane (PDMS), J. Polym. Sci. Part B. Polym. Phys., 36 (1998) 289-301.

[68] A. Morisato, B. D. Freeman, I. Pinnau and C. G. Casillas, Pure Hydrocarbon Sorption Properties of Poly(1-trimethylsilyl-1-propyne) (PTMSP), Poly(1-phenyl-1-propyne) (PPP), and PTMSP/PPP Blends, J. Polym. Sci. Part B. Polym. Phys., 34 (1996) 1925-1934.

[69] D. S. Pope, I. C. Sanchez, W. J. Koros and G. K. Fleming, Statistical Thermodynamic Interpretation of Sorption/Dilation Behavior of Gases in Silicone Rubber, Macromolecules, 24 (1991) 1779-1783.

[70] P. G. T. Fogg and W. Gerrard, Solubility of Gases in Liquids, John Wiley and Sons, New York, 1991.

[71] V. M. Shah, B. J. Hardy and S. A. Stern, Solubility of Carbon Dioxide, Methane and Propane in Silicone Polymers: Effect of Polymer Side Chains, J. Polym. Sci. Part B. Polym. Phys., 24 (1986) 2033-2047.

[72] M. S. Suwandi and S. A. Stern, Transport of Heavy Organic Vapors through Silicone Rubber, J. Polym. Sci., 11 (1973) 663-681.

[73] J. M. Prausnitz, R. N. Lichtenthaler and E. G. de Azevedo, Molecular Thermodynamics of Fluid-Phase Equilibria, 3rd ed., Prentice Hall, Upper Saddle River, New Jersey, 1999.

[74] DIPPR Chemical Database, Thermophysical Properties Laboratory, Brigham Young University, Provo, UT, *available at* http://dippr.byu.edu/public/chemsearch.asp.

[75] Y. Ichiraku, S. A. Stern and T. Nakagawa, An Investigation of the High Gas Permeability of Poly(1-trimethylsilyl-1-propyne), J. Membr. Sci., 34 (1987) 5-18.

[76] G. K. Fleming and W. J. Koros, Dilation of Polymers by Sorption of Carbon Dioxide at Elevated Pressures. 1. Silicone Rubber and Unconditioned Polycarbonate, Macromolecules, 19 (1986) 2285-2291.

[77] W. J. Koros, D. R. Paul and G. S. Huvard, Energetics of Gas Sorption in Glassy Polymers, Polymer, 20 (1979) 956-960.

[78] T. C. Merkel, V. Bondar, K. Nagai, B. D. Freeman and Y. P. Yampolskii, Gas Sorption, Diffusion, and Permeation in Poly(2,2-bis(trifluoromethyl)-4,5-difluoro-1,3-dioxole-co-tetrafluoroethylene), Macromolecules, 32 (1999) 8427-8440.

[79] H. J. Bixler and O. J. Sweeting, Barrier Properties of Polymer Films, in O. J. Sweeting (Ed.), The Science and Technology of Polymer Films, Vol. II, Wiley-Interscience, 1971, pp. 1-130.

[80] P. R. Bevington and D. K. Robinson, Data Reduction and Error Analysis for the Physical Sciences, 2nd ed., McGraw-Hill, Inc., New York, 1992.

[81] J. H. Petropoulos, Mechanisms and Theories for Sorption and Diffusion of Gases in Polymers, in D. R. Paul and Y. P. Yampol'skii (Eds.), Polymeric Gas Separation Membranes, CRC Press, Inc., Boca Raton, 1994, pp. 17-82.

[82] T. Masuda, Y. Iguchi, B. Tang and T. Higashimura, Diffusion and Solution of Gases in Substituted Polyacetylene Membranes, Polymer, 29 (1988) 2041-2049.

[83] I. Pinnau and L. G. Toy, Transport of Organic Vapors through Poly(1-trimethylsilyl-1-propyne), J. Membr. Sci., 116 (1996) 199-209.

[84] R. Srinivasan, S. R. Auvil and P. M. Burban, Elucidating the mechanism(s) of gas transport in poly[1-(trimethylsilyl)-1-propyne] (PTMSP) membranes, J. Membr. Sci., 86 (1994) 67-86.

[85] W. J. Koros, "Gas Separation" in Membrane Separation Systems - A Research and Development Needs Assessment, US Department of Energy, (1990).

[86] R. M. Barrer, J. A. Barrie and N. K. Raman, Solution and Diffusion in Silicone Rubber. I. A Comparison with Natural Rubber, Polymer, 3 (1962) 595-603.

[87] W. L. Robb, Thin Silicone Membranes-Their Permeation Properties and Some Applications, Ann. N.Y. Acad. Sci., 146 (1968) 119-137.

[88] A. Y. Alentiev, V. P. Shantarovich, T. C. Merkel, V. I. Bondar, B. D. Freeman and Y. P. Yampolskii, Gas and Vapor Sorption, Permeation, and Diffusion in Glassy Amorphous Teflon AF1600, Macromolecules, 35 (2002) 9513-9522.

[89] I. Pinnau, Z. He, A. R. Da Costa, K. D. Amo and R. Daniels, Gas Separation using C_{3+} Hydrocarbon-resistant Membranes, US Patent 6,361,582 B1 (2002).

[90] I. Pinnau, Z. He, A. R. Da Costa, K. D. Amo and R. Daniels, Gas Separation using Organic-vapor-resistant Membranes, US Patent 6,361,583 B1 (2002).

[91] R. Prabhakar, B. D. Freeman and I. Roman, Gas and Vapor Sorption and Permeation in Poly(2,2,4-trifluoro-5-trifluoromethoxy-1,3-dioxole-co-tetrafluoroethylene), Macromolecules, 37 (2004) 7688-7697.

[92] B. D. Freeman and I. Pinnau, Polymeric Materials for Gas Separations, in B. D. Freeman and I. Pinnau (Eds.), Polymer Membranes for Gas and Vapor Separation, Vol. 733, American Chemical Society, Washington, DC, 1999, pp. 1-27.

[93] A. J. Erb and D. R. Paul, Gas Sorption and Transport in Polysulfone, J. Membr. Sci., 8 (1981) 11-22.

[94] J. S. McHattie, W. J. Koros and D. R. Paul, Gas Transport Properties of Polysulphones: 1. Role of Symmetry of Methyl Group Placement on Bisphenol Rings, Polymer, 32 (1991) 840-850.

[95] K. Ghosal, R. T. Chern and B. D. Freeman, Effect of Basic Substituents on Gas Sorption and Permeation in Polysulfone, Macromolecules, 29 (1996) 4360-4369.

[96] V. Arcella, A. Ghielmi and G. Tommasi, High Performance Perfluoropolymer Films and Membranes, Ann. N.Y. Acad. Sci., 984 (2003) 226-244.

[97] V. Arcella, P. Colaianna, P. Maccone, A. Sanguineti, A. Gordano, G. Clarizia and E. Drioli, A Study on a Perfluoropolymer Purification and its Application to Membrane Formation, J. Membr. Sci., 163 (1999) 203-209.

[98] E. P. Wesseler, R. Iltis and L. C. Clark Jr., The Solubility of Oxygen in Highly Fluorinated Liquids, J. Fluorine Chem., 9 (1977) 137-146.

[99] M. H. A. Hamza, G. Serratrice, M.-J. Stebe and J.-J. Delpuech, Fluorocarbons as Oxygen Carriers. II. An NMR Study of Partially or Totally Fluorinated Alkanes and Alkenes, J. Magn. Reson., 42 (1981) 227-241.

[100] R. S. Prabhakar and B. D. Freeman, Fluoropolymer-Hydrocarbon Polymer Composite Membranes for Natural Gas Separation, in I. Pinnau and B. D. Freeman (Eds.), Advanced Materials for Membrane Separations, Vol. 876, American Chemical Society, Washington, DC, 2004, pp. 106-128.

[101] J. E. Jolley and J. H. Hildebrand, Solubility, Entropy and Partial Molal Volumes in Solutions of Gases in Non-polar Solvents, J. Am. Chem. Soc., 80 (1958) 1050-1054.

[102] S. M. Jordan, W. J. Koros and G. K. Fleming, The Effects of CO_2 Exposure on Pure and Mixed Gas Permeation Behavior: Comparison of Glassy Polycarbonate and Silicone Rubber, J. Membr. Sci., 30 (1987) 191-212.

[103] S. M. Jordan, G. K. Fleming and W. J. Koros, Permeability of Carbon Dioxide at Elevated Pressures in Substituted Polycarbonates, J. Polym. Sci. Part B. Polym. Phys., 28 (1990) 2305-2327.

[104] L. M. Robeson, Correlation of Separation Factor versus Permeability for Polymeric Membranes, J. Membr. Sci., 62 (1991) 165-185.

[105] W. J. Koros and M. W. Hellums, Gas Separation Membrane Material Selection Criteria: Differences for Weakly and Strongly Interacting Feed Components, Fluid Phase Equilib., 53 (1989) 339-354.

[106] W. J. Koros and G. K. Fleming, Membrane-based Gas Separation, J. Membr. Sci., 83 (1993) 1-80.

[107] M. R. Coleman and W. J. Koros, Isomeric Polyimides based on Fluorinated Dianhydrides and Diamines for Gas Separation Applications, J. Membr. Sci., 50 (1990) 285-297.

[108] G. S. Park, Diffusion of Some Halomethanes in Polystyrene, Trans. Faraday Soc., 46 (1950) 684-697.

[109] S. Prager and F. A. Long, Diffusion of Hydrocarbons in Polyisobutylene, J. Am. Chem. Soc., 73 (1951) 4072-4075.

[110] G. S. Park, The Diffusion of Some Organic Substances in Polystyrene, Trans. Faraday Soc., 47 (1951) 1007-1013.

[111] R. J. Kokes and F. A. Long, Diffusion of Organic Vapors into Polyvinyl Acetate, J. Am. Chem. Soc., 75 (1953) 6142-6146.

[112] C. E. Rogers, V. Stannett and M. Szwarc, The Sorption, Diffusion and Permeation of Organic Vapors in Polyethylene, J. Polym. Sci., 45 (1960) 61-82.

[113] R. M. Barrer, Nature of the Diffusion Process in Rubber, Nature, 140 (1937) 106-107.

[114] G. J. van Amerongen, The Permeability of Different Rubbers to Gases and its Relation to Diffusivity and Solubility, J. Appl. Phys., 17 (1946) 972-985.

[115] R. M. Barrer and G. Skirrow, Transport and Equilibrium Phonemena in Gas-Elastomer Systems. I. Kinetic Phenomena, J. Polym. Sci., 3 (1948) 549-563.

[116] R. M. Barrer, Permeation, Diffusion and Solution of Gases in Organic Polymers, Trans. Faraday Soc., 35 (1939) 628-643.

[117] G. J. van Amerongen, Influence of Structure of Elastomers on their Permeability to Gases, J. Polym. Sci., 5 (1950) 307-332.

[118] R. M. Barrer, Some Properties of Diffusion Coefficients in Polymers, J. Phys. Chem., 61 (1957) 178-189.

[119] D. R. Paul and A. T. DiBenedetto, Diffusion in Amorphous Polymers, J. Polym. Sci.: Part C, 10 (1965) 17-44.

[120] R. Y. M. Huang and V. J. C. Lin, Separation of Liquid Mixtures by Using Polymer Membranes. I. Permeation of Binary Organic Liquid Mixtures through Polyethylene, J. Appl. Polym. Sci., 12 (1968) 2615-2631.

[121] H. Fujita, Diffusion in Polymer-Diluent Systems, Fortschr. Hochpolym. Forsch., 3 (1961) 1-47.

[122] S. S. Kulkarni and S. A. Stern, The Diffusion of CO_2, CH_4, C_2H_4 and C_3H_8 in Polyethylene at Elevated Pressures, J. Polym. Sci. Polym. Phys. Ed., 21 (1983) 441-465.

[123] R. J. Young and P. A. Lovell, Introduction to Polymers, 2nd ed., Chapman & Hall, London, 1991.

[124] R. L. Scott, Solutions of Non-Electrolytes, Ann. Rev. Phys. Chem., 7 (1956) 43-66.

[125] R. L. Scott, Some Unsolved Problems of Liquids and Solutions, J. Chem. Ed., 30 (1953) 542-549.

[126] J. H. Hildebrand, The Entropy of Solution of Molecules of Different Size, J. Chem. Phys., 15 (1947) 225-228.

[127] R. L. Scott, The Solubility of Fluorocarbons, J. Am. Chem. Soc., 70 (1948) 4090-4093.

[128] J. H. Simons and R. D. Dunlap, The Properties of *n*-Pentaforane and Its Mixtures with *n*-Pentane, J. Chem. Phys., 18 (1950) 335-346.

[129] J. H. Hildebrand, B. B. Fisher and H. A. Benesi, Solubility of Perfluoro-*n*-heptane with Benzene, Carbon Tetrachloride, Chloroform, *n*-Heptane and 2,2,4-Trimethylpentane, J. Am. Chem. Soc., 72 (1950) 4348-4351.

[130] J. H. Simons and J. W. Mausteller, The Properties of *n*-Butforane and Its Mixtures with *n*-Butane, J. Chem. Phys., 20 (1952) 1516-1519.

[131] D. N. Campbell and J. B. Hickman, Solubility Characteristics of Some Binary Liquid Mixtures, J. Am. Chem. Soc., 75 (1953) 2879-2881.

[132] N. Thorp and R. L. Scott, Fluorocarbon Solutions at Low Temperatures. I. The Liquid Mixtures CF_4-CHF_3, CF_4-CH_4, CF_4-Kr, CH_4-Kr, J. Phys. Chem., 60 (1956) 670-673.

[133] N. Thorp and R. L. Scott, Fluorocarbon Solutions at Low Temperatures. II. The Liquid Mixtures C_2H_6-C_2F_6, C_2F_6-CHF_3, CH_2F_2-CHF_3, C_2H_6-CHF_3 and Xe-CHF_3, J. Phys. Chem., 60 (1956) 1441-1443.

[134] J. M. Smith, H. C. Van Ness and M. M. Abbott, Introduction to Chemical Engineering Thermodynamics, 6th ed., McGraw Hill, New York, 2001.

[135] A. J. Stone, The Theory of Intermolecular Forces, Clarendon Press, Oxford, 1996.

[136] J. H. Hildebrand and R. L. Scott, The Solubility of Nonelectrolytes, Reinhold Publishing Corporation, New York, 1950.

[137] F. London, On Centers of van der Waals Attractions, J. Phys. Chem., 46 (1942) 305-316.

[138] T. M. Reed III, The Theoretical Energies of Mixing For Fluorocarbon-Hydrocarbon Mixtures, J. Phys. Chem., 59 (1955) 425-428.

[139] S. D. Hamann, J. A. Lambert and R. B. Thomas, The Second Virial Coefficients of Some Gas Mixtures, Australian J. Chem., 8 (1955) 149-157.

[140] E. M. Dantzler-Siebert and C. M. Knobler, Interaction Virial Coefficients in Hydrocarbon-Fluorocarbon Mixtures, J. Phys. Chem., 75 (1971) 3863-3870.

[141] M.-G. De Angelis, T. C. Merkel, V. I. Bondar, B. D. Freeman, F. Doghieri and G. C. Sarti, Gas Sorption and Dilation in Poly(2,2-Bis(Trifluoromethyl)-4,5-Difluoro-1,3-Dioxole-Co-Tetrafluoroethylene): Comparison of Experimental Data with Predictions of the Nonequilibrium Lattice Fluid Model, Macromolecules, 35 (2002) 1276-1288.

[142] W. Song, P. J. Rossky and M. Maroncelli, Modeling Alkane + Perfluoroalkane Interactions using All-atom Potentials: Failure of the Usual Combining Rules, J. Chem. Phys., 119 (2003) 9145-9162.

[143] T. M. Reed III, The Ionization Potential and the Polarizability of Molecules, J. Phys. Chem., 59 (1955) 428-432.

[144] J. A. Beran and L. Kevan, Semiempirical Calculation of Molecular Polarizabilities and Dimagnetic Susceptibilities of Fluorocarbons, Substituted Fluorocarbons, Ethers, Esters, Ketones, and Aldehydes, J. Phys. Chem., 73 (1969) 3860-3866.

[145] R. J. Lagow and H.-C. Wei, Direct Fluorination of Polymers, in G. Hougham (Ed.), Fluoropolymers I, Kluwer Academic/Plenum Publishers, New York, 1999, pp. 201-221.

VITA

Rajeev Satish Prabhakar was born on June 20, 1976 to Satish and Vijayalaxmi Prabhakar in Bombay, India. He received his Secondary School Certificate from St. Michael's High School and Higher Secondary School Certificate from Mithibai College, both in Bombay. He received his undergraduate training at the Indian Institute of Technology at Kharagpur, India from where he graduated with a B.Tech.(Hons) in Chemical Engineering in May 1998. Then, he joined North Carolina State University in Raleigh, NC that same year. He was awarded a Master of Science (M.S.) degree in Chemical Engineering in December 2000. In January 2002, he transferred to the University of Texas at Austin and continued to work with the same supervisor, Professor Benny D. Freeman, in the Chemical Engineering department.

Permanent address: 1/24 Seema Society, N. Dutta Marg
Four Bungalows, Andheri (West)
Mumbai 400 053 INDIA.

This dissertation was typed by the author.